Radar Backscatter Modelling of Forests Using a Macroecological Approach

Matthew Brolly

Submitted for Doctor of Philosophy

The University of Edinburgh

May 2011

Acknowledgements

I'd like to formally thank all those who have helped scientifically in the formation of this thesis. Thanks to the inventors of RT2, WBE and SERA you have all made this possible. Thanks also to Dr. Mencuccini for his initial help with forestry matters and all those who have inspired me. Thanks especially to my supervisor Dr Iain Woodhouse for recruiting me and showing me how science can be done in the most relaxing way, thanks for the faith and ideas.

Inspirational.

To my friends in Edinburgh, thanks for keeping me stress free and happy, I owe a lot.

To Rocka Juniors, well played.

To Becki, it's finished so we can start. You are a radar detector.

To Mum and Dad thanks for all the meals and stuff, you've inspired me to do this ever since the moment I handed in my MSc and you said "Are you going to do a PhD?" and I said "No way." I hope this makes you proud.

To geniuses, thanks for the quotes.

"If the facts don't fit the theory, change the facts."
Albert Einstein

"Thank you, thank you, thank you, you're far too kind, now can I get an encore, do you want more?"
Shawn Corey Carter

Abstract

This thesis provides a new explanation for the behaviour of radar backscatter of forests using vegetation structure models from the field of macroecology. The forests modelled in this work are produced using allometry-based ecological models with backscatter derived from the parameterisation of a radiative transfer model. This work is produced as a series of papers, each portraying the importance of macroecology in defining the forest radar response. Each contribution does so by incorporating structural and dynamic effects of forest growth using one of two allometric models to expose variations in backscatter as a response to vertical and horizontal forest profiles. The major findings of these studies concern the origin of backscatter saturation effects from forest SAR surveys. In each work the importance of transition from Rayleigh to Optical scattering, combined with the scaling effects of forest structure, is emphasised. These findings are administered through evidence including the transition's emergence as the region of dominant backscatter in a vertical profile (according to a dominant canopy scattering layer), also through the existence of a two trend backscatter relationship with volume in the shape of the typical "saturation curve" (in the absence of additional attenuating factors). The importance of scattering regime change is also demonstrated through the relationships with volume, basal area and thinning. This work's findings are reinforced by the examination of the relationships between forest height and volume, as collective values, providing evidence to suggest the non-uniqueness of volume-to-height relationships. Each of the studies refer to growing forest communities not single trees, so that unlike typical studies of radar remote sensing of forests the impact of the macroecological structural aspects are more explicit. This study emphasises the importance of the overall forest structure in producing SAR backscatter and how backscatter is not solely influenced by electrical properties of scatteres or the singular aspects of a tree but also by the collective forest parameters defining a dynamically changing forest.

In summary, this work provides a new explanation to describe saturation behaviour associated with radar remote sensing of forests through analysis of Rayleigh and Optical scattering trends. The negative and positive exponential trends followed by the respective regimes for backscattering coefficient against branching level through the canopy, and the nature of the maximum value predicted by the model are evidence that the vertical profile, and indeed forest structure, influence backscatter and impact on interferometric height retrievals. The dependence of the saturation effect on basal area and the transition from Rayleigh to Optical scattering is also emphasised using modelled forests devoid of volume scattering (often assumed responsible for the saturation effect through attenuation). This is primarily considered a result of the proportionality of Rayleigh scattering to the target volume squared and the Optical scattering to basal area. Crucially this suggests that if the dominant scattering regime at any volume is Optical and basal area remains consistent then so will backscatter. This work links macroecology directly to radar backscatter, emphasising the importance of ecology in the interpretation of remotely sensed data to provide accurate forest parameter estimates.

The thesis is provided in the form of a series of prospective journal articles intended for submission or currently in review. As a result of the format several themes and equations are repeated.

Table of Contents

1 Introduction

1.1 Aim

The aim of this thesis is to analyse and determine the importance of macroecology in forest remote sensing, particularly in radar backscatter studies. Macroecology deals with the study of relationships between organisms and their environment at large spatial scales to characterise and explain statistical patterns of abundance, distribution and diversity. These attributes of an ecosystem are directly influenced by the surrounding environment in which they are placed and as a result are affected by environmental variations both internal and external in nature. The manifestation of these changes are the physical attributes exhibited by the system. In the case of a forest the dynamics of growth and size as well as mortality will be affected, producing unique forest systems for the environment they occupy.

The influence Macroecology has on the radar backscatter of a forest is believed throughout this work to emanate from the variations enforced by the environment on the branch and stem sizes and the number density within a studied forest. These physical aspects of a forest determine the different scattering mechanisms and the intensity of scattering produced. They are therefore believed to be in direct relation to macroecological changes. In this work the radar backscatter from a forest is linked to the specific Macroecological trends of self thinning, number density, forest height, basal area and most importantly to the volume and biomass of forests. The influence of Forest Macroecology on radar backscatter is highlighted to play a significant role in determining the trends exhibited by empirical studies and significantly, suggests that relationships between forest volume and forest backscatter are non-unique and are instead a consequence of Macroecological variations. The original scientific work of this thesis begins in Chapter 4 with an analysis of the forest height to forest volume relationships that are predicted by a forest growth model (SERA (Hammond and

Niklas 2009) see also Chapter 3.2). The direct implications for forest remote sensing are considered and the consequences of the use of allometry (Chapter 1.4) are also considered. The work which follows on from this analysis directly incorporates radar modelling and forest structure provided by the WBE model ((West et al. 1997) and Chapter 3.1). In Chapter 5 the vertical backscatter distribution of forests is examined with close attention paid to the effect of branch component number densities and size distributions. This is followed in Chapter 6 by an interferometric analysis of the backscatter profiles of Chapter 5 using coherence tomography techniques. Chapters 7 and 8 consider the effect of macroecological variation on the process of direct volume inferral from backscatter intensity measurements using the Matchstick Model (see Chapter 3.3) and SERA respectively. Each study considers the physics of scattering and the trends produced by backscatter modelling using RT2 ((Saich 1993) see also Chapter 3.4) to provide general reasoning related to macroecological behaviour for backscatter trends exhibited in empirical data. Chapters 1-3 provide background on forest modelling methods, the complementary use of allometry, the principles of SAR scattering and descriptions and uses of the specific models featured in this study.

This thesis aims to address the following key questions through the original work presented. Each experimental Chapter (4-8) offers a deductive approach to forest modelling. Some key questions this thesis addresses are:

1. How does the relationship between synthetic aperture radar backscatter and forest volume vary when forests are exposed to vertical and horizontal structure variation?
2. How consistent are the relationships between forest volume and forest height classifications?
3. How do any variations in height to volume relationships impact on the use of allometry to infer forest volume and biomass?
4. How does branch size and number distribution within the canopy influence backscatter interpretation?

5. Can forest backscatter be described through a comparison of scattering theory trends?
6. What are the consequences of the findings presented here for the future of forest biomass estimation through remote sensing?

1.2 Rationale

With the continuing debate over climate change in present day political and social environments there is pressing need for an accurate analysis of forest biomass for use as an effective measure of carbon sequestration. As a country's carbon usage can be offset by such methods (Brown et al. 2000a; Sedjo and Marland 2003) a lot of recent interest has been devoted to this subject by the academic community. Forest biomass estimates have commonly been carried out by taking advantage of allometric relationships originating from standard forestry measurements such as diameter at breast height (DBH) or basal area (Chave et al. 2004; Keller et al. 2001; Nelson et al. 1999); often requiring collection of data at ground level to develop site specific equations (Gehring et al. 2004; Ketterings et al. 2001). Complete global coverage using such methods remains difficult and as a consequence remote sensing has, as such, been nominated and begun to prove itself as the method to provide this coverage. Various works have enforced the importance of such research including that of (Treuhaft et al. 2003) who stated that balancing terrestrial carbon budgets, "*calls for global remote sensing of forest biomass*". Recent work has been hampered by underestimates of biomass using remote sensing (Chen et al. 2009; Sandberg et al. 2009) but the fact that relationships exist between microwave interactions and aboveground biomass suggests there is great scope for improvement in the understanding and application of SAR and other EM remote sensing methods.

Optical methods, including those using infrared for forestry applications, (Sellers 1992), have obvious flaws when confronted with cloud cover or other meteorological

barriers. These barriers strongly limit the number of available optical images (Bindlish and Barros 2001), in addition to the fact that collection can only take place during daylight hours. Contrary to these limitations, Synthetic Aperture Radar (SAR) is not hampered by atmospheric conditions in the same way, allowing it to stand out as the choice method for forest remote sensing exhibiting correlations between radar cross section and forest parameters such as biomass (Le Toan et al. 1992). The principles of SAR acquisition are described in detail in Chapter 2.

Forest modelling using SAR to obtain biomass values can be carried out in different ways; by analysing the values of the normalised radar cross section (Castel et al. 2002), by using interferometric (Floury et al. 1997) and polarimetric methods ((Mette et al. 2004a), or through a combination. These methods each have their advantages as well as flaws. Forest biomass shows a strong relationship with normalised radar cross section but only until a certain biomass level is reached. Normalised radar cross section saturation occurs at a point, typically associated with a biomass level relative to the radar frequency. Beyond this level it is generally accepted that no more information is perceived to be attainable (Imhoff 1995a) whether that be a result of signal attenuation or forest structure. SAR interferometric methods of biomass retrieval also have deficiencies as they rely on the ability to distinguish between height and ground contributions, errors are often apparent in the identification of the explicit height measurements (Papathanassiou and Cloude 2001). Polarimetry and interferometry have been used to avoid the limiting influence of saturation, but inaccuracies of up to 30% have been recorded (Mette et al. 2002). Height inaccuracies associated with interferometry are often due to coherence discrepancies. In forest scenarios coherence has been observed to reduce as stand height increases, and typically as biomass increases (Floury et al. 1996).

Approximately 38% of the world's vegetated surface area, containing 81% of the estimated total store of its biomass, is above the saturation limit of current radar systems with 62% of the Earth's vegetated surface area existing at biomass below the

saturation level for P-Band (Imhoff 1995a). This in turn contains only an estimated 19% of the total biomass represented by terrestrial vegetation. Experimental studies with airborne systems such as AirSAR and E-SAR over temperate, boreal and tropical forests; (Beaudoin et al. 1994; Dobson et al. 1992; Hoekman and Quiriones 2000; Le Toan et al. 1992; Quegan et al. 2000; Rignot et al. 1994), have indicated that saturation occurs at approximately 30, 50 and 150–200 tonnes/ha at respective C, L and P-Bands. While these systems can measure a large range of above-ground forest biomass, spaceborne radars currently available are limited by their operational wavelengths to biomass levels of less than 50 tonnes/ha with the longest wavelengths used being L-Band. The proposed P-Band ESA BIOMASS mission (Scipal et al. 2010) is one possible future system that aims to increase the biomass range of spaceborne systems, but currently the prospect of any longer wavelength systems in orbit provides major technical and financial difficulties. Nonetheless, the use of current systems provides the ability to monitor biomass and biomass increments of young forests below the saturation point, a valuable asset to carbon cycle studies (Kurz and Apps 1999). Future L-Band systems such as Tandem-L (Krieger et al. 2009) are hoped to be capable of more accurate biomass estimates using interferometry, even at post saturation biomass levels. A greater understanding of the relationship of normalised radar cross section with post saturation biomass, or a similar improvement in the understanding of height to biomass relationships to improve the accuracy of interferometric techniques is required to maintain the momentum of forest biomass research using remote sensing. With either option the accuracy of results could be significantly improved by modelling studies which incorporate environmental and biological information in to the modelling. With these considerations the accuracy of forest biomass estimation will definitely improve as the forest primarily dictates the backscatter both in terms of scatterer shape and size and through number density.

Enhancing forest remote sensing using biology can be done in two prominent ways. The first method involves the complete destructive sampling of a forest, allowing all

trees to be accurately measured and weighed. Such an approach has an obvious environmental impact.. The second method requires a more sample based measuring technique by selectively sampling trees of particular heights and breadths. These can then be used to approximate and represent the scaling relationships in the forest. Both methods can contribute to the enhancement and study of allometry which aims to develop equations to be used as an accurate representation of the scaling relationships exhibited by all trees within a forest.

Through the methods of allometry and remote sensing this work aims to provide alternative methods of estimating biomass by proposing links between the macroecological behaviour of a forest and the remote sensing measurements. Although backscatter is deemed proportional to biomass, the variations that have been recorded in this relationship (Patenaude et al. 2005) are proof enough that a greater understanding of what causes saturation and these variations is required. This thesis follows the recorded course of investigation due to the association of macroecology with the dynamics of a forest, and through these dynamics, with SAR backscatter. An enhancement in biological understanding of is hoped will help determine whether forests should continue to be viewed as random volumes above a surface, in a similar fashion to the Water Cloud Model of (Attema and Ulaby 1978) and Random Volume Over Ground model used by (Treuhaft and Siqueira 2000), or whether additional complexity associated with forest structure, macroecology and evolution is required.

1.3 Forest Modelling in Remote Sensing

1.3.1 Methods of Investigation

In general, the most prominent approaches of forest biomass estimation according to (Mette et al. 2003) are: the estimation from individual tree mapping (Needham 1987), estimation from optical and radar signal intensity using correlation between backscatter intensity and biomass (Le Toan 2001), allometric estimations based on

forest parameters closely related to biomass such as tree height (Mette et al. 2004b), or the less commonly used, within SAR studies, LAI (Dong 2003). The role SAR studies have played in the estimation of forest biomass can also be generalised into prominent approaches; the initial research period upon the initiation of SAR involving intensity measurements, the use of interferometry and incorporation of allometry, and most recently the use of polarimetric methods both alone and in combination with interferometry to take advantage of unique polarimetric responses of vegetation as a consequence of the nature of scattering.

In 1990 Richards published a review of current trends in forest research using radar backscatter (Richards 1990). Published prior to the onset of Pol-INSAR, this paper considered the challenges faced when modelling forests,

"the propensity for substantial energy penetration into the forest canopy, especially at longer wavelengths, suggests that the integrated backscatter observed from a forest environment must be a collection of scattering events involving the canopy, the tree woody matter and the understory or subsurface under the canopy".

This statement now appears obvious with regards to studies involving decomposition (Cloude et al. 1996) but it outlined the potential need for microwave backscatter to be modelled more directly with forest structure. Introducing a fully layered or allometrically based forest model, as undertaken in this thesis, to do just this is a logical step to effectively assess the contributions of forest structure on backscatter. Attempts to model backscatter with regards to realistic forest structures have been limited in the literature and tend to be more focussed on ideal structures with little basis in biological models. A prime example of this has been the widely used Water Cloud Model (Attema and Ulaby 1978). Richards also stated that forest modelling using radar, in general, takes on three different guises. The analytical approach, based on electromagnetic theory and well known expressions for radar backscatter coefficients (Saatchi and Moghaddam 2000); regression models which aim to fit

experimental data (Eom 1986); and phenomenological models concerned with biological processes (Freeman et al. 1992). This thesis aims to employ these guises with particular emphasis on the biological influence of forest dynamics. The complex nature of modelling energy interactions within forests raises the possibility that to achieve the most accurate forest biomass estimates using microwave remote sensing any chosen technique should involve a combination of each, taking advantage of their individual strengths to negate any inherent weaknesses.

Sacrifices of realism have often been a feature of forest modelling in order to limit complexity. (Karam and Fung 1988) created a model consisting solely of branches and surface, while (Lang 1985) in a similar effort to simplify used a model devoid of branches. Importantly these models maintained a link with the biological structure of a forest, but did not venture as far as to explore how differing forests on a macroecological level produce different backscatter. The inclusion of biological realism in forest models for radar studies can be used to maintain the essential simplicity and tractability of many existing models with only a negligible increase in complexity. Such an attempt is made in this thesis in which simple structures are used but within the simplicity of the structures is a scaling regime built on models derived from empirical evidence and factoring in the effects of forest thinning. Improving relationships between nature and models used in remote sensing does not necessarily lead to an escalation in complexity. By refining allometric relationships of particular features and modelling significant growth more accurately it is believed that greater understanding of forest microwave interactions can be revealed. This is done in this thesis using the models described in Chapter 3.

1.3.2 A History of Forest Modelling using SAR Backscatter

In many theoretical models, vegetation canopy is treated as a uniform layer of specified height containing a random distribution of scatterers (Attema and Ulaby 1978) (Karam and Fung 1988). Limitations in these theoretical scattering models are

associated with scatterer assumptions. In such models the scatterers, for simplicity, are often located in one layer above the soil surface, an arrangement which negates the trends of many forests, particularly managed ones in which the vertical structure is highly organised. (Ulaby et al. 1990) was one of the first works to successfully introduce multi-layered models. In contrast to idealised theoretical models (Yueh 1992) showed that it may be necessary for theoretical models to take into account vegetation architecture, the aspect of modelling most often sacrificed. In this thesis branching architecture is featured in the experimental chapters 5 and 6 with more idealised but applicable to long wavelength SAR structures used in 4, 7 and 8. This thesis is an example of how different methods may be complementary.

The model presented by (Attema and Ulaby 1978) is a widely referenced work for experiments modelling microwave-canopy interactions due to its mathematical ease and effective results with both crop (Graham and Harris 2003; Wigneron et al. 1999) and forest modelling (Askne et al. 1997; McDonald et al. 1990). In the model, the canopy is represented as a distribution of isotropic point scatterers with only single scattering events considered. As such the vegetation layer can be modelled as a "Water Cloud", hence the commonly held name "Water Cloud Model" (WCM). This model uses the same physics for modelling forest backscatter as that used for clouds, assuming the canopy to be composed of spheres of equal size. Although extremely simple, it provides one explanation to the "saturation" effects observed when plotting SAR backscatter against biomass. To increase biomass in this model the depth of the layer must be increased, with depth increasing until it is eventually considered opaque. The only significant variables are the height of the canopy layer and the cloud density. The geometry of this model allows it to be easily modified and used in conjunction with other models such as the radiative transfer models of (Ulaby et al. 1990), known as MIMICS, or RT2 (Anderson 2000; Saich 1993; Saich 2002; Saich et al. 1995), which is used effectively to model multi layer scenarios in this thesis but also in the work of (Balzter et al. 2003b; Brown et al. 2000b; Cookmartin et al. 2000; Saich et al. 2001; Woodhouse 2006b) for both agricultural and forest applications.

RT2 is very important to the work of this thesis and is discussed in Chapter 3.4. The MIMICS model is based on a first order solution of the radiative transfer equation (see Chapter 2.2) for a tree canopy comprising a crown layer, modelled by a distribution of dielectric cylinders representing branches, and discs representing leaves. The trunks are treated as dielectric cylinders of uniform diameter. It is stated in (Ulaby et al. 1990) that the major shortcomings of previous available models were that they treated the canopy as a continuous layer in the horizontal direction, as well as assuming the canopy to have uniform properties in the vertical direction with scatterers in the crown volume uniform in size, shape and dielectric properties. These shortcomings are acknowledged in the choice of scattering model used in this thesis. The ability of RT2 to model layer-ground interactions from each modelled canopy layer (considered an important component of long wavelength SAR forest scattering such as that exhibited at P (Saatchi and McDonald 2002) and VHF (Fransson et al. 2000a; Hallberg et al. 2005) bands) in addition to the individual scattering mechanisms makes it a more appropriate model for this study.

There has been a relative lack of work broaching the subject of linking forest modelling using SAR and biological growth models. The "Water Cloud Model" is still continually used in its original form (Bindlish and Barros 2001); (Askne et al. 1997), while its use in (Richards et al. 1987) is applied with the view of developing a theoretical radar backscatter model through characterisation of tree component scattering properties and through imposition of empirically derived spatial distributions. The model produced a simplistic interpretation of the forest structure in keeping with the WCM's simplicity but highlighted the significance of the tree trunk to the backscatter response. Although empirically derived, the fact remains that the growth of individual trees was not analysed in Richard's work, resulting in a site specific model rather than a more generic interpretation applicable to other forests as attempted in this thesis. The growth models used in this thesis are based on the biophysical and allometric relationships exhibited by species of multiple ages from multiple locations. The West, Brown and Enquist model, WBE (West et al. 1997) is

based on the requirements of resource distribution using a branching structure in accordance with biological, hydraulic, and mechanical theories, while the SERA model is more empirically based with a large influence placed on a single plantation monitored over a 100 year period but with inputs from many field study sites through the Cannell compendium(Cannell 1982). Both models are also easily manipulated in this thesis to account for changing conditions in terms of environment and scaling and are described with reference to their applicability to this thesis in Chapter 3.

Other approaches to remote sensing vegetation modelling have been made by (Lang 1983) using a set of dielectric discs with specified statistical distributions of angular orientation to represent foliage. This has been effectively used in inversion procedures by (Lang and Saleh 1985). (Eom and Fung 1986) investigated the usefulness of needle and disc models, while previously (Tsang 1981) attempted to model the canopy layer by simulating a dielectric slab with a randomly fluctuating dielectric constant. In (Karam and Fung 1988) a scattering model for defoliated vegetation was developed by treating a branching layer within a canopy as a collection of randomly oriented dielectric cylinders of finite length over an irregular ground surface. Both the polarised and depolarised backscattering were computed for this setup and their behaviour versus the volume fraction, the incidence angle, the frequency, the angular distribution and the cylinder size were illustrated.

Further models have been created which have been designed with the compromise between complexity and tractability firmly in mind. A multi-layered model of the forest structure was derived in (Karam 1995), in the sequel to the work of (Karam et al. 1992), which built upon the “Water Cloud Model” and progressed the work of (Karam and Fung 1988). In this work, vegetation was modelled using a randomly oriented disc analogy, an aspect further explored in, (Treuhaft et al. 1996) and (Treuhaft and Siqueira 2000) in compiling the RVoG, or Random Volume Over Ground model. The original (Karam et al. 1992) model accounted for first and second–order scattering within the canopy, surface roughness in canopy-soil

interaction, and allowed variation in branch size and orientation to be included, in a similar manner to RT2. These characteristics were maintained in subsequent model developments. This approach showed that for a match between calculated and measured values of backscattering coefficients the branch size distribution was important and so much so that the use of only one or two average branch sizes within the canopy would not be sufficient to explain multi-frequency data; an aspect addressed by (Woodhouse and Hoekman 2000). The (Karam et al. 1995) model furthered the work by considering a fully polarimetric canopy based on a second order solution of the radiative transfer model.

The RVoG model is commonly used as the model inverted in polarimetric interferometry to derive canopy height in work such as (Cloude and Papathanassiou 2003). In a similar manner to the WCM it increases forest volume by increasing canopy depth but features scatterers more suited in size and shape to describing scattering from branches. The resulting backscatter profile using these models is a function of extinction with homogeneous number density throughout the modelled forest. In conjunction with interferometry and polarimetry the RVoG model can be used to estimate vertical-structure parameters due to its simple description of extinction with increasing canopy depth (the applicability of such methods to RT2 modelled data is investigated in Chapters 5 and 6). The usefulness of interferometry in forest modelling is that it responds primarily to the location and distribution of vegetation components and underlying surfaces, while for polarimetry it is known to respond primarily to the orientation and shape of scatterers (Treuhaft and Siqueira 2000). Methods of remote sensing which can be used to distinguish such details of forest composition identified by interferometry and polarimetry call for the use of forest models based on biological processes, and realism such as offered by WBE and SERA (Hammond and Niklas 2009; West et al. 1997).

Although each of these theoretical works remain important land marks in this field of research, the common factor missing continues to be a direct relationship to biology

and the macroecological relationships governing the growth of forests. It is believed here that this is necessary to emphasise the importance of the relationships existing between forests as a consequence of sharing a common functionality. Such consideration was taken by (Woodhouse 2006b) by combining the WBE model with the WCM to take advantage of the relative simplicity of both, and in doing so to highlight the potential of such alliances. It is upon that work which this thesis aims to improve.

1.3.3 Interferometry and Polarimetry in Forest Modelling

Prior to the development of radar interferometry as a technique for forest structure modelling, remotely sensed biomass was mainly derived from the power of the microwave returns (Treuhaft et al. 2003). Inaccuracies in this method were apparent when it came to larger scale biomass estimates with volume saturation occurring at biomass levels as low as 150ton/ha at the lowest useable microwave frequencies (Patenaude et al. 2005) (Imhoff 1995a). Interferometry and Polarimetry offer alternatives.

Two factors constrain the use of interferometry in SAR for evaluating the relationship between the interferometric observables and the parameters of the scattering process (Cloude and Papathanassiou 1998). One is that a conventional interferometric system operating with a fixed polarisation at a single frequency is not able to provide enough independent parameters necessary to describe natural scattering processes. The second is in the interpretation of the interferograms; involving an estimation of the location of the effective scattering phase centres (dominant backscatter location), with dependence on wavelength, polarisation and other physical and geometrical parameters of the scatterer. These problems have been broached by using multi parameter techniques including multi-temporal (Papathanassiou et al. 1997), taking advantage of the temporal decorrelation, multi-frequency (Papathanassiou et al. 1997) (Lanari et al. 1996) making use of the frequency dependent behaviour of the

interferometric coherence and the varying depth penetration achieved with varying frequencies, and multi-baseline (Treuhaft et al. 1996) which extends the number of independent observations.

Accuracy in forest height estimation using interferometry is dependent on the identification of scattering centres and remains an ongoing challenge. In effect this technique relies upon the idenitifcation of distinguishable areas of backscatter within the vertical profile with interferometric canopy height highly significant. Due to the common misinterpretation of the origin of scattering phase centres, using heights retrieved from interferometry to ascertain biomass is not necessarily an accurate method. Understanding which height these phase centres refer to, whether that be maximum, average or a weighted average, and how the retrieved height is related to the biomass are extremely important considerations for maximising the ability of interferometry. These deficiencies are addressed in the work of this thesis both through an explanation for the occurrence of scattering centres and through a description of the relationships of various height classifications to volume in Chapter 4. Chapters 5 and 6 also analyse how these phase centres can vary in location as a consequence of structural variation.

In (Treuhaft and Cloude 1999) the identification of the top of the canopy and knowledge of an underlying topography were to lead to reported vegetation height accuracies in the 2-8m range. This was dependent on parameters such as the level of orientation of the vegetation, average extinction, and other forest characteristics. Treuhaft and Cloude (1999) provided a method of garnering parameter estimates using the characteristics of the eigenpolarisations estimated from the co-polar and cross-polar combinations of the signal used to analyse forest structure. In the representation of a randomly oriented volume the vegetation parameters on which the cross correlation was identified to depend were given as, the vegetation layer, the altitude of the bottom of the vegetation layer and the extinction coefficient. As there were three parameters to be found from the two observations of amplitude and phase

it was clear that a single observation could not be used to accurately estimate the required parameters. The solution being to feature more than one observation to provide enough interferometric amplitudes and phases to accurately estimate structural parameters and the extinction coefficient but even with the greatest accuracies the indirect nature of biomass retrieval using interferometry is dependent on the accuracy of allometric relationships (Chapter 1.4).

Polarimetric SAR interferometry for forest applications was developed by (Cloude and Papathanassiou 1998). In this work a canopy penetration model was presented. The model was an electromagnetic model which had been simplified for the scenario of backscatter radar signals from vegetation, with the intention to showcase the significant role that polarimetry could play in interferometric applications. In its original form the method was a process of generating phase differences between interferograms using different polarisation combinations. Through analysis of the phase differences, a correlation with the vegetation height was observed.

A fundamental quality of polarimetric interferometry is shown by (Isola and Cloude 2001) in which a validity test for a model was carried out. In this model four unknown parameters existed with only the measurements of amplitude and phase of coherence available for determination; a similar situation to that seen in (Treuhaft and Siqueira 2000). By employing fully polarimetric interferometry it was proved that the ratio of unknowns to measurements became equal with the introduction of a polarimetric channel, bringing about one unknown parameter and two further measurements. This led to a 6 observables, 6 measurements ratio through the incorporation of two polarimetric channels. (Cloude and Papathanassiou 2003), further proposed a method of relating the polarimetric SAR interferometry observables to the physical parameters of a forest in order to establish the thickness of the vegetation cover including the extinction coefficient. Although, the techniques used have been shown to mainly underestimate tree heights (Cloude et al. 2001). The estimation of the extinction coefficient was seen to improve with increasing tree

height, ultimately showing its applicability for use in forestry applications while also highlighting the inaccuracies that may be a feature of height to volume relationships and ultimately allometric conversions to obtain biomass as was the focus of (Mette et al. 2003) and (Mette et al. 2004b).

In polarimetric terms the polarisations HH and HV, which show the most sensitivity to specular scattering mechanisms i.e. the trunk and ground surface, are also said to show the highest sensitivity to biomass (Bindlish and Barros 2001). It is also known that cross-polarisation signatures are more sensitive to crown structure than the co-polarisation signatures (Sun 1995). Within this thesis the presence of canopy scatterers determines the polarisations used. In their presence the chosen polarisation is HV due to the depolarising effects of volume scattering (Mougin et al. 1999; Richards et al. 1987) and the heightened sensitivity to forest biomass shown by this polarisation (Ranson and Sun 1994b) see Chapters 5 and 6 for their use in this thesis. Where only the stems are concerned the co-polarisations are preferred due to the enhanced contribution of the double bounce mechanism (Moghaddam and Saatchi 1995) and are chosen according to their relative emphasis, see Chapters 7 and 8. This simple consideration is just one example of how multi polarisation data can be used as a complementary data source with or without interferometry.

The heights extracted from the PolInSAR data in (Mette et al. 2004a) showed a good correlation with the H100 forestry value, a sample height taken as the mean of the 100 trees with the greatest diameter at breast height, and showed how the consideration of the source of a scattering phase centre is crucial for accurate parameter estimation. It also highlighted the possibility that allometric equations may not suffice for forest scenarios and forest height classifications such as H100 if they were developed initially for individual trees rather than for a forest collective as shown in (Mette et al. 2004a). The significance of this is that forest height can be classified in numerous ways and identifying which height the scattering phase centres refer to is crucial to improve biomass estimation. The successful use of polarimetric

interferometry in conjunction with scattering models would suggest that greater success could be achieved through the consideration of forest models featuring accurate descriptions of scaling, number densities, and architecture. Although the scattering mechanisms associated with the phase centres are known, it is just as important to understand what macroecological factors determine their location within a forest canopy. Of particular importance is the scattering centre associated with the height of the canopy used to indirectly infer biomass through allometry in interferometric studies.

1.4 The Role of Allometry

The word allometry comes from the Greek word, *allos* meaning other, and *metron* meaning measure. Allometry is the comparative measurement of the growth and the size of parts of an organism's body in relation either to other parts of the same organism's body, or to the same body part in a conspecific or another species. Allometry forms a large part of this thesis through the SERA and WBE models with one or the other used in each experimental chapter of this thesis.

Allometric growth represents differential rates of growth of two measurable traits of a living organism and are typically related by power laws:

$$Y=Y_0M^b \tag{1.1}$$

with Y, describing the magnitude of the organ; M, the body size; b, growth ratio; and Y_0, a constant with a biological meaning. Similarly the power law could be expressed as the logarithmic equation:

$$\log Y = b \log M + \log Y0 \tag{1.2}$$

When 'b' is less than 1 there is a negative allometry which means that as M increases, Y increases at a reduced rate. When b is more than 1 there is a positive allometry

which indicates that as M increases, Y does so also but at an increased rate. If b is equal to 1 there is isometric growth indicating no change in shape. An isometrically scaling organism would experience all volume-based properties changing with mass to the first power, all surface area-based properties would change with mass to the 2/3 power, and all length-based properties would change with mass to the 1/3 power.

Variations of allometry exist. Interspecific allometry is concerned with the comparison of the traits of same aged individuals of different species. Intraspecific allometry is concerned with the comparison of the traits of individuals of all ages within a species (Ontogenetic allometry), or the comparison of individuals of the same age within a species (Static allometry). Human adults tend to have the same proportions; around the value of $b = 1$ but as much as 2.5 (Burton 2010) while another example of allometry in humans is Kleiber's Law (Smil 2000) which describes the relationship between metabolic rate and body mass. Plant specific allometry is of primary relevance here. The partitioning of total body biomass among leaves, stems, and roots; the annual growth rates for new leaf, stem and root tissues, and the biomass annually invested in reproductive effort at the level of the individual plants are three instances of allometry in plant biology. These allometric cases are featured in (Niklas and Enquist 2001) where plant allometry is explored in terms of the relevance of the scaling of annual growth as the ¾ power of body mass, and that annual growth remains proportional to the capacity of the individual to intercept sunlight.

1.4.1 How are allometric equations created?

Allometric equations in forestry rely on empirical information to determine relationships that exist between forest structures. To conduct the empirical studies it is often the case that destructive sampling is required. All tree parameters are measured including the mass and dry mass of the tree. Other useful parameters are diameter at breast height and height of tree. Although it is a necessity to conduct

destructive sampling to determine mass measurements the other external parameters can be measured more easily. Field measurements using non destructive methods are more environmentally friendly as well as more efficient measurement techniques in terms of time and money. Height remains the most difficult parameter to accurately measure and as such many allometric equations are created with only DBH used to determine biomass.

Allometric equations can vary even within a single species as shown by (Zianis and Mencuccini 2004). It has been shown to vary within a species as a matter of age (Hammond and Niklas 2009) which creates problems with regards to consistency. It is important then that the sampling involves only trees greater than a particular size for a single equation; often indicated by stems with DBH > 10cm. The general result being that allometric equations are most suited to mature trees. Allometry has been used as a powerful tool to complement forest remote sensing for several years. Studies that have involved the collaboration of allometry and remote sensing have been used to investigate parameters such as biomass through LAI (White et al. 1997), height (Mette et al. 2004b), and canopy coverage (Lefsky et al. 2002).

The role allometry plays in the forest remote sensing process, is to convert the remotely sensed data into useful information regarding the forest. In order to do this there must be some measurable aspect of the data that shows a correlation with a forest parameter. For example, canopy coverage detected using photogrammetry, LiDAR or SAR have all been shown to possess a correlation with biomass (Suganuma et al. 2006). Each technique can be used to establish an estimate of a further parameter using allometric equations.

1.4.2 Allometry and SAR Remote Sensing in the Literature

While improvements to the techniques involving polarisation and interferometry continue to be made, an uninterrupted direct correlation with biomass remains elusive due to saturation. If this parameter were to be inferred using measurements from polarimetry and interferometry studies then a further calculation using a relationship between the retrieved height and the required biomass measurement would need to be introduced such as in (Mette et al. 2002) and introduced in a previous section, where a method for biomass estimation through forest height using a particular allometric relationship and polarimetric SAR interferometry data is proposed. Developments of this method were shown in (Mette et al. 2004b) where they further considered the relationship to biomass of other important forest parameters and not just height. Figure 1.1 is taken from this work and shows a consideration of the accuracy of the allometric links of forest parameters with forest biomass. A modified allometric relationship that compensated for typical overestimation existing from forestry table estimates was proposed. With basal area and canopy height believed to be correlated, the biomass was shown in theory to be defined using just canopy height. The relationship between biomass and height is immediately obvious across species in comparison with the relationships between biomass and other selected forest parameters.

In Figure 1.2 my own study of the yield table information from British forests from 1946 are shown including individual yield classes. The different trajectories are apparent and similarly to the work of (Mette et al. 2004b) the effects of different yield classes can be seen. The correlation of height with biomass is here represented by assuming its proportionality to volume, with the relationship again more obvious than that exhibited by parameters such as age. Specific wood density information was not available within the yield tables to allow biomass conversion.

Biomass underestimation and overestimation is a known occurrence in radar studies due to inaccurate height estimates (Kugler et al. 2006; Mette et al. 2004b; Wallington and Woodhouse 2006; Woodhouse et al. 2006) possibly resulting from a misunderstood relationship between the location of the canopy scattering centre and the height of the forest. Understanding what height this scattering centre refers to is key to a better understanding with the relationships of stand heights as analysed in (Guo et al. 2008), and (Mette et al. 2004a).

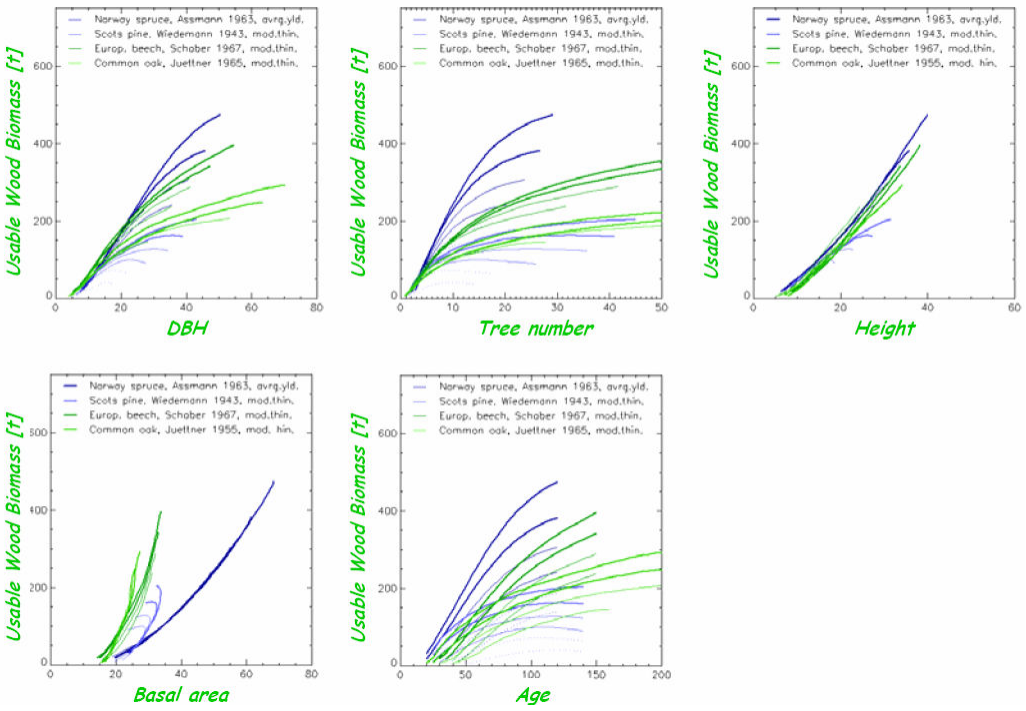

Figure 1.1. Forest biomass allometry from yield tables of temperate forest species. Each plot represents four species, represented by different colours, and representing different yield classes. Taken from (Mette et al. 2004b).

To allometrically relate biomass to forest parameters, alternatives to height have been used. (Treuhaft et al. 2003) indirectly used leaf area index to normalise relative density profiles retrieved from SAR interferometry and producing leaf area density values which identified agreements between field and remotely sensed biomass, while DBH in (Ranson and Sun 1994a) was used to validate SAR biomass estimates

through the use of allometric equations developed by (Young et al. 1980). Relatively simple empirical or semi-empirical models have also been shown to describe the average behaviour of radar interferometric coherence as a function of forest stem volume which can then be used to infer biomass (Askne et al. 1997; Fransson et al. 2001). The best interferograms in (Fransson et al. 2001) show a linear relationship between stem volume and coherence with a RMSE of approximately 20% of the average stand stem volume density.

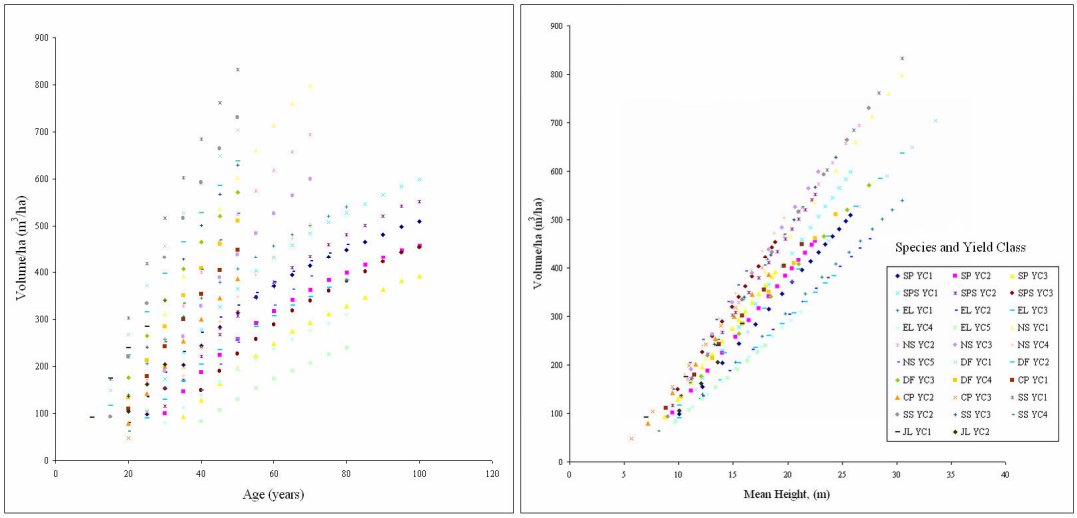

Figure 1.2. 1946 British yield table data showing the correlation with volume density of two independent variables, height (left) and age (right). Colours represent 8 different species and their different yield classes. SP= Scots Pine, CP=Corsican Pine, NW=Norway Spruce, DF=Douglas Fir.

1.4.3 Consideration of Biological Realism and Scattering Processes

As has been outlined, SAR has the ability to directly and indirectly measure the biomass of forests. One particular problem with many models used in collaboration with remote sensing has been that they do not include a true forest representation based on biological processes or allometric scaling. In addition, advanced techniques are continually associated with inaccuracies regarding remotely sensed height estimations.

Technological and theoretical advances have continued to provide new methods such as InSAR (Balzter 2001), PolInSAR (Cloude and Corr 2003) and coherence tomography (Cloude 2006) but the limitations these processes face with regards to their dependence on allometry and correct identification of scattering phase centres would suggest that consideration of biological realism and a more thorough understanding of the scattering processes is a requirement for future developments. The aim of producing and incorporating a more realistic representation of branching processes into forest remote sensing studies using the rules of allometry would be a suitable course of action. The biological aspect of forest modelling using SAR should make a significant contribution to an accurate model with many factors from number density to size distribution of the forest constituents needing to be taken into account to achieve a greater accuracy than presently possible. It may not be the case that more parameters must be modelled to achieve a greater accuracy but rather that more accuracy is required in the choice of the modelled parameters.

Work such as (Woodhouse and Hoekman 2000) has attempted to consider the structure of the forest in terms of branching but the weak point of this model like many others has been the unrealistic description of the spatial distribution of the canopy scatterers within the backscatter model which remains technically unrelated to actual biological processes. Like other methods an overall underestimation of forest height and biomass is often the result. (Richards et al. 1987) produced two figures in their work on L-Band forest modelling showing how simulated backscatter as a function of tree height and tree area density comprise different forest component contributions. The figures show that the trunk is the most significant contributor at L-Band for an incidence angle of 30 degrees. As the heights of simulated trees increase from 10m it was shown that the double bounce contribution of the trunk increases while at the same time the ground and forward scattering effects drop. Volume scattering was shown to increase with size but not proportionally to the increase in trunk scattering. These figures are shown below with 1.3 (a) showing a representation

of the notion of "saturation" with the contributions of all components seen separately to tail off at heights around 30m. These figures show how the contributions to the backscatter with and without the trunk contribution are significant, with the volume contribution dominating only if the trunk scattering is discounted. Accurately representing the stem component of forests is the most significant biomass contributor to a forest and at long wavelengths the greatest contributor to backscatter levels. The crucial consideration here is that the backscatter from stems must be accurately represented to interpret forest backscatter accurately.

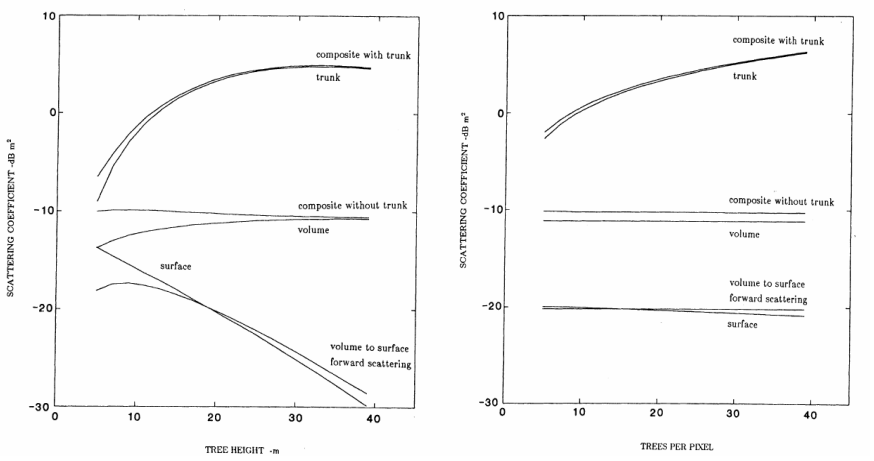

(a) (b)

Figure 1.3. Simulated forest backscatter from forest components (a) as a function of tree height, at an incidence angle of 30 degrees and for 20 trees. (b) as a function of stand density, at an incidence angle of 30 degrees and for a tree height of 20m. All data L-Band and HH polarisation. Taken from (Richards et al. 1987).

If the scattering processes can be more thoroughly understood then the only further improvement that can be made to the process of forest biomass estimation would concern the forest model.

2 RADAR Scattering Principles

In radar measurements the quantity measured is the radar cross section for an isolated target or scattering coefficient for an area extensive target. To measure the radar cross section the size of the target must be smaller than the coverage of the radar beam, and the reverse is true for measuring the scattering coefficient. The radar cross-section has units of m² and if all incident radar energy on the target is reflected equally in all directions, then the radar cross section would equal the target's cross-sectional area. This represents an ideal case as inevitably some energy is absorbed while the reflected energy is not distributed equally in all directions. Because of the reality of the situation radar cross-section is difficult to estimate.

An object can scatter an incident wave in all possible directions with varying strength. This scattering pattern should vary with the incident direction. For the radar cross section of an object the common reference is an idealised isotropic scatterer. The radar cross section of an object observed in a given direction is the cross section of an equivalent isotropic scatterer that generates the same scattered power density as the object in the observed direction. The radar cross section of an object is the ratio of the total power scattered by an equivalent isotropic scatterer to the incident power density on the object. The radar cross section can be written as below:

$$\sigma = 4\pi R^2 \frac{|P_d|^2}{|P_s|^2} = 4\pi R^2 \frac{|E^s|^2}{|E^i|^2} = 4\pi |S|^2 \tag{2.1}$$

Where P_d is the incident power density measured at the target and P_s is the scattered power density at a distance R. It can also be written in terms of the electric field intensities with E^{i} being the incident field and E^{s} the scattered field along the direction under consideration or using the scattering amplitude S.

A transmitter generates a wave of power density P_d which interacts with the target, given by:

$$P_d = \frac{P_t G_t}{4\pi R^2} \tag{2.2}$$

where G_t is the transmitter-antenna power gain, P_t is the transmitted power and R is the range to target. The target "intercepts" a certain fraction of this wave and re-radiates, generally in all directions with a complicated pattern of which only the direction returning to the receiver is important. It can be imagined that the object scatters equally in all directions, i.e. an isotropic scatterer. The scattered field at the receiver is then written as:

$$P_s = \frac{P_d \sigma}{4\pi R^2} \tag{2.3}$$

Where P_d σ is the total power that must be re-radiated by the target to produce the observed power density. The total received power is then $P_r = P_s A_r$ where A_r is the receiver-antenna aperture given by $\lambda^2 G_r / (4\pi)$ with G_r the transmitter-antenna power gain. Combining equations (2.2) and (2.3) to give a new form of P_s then gives the radar equation for a two way monostatic system. Representing the returned power in radar backscattering measurements of an isolated target of cross section σ:

$$P_r = \frac{P_t G_r G_t \sigma \lambda^2}{(4\pi)^3 R^4} \tag{2.4}$$

In equation (2.4) only the radar cross section is related to the properties of the target. The radar equations defined above cover the scenario of point targets but are not formulated for area extensive targets and do not include polarisation effects. For area extensive targets such as forests where the target is larger than the incident beam the scattering coefficient is written as σ^0, the radar cross section per unit area or normalised radar cross section. A dimensionless quantity. The total averaged power for an area extensive target is the integral over the illuminated area, A_0, with ds representing the differential area occupied by each target.

$$P_{\mathrm{r}} = \iint_{A_0} \frac{\left(P_{\mathrm{t}} G_{\mathrm{r}} G_{\mathrm{t}} \sigma^0 \lambda^2\right)}{(4\pi)^3 R_{\mathrm{r}}^2 R_{\mathrm{t}}^2} ds \tag{2.5}$$

The new term of normalised radar cross section is shown as the radar cross section divided by the illuminated area, A_0, and is given in terms of the scattered and incident fields in equation (2.6).

$$\sigma^0 = \frac{\sigma}{A_0} = \frac{4\pi R^2 \dfrac{|E^s|^2}{|E^i|^2}}{A_0} \tag{2.6}$$

To incorporate polarisation effects into the radar equations consideration must be given to the electric fields and their corresponding powers. These are the quantities directly dependent on polarisation. The general form is to consider the subscript *p* as denoting the incident polarisation and *q* as the scattered polarisation with either being horizontal or vertical. The radar equation can then be written as (2.7):

$$P_q = \iint_{\mathrm{A}_0} \frac{\left(P_p G_r G_t \sigma_{qp} \lambda^2\right)}{(4\pi)^3 R_r^2 R_t^2} ds \tag{2.7}$$

The scattered power considered by the radar equation does not account for both amplitude and phase. When measurements of the scattering field are taken at large distances from the scatterer the scattered waves can be considered spherical due to the oscillations occurring perpendicular to the propagation direction. The scattered intensity and the incident intensity of a plane wave illuminating a rough surface area can be described using the vertically and horizontally polarised scattered field components. The scattered field *E*, at a range *R* from the scatterer can then be represented as:

$$\begin{bmatrix} E_p^s \\ E_q^s \end{bmatrix} = \frac{e^{-ikR}}{R} \begin{bmatrix} S_{pp} & S_{pq} \\ S_{qp} & S_{qq} \end{bmatrix} \begin{bmatrix} E_p^i \\ E_q^i \end{bmatrix} \tag{2.8}$$

Equation (2.8) shows that the amplitude, phase and polarisation of E_s are modified with respect to E_i with the scattering matrix containing information on the nature and characteristics of the observed media. The scattering matrix is then related to the radar cross section through equation (2.9):

$$\sigma_{pq} = 4\pi R^2 \frac{|E_s|^2}{|E_i|^2} = 4\pi |S_{pq}|^2 \tag{2.9}$$

2.1 Vegetation Scattering

The backscatter from vegetation canopies can be determined using six factors (Bindlish and Barros 2001):

1. The dielectric properties of the vegetation material.
2. Size distribution of canopy scatterers.
3. Shape distribution of canopy scatterers.
4. Orientation distribution of canopy scatterers.
5. Canopy cover geometry.
6. The roughness and dielectric constant of underlying soil surface.

Vegetation scattering can typically be described as scattering occurring from a volume of discrete plant components such as leaves, branches and stems. The radar waves that interact with vegetation components of approximately the same size as the wavelength produce the strongest scattering. Shorter wavelengths are therefore recommended for the investigation of smaller tree components and longer wavelengths for the investigation of trunks and larger branches. The Microwave spectrum spans a similar order of wavelengths as the branch sizes expected within a forest with typical frequencies of P-Band and X-Band representing 0.7m and 0.03m respectively. Energy that penetrates the canopy will also produce direct and indirect surface scattering from the ground through double bounce and other multiples of scattering.

In the study of vegetation scattering problems, several approaches have been used. One method is to expand the wave integral equation in the form of a Born Series. Although a rigorous approach, it is most practical for dealing with low permittivity contrast media (Hill 1988). One way around the limitation of this wave theory is to apply the strong fluctuation theory and Distorted Born Approximation. This involves complicated mathematical manipulation and is impractical to extend to high order scattering effects as featured in the work of this thesis. This method is used for a two layer canopy case in (Saatchi and McDonald 1997) while in (Chauhan et al. 1991) for a simple one layer case. In contrast, solutions to radiative transfer theory are easier to carry out and can be extended to higher scattering orders.

2.1.1 Radiative Transfer Theory

Radiative transfer theory refers to the propagation of energy by radiative processes. Radiative transfer is complicated due to the interaction of energy with matter within the medium through which energy propagates. Through these interactions the original energy is exchanged as a result of collisions with particles within the medium. It is therefore a direct study of energy transport, including absorption, emission, and radiation effects.

When radiative transfer theory is used to describe energy passing through a vacuum it is conveniently known that the medium will be constant and energy will not suffer from extinction. As soon as atmosphere is encountered extinction becomes an issue and complications arise. For a forest scenario these complications are increased. If we assume the medium to be filled with some material with a known extinction coefficient α, with units 1/cm the equation of radiative transfer can be written as:

$$\frac{dI}{ds} = -\alpha I \tag{2.10}$$

Where I represents intensity and s the path length with d representing the derivative. If the variables are changed to represent optical depth τ, where $d\tau = \alpha\, ds$, we obtain

$$\frac{d\,I}{d\tau} = -\,I \tag{2.11}$$

Which has a solution of:

$$I = I(0)\, e^{-\tau} \tag{2.12}$$

As matter not only attenuates radiation but also emits radiation an emissivity coefficient j must be added:

$$\frac{dI}{ds} = j - \alpha I \tag{2.13}$$

Changing variables again with $d\tau = \alpha\, ds$ we get

$$\frac{d\,I}{d\tau} = \frac{j}{\alpha} - I \tag{2.14}$$

The ratio given by j/α represents the source function in radiative transfer denoted by S which along a ray through a medium gives:

$$\frac{d\,I}{d\tau} = S - I \tag{2.15}$$

If the source function is equal for both depth and path length, so that $S(s)=S(\tau)$ then the solution of the equation is:

$$I = I(0)\, e^{-\tau} + S(1 - e^{-\tau}) \tag{2.16}$$

This shows that in a medium with a sufficiently large optical depth τ the original input intensity (before the ray entered the medium) $I(0)$ is gradually replaced with the intensity $I = S$ inside the medium. This is the derivation of the formal radiative transfer equation and can be solved along each ray through the medium. The complications with radiative transfer lie in the fact that the source function is often

unknown in advance and depends on the outcome of the equation itself (Rybicki and Lightman 1979). For the forest case this is a complex scenario of absorption and emission.

The equations governing Radiative Transfer (equations 2.10-2.16) have attenuation effects inbuilt inherently. Through the inclusion of an extinction coefficient a proportional loss of energy, equivalent to an exponential decay in power, is exhibited as incident waves travel through a homogeneous medium. This represents the energy loss that can occur even through a medium consisting of only air particles. For a wave transmitting through a forest canopy the extinction rate will be increased due to the greater attenuating factor of branches, particularly of those of similar size to the microwave lengths used in radar studies. Removing the branches from such a scenario would result in an extinction reduction meaning attenuation would predominantly result from the inherent energy decay associated with energy propagation through a medium. As the loss of energy through extinction is an inherent property of radiative transfer, where radiative transfer is used to model energy propagation through layers the attenuation is always a factor. Within RT2, the radiative transfer model used here, the extinction and phase matrices calculated using radiative transfer determine how much energy is reflected back to the receiver and how much is transmitted through to the next layer. All the scatterers within a layer of RT2 are exposed to the same power. This means that within the single layer case the inherent radiative transfer attenuation will not figure. The absence of attenuation discussed as a result of canopy removal in this thesis (Chapters 7 and 8) refers to the significant contribution of the canopy scatterers as a consequence of increasing number density within each layer of the canopy. In their absence attenuation is greatly reduced. Radiative transfer theory does not consider the effects of diffraction and interference with regards to the particle interactions and assumes no correlation between fields as by its nature the radiative transfer equation ignores coherent effects (Battaglia et al. 2010). It does however account for each scatterer through the addition of backscatter power incoherently (Saatchi and McDonald 1997).

Radiative transfer models can treat single homogeneous layers analytically and can be extended to include multi-scattering effects. For multi layered, multi scattering scenarios the solution becomes complex due to inter layer interactions that occur and can require an iterative approach to solve (Liang and Jin 2003). Using multi-layered models is particularly appropriate in forest modelling.

According to (Saatchi and McDonald 1997) the validity limits for both Radiative Transfer theory and the Distorted Born Approximation, for use with forest backscatter models, are as follows. The individual scatterers in the medium must be located in the far zone of each other. If the source has a maximum overall dimension D that is large compared to the wavelength, the far-field region is commonly taken to exist at ranges $> 2D^2/\lambda$ from the source, and therefore the coherent effect between scatterers is small. The coherent effect due to scattering between individual scatterers and the reflective boundary must also be small. The same approximations for solving the multiple scattering problems are applied for both scattering solutions. For radiative transfer theory this is through the small extinction length and for the Distorted Born Approximation through the mean field approximation. Both methods also predict the same number of scattering mechanisms in the backscattering coefficients as well as identical results for the mean backscattering cross section when the volume scattering from randomly positioned scatterers is considered (Smith 2000).

The main differences between the two approaches are based on the presence of coherent scattering in the Distorted Born Approximation, specifically in the terms representing volume surface interactions. A particular example highlighting this difference is when a reflective ground surface is considered, with the scattering from the volume surface constructively interfering with the inverse wave. The coherent addition then results in a doubling of the backscatter in the Distorted Born Approximation but not for the Radiative Transfer solution.

In this work Radiative transfer theory is used to model forest interactions. The use of RT2 (Balzter et al. 2003b; Cookmartin et al. 2000; Knight 1997; Saich 1995; Saich et al. 1995), used for both crops and forests, allows a multi-layered description of the subject area and is ideal for use with the models used in this thesis, see Chapter 3. RT2 is a second-order solution to the vector radiative transfer equations as outlined in (Tsang et al. 1985). The formulation for the vegetation components in RT2 is sufficiently general to allow determination of the microwave backscatter from either forest stands or agricultural crops (Cookmartin et al. 1998). The RT2 model does not provide locations of scatterers within the defined layers but instead produces backscatter values using code to calculate the backscatter of individual components (Cookmartin et al. 1998) rather than through ray tracing techniques. As a result of this it is assumed that no two scatterers can occupy the same space as would potentially be the case for ray tracing models which require more specific location details. The dielectric properties of each component are calculated from its gravimetric water content using the empirical dual-dispersion model of (Ulaby and El-Rayes 1987). The soil dielectric properties are derived from its volumetric water content using the empirical model of (Hallikainen et al. 1985), in each case both of these are assumed constant while forward scatter from the soil surface is calculated using specular coefficients alone. Further discussion is provided in Chapter 3.4.

2.2 Forest Scattering Mechanisms

When considering forest scattering, single and multiple scattering events occur. The single scattering terms result from surface scattering from the ground, scattering from the trunk, and scattering from the canopy. The normalised radar cross section of the single scattering events can be deemed a summation of the separate contributions (Le Toan et al. 1992). The double scattering events associated with layer-ground interactions are a consequence of scattering from canopy to ground, trunk to ground, and multi scattering events occurring within the canopy. Each of these scattering events can occur in the reverse situation giving six double scattering mechanisms.

Similarly to the single scattering contributions the double bounce scattering contributions can be coherently summed to include the forward and reverse instances of each scattering mechanism. An overview is shown in Figure.2.1. In this thesis the different forest models incorporated provide different forest formations as described in the next chapter. The difference in these formations are such that different scattering mechanisms will be more dominant with each model. Using a scattering model that can account for as many of these mechanisms as possible is a requirement for this study.

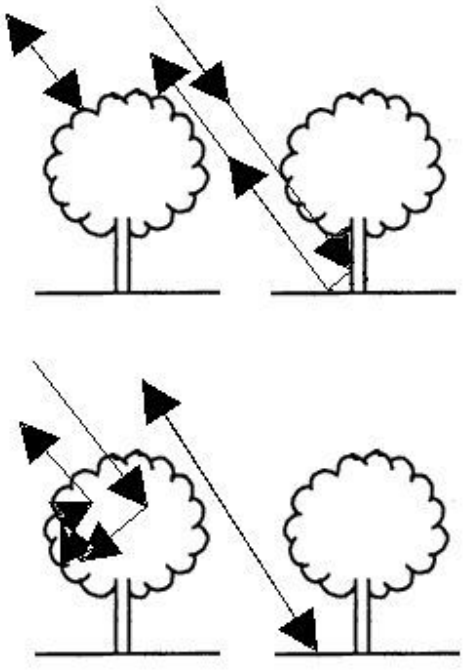

Figure 2.1. Dominant forest scattering mechanisms. Clockwise from top left: volume scattering from canopy, layer ground scattering, intra layer volume scattering, surface scattering from the ground.

2.2.1 Influence of Shape

Forest scattering is variable between species and locations due to the natural variations in shape and structure. No trees are identical but many can resemble one another's characteristics. Knowing that many trees are made up of the same constituent factors, forest modelling can be approached assuming a generic structure

to represent branching elements. In modelling exercises branches are typically represented by cylinders (Woodhouse and Hoekman 2000), while leaves can be represented as discs (Ferrazzoli and Guerriero 1995) or needle like shapes (Eom and Fung 1986) dependent on whether coniferous or deciduous forests are modelled. Some studies also consider the canopy to consist of a collection of spherical scatterers (Attema and Ulaby 1978; Bindlish and Barros 2001; Nghiem et al. 1993). Other descriptions are possible but these are deemed the simplest forms. The shapes for modelling are chosen due to their ability to closely resemble the scattering behaviour exhibited by the forest as well as to mimic the structural and physical appearance. In both instances a consideration of naturally occurring forest shapes is desired to enable the shapes used within the modelling to best represent those of the canopy while not overcomplicating the scattering scenario. Although this aspect does not improve the realisation of a forest it enables the model to operate effectively without creating excessively complex calculations particularly if the aim is to identify specific backscatter trends.

2.2.1.1 Cylindrical Scatterers

For microwave remote sensing of forests the constituent scatterers can range from sizes smaller to larger than the incident wavelength. This particular problem of size to wavelength ratio was addressed by (Mie 1908) and (Debye 1909). Their theory had the ability to model the scattering around a sphere of any size in comparison to the wavelength. Due to the smaller size of the wavelength in comparison to the scattering particle many dipole moments were induced which could be managed individually. This was laid out by Rayleigh in his original proposition through the solving of Maxwell's equations in the far field and then by predicting the amplitude of the secondary electric field, as a consequence of many dipoles, for all scattering angles.

The interaction of electromagnetic waves with spherical scatterers were considered in (Tsang and Kong 1977) who solved the radiative transfer equations using a Mie

scattering phase function and have since been used to model vegetation such as in (Attema and Ulaby 1978).

In this thesis the scattering simulations are limited to cylindrical shapes. The first presentation of an exact solution for the scattering of a plane wave from an infinite circular cylinder was published in (Wait 1955). This solution has been thoroughly used appearing in literature such as (Richmond 1965), (Marin 1982), and adapted for the finite case in (Bansal et al. 1982), (Karam and Fung 1988), (Seker and Schneider 1988), (Sarabandi and Senior 1990), (Lang et al. 1994) and (Stiles and Sarabandi 1996). The Rayleigh approximation can be applied to thin cylinders whose radius is much smaller than the wavelength.

A study of particular interest concerning scatterer shape is (Karam and Fung 1988) in which the field solution proposed in (Wait 1955) is adapted to show the scattering from an arbitrarily oriented finite length cylinder. A scattering model is presented which represents defoliated vegetation as a collection of randomly oriented dielectric cylinders of finite length. For consideration with vegetation this study uses the finite case incorporating cylinder dimensions similar to the wavelengths of microwaves. To use a finite length cylinder within a scattering scenario requires an assumption that the internal fields induced are the same as those of a similar cylinder of infinite length with constant dielectric properties.

2.2.2 Influence of Composition

2.2.2.1 Dielectric Properties

Dielectric properties of forest scatterers must be adequately modelled due to their relative backscatter influence (Shao et al. 2003). The relative dielectric permittivity measures the degree to which a medium resists the flow of electric charge divided by the degree to which free space resists such charge. The degree is defined as the ratio

of the electric displacement to the electric field strength. The dielectric constant can be written as the complex number:

$$\varepsilon = \varepsilon' - i\varepsilon'' \tag{2.17}$$

where ε''is the imaginary part of the permittivity, which is related to the dissipation of energy within the medium and ε' represents the real part related to the stored energy within the medium.

The greater the relative dielectric permittivity of a material, the slower the radar energy will move through it and as such can be seen as a measurement of the ability of radar energy to be transmitted to depth. In GPR studies this parameter is used to measure velocities of propagating radar energy through different media with the relative dielectric permittivities of materials varying from one to another. The greatest factor affecting the dielectric constant is the moisture content level and the distribution of this throughout the material. The backscattering coefficient of radar will increase when incident on an increasing dielectric constant (Fung 1994).

With regards to forest remote sensing the dielectric constant can vary from species to species and both temporally and spatially. (Salas et al. 1994) show that the dielectric constants of forests are strongly correlated with the water content of trunks and that apparent diurnal fluctuations of the dielectric constant result from the same temporal variations in the water potential of the area, results similarly reported in (Way et al. 1991) and (Weber and Ustin 1991). Any lag between water potential and dielectric variations are also reported to be partly influenced by the structure of the tree. The dielectric constant of vegetation is also influenced by water variations imposed by atmospheric conditions. Clouds limit the incident radiation on the earth's surface and so can change the surface or vegetation water content. The presence of cloud can then decrease or stop vegetation transpiration affecting the water potential, dielectric properties and therefore backscatter (Lillesand and Kiefer 1987). Water content has been shown to directly affect backscatter measurements in radar studies involving

soils, e.g. (Dobson and Ulaby 1986). In vegetation studies canopy moisture is also shown to have a distinct effect on backscatter measurements (McDonald et al. 1991). The influence of water on the dielectric constant of a tree is highly likely due to the large difference between the values of water, with a high dielectric constant (~ 80, (Davis and Annan 1989), and wood (2 to 5 at room temperature, (Laboratory. 1999). The existence of varying dielectric constants within a single tree, let alone within a forest, make the concept of dielectric properties a significant obstacle for radar forest modelling. This is avoided most often by assuming constant properties within all trees of a particular species within a medium as assumed throughout this thesis. Other methods adopted to mimic the dielectric properties have been to use an infinite medium regarded as a slab with homogeneous or fluctuating dielectric properties (Bush and Ulaby 1976); (Isaacs et al. 2002); (Tavakoli et al. 2002). If a species can be defined by a dielectric constant then there would be problems involved with the species variations presented in this thesis in which a constant term is used regardless. However, this assumption is not detrimental due to the attention here paid to trends rather than absolute values of backscatter which requires the assumption that a linear relationship exists between species. Typical values of relative dielectric permittivity (RDP) for some common materials are given below in Table 2.1.

Table 2.1. Material RDP values, (Davis and Annan 1989):

Material	RDP (F/m)
Air	1
Dry Sand	3-5
Ice	3-4
Granite	4-6
Concrete	6
Saturated Silt	10-40
Organic Rich Soil	12
Forested Land	12
Saturated Sand	20-30
Fresh Water	80
Sea Water	81-88

2.3 The Influence of Scattering Regimes

The interaction of microwaves with forest canopies is very complicated. If the interaction of each individual component of the canopy is considered then a solution to Maxwell's equations must be found. In addition if a twig is much smaller than the wavelength being used there is Rayleigh scattering, with backscatter proportional to the square of the volume, while if the twig is much smaller than the wavelength there is Optical scattering and the backscatter is proportional to the physical cross-section. The situation is further complicated by Mie scattering in the region between these scattering regimes (Woodhouse 2006a) and is considered as a significant component in modelling in Chapter 7.4.3. The assumptions applied to the modelling of backscatter in this thesis consider the limiting case of cylinders with circumferences smaller than one tenth of a wavelength, and those much larger than ten wavelengths on the other and are rather crudely referred to as the limits corresponding to “Rayleigh” and “Optical” scattering, respectively. At the transition between these two regimes lies the resonant behaviour of Mie scattering and throughout this thesis an approximation is made that assumes an “averaging”of this resonance due to the cumulative effect of stem size distribution. This is supported by empirical results in (Lopes et al. 1991), and (Mougin et al. 1993) and is assumed to take on the form of Optical scattering within this region as proposed by (Crispin Jr and Maffett 1965), see also Figure 2.2.

A major influence for the work of this thesis is the data shown in (Crispin Jr and Maffett 1965), Figure 2.2. In this diagram the results of Rayleigh theory and geometric optics are plotted to show the ratio of normalised radar cross section to the wavelength squared with respect to the value of the diameter of a sphere divided by the incident wavelength. Also plotted in this figure are the results from the exact EM theory. The exact solution is adequately represented by two linear equations representing Rayleigh scattering and Optical scattering respectively with the Optical

version representing an average of the EM theory. In a similar fashion to this figure the normalised radar cross section saturation over a forest with increasing volume can be assumed to consist of two parts. Linking the concept of this figure with an empirical example such as (Neeff et al. 2005), shown here in Figure 2.3, leads to an assumption that saturation effects seen in forest radar studies could be a consequence of structural changes. Particularly through the existence of larger stems and branching components as forest biomass density increases, forcing a dominant scattering regime change. Although the figure presented in Crispin and Maffett represents scattering within the resonance region where Mie scattering takes place it also serves to show that resonant scattering can be well approximated by geometric optics. In effect it suggests that radar scattering over a forest can be addressed by assuming that all scattering can be a product of Rayleigh or Optical scattering with Optical scattering independent of frequency and solely affected by the scatterer cross section. These assumptions are maintained throughout this thesis and are crucial to the findings of Chapters 5, 7 and 8 and overall.

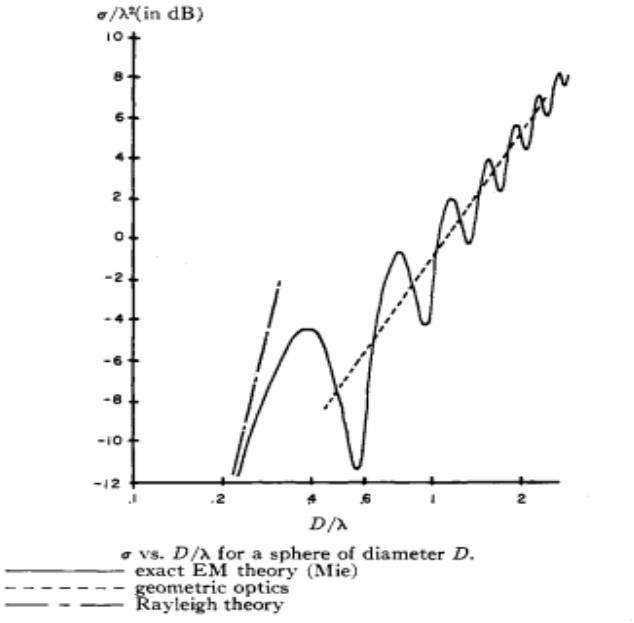

Figure 2.2. Example of EM theory backscatter including Mie scattering described by Rayleigh scattering and geometric optics alone for a sphere of diameter D. Taken from (Crispin Jr and Maffett 1965).

Within the resonance region it is known that two or more mechanisms may combine in and out of phase with one another to produce the undulating effect of radar cross section which defines the resonance region of Mie scattering (Knott et al. 2004). For a sphere the mechanisms are simply the specular reflection from the front of the sphere and the effect of the creeping wave that circles around the shadowed side, see Figure 2.4. If only the specular reflection is significant the radar cross section of the object is perfectly replicated by the physical cross section of the object (Skolnik 1970). The existence of this mechanism within the resonance region implies that a significant contribution is made by the optical description of radar cross section and in conjunction with the examples of (Crispin Jr and Maffett 1965) would provide justification for following optical theory within the resonance region for the purpose of this thesis. A representation of the different scattering regimes is given in Figure 2.4.

"With the exception of the few bodies for which exact solutions are available approximate methods appropriate in the resonance region are usually extensions of optics or Rayleigh techniques."

(Crispin Jr and Maffett 1965)

Rayleigh scattering takes place when the frequency of the incident radiation is "low" and consequently its wavelength "long" (Kleinman 1965) and is typically apparent when the scattering object is described by, $2\pi r << \lambda$. On a general scale the region in which this type of scattering occurs is the range where the wavenumber, k, for the scattering cross section can be expanded in a convergent series of positive integral powers of k, forming a Rayleigh series. It is also reasonable to assume that the Rayleigh region can be approximated by the first Rayleigh series term. The critical parameter in Rayleigh scattering is the volume of the scatterer and for spheres and spheroids the radar cross section is proportional to the wavenumber to the power of 4 multiplied by the volume to the power of 2 as shown in equation (2.18).

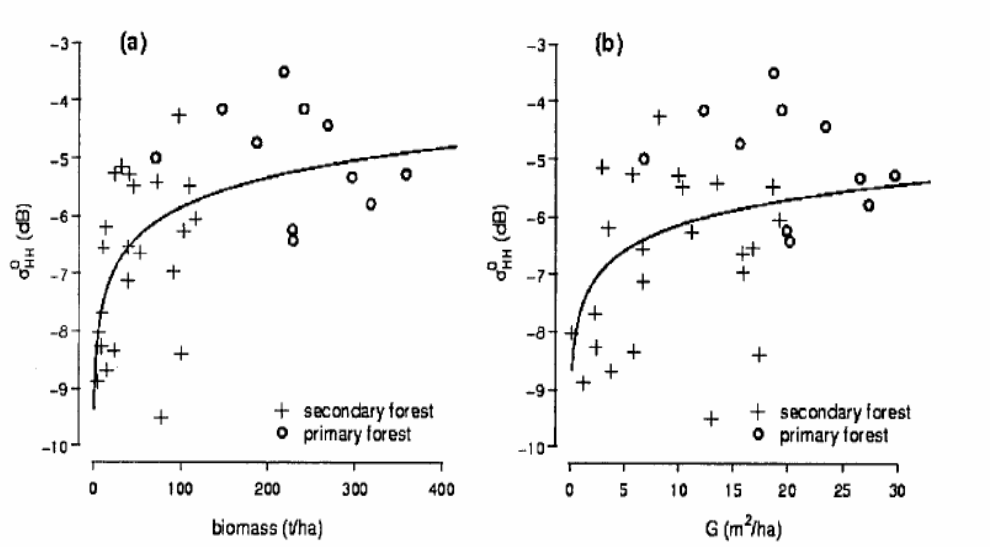

Figure 2.3. Backscatter saturation effect for forest biomass and total basal area. (a) Scatterplot of HH radar backscatter versus forest biomass. (b) Scatterplot of HH radar backscatter versus total basal area G. Points are distinguished by primary and secondary-growth forest, and logarithmic regression curves are displayed. Taken from (Neeff et al. 2005).

The formulation by (Smith and Ulander 2000) based on VHF backscatter from individual stems at polarisation *P*, is as follows for a single stem:

$$\sigma_{PP} = \frac{4k^4 \left| r_P(\theta) \right|^2}{\pi L^2} \left| \frac{(\varepsilon_r - 1)}{(\varepsilon_r + 1)} \right|^2 V^2 \tag{2.18}$$

where V is stem volume within the area, $r_p(\theta)$ is the Fresnel reflection coefficient of the surface with θ representing the incidence angle from normal, ε_r is the relative dielectric permittivity of the trunk, and L the attenuation. Due to the simplifications assumed in this thesis it is reasonable to assume that these parameters all remain constant within any particular run of a model aside from volume, with attenuation only varying within the work involving WBE branching architecture (Chapters 5 and 6). Reflection coefficients and permittivities remain constant as defined by the models used, while wavenumbers are dependent on frequency choices determined prior to simulations. As this equation represents the backscatter for VHF radar it is a representation of Rayleigh scattering, hence the dependence on volume squared.

Assuming that all backscatter will be Rayleigh scattered in the VHF band is a result of the transition from Mie to Optical scattering being defined by a sphere with a radius of approximately 9.54m when a 6m wavelength is incident. Dimensions such as this do not exist in a forest environment but if the Mie region is assumed to scatter optically then radii of approximately 0.095m are all that are required.

As the ratio of scatterer size to incident wavelength increases, or the wavelength reduces, Optical scattering occurs. Optical scattering can be described by either a physical optics or geometric optics description and is typically described by the relationship, $2\pi r >> \lambda$.

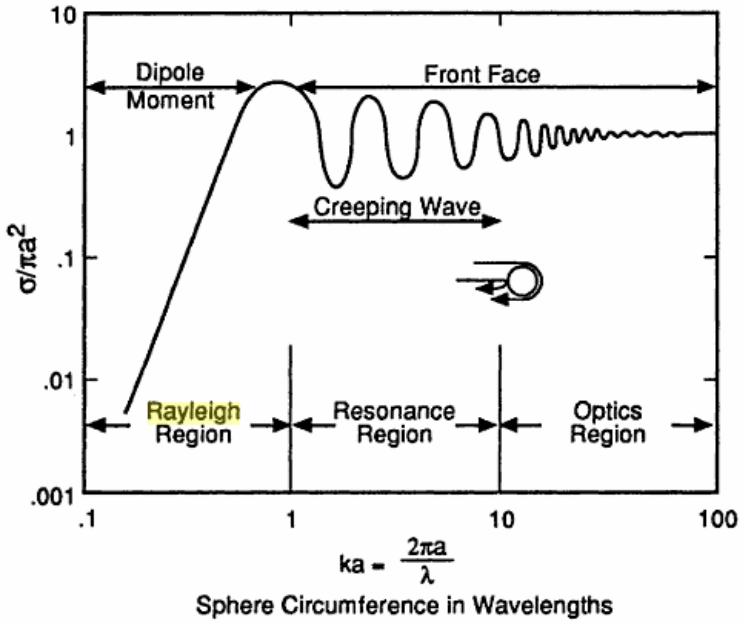

Figure 2.4. Radar cross section of a sphere as a ratio with physical cross section plotted against 2πr/λ. Figure represents the 3 regions of interest Rayleigh, Mie and Optical and their transitions as the sphere radius increases. Taken from (Knott et al. 2004).

For Optical scattering, the normalised radar cross section scales with the physical cross-section with N representing numerical value and A the physical cross section:

$$\sigma^{0}_{optical} \propto N\ A \tag{2.19}$$

This is in accordance with the laws of geometric optics which under certain limitations is an acceptable simplification of the scattering formula for the physical optics of a cylinder. The physical optics formula for the radar cross section of a cylinder is shown below where k is the wavenumber, r the cylinder radius, l the cylinder length and θ represents the incident angle from broadside:

$$\sigma_{cyl}^{0} = krl^2 \cos^2\theta \left[\frac{\sin(kl\sin\theta)}{kl\sin\theta} \right]^2 \tag{2.20}$$

By taking an average value over a symmetric window of incidence angles centred at $-\theta_w \leq 0 \leq \theta_w$ the average radar cross section of a cylinder becomes the integral:

$$\overline{\sigma_{cyl}^{0}} = \frac{1}{\theta_w} \int_0^{\theta_w} krl^2 \cos^2\theta \left[\frac{\sin(kl\sin\theta)}{kl\sin\theta} \right]^2 d\theta \tag{2.21}$$

As this window approaches zero the small angle approximations of $\cos\theta=1$ and $\sin\theta=0$ apply, and following a change of variable and subsequent integration we get the closed form formula for the average RCS of a cylinder around broadside, equation (2.22) (see also Hestilow 2000):

$$\overline{\sigma_{cyl}^{0}} = \frac{rl}{\theta_w} \left[Si(2kl\theta_w) - \frac{\sin^2(kl\theta_w)}{kl\theta_w} \right] \tag{2.22}$$

According to the rules of the sine integral function Si(x), as the argument (x) approaches zero, Si(x) will tend to x. Similarly by taking the limit of the angular window tending to zero we can rewrite equation (2.22) as below:

$$\overline{\sigma_{cyl}^{0}} = \lim_{\theta_w \to 0} \frac{rl}{\theta_w} \left[Si(2kl\theta_w) - \frac{\sin^2(kl\theta_w)}{kl\theta_w} \right] = \frac{rl}{\theta_w} \left[2kl\theta_w - kl\theta_w \right] = krl^2 \tag{2.23}$$

Where the window tends to zero and is approximately representative of the broadside angle the average radar cross section is proportional to the frequency and the cylinder volume. But in the limit of large arguments where $2kl\theta_w$ is large the function

Si(∞) tends to $\pi/2$, and is known as the Dirichlet integral. Under the limits of $kl\theta_w$ tending to infinity (equation (2.24)) we can write the equation for average radar cross section of a cylinder as in equation (2.25). This frequency invariant equation is then a function of the physical cross section of the cylinder in accordance with geometric optics. A full progression of the working is found in (Hestilow 2000).

$$\lim_{kl\theta_w \to \infty} \frac{\sin^2(kl\theta_w)}{kl\theta_w} \to 0 \tag{2.24}$$

$$\overline{\sigma^0_{cyl}} = \frac{\pi r l}{2\theta_w} \tag{2.25}$$

In the presence of a single scattering object Mie oscillations are expected, and it is assumed that the same behaviour, to some extent, is exhibited with a collection of identical stems. As such, these oscillations are not generally seen or noted in empirical data possibly due to the number of stems present and their size variability. When mono size stands are considered in this thesis, oscillations are visible in the radiative transfer derived data (see Figure 7.8) but when forests of various sized stems are considered there is a reduced oscillatory contribution.

2.4 Forestry applications of SAR

2.4.1 Synthetic Aperture Radar

Synthetic Aperture Radar (SAR) is an active microwave remote sensing tool with the antenna and receiver co-located. SAR is side looking and captures data from a parallel path to the trajectory of the carrying platform. How it differs from conventional radar is that the actual size of the aperture used does not correspond to the actual size of the image it can produce. The synthetic aperture is created by collecting data over a target area for a known period of time as the sensor traverses the location. As the sensor passes over it will record multiple datasets along this

traverse. These collected data are then formed into a single image using the principles of Doppler Shift (Raney 1971) to position multi frequency data in the correct location. As the platform moves towards a target the scattering frequencies received will increase; as it moves away they will reduce. With the technical specifications of the system known, particularly the transmission frequency, these data can be used to unravel data acquired over the footprint by the synthetic aperture. This technique allows much larger areas to be covered in a shorter time and allows the use of small aperture sensors, providing benefits such as payload reductions, and a decrease in the size of the system required to obtain equivalent data. SAR systems exist in multifrequency and polarisation varieties such as RADARSAT (C-Band and HH polarisation), JERS-1 (L-Band and HH polarisation), and the ASAR instrument aboard ENVISAT (C-Band and multi-polarisation) and are used for purposes including topography studies, ice monitoring, disaster prediction, and forest remote sensing. The geometry of a typical acquisition is shown in Figure. 2.5.

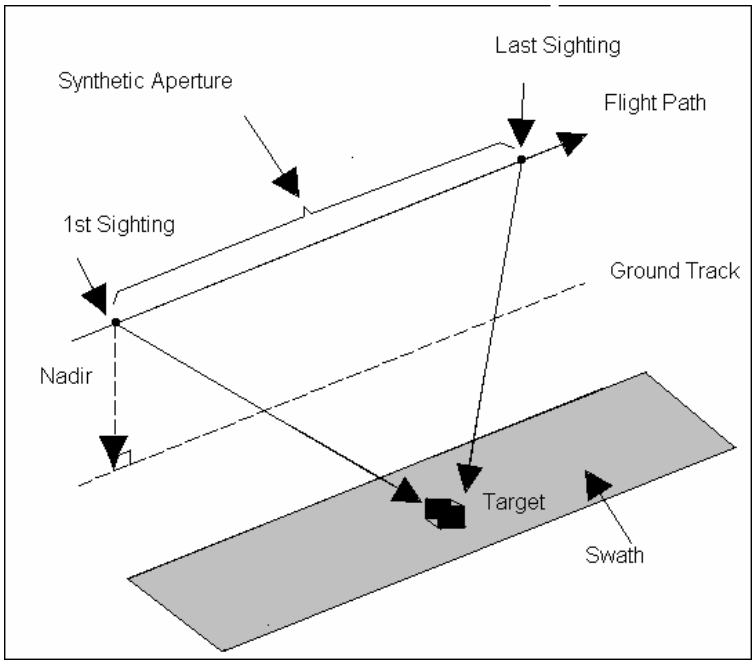

Figure 2.5. SAR acquisition geometry of system moving from centre left towards top right of figure.

2.4.2 How is SAR polarisation affected by forest scattering?

Radar wave polarisation determines the orientation of the electromagnetic field energy as it propagates through a medium, this includes waves after emission or during reception by the radar system. Within a forest environment the contribution of each individual scattering mechanism can be established through polarimetric analysis. SAR systems have the ability to transmit and receive bistatically at many frequencies and in polarisation configurations including co-polarisation, cross-polarisation and quadrature polarisation. The polarisations defining full quadrature polarisation are horizontal transmit and receive (HH), vertical transmit and receive (VV), horizontal transmit and vertical receive (HV), vertical transmit and horizontal receive (VH). If an object is a depolariser it will cause the original polarisation of the incident wave to be lost, this can refer to a change in orientation causing a horizontally transmitted polarisation to be scattered vertically. In radar terms this depolarisation can be detrimental or beneficial to a study dependent on the capability or system setup.

In (Fung 1966) it is proved that the absolute magnitude of the backscattered horizontal field component obtained by transmitting a vertically polarised field is the same as that of the backscattered vertical field component obtained by transmitting a horizontally polarised field in accordance with the reciprocity theorem in electromagnetic theory. A forest can behave as a depolariser due to the inhomogeneous nature of the medium described by the canopy. When electromagnetic waves are scattered a fraction of the energy can be lost from the original orientation of the wave. If this original orientation is horizontal, when scattered there may be components from all orientations, inevitably resulting in a vertical scattering component. Where forest canopy is used in the experimental work of Chapters 4 and 5 the cross polarisation state HV caused by depolarisation is used to take advantage of the sensitivity of this polarisation to random media. Depolarisation of electromagnetic waves occurs when vegetation is encountered due

to the induction of current in the foliage by the incident electromagnetic field. As the foliage is randomly oriented the resulting scattering is depolarised in comparison to the incident field (Swarup and Tewari 1979).

In the presence of vertical stems a vertically polarised electromagnetic wave will be depolarised to a greater extent than a horizontally polarised wave (Tewari et al. 1990). Similarly a horizontally polarised wave will be depolarised to a greater extent in the presence of horizontal branches. For these reasons polarisation can be a very useful aspect of radar scattering in a forest environment. This is especially so for determining volume scattering within the canopy layer which results in depolarisation and a large backscattering component orthogonal to the transmitted polarisation. A setup of HV or VH is particularly useful for determining canopy scattering with the random orientation of scatterers ensuring a large backscattering contribution orthogonal to the transmitted polarisation. The extra information that polarisation provides can be utilised to identify the contributions of different scattering mechanisms within the forest environment as in (Freeman and Durden 1998) who also hint at the potential importance of forest thinning on the resultant backscatter.

Cross-polarised data will provide strong information on canopy scattering, while a weaker response will be caused by surface scattering or double bounce even when the surface is rough enough to cause multiple reflections. Strong HH or VV contributions are a consequence of vertically of horizontally oriented scatterers with both polarisation states providing stronger returns than the weak HV response would produce for similar structures. Chapters 7 and 8 concentrate on the like-polarisations due to the sole presence of vertical scatterers. The polarisations chosen to display the data are chosen to best emphasise the data trends.

2.4.3 SAR Backscatter and Saturation Over Forests

SAR backscatter in the form of normalised radar cross section has been shown to be directly related to forest biomass (Le Toan et al. 1992). The problem lies in the fact that a saturation effect occurs at an apparent incident frequency dependent biomass level. This saturation level will occur at higher biomass as the SAR frequency is reduced and the wavelength increased. This observation suggests that saturation is possibly dependent on scatterer size. The saturation occurrence highlights the importance of understanding SAR backscatter saturation curves more definitively. It also shows how important it is that developments continue in the fields of polarimetry and interferometry in order to remove the inherent inaccuracies associated with biomass estimation and backscatter saturation.

Prior to the development of radar interferometry as a technique for modelling forest structure, remotely sensed biomass was mainly derived from the power of the microwave returns (Imhoff 1995a; Le Toan et al. 1992). Estimates of biomass and tree height using this technique were obtained from the backscattering coefficient; an example of this process is shown in (Ballester-Berman 2005; Bouman 1991) in the study of crops, and.(Dobson et al. 1992; Hussin et al. 1991; Imhoff 1995b; Le Toan et al. 1992) for forests. Difficulties in the application of this method were apparent when it came to larger scale biomass estimates with typical volume saturation occurring when biomass levels were of greater than approximately 150ton/ha at the lowest microwave frequencies, typically P (Imhoff 1995a), or less for L-Band (Dobson et al. 1992). Work regarding forest backscatter saturation is largely conducted using the explanation provided in (Dobson et al. 1995) with the cause said to be the relative opaqueness of the canopy to the frequency of incident wave. An example of the saturation effect is shown in Figure. 2.6.

(Imhoff 1995b) states that many studies show correlation between radar backscatter and forest parameters. These include height, age, basal area, and biomass. Imhoff

poses the question “How universal is the phenomenon of SAR backscatter saturation with respect to biomass?”. The work includes the use of heterogeneous and monospecies forests with the age of stands varied. Results showed that the polarimetric differences between these forest types supported reports of techniques using SAR to distinguish between coniferous and broadleaf forests (Imhoff 1995b). Figure. 2.6 highlights the nature of the saturation curve and how saturation varies for different structures under different polarisations.

The explanation of the saturation curve can usually be disseminated by stating that the forest becomes more opaque the thicker it is. For example (Martinez et al. 2000) attribute backscatter saturation to a higher number of scatterers. This explanation would suffice if a forest consisted of a series of continually homogeneous layers but, as nature shows, the general geometry of trees is to have few large elements at the bottom and more numerous small elements at the top. The idea of opaqueness as the sole cause appears less feasible when this is considered. The saturation curve is most dependent on frequency, and therefore the wavelength incident on the canopy. Within the microwave bands used for forest imagery different amounts of scattering from each regime will take place dependent on the frequency and the size of the scatterers which within a canopy could range from mm to m scales. It is therefore legitimate to hypothesise that the saturation curve is affected by the nature of the scattering within the canopy (see Chapter 2.3) and in particular its reliance on the dominant scattering level, within the vertical profile of the canopy.

The saturation curve is explored further in (Imhoff 1995a) by investigating the relationship between surface area and volume with regards to backscatter. A particular statement refers to an often recalled assumption about forest backscatter, “If SAR backscatter is solely responding to the total volume, therefore biomass, of vegetation in a stand, then structural differences are irrelevant”. Several works have contradicted this statement and shown structure to be particularly important including Imhoff himself (Beaudoin et al. 1994; Castel et al. 2002; Imhoff 1995b; Rignot et al.

1994; Woodhouse 2006b). The association (Martinez et al. 2000) make between backscatter saturation and the higher number of scatterers would be sufficient for an attenuation centred explanation. If attenuation were ignored it would no longer hold. In Martinez's work graphical displays of the backscatter coefficient with respect to distance above the ground are presented for like and cross polarised X-band microwaves with a distinctive feature being the peak response of backscatter coefficient, evident for each polarisation and seen higher in the canopy for older stands. This, as predicted by (Woodhouse 2006b) is possibly the result of scattering regime transition from Rayleigh to Optical. As Woodhouse predicts, for the ideal pipe model (Fransson et al. 2000b; Shinozaki et al. 1964), saturation occurs at lower biomass levels for older stands with reduced stem number density. Due to the additional growth vertically in the stem, the transition region moves away from the ground and particularly for the higher microwave frequencies the contribution from layers closer to the ground will contribute less to the total backscatter due to their increasing size with age.

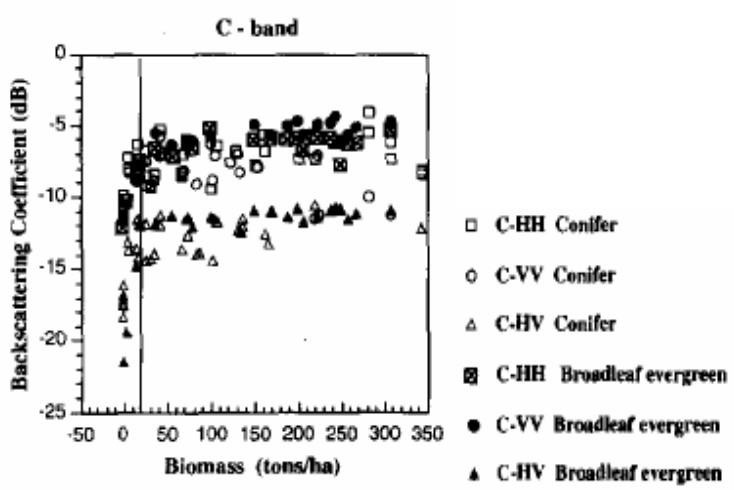

Figure 2.6. Calibrated SAR backscatter plotted against total above ground dry biomass for broadleaf evergreen forests in Hawaii and conifer stands in North Carolina and France at C-Band multiple polarisations. Taken from (Imhoff 1995a).

Saturation has not been proved in the literature to occur at all frequencies. When VHF band is used, the corresponding wavelengths are between approximately 3 and 15m. Branching elements will therefore have smaller diameter ratios to the size of the wavelength throughout and as a consequence the contribution to scattering will be dominated by the Rayleigh regime. The larger elements deeper in the canopy will be the dominant scatterers. This thesis approaches this scenario by suggesting that the macroecological conditions must fit particular criteria in order for saturation to be measured according to the nature of Rayleigh and Optical scattering.

In (Fransson et al. 2000b), in which relationships between VHF band backscatter and forest parameter relationships were investigated, no backscatter signal "saturation" was seen up to the maximum volume of the forest, this being a biomass level of 375 tons/ha. This is in stark contrast to the biomass saturation limits of P-band known to exist between 100-200 tons/ha. With the sensitivity to stems that VHF band possesses, it would appear that two possibilities exist for why saturation is avoided, either due to its lack of consideration of smaller branching elements and their attenuating effects, or possibly due to the structure of the forest reducing the impact of a scattering regime transition from Rayleigh to Optical and is a scenario that is explored in Chapters 7 and 8.

Observations of forest remote sensing using low frequencies only allow postulations as to the effect of Rayleigh and Optical scattering when regime change occurs. This is due to the lack of feasible comparison studies. With other frequencies much backscatter data are available and different levels of saturation have been assumed, (for comparison see (Patenaude et al. 2005)). As with all microwave frequencies it is assumed in this thesis that if the scatterers are allowed to grow large enough to scatter in a non Rayleigh manner then saturation is possible regardless of canopy density due to the relationships exhibited in Figure 2.4 in Chapter 2.3 . If saturation is not dependent on canopy opacity then a reduction in number density would not necessarily remove the possibility of saturation as shown in (Woodhouse 2006b).

Results such as this cast doubt on the typical saturation explanations with the work of this thesis aiming to further emphasise this doubt. When transition from Rayleigh scattering occurs, with the forest as a whole, the level of backscatter per unit volume increase is known to reduce greatly with this transition assumed from the increasing biomass of the forest. This is shown in backscatter to biomass curves as in Figure 2.6 for C Band where only very low volumes scatter in a Rayleigh manner. Other examples such as in (Santos et al. 2003) provide data exhibiting more gradual changes in the rate of backscatter per unit volume as is common with longer wavelength SAR data.

"It is important that we understand what effect stand-level canopy structure has on SAR backscatter. The lack of such knowledge has impeded an explanation, in real physical terms, of the mechanism by which SAR backscatter is positively correlated with biomass".

(Imhoff 1995b)

3 Modelling Methods

In this thesis all novel work relies upon modelling in some capacity. The models used consist of forest growth models, models of backscatter prediction and models of radiative transfer. Although the fact that this thesis relies primarily on modelled data limits the applicability of the findings to real world situations, the theories presented are tested thoroughly in the modelling environment. This allows the findings to be reported with sufficient confidence and results to be presented at a publishable level. Where possible all model results have been compared with empirical examples with appropriate reference in the text. This chapter provides descriptions and evidence for the appropriate use of each model featured in this thesis and the justifications for their use in particular situations.

3.1 The WBE Model

The WBE Model (West et al. 1997) is a model that serves to explain the origin of the ¾ power scaling rules displayed by living organisms across many functions. The working theory of WBE is that allometric scaling relations, including the ¾ power law for metabolic rates, are characteristic of all organisms. It describes how essential materials are transported through space-filling fractal networks of branching tubes. It also assumes that energy dissipated is minimised and that terminal tubes do not vary with body size. A more general description of the model is that it predicts structural and functional properties of plant vascular systems making it of particular interest to forest modelling. With its roots in a macroecological approach to explaining the origin of allometric scaling laws the WBE model was also modified to describe plants with branching architectures.

As shown in equation (1.1) it is stated how the dependence of a biological variable Y on body mass M is typically characterised by an allometric scaling law where b is the scaling exponent and Y_0 a constant that is characteristic of the organism. These

relations have been shown to reflect geometric constraints, indicating that *b* should be a simple multiple of 1/3 but according to the WBE model, and the work of (Peters and Wassenberg 1983) and (Niklas 1994), most biological phenomena scale as ¼ rather than 1/3 powers of body mass. As an example the cross-sectional areas of tree trunks scale to $M^{3/4}$. It is the purpose of the WBE model to offer an origin of these laws. The proposition is that a common mechanism underlies these laws and so the WBE model is presented as a quantitative model explaining the origin and ubiquity of quarter power scaling.

The model predicts essential features of transport systems based on three unifying principles. Firstly, for the network to supply the entire volume of the organism a space-filling fractal-like branching pattern is required, similar to that described by (Mandelbrot 1977). Secondly, the final branch of the network must be size invariant. Thirdly, the energy required to distribute resources is minimised; directly related to the minimisation of the system's total hydrodynamic resistance. The distribution system, for the most part, can be described as branching networks in which the sizes of tubes regularly decrease. In vascular plants this process is similar to the pipe model (Shinozaki et al. 1964) and is thought that biological species exhibit essentially the same scaling laws. It is this theory that is presented mathematically by WBE. According to (West et al. 1997) the ¾ power scaling law arises in the simple case of the classic rigid-pipe model, where branching is assumed to be area-preserving.

The WBE model attempts to understand the full allometric scaling of organisms, by formulating an integrated model for the entire system. The model provides a theoretical, mechanistic basis for understanding the central role of body size in all aspects of biology. Given the need to redesign the entire system whenever body size changes, small deviations from ¼ power scaling are thought to sometimes occur, as shown in (Peters and Wassenberg 1983). However, when body sizes vary over many orders of magnitude, these scaling laws are obeyed with remarkable precision.

The work of West, Brown and Enquist (Enquist et al. 1998a; Enquist and Niklas 2001; West et al. 1997, 1999b) are major influences for the work carried out for this thesis. Its biological basis and the mathematical arguments to reinforce the theories makes it an ideal starting point for developing methods for use in remote sensing collaboration. In these referenced works the key macroecological considerations for plant communities are discussed. From a forest macroecology point of view these works provide important information regarding the relevance of the use of the model in forest studies. In (Enquist et al. 1998a) the ¼ power scaling relationship was used to develop a further mechanistic model for describing the relationships between density and mass in resource-limited plants. The model implies that fundamental constraints on metabolic rate are reflected in the scaling of population density and other ecological and evolutionary phenomena, including the finding that resource allocation among species in ecosystems is independent of body size; a significant factor in affecting remote sensing measurements as discussed within the work of this thesis.

According to WBE, when the dry mass of the average plant in mature populations is plotted against the maximum plant density there is a distinct upper boundary traditionally characterised by a power law with an exponent of -3/2 (Yoda 1963). This thinning law has been shown to hold for plants in both single and mixed species stands and over a range magnitude orders. The fact that a plant fills a volume and covers an area has suggested a simple explanation for the -3/2 thinning law. WBE also addresses the relationships between maximal population density and average plant mass in ecological communities. The assumptions made are that sessile plants compete for spatially limited resources, their rate of resource use scales as $M^{3/4}$, and plants grow until they are limited by resources. So the maximum number of individuals that can be supported is related to the rate of resource supply and the average rate of individual resource use. At equilibrium in any given environment resource supply is constant so the maximum number of individuals supported is said to be proportional to $M^{-3/4}$.

The macroecological implications of WBE are significant in challenging widely held beliefs. WBE does not predict aspects such as the thinning trajectories of trees but it does predict that the rate of resource use per unit area varies among plant communities with differences in resource supply but essentially not as a result of plant size.

3.1.1 Application of WBE Model to Forest Remote Sensing

Despite some important limitations this model has some key advantages that make it an appropriate first-order linkage between simple backscatter modelling and models of biological function. In particular, it allows sufficient generalisation of plant structure so that it can be used with radiative transfer models that describe the interaction of microwaves with forest canopies such as RT2 (Anderson 2000; Attema and Ulaby 1978; Imhoff 1995b), see also Chapter 3.4. The important aspect of the WBE model is that it links plant branch structure to plant function and total standing biomass which is an important qualification for answering questions posed in this thesis. In (Enquist et al. 1998a), this same approach was employed to model the structure of plant populations and communities, resulting in a resource-based thinning law that predicts the scaling of populations. The methods involving the WBE model here were first used in (Woodhouse 2006b) with similar equations and justifications reproduced in the following section.

The WBE model is a generic scaling model that describes the relationship of the size and number densities of branch elements with the aim of explaining the origin of allometric scaling laws. General scaling principles are evident in tree architecture with branch sizes decreasing with branching generation, for instance, and as branch elements become smaller with increasing height into the canopy they become more numerous. This fractal-like nature of trees has already been utilized by some authors as input to a backscatter model using an L-system approach (Lin and Sarabandi

1999a, b). However the L-system model is a mathematical characterisation of particular trees and is not a general description of tree structure, whereas the WBE model is based on consideration of biological principles of resource distribution through a branching network and results in a space-filling rather than fractal network. The WBE model is not designed to describe the properties of any individual tree, or tree species, but describes "tree-like" branching resulting as a consequence of the underlying biophysical constraints of fluid flow and rigidity. In the current context, the fact that it is a generalised description of tree structure maintains a level of simplicity that is in keeping with the spirit of the Water Cloud Model (Attema and Ulaby 1978).

This thesis does not attempt to evaluate the validity, or otherwise, of this model but simply to use the allometric scalings it provides as a means of exploring the expected backscatter responses of "generalised" forests. The WBE model does not describe the size and shape of leaves directly, with the closest parameter being that of the leaf petiole radius. Due to the progression in growth by discrete steps the model is not well-suited for describing continual tree growth, but is designed to describe climax forests and those that are at, or near, equilibrium with regards to availability and use of resources. This relationship is expected to hold when all available space is occupied and the rate of resource use equals the rate of resource supply. The key impact of such assumptions, however, is on the resulting predictions about the biological processes, which remain debatable. In this study the impact of such assumptions are minimised by considering a range of empirical values of the key variables, rather than relying solely on those preferred by (West et al. 1997).

3.1.2 Allometric Predictions

Part of the contention of the WBE model stems from the original authors' claim that the special case of $a=1$ (describing the area-preserving "pipe model" (Shinozaki et al. 1964)) has unique significance, as a result the model has been known to make global

generalizations that are not generally accepted within the ecological community. In this thesis such debatable points are avoided by considering variables over a range of values implied by empirical evidence to assess the applicability of the trends related to the pipe model.

The WBE model characterises geometric plant structure through power laws derived from biological and biomechanical considerations of resource distribution within the plant (Enquist et al. 1999; Enquist et al. 1998a; Enquist et al. 1998b; West et al. 1997, 1999b). It is used for its relative simplicity but also for its clear advantages over the standard random volume over ground model (RVoG) (Treuhaft and Siqueira 2000).

The model uses five variables to describe the size and number of branch elements of a tree: (1) a scaling factor, a, determining how radii of branches change, or scale, within the plant;

$$l_k \propto r_k^{2/3a} \tag{3.1}$$

with l representing the branch length, r the radius, a the scaling factor, and k the branch level. (2) the branching ratio, n, the number of daughter branches derived from one parent; (3) the length-to-radius constant of proportionality, m; (4) radius of leaf petiole, r_N; and (5) number of branching levels N. In actual trees, all five of these parameters lie within a small range of values, (see Appendix 1 Chapter 12.1), and are likely species-specific. In broadleaf species N is likely to be related to the tree age and is the only variable that would normally change over time. Significantly in this thesis a range of values are experimented with in a similar manner to (Woodhouse 2006b) to avoid the restrictions and criticisms that (Kozlowski and Konarzewski 2004) associated with the WBE model. The values are influenced by allometric studies such as (Zianis and Mencuccini 2004).

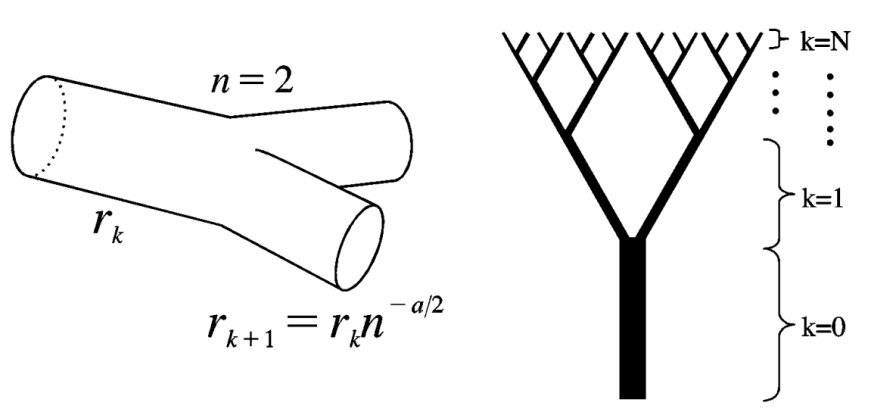

Figure 3.1. Representation of main parameters in WBE model: scaling factor *a*, branching ratio *n*, branching level *k*, total number of branching levels for particular tree, *N*.

The WBE branching network runs from the trunk (level 0) to the leaf petiole (level *N*) (see Figure 3.1) with an arbitrary level in the plant branching network denoted by *k*. Note, however, that we might expect biomechanical properties of tilted branches in the canopy to differ from a vertical stem. The value of *n* is typically 2 for broadleaf (decurrent) species, and larger (up to 5 or more) for conifers (excurrent). Within empirical studies, and specifically within the literature on modelling radar backscatter, the value of *a* ranges from 2/3 to 4/3, with values occurring out with this range very rarely, and are usually associated with stem allometry (Woodhouse 2006b; Zianis and Mencuccini 2004). For excurrent trees, the value for *a* in the branching structure is often approximately 2/3, representing geometric similitude, but stems can be better represented by some value greater than 7/6, similar to the case of stress similarity related to $a = 4/3$. Note that a value of $a=2/3$ coincides with a geometric similitude model of plant structure, consistent with many observations of conifers (Niklas 1994), but not dicots, which are more appropriately described by the elastic similarity model, $a \approx 1$. Values of $a > 1$ for stems are also suggested by other empirical data (Zianis and Mencuccini 2004). When the scaling factor is $a=1$, this describes the special case of the area-preserving "pipe model" (Shinozaki et al. 1964), whereby the plant is described by a tightly packed pipe bundle.

3.1.3 Relating WBE to Biomass

Allometric relationships for individual tree height to trunk volume are commonly used to determine trunk volume or biomass (Baker and Luckman 1999; Imhoff 1995b) whereby the volume, or biomass, of each tree trunk scales as:

$$V \propto M \propto r_0^2 l_0 \propto r_0^b \tag{3.2}$$

Here the original DBH and tree height have been replaced with r_0 and l_0 to coincide with the general model. The use of the exponent on the stem radius rephrases the equation as a standard allometric relationship (since stem height is often inferred from DBH). The constant of proportionality (not shown) usually incorporates a species-dependent shape factor. From summation over the branching levels in the WBE model it can be shown that for large N, the mean mass of a tree is given by:

$$\overline{M} \propto r_0^2 \, r_0^{2/3a} \propto r_0^{2(3a+1)/3a} \tag{3.3}$$

3.1.4 WBE Prediction for Populations

Due to resource limits as plants in a population grow larger, a given area can support fewer of them, with a forest carrying out self-thinning as a result of competition. When considering measurements at the population level, an additional "thinning factor" must therefore be included to describe the depletion of tree density with stand age (Enquist and Niklas 2001), (Baker and Luckman 1999). An estimate has been derived by (Enquist et al. 1998a) using the WBE model to consider the resource use as a function of plant size and from this predict that the maximum total number of individuals scales as the power of the body mass , which is in good agreement with many data (Enquist and Niklas 2001). This relationship is expected to hold for the intraspecific case i.e., for a forest observed over time in populations of single species, among growing individuals subject to density-dependent mortality. We assume here that it is also a good approximation of the interspecific case of scaling of plant size and number across stands of species that differ in average size at maturity.

Biomechanical and allometric theory also predicts that the mean plant mass is proportional to the stem radius r_0 to the power of some factor. The WBE provides the relationship of equation (3.3) with N_{max} being the total number of individuals and will scale as:

$$N_{\max} \propto \overline{M}^{3/4} \propto r_0^{-(3a+1)/3a} \tag{3.4}$$

When $a=1$, N_{max} would be inversely proportional to the basal area due to the negative two exponent. Despite global variations in tree densities and biomass the exponent of the size-frequency distribution of individual forest communities around the globe appears to lie mostly within d values of 1.5 to 2.5, with forests at high latitude being the general exception, with exponents approaching 0.5 (Enquist and Niklas 2001). In this thesis, the number density is generalised to:

$$N_{\max} \propto r_0^{-d} \tag{3.5}$$

With d the "thinning exponent.". $d=0$, corresponds to constant number density (i.e., no thinning), whereas a value of $d=3$ corresponds to a high rate of stem mortality (Coomes et al. 2003). Many radar studies report that number densities within a forest decrease with increasing biomass (or age) (Baker et al. 1994; Le Toan et al. 1992) although variations in number densities are often not explicitly given. In (Ferrazzoli and Guerriero 1995) both a conifer and deciduous scheme have number densities described by $d=2$. Other values reported include $d=1.9$ and $d=1.1$ (Baker et al. 1994), and (Quiñones and Hoekman 2004). This definition of thinning is used in Chapters 5 and 6 where the full WBE model is used but also in Chapter 7 where the Matchstick Model, described in Chapter 3.3, is used.

3.1.5 WBE Height and Biomass

For individual tree height, h, the WBE model predicts a power relationship with mean plant biomass such that:

$$\overline{M} = mh^{3a+1} \tag{3.6}$$

where $\overline{M}$ is the mean plant mass, m is the constant of proportionality related to the scaling factor of length to breadth of a branch (and incorporating the wood density), and a is the scaling parameter that determines how the size of the branches change. However, what is required in this thesis is a relationship between height and biomass density, rather than tree biomass so using N_{max} as the area density gives a biomass density M, as:

$$M \propto \overline{M} N_{\max} \tag{3.7}$$

so that:

$$M \propto h^{(6a+2-3da)/2} = h^{\alpha} \tag{3.8}$$

With α representing the height exponent which varies from approximately 0 to 4 within the range of a and d values used in this thesis. The majority of variation in this exponent is due to a sensitivity in the thinning exponent and not the species related scaling factor. For expected values of $d=1.5$ to $d=2$ values predicted for α in remote sensing literature have been shown to be 1.3 (Baker et al. 1994), 1.5 (Quiñones and Hoekman 2004); (Kasischke et al. 1995; Mette et al. 2002), 1.76 (Mette et al. 2002), 2.0 (Mette et al. 2003), and 2.17 (Askne et al. 1997).

3.2 The SERA Model

SERA (Hammond and Niklas 2009) is a forest growth model which accurately reproduces the community dynamics of a collection of trees competing for light and space. It is used as the forest growth model in Chapters 4 and 8. According to (Enquist et al. 1998a) a variety of plant ensembles are observed to "self-thin" in accordance with same or very similar scaling exponents. SERA was designed to incorporate, as a major function, this self management technique as it evaluates how

different species compete in a world space in which the physical attributes, such as the direction and intensity of incident sunlight are defined. Within SERA each plant is intentionally simplified to consist of a single photosynthetic surface elevated by a single stem. Similar concepts have been explored in (Niklas 2000) and (Chave 1999). Where some models represent the canopy as a flat disc, SERA treats each canopy as a hemisphere of uniform thickness. The angle of solar incidence on the forest is time averaged within the construct of the model to be 0 degrees such that the projected area of the canopy is the total photosynthetic area. This is an accurate description for tropical forests but is less representative of the light captured by boreal forests but is a simplified description of how trees acquire light from vertically above within a forest environment rather than from the sides.

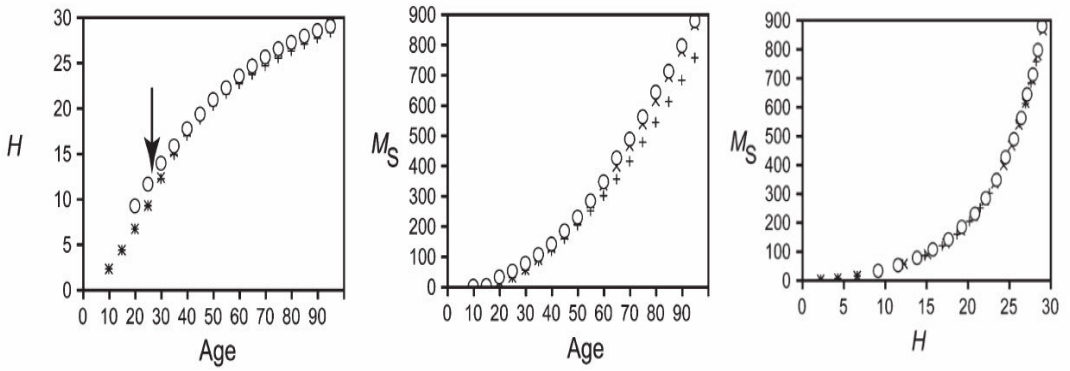

Figure 3.2. Bivariate comparisons among observed size-dependent trends (in 5-yr intervals) in an *Abies alba* population (denoted by o) and those predicted by SERA emulating normal reproductive effort and three times normal effort (x and +, respectively). H represents tree height (m), and M_S represents stem mass (kg). Arrow represents maturity onset. Taken from (Hammond and Niklas 2009).

To generate a single species within SERA six scaling exponents are required. These scaling exponents are the photosynthetic growth exponent, young canopy mass exponent, mature canopy mass exponent, stem mass exponent, stem diameter exponent, and young stem height exponent. The relationships that govern allocation of stem mass to stem diameter and height allow a transition in allometry from geometric self similarity to geometric non-similarity. Unlike WBE, SERA allows this

scaling exponent to change within the lifetime of a stem with a change in scaling found empirically to occur around the onset of maturity. Data from the original SERA paper (Hammond and Niklas 2009) is shown in Figure 3.2 and Table 3.1 and show the accuracy to which SERA replicates natural behaviour.

SERA consistently predicts plant life-span to scale as the ¼ power of body mass in a similar manner to WBE, a scaling relationship that has been reported for diverse plant species (Marbà et al. 2007). A number of naturally occurring scaling relationships also emerge as the direct result of competition for light and space. Many of the scaling relationships predicted by SERA also emerge from WBE suggesting that the empirically verified SERA and mathematical explanations for scaling relationships such as WBE have conceptual common ground.

Table 3.1. Comparisons between observed and predicted scaling exponents (α and 95% CIs) for observed and predicted scaling relationships of *Abies alba*, generalised conifer and angiosperm populations. G_T(kg/yr), M_T(kg), G_S(kg/yr), G_L(kg/yr), M_L(kg), M_S (kg), D(m), and H(m). G represents growth per year, M mass, D diameter, and H height. Subscript T denotes "total", L represents "leaf", S represents "stem". Taken from (Hammond and Niklas 2009).

	Abies alba		Generalized conifer		Generalized angiosperm	
Scaling relationship	Observed	Predicted	Observed	Predicted	Observed	Predicted
G_T vs. M_T	0.67 (0.65, 0.68)	0.66 (0.65, 0.67)	0.80 (0.75, 0.86)	0.80 (0.78, 0.82)	0.76 (0.72, 0.81)	0.75 (0.73, 0.77)
G_S vs. D	1.18 (1.10, 1.27)	1.18 (1.08, 1.28)	2.04 (1.98, 2.11)	2.05 (2.04, 2.06)	2.04 (1.93, 2.15)	2.02 (2.00, 2.04)
G_L vs. D	0.72 (0.58, 0.87)	0.64 (0.19, 1.09)	1.95 (1.87, 1.96)	1.95 (1.93, 1.97)	1.79 (1.75, 1.80)	1.80 (1.79, 1.81)
G_T vs. M_L	0.60 (0.58, 0.61)	0.57 (0.56, 0.58)	1.00 (0.98, 1.03)	1.00 (0.99, 1.01)	1.15 (1.07, 1.23)	1.15 (1.13, 1.18)
M_L vs. M_S	0.99 (0.93, 1.05)	0.95 (0.94, 0.96)	0.78 (0.74, 0.81)	0.78 (0.77, 0.79)	0.73 (0.71, 0.74)	0.74 (0.73, 0.76)
M_L vs. D	1.91 (1.89, 1.94)	2.03 (1.86, 2.21)	1.93 (1.85, 2.02)	1.98 (1.96, 2.00)	1.86 (1.72, 2.00)	1.98 (1.96, 2.00)
M_S vs. D	2.54 (2.53, 2.55)	2.54 (2.53, 2.55)	2.48 (2.39, 2.56)	2.44 (2.42, 2.47)	2.63 (2.55, 2.70)	2.66 (2.62, 2.67)
M_S vs. H	2.98 (2.90, 3.06)	2.84 (2.81, 2.88)	2.59 (2.47, 2.71)	2.60 (2.59, 2.61)	3.12 (2.88, 3.35)	3.10 (3.08, 3.13)
H vs. D	0.85 (0.83, 0.88)	0.89 (0.79, 0.99)	0.93 (0.88, 0.97)	0.94 (0.93, 0.97)	0.83 (0.75, 0.91)	0.86 (0.80, 0.87)

Within SERA the growth of plants is uninhibited but when plants violate physical laws the result is death. Mortality also results from light deprivation or stochastic/ age-dependent processes. By adhering to these rules the generated forests follow empirical trends of "self-thinning". The SERA model, being fully independent, was assessed biologically by comparing the ensemble behaviour of predicted against observed species for which sufficient empirical data existed. The world wide

compendium for forestry data compiled by (Cannell 1982) was initially used to identify long term studies of monospecific ensembles, with the most useful data set being a single *Abies Alba* population documented every 5 years for 95 years starting 10 years after planting (Cantiana 1974); (Hellrigl 1974). The (Cannell 1982) dataset was then used to characterise 332 angiosperm and 343 conifer communities to emulate the dynamics of "generalised" populations.

SERA possesses the ability to vary light intensity within the world space, to plant various species at user defined locations, and to vary the distribution space. In this thesis all available options are used in order to investigate the resulting variations in forest parameters and to observe backscatter. The user defined simulation parameters of SERA include, world size, starting population, maximum population, and maximum number of cycles. Additionally the species composition of the original plantings is preselected at the commencement of the program. A full description of *Abies Alba*, *Cryptomeria*, Generic Angiosperm and Generic Gymnosperm is given in Appendix 2 Chapter 12.2. The default values of SERA provide initial inputs regarding the desired environment and also prevent two plants from occupying the same space, for plants to grow partially outside the world space, and for Euler-Greenhill scaling to be violated. The stochastic nature of reproduction and success means that no two forests will be identical but will tend to optimum conditions due to the limits of resource and space. Appendix 4 of Chapter 12.4 shows how SERA can also be used to determine the vertical distribution of biomass within a multi age forest canopy.

Because of their grounding in allometric principles, WBE and SERA continually replicate the behaviour exhibited by trees in nature. Where the two models differ significantly is their application. The WBE model is fractal-like, making it an ideal descriptive tool for generating a single multi layer tree, while SERA can successfully predict the stem growth of a tree as well as model community growth. The main

allometric linkages that exist in SERA lie with the stem growth, the canopy of SERA serving as a means of collecting light without featuring branching architecture.

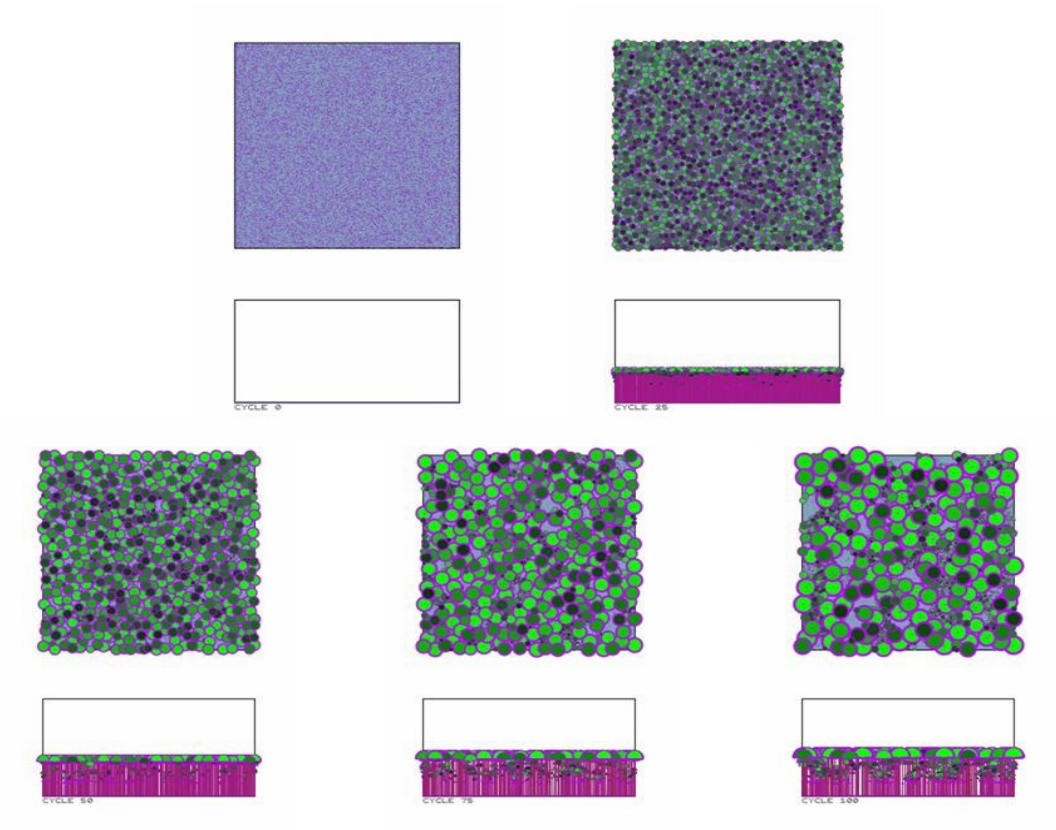

Figure 3.3 Angiosperm forest horizontal and bottom-up representation. Glimpses at 0, 25, 50, 75 and 100 years over 1ha.. Purple represents stems, darkness of green represents shading level. Blue indicates zero canopy cover.

The modelling undertaken within this thesis employs both models but independently. Despite limitations the WBE model has key advantages. The WBE model is generically based on biomechanical constraints and resource distribution and the generic nature allows it to adequately describe "tree-like" branching constrained by fluid flow and rigidity (unlike fractal scaling models), but as a consequence of its generic nature it is not well suited to describing properties of a particular tree species. WBE characterises the geometric structure of a plant through power laws derived from biological and biomechanical considerations of resource distribution within the

plant. It is used for its relative simplicity but also for its clear advantages over models such as RVoG (Treuhaft and Siqueira 2000) for representing structure. Being a fully developed and interactive model, SERA, is a more appropriate method for modelling specific forests than WBE. SERA's appropriateness lies in its ability to accurately model single trees as well as simulate population dynamics through community growth, regrowth and mortality. SERA is unable to model the branching structure of canopies and in this sense WBE is advantageous and essential for the studies in this thesis concerning vertical structure but where SERA is most appropriate is in describing the relationships between forest height and volume, see Chapter 4, and for providing heterogeneous forests for long microwave SAR studies, see Chapter 8.

The visual capabilities of SERA are shown in Figure 3.3 where an Angiosperm forest growing over a 100 year period is visualised in 25 year increments. Not only does it provide location details but as can be seen in the figure the varying degrees of canopy shading are shown through the brightness of the canopy colour.

3.3 The Matchstick Model

Simple, single layer models of microwave scattering from a forest have typically treated the target surface as either a dielectric slab with constant properties suspended above the ground (Bush and Ulaby 1976) or a layer of sparsely distributed identical dielectric scatterers. These scatterers can be spheres, as in the Water Cloud Model (Attema and Ulaby 1978), or random cylinders (Peake 1959) which may be randomly oriented like the RVoG model, (Papathanassiou and Cloude 2001), (Mette et al. 2004a) or with a systematic orientation (Treuhaft et al. 1996), (Smith et al. 2002). These models share one important common feature in that none of them considers the change in number density of tree stems associated with biomass changes.

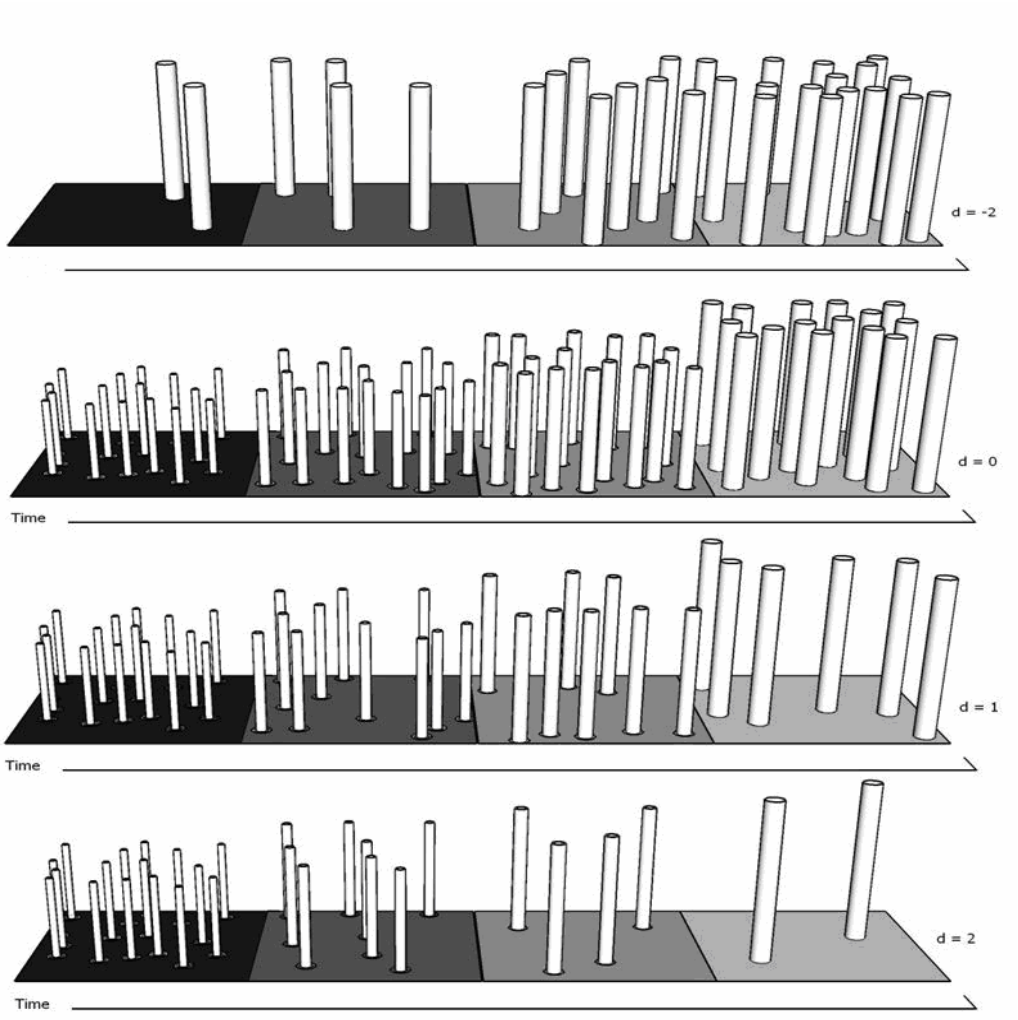

Figure 3.4. Representation of collection of cylinders in four forest settings. Area is schematic representation. From top to bottom d=-2, d=0, d=1 and d=2 representing various thinning regimes. Where d is positive the progression from left to right can represent a single stand changing over time or simply the state of four neighbouring plots at any one time. When d is negative the progression can not be considered with respect to time but can represent neighbouring stands, shown here with no stem size variation.

Remaining within the tradition of simple, single-layered models, a model based on a single layer of stems is described. Here called the 'Matchstick Model'. It is an oriented layer of cylinders and as such the model is most suited to P-band wavelengths or longer. The stems are identical and always (near) vertical, and do not

account for tapering. The forest biomass is assumed to be directly related to the total volume of the cylinders in a similar fashion to the relationships explored in (Fang et al. 1998) in which a simple linear relationship between stand biomass and volume is shown to exist for all the main forest types in China. In that work a direct relationship was also established between stem volume and biomass shown to slightly underestimate biomass. Similar relationships are used in (Valentine et al. 1984) and documented in (Philip 1994), while (Le Toan et al. 1992) states the link between stem volume and biomass within the context of a radar survey. Changes in area biomass are therefore a result of changes in cylinder size and number density. The primary purpose of the Matchstick Model is to explore *trends* in backscatter associated with biomass changes rather than simulate absolute values. A visual representation of the model is demonstrated in Figure 3.4 with d indicating the thinning parameter as introduced in equation (3.5) of Chapter 3.1.4.

The following sections describe how we can characterise the changes in stem size and number density using general macroecology principles which define the model. When using the Matchstick Model the modelled scenario is that of a developing forest. Although it can be assumed that the data points represent a single hectare forest changing over time as in the cases of $d=2$, $d=1$, and $d=0$, they can just as easily refer to neighbouring hectare plots at differing stages of growth within a large forest or plantation as for all cases featured in Figure 3.4, including $d=-2$. This is particularly relevant in an expanding forest where a plot of new growth would mimic the characteristics of early stage forest. Modelling a single stand across a number of years does not account for variations that may exist in terms of ground conditions and other environmental factors that may directly affect the growth of the forest, but in spite of this, this method allows a direct analysis of the effect of size and number distribution on the trends of backscatter return. This method of forest modelling is therefore directly relevant to studies presented in the literature as the acquisition of a wide range of biomass values to enable scientific analysis involves the survey of forest stands of varying stages of growth. It is particularly true within monospecies stands in

which the allometry of individual trees is assumed to vary very little and resource levels to remain fairly consistent within neighbouring stands.

3.3.1 Individual Stem Characteristics

When the Matchstick Model is used in this thesis in Chpater 7 the variables that determine individual stem sizes are (1) a scaling factor, a, which determines proportional change of cylinder shape to cylinder size, (West et al. 1997), (Woodhouse 2006b) as defined in equation (3.1) and (2) the length-to-radius constant of proportionality, m, so that:

$$l = mr^{2/(3a)} . \quad (3.9)$$

This allometric formulation utilises biomechanical constraints that predict some optimal relationship between l and r in the same manner as the WBE model. Decurrent trees (most broadleafed species) are appropriately described by the elastic similarity model, $a = 1$, whereas $a = 2/3$ is the value that represents geometric similitude, $l \propto r$, which (Niklas 1994) reports is consistent with many observations of excurrent species (most conifers). Empirical data suggests that stems have often been better represented by some value greater than $a = 7/6$, similar to the case of stress similarity, a condition related to $a = 4/3$. The constant of proportionality, m, is more diverse than observed values of a. Reported values range from approximately 5 to 163 in the dataset of (Cannell 1982) which includes 675 forest communities.

3.3.2 Stem Number Densities (Populations)

In radar measurements it is not usually possible to measure individual trees. The Matchstick Model therefore incorporates variability in both stem size, and stem number density within a population. In the current work we only consider populations of identical stems so that variability of biomass per unit area is governed only by variability in size and number. This is a good representation of managed

monocultures, but also a reasonable model for many single species forest areas (Christensen and Emborg 1996).

In any forest biome, the number of trees of a given size is limited by the available resources, and the balance between new growth and tree mortality (including herbivory and fire). These may vary both spatially and temporally. In the Matchstick Model the relationship between the size (radius, r) and number of trees, N, can be characterised by the thinning factor, d, such that:

$$N \propto r^{-d} \tag{3.10}$$

Thinning in the Matchstick Model is related to the radial increases in the stem through the equation:

$$N = r_k^{-d}.r_0^{d}.pdens \tag{3.11}$$

Where subscript $_k$ represents an incremental increase in radius from the initial radius value associated with $_0$. This zero value is related to the WBE model as it represents the petiole radius when WBE is used to implement size as described in Chapter 3.1 but also later in its use in Chapter 5 (See also (Woodhouse 2006b)). The variable *pdens* simply represents the initial planting density of the forest.

Although called a "thinning factor" it need not apply only to the change in a population over time (or a spatial surrogate, as in different aged managed stand) – we use it here as a general description of the size-number relationship. Figure 3.4 visually describes the impact of d and demonstrates the relationship between size, number density and volume. The typical range of d observed globally (Niklas et al. 2003) is shown. When $d=0$, N is constant and total volume increases linearly with the volume of each stem. This is typical of young, actively growing forest (such as regeneration) where trees have yet to utilize all available resources, and tree mortality is near zero. When $d=2$, there is a dramatic decrease in N. The total volume still increases since the collective basal area remains constant (since each stem increases

with r^2) while stem height increases. This is typical of many forests, especially in the tropics, or in managed forests where thinning has been applied in order to maintain basal area. It is exactly this dramatic change in structure associated with increasing area volume that the Matchstick Model tries to characterise (and is not incorporated into other simple single layer models). For $d=-2$ (relating number increases and neglecting corresponding radius increases) the cylinders are identical; increasing volume per unit area corresponds to increasing N. This is typical of a resource-limiting case, such as savannas, whereby tree numbers are limited due to competition for scarce resources such as water, but where trees do grow they often need only grow to a sufficient height to outperform grasses and avoid fire and herbivory (Sankaran et al. 2008).

3.3.3 Scattering Considerations

The simple formulation of the Matchstick Model considers the limiting case of cylinders with circumferences smaller than 0.1λ on the one hand, and much larger than 10λ on the other. For the sake of simplicity, these limits are referred to as corresponding to "Rayleigh" and "Optical" scattering, respectively. In the Rayleigh case we assume the backscatter from each cylinder increases with the square of the cylinder volume, and for the latter, it increases with the physical cross-section (Kononov and Ka 2008). At the transition between these two regimes lies resonant scattering, here we make an approximation that assumes the resonant behaviour "averages out" across this region due to the cumulative effect of a distribution of stem sizes. This assumption is supported by empirical results in (Lopes et al. 1991), and (Mougin et al. 1993).

An additional feature of the Matchstick Model is the absence of scatterer attenuation due to the absence of canopy. A compelling case for the importance of attenuation would normally be made based on evidence of saturation in the backscatter-biomass curves. However, it is just such an interpretation based on the Water Cloud model

(Attema and Ulaby 1978) that we wish to challenge with the Matchstick Model. Indeed, the results presented in this thesis demonstrate that the impact of thinning on the backscatter can be sufficient to cause saturation even when attenuation due to a thickening canopy and increasing number of scatterers is ignored. Saturation modelled by the Matchstick Model in itself is therefore not evidence of increasing attenuation by the forest layer.

In summary the trend in backscatter from each stem in the Matchstick Model is characterised as follows. For Rayleigh scattering where σ represents the radar cross section and V the volume :

$$\sigma_{Rayleigh} \propto V^2 \tag{3.12}$$

Using the relationship between length and radius of equations (3.1) and (3.9), the proportional relationship can then be written with respect to radius, *r,* and scaling exponent, *a,* as follows. Normalised radar cross section is proportional to the cylinder volume where l represents the scatterer length and N the number of scatterers:

$$\begin{aligned} &\sigma^0_{Rayleigh} \propto N\, r^4 l^2 \\ &= Nr^{(12a+4)/3a} \end{aligned} \tag{3.13}$$

For Optical scattering, the normalised radar cross section scales with the physical cross-section, A:

$$\begin{aligned} &\sigma^0_{optical} \propto N\, A \\ &= Nrl \\ &= Nr^{(3a+2)/3a} \end{aligned} \tag{3.14}$$

This is in accordance with the laws of geometric optics which under certain limitations is an acceptable simplification of the scattering formula for the physical optics of a cylinder as described in Chapter 2.3.

If the geometric optics is valid it can be stated that within P-Band at 429MHz the radius value of a scatterer coinciding with the transition from Rayleigh to Mie is about 0.01m and the radius value of a scatterer which coincides with the transition from Mie to Optical is approximately 1.1m. Scatterers greater than 0.01m are deemed by the Matchstick Model to be Optical scatterers at P-Band.

The application of the Matchstick Model is shown in Chapter 7 in which it is used to investigate the effects of stem number density and size variations on backscatter modelled by the radiative transfer model RT2.

3.4 RT2 to model SAR Scattering from Forests

RT2 Version 3e (Anderson 2000; Balzter et al. 2003b; Cookmartin et al. 2000) is a second order radiative transfer model developed in 2000 based on an earlier first order version of the model produced by Paul Saich (Saich 1993; Saich et al. 1995). It is used in Chapters 5, 6, 7, and 8 to provide SAR backscatter data at multiple frequencies. RT2 version 1 could initially support a layered structure of up to 3 layers, with a maximum of five scatterer types in each layer. Version 2 a greater availability of scatterer orientation distributions, and the inclusion of empirical ground scattering models. Version 3e is a more complete model ideally suited for forest geometry parameterisation. Specifically the allowance of more layers, up to 20 used in this thesis, enables a detailed forest structure to be constructed with each layer potentially used to model different branch sizes. In addition there is a capacity for up to 64 scatterer sizes within a single layer or within a single forest simulation. This feature is advantageous when RT2 is parameterised by SERA allowing 64 class sizes for the description of multi-age stems within a single forest. Version 3e also benefits from the addition of new ground scattering models, scatterer types, permittivity models and scatterer orientations.

In addition to the parameterisation of layers using forest geometry, RT2 allows the user model choices to represent environmental conditions as well as models to determine composition and scatterer position. The subsidiary models available refer to the scattering of the geometrical shapes, the scatterer orientation distributions, the ground scattering, the ground permittivity, and the vegetation permittivity.

Each parameter file in RT2 must include information regarding each layer, the ground, and the modelled incident electromagnetic wave. Within the header file the constant terms of a particular simulation are included, consisting of the incident frequency information, both angle and wavenumber, the scattering types to be modelled (direct, layer-ground, layer-layer backscatter), the ground scattering model and the ground composition.

3.4.1 Ground Scattering Model

The theoretical ground scattering models available within RT2 are the Small Perturbation Model, Kirchoff Geometric Optics Model, and Kirchoff Physical Optics Model. Each of these can be used with a Gaussian surface correlation function. In addition, empirical ground models of (Ulaby 1995), (Dubois et al. 1995), and (Oh et al. 1992) are available but their use in this thesis is not appropriate due to the concentration of this thesis on low radar frequencies in comparison to those used to devise these models.

The ground scattering model chosen in this study is the Kirchoff geometric optics model using a Gaussian surface correlation function. The geometric optics approximation is based on the Kirchoff-tangent plane approximation, which assumes that each point of a rough surface can be considered as locally flat (Pinel et al. 2010). In addition to scattering model choice, parameters indicating the surface roughness of the ground must be determined. Using the criterion shown in (Ulaby 1982) also known as the Fraunhofer criterion, the ground surface can be considered smooth if the

phase difference is less than an eighth of π. Within this study the ground conditions have been chosen to represent a rough surface at the limits of the geometrical optics approximation, verified in (Tang and Buckius 1998; Tang et al. 1996), in order to reduce the direct backscatter contribution from the ground surface and emphasise the contribution of the forest and the resulting double bounce. Simulations were carried out using a fixed incidence angle of 35 degrees and frequency of 429MHz to compare the backscatter effects of various correlation lengths and RMS surface heights from within the validity area of geometric optics. The variations in data resulting from different ground roughness are shown in Figures 3.5 and 3.6 for two cases. The first exhibits the data from an initial population of 500000 stems with scaling parameter a=2/3 as defined by equation (3.1), undergoing d=2 thinning as defined by equation (3.11) representing a relatively small forest, while the second example exhibits the data from an initial population of 1000000 stems with scaling parameter a=1, undergoing d=2 thinning representing a relatively large forest. d=2 thinning is the exact value that maintains total basal area of the forest as forest volume increases (see Figure 3.4) and is responsible for the rapid reduction in stem numbers with each increment of age to represent more natural stem number densities. Lower values indicate a level of thinning that will continue to increase basal area as volume increases even though tree numbers are reduced. The size of the forest can be compared using the volume values with both consisting of solely vertical stems.

The backscatter values in relation to default RMS surface roughness and correlation length choices suggest that the ratio of these values is a defining aspect, as shown in (Tang et al. 1996). The datasets possessing approximately the same ratio between these two values produce approximately the same backscatter and so, within the context of this thesis, this ratio will be kept at a value denoting a rough surfaceof correlation length 0.15 and RMS surface height 0.014. If a very rough surface is used the result will be that direct backscatter from the ground will dominate and render the forest invisible. Similarly, if a surface too smooth is used, the direct ground contribution will not be apparent due to specular reflection dominance. Although the

default setting used in this thesis lies at the limit of validity, in accordance with (Tang et al. 1996) ground representations that lie at other locations within the range of validity produce almost identical results as shown in Figures 3.5 and 3.6 with the trends even more closely matched. Significantly for this study the trends remain the same regardless of the absolute backscatter values depicted, unless the surface is modelled as very rough.

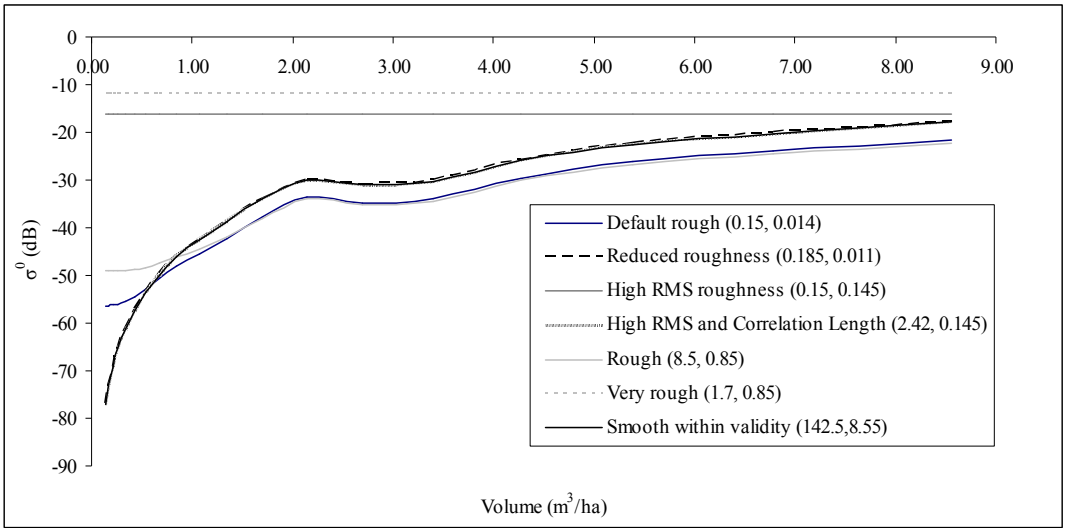

Figure 3.5. RT2 simulated P-Band VV data for surface roughness variation sensitivity test. Planting density (500000), Scaling (a=2/3), Thinning (d=2). Numerical values represent (correlation length, RMS surface height) defining roughness. Default setting used in thesis best described as rough surface for validity with Geometric Optics.

The ground composition must also be defined in the header file through the choice of ground susceptibility parameters. To model the ground the susceptibility model of (Hallikainen et al. 1985) is used, requiring a description of the soil in terms of sand, clay and silt content. In addition a volumetric water content must be defined. Similar to the choice of low surface roughness the volumetric water content of the ground is kept low to reduce the dielectric constant value and reduce the influence of direct ground backscatter. As shown in (Hallikainen et al. 1985) a low value for volumetric water content can still produce a significant dielectric constant to allow scattering.

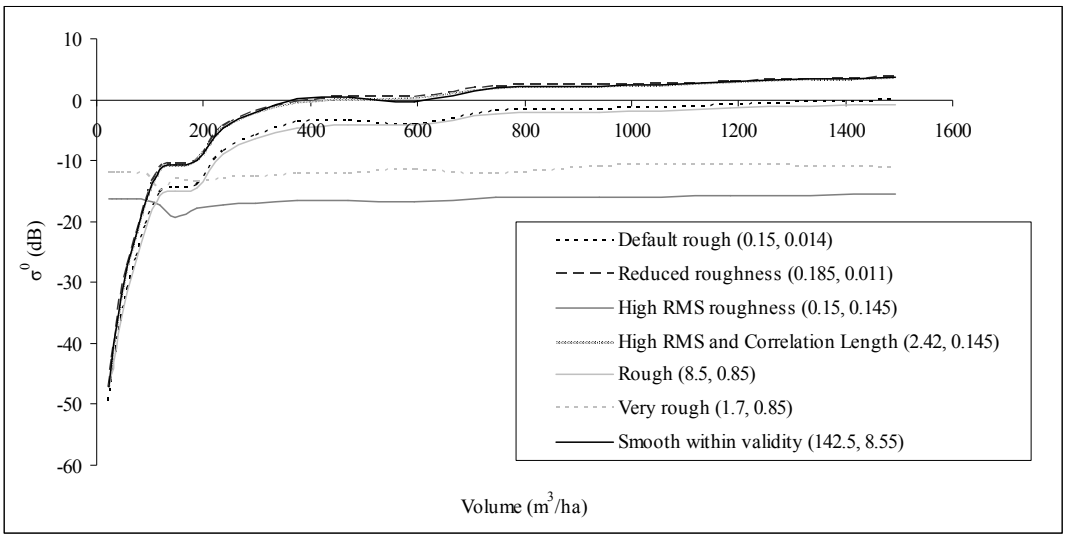

Figure 3.6. RT2 simulated P-Band VV data for surface roughness variation sensitivity test shown for planting density (1000000), Scaling (a=1), thinning (d=2). Numerical values represent (correlation length, RMS surface height) which define roughness.

3.4.2 Canopy Scatterers

Each individual scatterer type used in an RT2 simulation must be defined according to a series of parameters. These are the shape, height, half length, radius, number of scatterers per cubic metre, inclination angle, axial angle, and susceptibility. For each simulation the height defines the height of the layer while the half length input allows several branch sizes to be represented within the layer boundaries. The parameters that remain constant within a simulation and within the context of this thesis are the susceptibility values using the dual dispersion model for branches and trunks (Ulaby and El-Rayes 1987) which require constant inputs of gravimetric water and temperature. The shape of scatterer used throughout this thesis is cylindrical with the "infinite" cylinder approximation used throughout rather than the alternative and less applicable, for this scenario, needle and disc models which would be considered if foliage modelling was required in this study.

With regards to inclination and orientation, when the Matchstick Model (Chapter 7) or SERA (Chapter 8) is featured the stems are deemed vertical with zero inclination unless stated. For the work using the branching of the WBE model the orientation of the branches are uniformly distributed within an angular range of -180 to 180 degrees. The branch inclination is represented by spherical distribution. Evidence for the use of RT2 as an effective tool for backscatter modelling of vegetation of both forests and agricultural crops can be found in (Balzter et al. 2003b; Luo et al., 2000) and (Cookmartin et al. 2000). Further information about other models featured within RT2 and alternative setups can be found in the user guide (Anderson 2000).

3.4.3 Preliminary Backscatter Findings

Preliminary modelling for this thesis has analysed the effect on RT2 backscatter calculations resulting from variation in scaling parameter '*a*', planting density, and incident frequency. For scaling parameters of a=1 and a=2/3 frequencies of 50MHz, 429MHz, 1.5GHz, and 3GHz at an incidence angle of 25 degrees have been investigated with initial planting densities ranging from 10000 to 5000000 stems per hectare. Although these planting densities may appear unrealistic they represent the number of seeds and are subject to d=2 thinning (see Equations (3.5, 3.10, 3.11) and Figure 3.4) which maintains a constant total basal area for the forest throughout the experiment. The WBE model is used to generate the test forests using constants defining the geometry of an 18 layer forest with d=2 thinning incorporated.

Figures 3.7-3.9 show the results from varying incident frequencies and scaling parameters (comparison of Figures 3.7 and 3.8) and planting densities (Figure 3.9). RT2 reproduces expected trends in backscatter with higher illuminating SAR frequencies providing higher backscatter intensity for any particular volume as well as lower "saturation" points in keeping with the theories of extinction (Attema and Ulaby 1978) and of a scattering transition driven saturation (see Chapter 2.3). This is a prime example of how RT2 can successfully model backscatter effects from forests.

In addition to these expected trends RT2 shows how the saturation point can vary as a result of scaling parameter and planting density variations. These variations form a significant focus of the work conducted in this thesis.

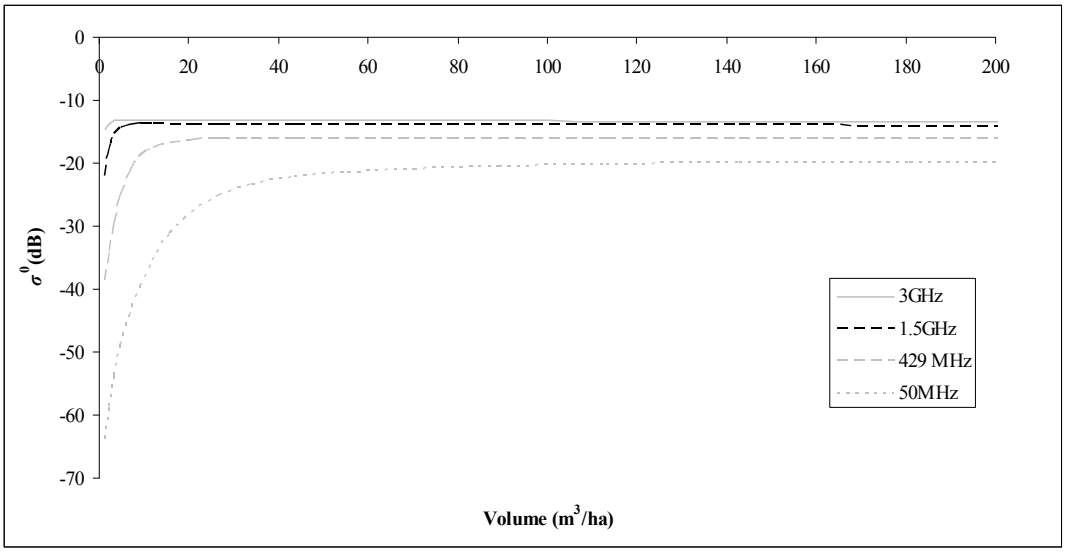

Figure 3.7. RT2 HV backscatter with increasing volume for varying frequencies at initial planting density 1000000, scaling factor *a*=1 for 18 layer forest. *d*=2 thinning ensures constant basal area.

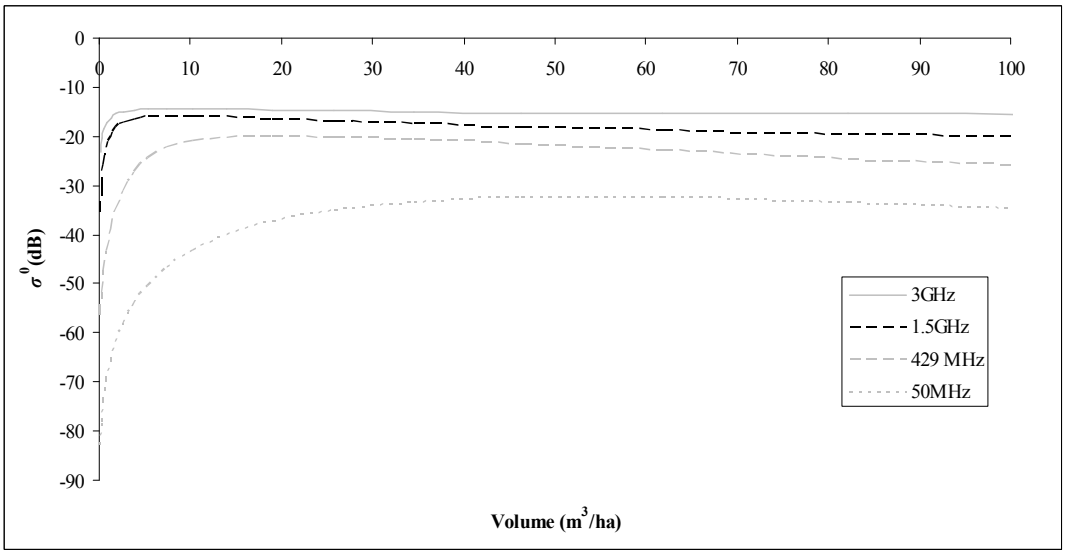

Figure 3.8. RT2 HV backscatter with increasing volume for varying frequencies at initial planting density of 1000000, scaling factor *a*=2/3 for 18 layer forest. *d*=2 thinning ensures constant basal area.

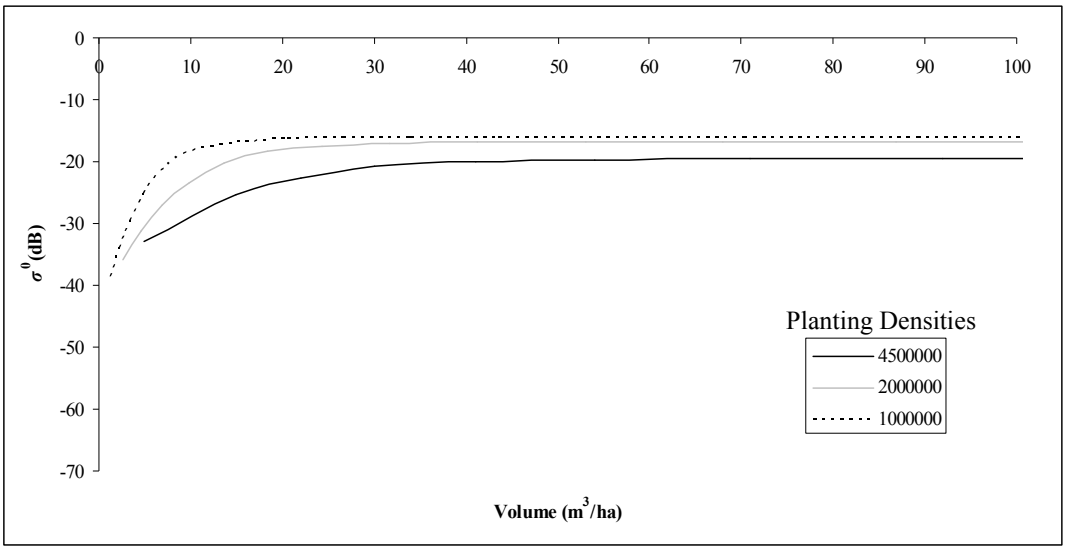

Figure 3.9. RT2 HV backscatter for 429MHz with increasing volume for varying frequencies at 3 different planting densities. Data for 18 layer forest with Scaling a=1 and thinning d=2.

Where the scaling parameter is varied the scattering values are shown to vary where similar volumes and incident frequencies are considered. This is in keeping with empirical findings such as those shown in (Castel et al. 2002) and (Imhoff 1995b). In addition here the volume of saturation is seen to vary when the same frequency is analysed. This behaviour is seen when comparing empirical surveys which report different saturation levels for the same incident frequency but over different forests, for example (Luckman et al. 1998), (Fransson and Israelsson 1999), and (Mitchard et al. 2011) all reporting for L-Band using the same survey system. Environmental conditions could be responsible for these differences but it is likely that forest structure plays a critical role as predicted by RT2 modelling and is investigated in the experimental chapters. For the a=2/3 case the gradient of the curve is seen to be negative after the maximum value associated with "saturation" has been reached, while an approximate zero gradient is consistently seen following "saturation" for the a=1 case. This is an attenuation effect due to bunching of scatterers in thinner layers brought on by lower scaling parameters. The way in which RT2 models attenuation mimics that expected in nature with Figure 3.10 representing an attenuation test of RT2. This test ensures that RT2 models typical RVoG behaviour (see Chapter 1.3.2).

Identical layers are modelled in this example with extinction set to allow transmission through all layers to show how the signal is attenuated exponentially through the canopy. The attenuation through a forest canopy would not be expected to follow this exact trend due to the non uniform distribution of branching within a forest but is typically used in interferometric studies of forests (see Chapter 6).

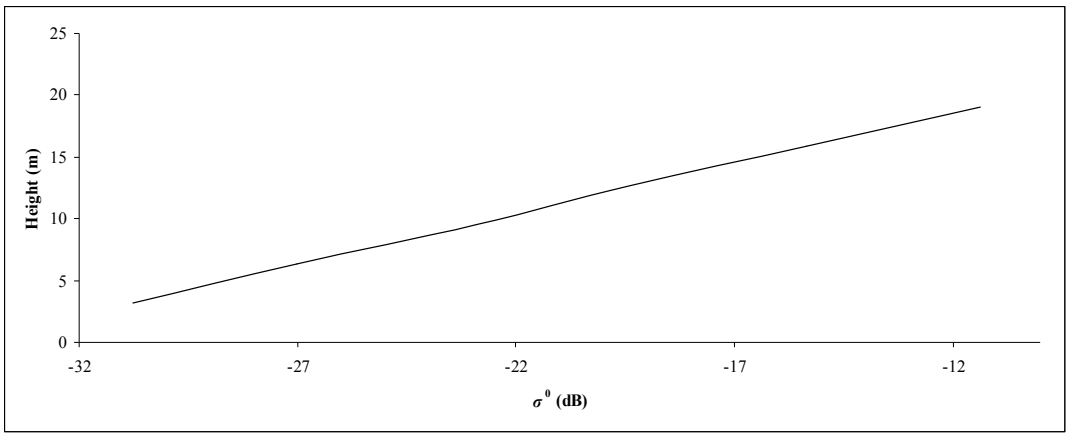

Figure 3.10. RT2 HV normalised Radar Backscatter from a 6 layer model of identical layer composition, number and volume of scatterers. Same trends shown for HH and VV.

Other examples of saturation behaviour can be found in Chapters 7 and 8 with Figure 8.12 in particular showing how the saturation level can vary in the presence of a heterogeneous forest.

3.4.4 Dominant radii in RT2 scattering

Common to all datasets is the presence of a dominant scattering layer. Figure 3.11 is an example of backscatter distribution around the dominant radius with the contribution from radii below the dominant radius thought to be the Rayleigh contribution (see Chapter 2.3) which increases with radii increase, while for radii above the dominant radius it is considered the Optical contribution which reduces with increasing radius. This represents an equi-biomass multi-layer model. In a similar way Figure 3.12 shows scaling variation effects with dominant radius

unaffected by scaling change as it is a consequence of incident frequency, in keeping with theories that predict maximum backscatter from scatterers of radii within the resonance region. The existence of a dominant radius is a relevant prerequisite for the work carried out in Chapter 5 regarding the vertical backscatter profile of forests.

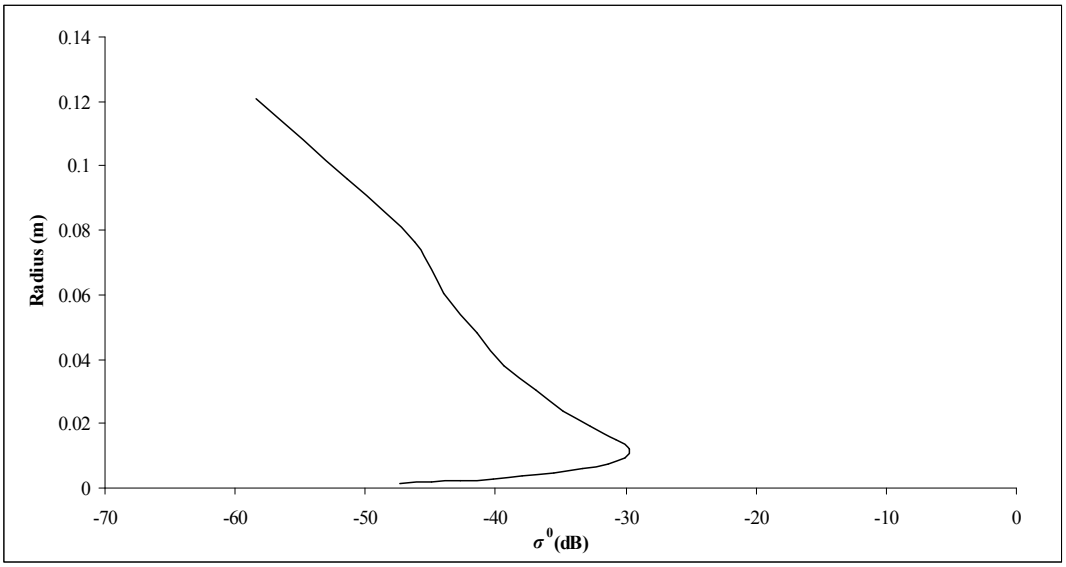

Figure 3.11. RT2 HV429MHz backscatter as function of branching radius with initial planting density of 500000 and biomass density of 54.43 m^3/ha. Scaling a=2/3 in 20 layer WBE modelled forest.

The following experiment explores the backscatter ramifications of a forest consisting of five branching levels representing five stages of branch growth. One tree is planted and grows through five layers/branching sizes. From this tree two separate trees are seeded which begin growth one branching order behind the original tree continuing through the remaining growth periods. Each branching element seeds 2 daughter branching elements for the next stage of growth.

The largest tree possesses one large stem (B1) in the base layer, two large branches (B2) in layer 1, four smaller branches (B3) in layer 2, eight smaller still branches (B4) in layer 3 and sixteen leaf petioles (B5) in layer 4. Once the largest stem has reached this growth increment the second largest trees will be one growth increment behind, and so on. The

base layer of the forest will therefore have 1 x B1, 2 x B2, 4 x B3, 16 x B4, and 32 x B5 and contain all the branching of the 4th and 5th generation trees.

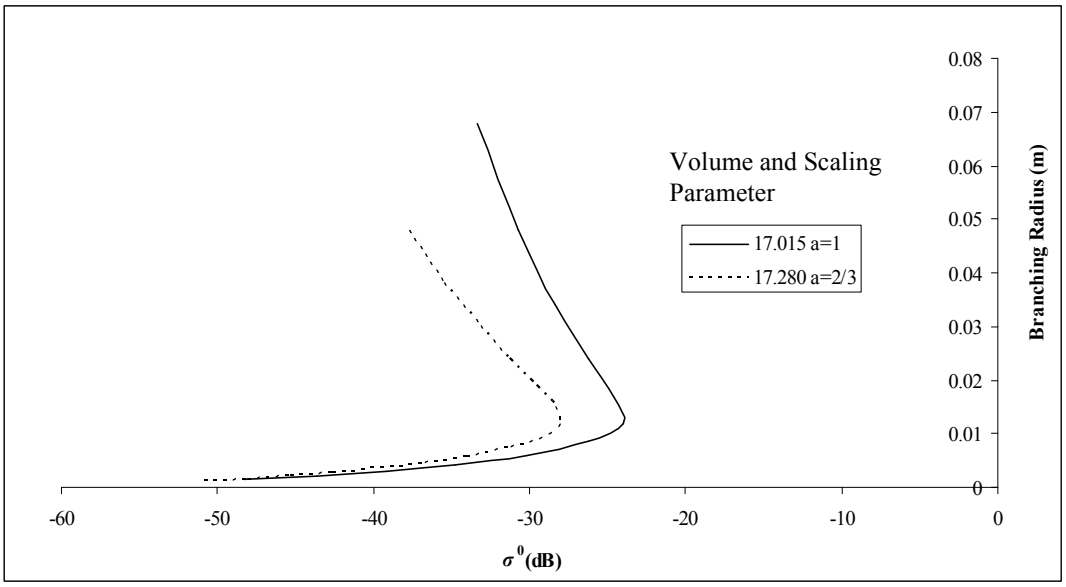

Figure 3.12. RT2 HV 429MHz backscatter as a function of branching radius shown for similar volumes with different scaling parameters. Biomass values in terms of m^3/ha shown in legend.

Figure 3.13 shows volume backscatter data from the forest configuration described in the above paragraphs. The data points in the figure are associated with the top of the layer so that the first point is located at 5.7m. The single large stem case is accompanied by simple multiplications of the configuration to 300, 500, 800 and 1000 so each time the number of the largest stems will be represented by this value. In its simplest form the dominant backscatter originates at the forest base from the location of the largest stem as well as the largest concentration of forest volume. This is a result that would be expected if backscatter were correlated with forest volume but interestingly there exists an anomaly higher in the canopy which gradually becomes the dominant source of backscatter around 16m height as multiplication is increased. The anomaly corresponds with the 4th layer which contains a volume significantly lower than the base layer, (extinction occurs only in the 1000 multiplication example in which the penetration depth through the base layer is 1m short of the ground). The anomalous result indicates

sensitivity to the size of scatterer at P-Band of the 4th layer which is occupied by the B4 and B5 branches as well as displaying possible attenuating effects which reduce the contributions from lower down. The wavelength of P-Band used here is 0.7m showing a sensitivity to scatterers of the size 0.01m x 2m and 0.016m x 2.52m with the transition from Rayleigh to Mie scattering associated with the P-Band radius dimension of 0.011m. This experiment provides an example of how forest scattering is not dominated by attenuation by exhibiting how greater values of backscatter can be found below the surface of the canopy using a model that models attenuation effects and resonant effects.

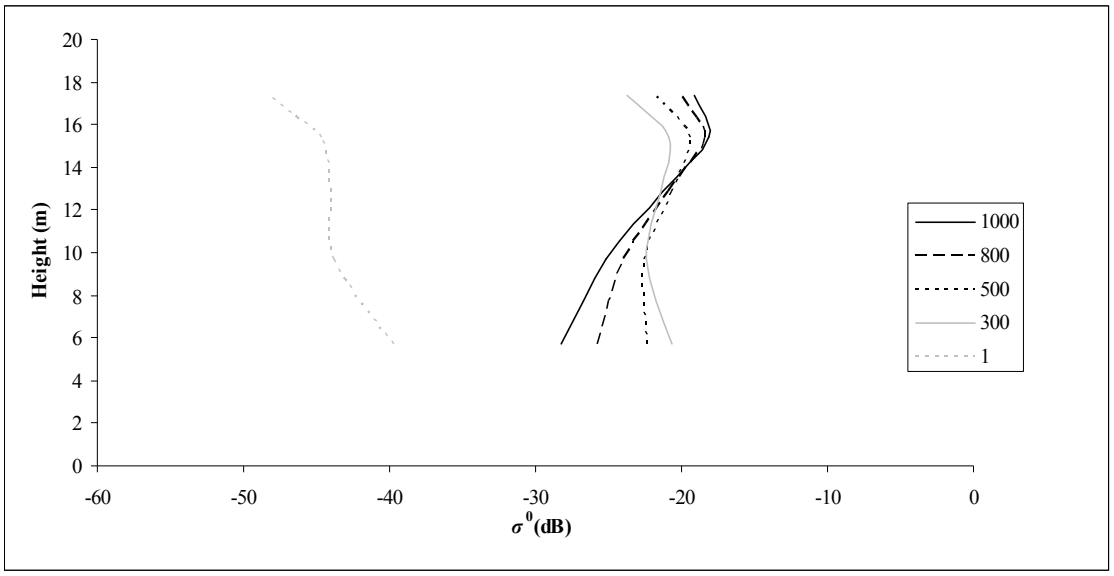

Figure 3.13. RT2 HV backscatter from forest branching levels corresponding to configuration described in text above. Legend denotes number of largest trees.

To further this experiment into this structure an extra layer was inserted to investigate the sensitivity of P-Band to particular dimensions of scatterer. Into this layer the branch sizes B3 (3rd generation), B4 (4th generation) and B5 (5th generation) were placed alternately while maintaining the same total volume. The backscatter data is shown in, Figure 3.14.

From the data it is apparent that backscatter from the uppermost layers in the canopy produce the same backscatter values albeit at different heights as a result of the total

height of the tree affected by the components of the test layer. As the backscatter values from lower in the canopy are analysed, the largest of the three tested branches, the 3rd generation, produces a backscatter level that can be clearly seen to drop off in intensity in the approximate region of 15m height. For the 4th and 5th generation branches this drop off is not as clear. At the lowest layers the backscatter response is larger for configurations featuring larger branching sizes within the test layer due to higher attenuation experienced by the more numerous and smaller scatterers required to maintain similar volume levels. Each example features identical configurations below the test layer with the level of backscatter below this layer dependent on the amount of backscatter attenuated above. The key thing to come from this group of figures is that RT2 shows sensitivity to size and number density distributions and is further evidence for the usefulness of RT2 in predicting backscatter from forest structures in accordance with the scattering theories presented in Chapter 2.3.

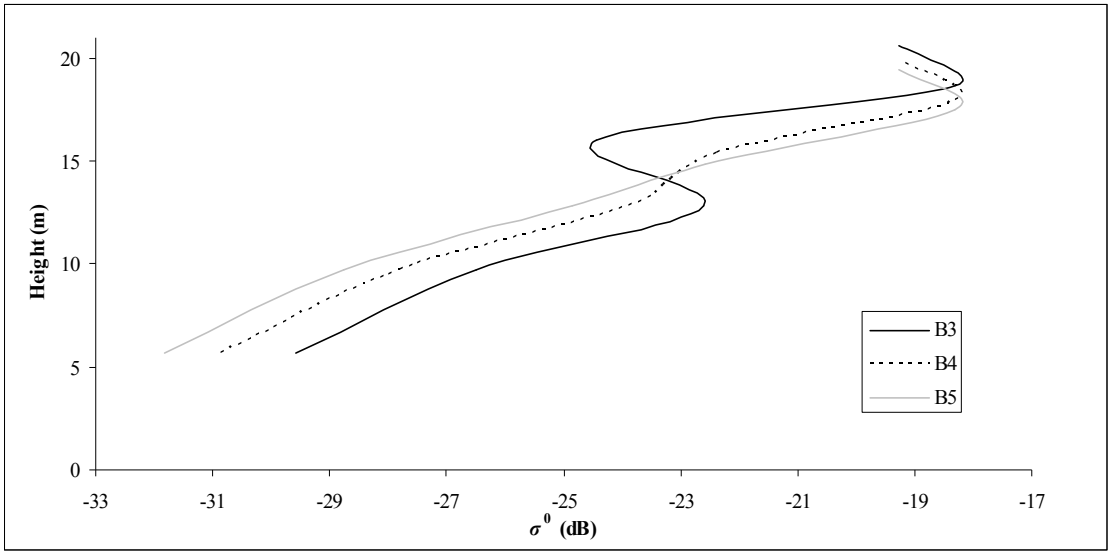

Figure 3.14: RT2 HV vertical profile backscatter data showing direct backscatter contribution from each layer with each dataset containing an additional layer of 3rd, 4th or 5th generation branches of equi-volume. Maximum heights vary as a result of the test layer height variation.

3.5 Structure of Experimental Modelling Within Thesis

The original experimental work of this thesis is presented in the following Chapters (4-8). Each chapter as its focus has the consequences of variations in macroecological forest parameters on remote sensing data, particularly SAR. Of significance are the forest parameters of number density and size which are both ultimately controlled by the self thinning of the forest. Each chapter presents its findings in terms of modelling results with forest structures provided either by the SERA model (Hammond and Niklas 2009) (Chapters 4 and 7) or the WBE model (West et al. 1997) (Chapters 5, 6, 7) which have both been introduced previously in this chapter (see Chapter 3.1 and 3.2). Backscatter data is provided either through Matchstick Model (Chapter 3.3) predictions or RT2 radiative transfer backscatter (Chapter 3.4).

The modelling work is conducted to address the questions set out in the Introduction of this thesis and to provide new ideas and methods to add to the scientific knowledge of radar remote sensing which was discussed in the first two chapters of this thesis. The flow of the experimental work begins with an introduction to forest remote sensing by examining the consequences of height to volume relationships that exist within forests. Using SERA the trends of typical height classifications used in forest remote sensing are analysed for forest stands made up of various planting densities, species mixtures, and resource restrictions. The aim of the work is to highlight how the association of forest height with forest volume can result in various volume estimates dependent on the height classification used. The simple analysis of how structure can affect simple forest relationships is a relevant consideration prior to analysis of backscatter variations caused by the same structures. The relevance for remote sensing lies in the use of interferometric SAR and LiDAR remote sensing which rely on accurate height values to infer forest volume or biomass. What this study highlights is that the vertical structure of the forest as a whole can influence the height to volume relationship whether that be maximum height, H100, or mean height so that if anything from planting density, resource availability, or species composition

is changeable then the relationship between height and volume maybe also. In addition, the study aims to predict the most appropriate height classification for use in forest remote sensing based on the accuracy levels across changing parameters, but also with consideration to the physics of scattering. Chapter 4 serves as an introduction to the forest remote sensing modelling that is conducted in the subsequent chapters and the way in which forest models are used as a tool to analyse remotely sensed data, particularly for the retrieval of forest structure data. The work in Chapter 4 also introduces the idea of the existence of dominant scattering layers within the vertical structure corresponding to interferometric scattering phase centres and suggests why particular height classifications may correspond to these centres. The importance of forest basal area as an indicator of both backscatter behaviour and subsequently biomass levels is also discussed.

Chapter 5 continues on the theme of vertical structure by introducing SAR backscatter modelling using RT2 (Saich 1993) (Chapter 3.4) to investigate the consequences of vertical structure variations on the analysis and interpretation of backscatter data. Using the WBE model described in Chapter 3.1, forests are modelled at a particular stage of growth as a collection of identical trees represented by branching layers consisting of identical sized cylinders. These cylinders get smaller with increasing layer number and therefore height from the ground. The investigation focuses on the potential existence of dominant scattering layers within a forest canopy related to both size and number density by generating a vertical scattering profile of the forest. The working hypothesis of the Chapter is that a dominant branching layer will exist as a result of a trade off between size of scatterers and their number density at a location determined by a transition from Optical scattering (predicted to be dominated by number density) to Rayleigh scattering (predicted to be dependent on scatterer size). The ratio of the size of the scatterer to the incident wavelength determines this size of transition as described in Chapter 2.3. Although a dominant scattering layer is predicted by traditional thinking to be located at the top of the canopy in accordance with the theory of attenuation. The difference

between the maximum backscatter resulting from resonance (Figure 2.4) and the scenario exhibited here is that the number density within each layer is changing in accordance with the branching of the WBE model. The investigation attempts to determine whether a dominant scattering layer exists within the canopy, not as a consequence of attenuation, or due to resonance but due to the size of the scatterers and their number density within any particular layer.

As a consequence of the hypotheses and findings of Chapter 5 and the relationship to interferometric remote sensing of Chapter 4, Chapter 6 features a short study that incorporates both vertical backscatter profiles and the methods of forest height retrieval using interferometric methods. In this case the method of interferometry is Coherence Tomography (Cloude and Papathanassiou 2008a). The work in this chapter uses RT2 vertical backscatter profiles of WBE modelled forests which were created to allow comparison with empirical data collected at the Remningstorp test site in Sweden. The backscatter data was modelled using L-Band to match empirical data rather than the longer wavelength P and VHF Bands used throughout the rest of this work. The RT2 vertical profiles are used to compare coherence data and subsequently height retrievals obtained from inverting different model solutions. These model solutions being the RVoG model (Treuhaft and Siqueira 2000), and the Gaussian and Legendre spectrums. The work serves to identify whether these solutions are appropriate for describing vertical backscatter of forests and whether volume backscattering profiles can be used as adequate descriptions of forest scattering behaviour and for accurate use in forest height retrieval.

With Chapters 4, 5 and 6 concentrating on the vertical structure of forests and the consequences for volume and biomass retrieval, Chapter 7 incorporates the Matchstick Model introduced in Chapter 3.3 to explore horizontal structure variations exhibited by number density and size variations of stems. The work of this Chapter investigates the theories of the Matchstick Model in comparison to RT2 modelled backscatter data produced following its parameterisation using the same vertical

stems. The key aspects of the Matchstick Model are that it is applicable at long wavelengths (P-Band or longer) and describes forests as a series of identical cylindrical stems with size increments based on WBE model scaling. It also allows the backscatter consequences of number density and size variations within forests to be identified in the absence of canopy attenuation. With the importance of basal area with regards to radar scattering, touched upon for the vertical profile case in Chapter 4, it is discussed in Chapter 7 for its importance in the horizontal case; referring to the total backscatter behaviour over a forested area. The idea of saturation and its causes are investigated by focussing on the relevance of scattering transitions to the trends existing between backscatter intensity and forest volume. As with the other Chapters of this thesis the approach to modelling is a deductive process analysing the consequences of general scattering behaviour to provide explanations for specific behaviour seen in empirical studies. The general behaviour here being that forests consist of vertical stems growing at similar rates, causing a transition in scattering as they achieve a particular size, and whose scattering can be described either as solely volume dependent Rayleigh scattering or area dependent Optical scattering depending on the scatterer size to incident wavelength ratio. Describing forest scattering in this way is similar to the methods used to predict vertical backscatter behaviour in Chapter 5. The theoretical data of the Matchstick Model and RT2 modelled backscatter crucially suggest that saturation is not necessarily determined by attenuation levels. One of the key questions of Chapter 7 is whether backscatter is a trustworthy indicator of forest volume or biomass? This question is analysed for varying volume levels at which scattering transitions by stems take place and through number density variations resulting from thinning behaviour which impacts directly on forest basal area.

Chapter 8 is the final experimental chapter of the thesis and is primarily a further study of the Matchstick Model description of forests and forest backscatter. In addition to exploring the theories of the Matchstick Model it utilizes the SERA model, introduced in Chapter 3.2 and featured in Chapter 4 to provide the forest

description. Due to the level of detail provided by SERA and its depictions of forest stands as multi-age, and potentially multi-species collectives, the forest can be segregated into Optical and Rayleigh scatterers according to stem sizes at each stage of growth. This allows backscatter to be calculated in terms of all scatterers present, or solely for the Rayleigh or Optical scatterers alone. This is a clear advancement on the scattering scenario provided by the Matchstick Model forest as it allows a more realistic distribution of stems through its ability to model multiple aged stems within the same stand as a consequence of mortality and subsequent regrowth. Chapter 8 provides an analysis of the scattering behaviour predicted throughout this thesis in a setting more closely linked to the natural arrangement of forests. Where in Chapter 7 the user was required to define thinning behaviour and scaling values using the WBE framework the work of Chapter 8 is less user driven and more dependent on growth behaviour provided by the SERA model as a consequence of competition for light and space. The existence of competitive behaviour within the model allows a forest to vary its thinning rate, to encourage regrowth, to cope with mortality, and to provide a more heterogeneous environment in keeping with forests which may have been involved in previous remote sensing studies. An advantage of the approach adopted in Chapter 8 is that the scattering behaviour typically associated with empirical studies can be described in terms of all scatterers present within the forest rather than according to samples as may be the case with forest field measurements. This is not to say that modelled data is more advantageous than empirical data but rather that it provides a more controlled environment to investigate specific influences. This is especially true if the data correspond closely with published trends and an alternate explanation for backscatter saturation behaviour can be provided.

The experimental work of this thesis aims to produce novel work to accompany those discussed in Chapter 1.3 by answering the questions of Chapter 1.1. Particular attention is paid to the influence of forest structure on the vertical and horizontal backscatter profiles, and the consequences for interferometric measurements. The findings are discussed in Chapter 9 with the conclusions given in Chapter 10.

4 A Macroecological Analysis of SERA Derived Forest Heights and Implications for Forest Volume Remote Sensing

Matthew Brolly and Iain. H. Woodhouse

Summary

This chapter was initially written in 2010 and submitted to PLoS ONE Open Access Journal in 2011, it is currently in review. The work presented in this paper is a study of the relationships between forest height classifications and forest volume values. The findings of the work are intended to inform on the indirect forest volume retrieval methods using allometry (See Chapter 1.4) and forest height data retrieved from InSAR and LiDAR methods. As a tool for investigation the forest model SERA (Chapter 3.2) is incorporated into this study to provide in depth details of forest geometry on a stand level. SERA can be used to monitor the effects of macroecological variations on the relationship between height and volume with analysis of all trees within a stand. As a modelling exercise this chapter is intended to highlight potential pitfalls in using forest height as an indicator of forest volume but also to discuss the importance of correctly classifying height for volume conversion particularly when height is associated with interferometric processes.

The work is presented here as a stand alone article but also as an introductory experimental chapter for the thesis that serves to highlight the usefulness of forest growth models particularly in providing data on size and number distributions. As a precursor to backscatter modelling incorporated in the following chapters it highlights how simple structural variations can impact on macroecological relationships and subsequently on the interpretation of remotely sensed data. SERA is also used in Chapter 8 to interpret backscatter relationships with macroecology while the vertical

structure and consequences for interferometry are covered in Chapters 5 and 6 immediately following this work.

This chapter aims to address the following questions:

1. What correlation is predicted by SERA to exist between forest height and forest volume?
2. How does this correlation vary when height is described in different ways, across number density variations, species definition, and resource restrictions?
3. What implications do the relationships described by SERA have for remote sensing studies used to determine forest height such as SAR interferometry and LiDAR?
4. Is there a height classification predicted by SERA to be suited in terms of a physical connection with scattering behaviour that is also related to volume?

The work featured in this paper was entirely produced by myself including idea formulation and work undertaken. Influence was provided by S. Hammond and Prof. Niklas of Cornell University regarding the effectiveness of their SERA model acknowledged as a significant contribution to this work. Help was provided by Dr. Woodhouse with editing and inspiration within a supervisory role.

4.1 Abstract

Individual trees have been shown to exhibit strong relationships between DBH, height and volume with studies citing these as justification for use in forest volume estimation through remote sensing. With resolution of common remote sensing systems generally too low to resolve individuals and a need to cover larger areas, these systems rely on descriptive heights which account for collections of trees in forests. For remote sensing and allometry applications this height is not entirely understood in terms of its vertical location, but here we ask whether an

understanding of this height value is required to make accurate forest volume estimates?

A forest growth model (SERA) is used to analyse forest canopy height relationships with forest wood volume. The heights maximum, Mean, H100, and Lorey's are examined for their variability under number density, resource and species variations. Findings are analysed for their implications to forest remote sensing techniques such as LiDAR and radar interferometry.

Traditional forestry measures of maximum height, and to a lesser extent H100 and Lorey's are shown to exhibit little consistent correlation with forest volume across modelled conditions. Implications being, that using forest height to infer volume or biomass, remote sensing would require species and community behavioural information to infer accurate estimates using retrieved height alone. SERA predicts Mean height to provide the most consistent relationship with volume of the height classifications studied and overall across all forest variations.

Height classifications investigated here are potentially linked to radar scattering centres with implications for their use with allometry. These findings may be used to advance forest biomass estimation accuracy through remote sensing. Furthermore the use of Lorey's height with its specific relationship with remote sensing physics is recommended as a more universal indicator of volume when using remote sensing than can be achieved through either maximum height or H100.

4.2 Introduction

Accurate global forest inventory and above ground biomass estimates remain an uncertain element in our understanding of the global carbon cycle (Cramer et al. 2004; Magnani et al. 2007). Remote sensing by current and future techniques using

SAR and LiDAR are expected to play an increasing role in reducing such uncertainties; alone and in synergy (Sun et al. 2011). Both of these techniques suffer from inaccuracies associated with their estimation of biomass. For SAR there are empirical results showing that relationships exist between the intensity of backscatter and the biomass of a forest so that an accurate estimate of biomass can be determined directly, but this technique is hampered by the existence of a saturation effect (Dobson et al. 1992; Imhoff 1995a) seen both in empirical (Dobson et al. 1992) and theoretical studies (Bergen and Dobson 1999), and through a lack of consistency across different forest types. The source of the saturation effect and the information that can be extracted at volumes above this saturation biomass are a topic of debate ((Imhoff 1995a; Wang and Ouchi 2005; Waring et al. 1995; Woodhouse 2006b). A significant problem is that approximately 81% of the world's forests contain biomass beyond the saturation level currently associated with P-Band SAR (Imhoff 1995a) -- the frequency of choice for the proposed European Space Agency mission, BIOMASS (Lin et al. 2008)). The level of this saturation is approximately 100-200t/ha (Patenaude 2003).

For SAR height, values can be inferred from polarimetric-interferometric radar (Hajnsek et al. 2009). The estimation accuracy, with respect to forest height, has been shown to be in the order of 10-15% for particular studies (Mette et al. 2002) but still requires the use of allometric equations to convert to biomass. For LiDAR the relationship between the LiDAR return and the height of the forest is more direct, with uncertainties associated largely with footprint size. For both large footprint (>10m) LiDAR and SAR, the direct relation to "canopy height" as measured in the field is not well-defined, and different methods of calculating a mean, or representative height are used (e.g. H100, Lorey's height, etc.). Some examples of the variations in LiDAR recorded height are quantified in terms of system and survey characteristics in (Disney et al. 2010).

In both the LiDAR and SAR cases allometric equations are required to determine biomass and this entails a high degree of uncertainty. Allometric equations are traditionally based on the properties of individual trees, with power law relationships between DBH, stem height, or a combination of the two. Now that height is measurable over large areas, there is growing interest in the allometry at the stand or plot level, so that the allometry takes the form:

$$M_{Forest} = aH^c \tag{4.1}$$

Where H is some average forest height, and a, and c are constants that vary with species, forest type, etc. An average height is typically used as Maximum height is not necessarily a good indicator of forest volume. This is the focus of this paper, namely to evaluate the following alternative height descriptions as indicators of biomass: Mean height, H100 and Lorey's height, and to consider how their relationship to biomass varies with respect to population, species, resource, and area variations.To achieve this, the forest growth model SERA (Spatially Explicit Reiterative Algorithm) is used to investigate the height-volume relationships at plot scale of simulated forests (Hammond and Niklas 2009). This allows the evaluation of several different descriptions of height as an indicator of plot level volume. Our link to biomass depends on the assumption that wood density is relatively consistent for any given forest composition, with genus level means giving reliable approximations of species values (Chave et al. 2006), and cross species examples explored in terms of both biomass and volume units where wood density variations may impact on results.

4.3 Methodology

4.3.1 SERA

SERA (Hammond and Niklas 2009) models tree growth within a population through the incorporation of ensemble behaviour. Due to the inherent constraints of space and

light within SERA and the allowance of species variation, it is able to mimic forest dynamics resulting from competition. As an output, SERA provides information regarding canopy size and composition as well as stem information including volume, weight (based on species-specific wood density), size, and location. SERA can be programmed to model a user-defined area, as well as user-defined conditions such as light intensity and number of seeds planted. In all cases the topography is flat. The model can also be set to span a user-defined number of years. SERA has accurately predicted several relationships that have been identified within an empirically modelled *Abies Alba* population (Hellrigl 1974). Of these relationships the two of particular importance, and the reason for this model's significance here, are the relationships between mass/volume and height, and of height to diameter. The model is used to investigate the variations in these relationships when forest community conditions are altered in terms of number density, resource availability, and species variation.

Within SERA each plant is intentionally simplified to consist of a single photosynthetic surface elevated by a single stem, but in this work the canopy is only used to determine ensemble growth. The stem is used to determine volume/biomass. SERA has the ability to predict the fate of a species under varying degrees of spatial and temporal heterogeneity, primarily through space and light variations. SERA's ability to model backscatter is studied in Chapter 8 with the model introduced in Chapter 3.3.

4.3.2 Height Classifications and Remote Sensing

In principle, the height of a tree can be defined as the distance of the maximum point vertically from the ground surface (even though other height measures can be used for specific purposes). For a community of trees, the average height can be described in several ways. The Maximum canopy height represents the height of the tallest tree; the Mean height represents the arithmetic mean of the summed trees; H100 represents

the mean height of the 100 trees with the largest DBH within one hectare; Lorey's height refers to the height of the trees weighted by each basal area. With the ability to quantify community height in several ways it is important to consider how heights obtained from SAR, LiDAR and traditional Optical remote sensing compare to these various height descriptions. Mean canopy height is extremely difficult to measure in the field due to the need to account for every single tree (additionally, due to its unweighted nature it is easily influenced by mortality of tall individuals). Average height can be simply the arithmetic mean as featured here but can also be sample based if all trees are not measured (typical of larger stands). H100 remains less complicated due to the requirement to identify and measure 100 trees but in a stand of 1 ha size such a measurement will likely be very close to the Maximum tree height which remains the simplest measurement due to the need to identify and measure only the single largest tree. H100 (Mette et al. 2004a) and Maximum height (Lefsky et al. 2005a) are expected to resemble one another very closely, particularly for mature stands while Lorey's height is a basal area weighted mean height, equation (4.2) (Lefsky et al. 2005b). The difficulties in acquiring such field measurements are great due to the need to measure all trees, but due to the influence of larger trees on this height class the omission of smaller stems will have less of an impact than exhibited on Mean height. For Lorey's Height, H_i and A_i represent the individual characteristics of each tree within the sample area in terms of height and area respectively.

$$H_{Lorey} = \frac{\Sigma\left(H_i \text{ x } A_i\right)}{\Sigma\left(A_i\right)} \tag{4.2}$$

Trees with a large basal area, and therefore large volume, contribute more to Lorey's Height than trees of a small basal area (allometry suggests that these trees will also tend to have the smallest heights and volumes). Lorey's height is therefore also approximately weighted by crown area (on the assumption that crown size is correlated with basal area). These properties make it very appropriate for remote sensing, given that any pixel-based height determination will be influenced most by

the larger trees. Lorey's height highlights the larger trees, in a similar way to the contribution we might expect from each tree within a collection of SAR pixels, or a large LiDAR footprint.

4.3.3 SAR Inferred Forest Height

Forest height retrieval using SAR interferometry has been employed as a technique for more than a decade and has taken on several guises. Single pass interferometry (Faller and Meier 2002; Kobayashi et al. 2002; Treuhaft and Siqueira 2000), repeat pass interferometry (Askne et al. 2003; Floury et al. 1997; Hagberg et al. 1995; Hyyppä et al. 2000; Wegmuller and Werner 2002); single baseline polarimetric interferometry (Cloude et al. 2009; Cloude and Corr 2003; Cloude and Papathanassiou 1998, 2003; Papathanassiou and Cloude 2001, 2002; Treuhaft and Cloude 1999, 2002); multi-baseline interferometry (Treuhaft and Cloude 1999; Treuhaft et al. 2004); and multi-baseline polarimetric interferometry (Stebler et al. 2002).

When using interferometry, identifying the phase centres corresponding to the canopy and the ground is a necessary requirement for canopy height estimation. The phase differences between interferograms represent the height difference between the effective phase centres of the corresponding scattering mechanisms. The interferometric scattering phase centre height from SAR interferometry is therefore the vertical location within the canopy from which most of the backscatter signal is returned. For dense forests and short wavelengths the scattering phase centre can be close to the canopy top, while for sparse forests with gaps or using longer wavelengths this can be closer to the forest floor (Madsen et al. 2002). Additionally, when applying polarimetry to interferometric SAR (InSAR) (Cloude and Papathanassiou 1998) the existence within the forest of different scattering processes, occurring at different heights, produces different polarimetric results. High interferometric decorrelation results in high errors which propagate through to

biomass estimation. Forest structure has been shown to have a high impact on interferometric coherence (Cloude et al. 2009).

4.3.4 LiDAR Inferred Forest Height

In order for LiDAR to calculate forest height, identification of the ground is also required. In order to create an accurate representation of the ground all returns identified as being non-ground must be removed from the analysis. Different filtering techniques exist but the major assumption made is that in discrete return LiDAR the last returns are ground returns (Dubayah and Drake 2000). The surface model is generally derived from the distribution of the first returns while the terrain model is generated through the filtering of the last returns to isolate ground reflections. For full waveform LiDAR, canopy height is calculated through conversion of the two-way travel time differences between the two most prominent modes in the amplitude waveform which is then converted into a distance measurement. The difficulties here lie in the fact that the identification of the two most prominent modes may not always correspond to the highest point in the canopy but instead be a function of canopy structure (Nelson et al. 1984). Large footprint systems are most effective when the canopy profile metrics are to be derived while the use of small footprint radar systems are applicable for more small scale surveys related to forest management, as crown diameter can be estimated and species identified.

Comparative results of LiDAR against InSAR canopy height estimation have been published in work such as (Balzter et al. 2007) and (Andersen et al. 2003).

4.4 Results

4.4.1 Forest Height Analysis

SERA was used to produce forest stands of both angiosperm and gymnosperm communities. With *Abies Alba*, European Silver Fir being the most thoroughly researched forest structure input into the SERA model it is important that this species features heavily. *Cryptomeria*, Cedar, is also included as a specific species while generic representations of angiosperms and gymnosperms are included. For each forest identity, planting densities are varied to cover the possibilities of 1, 100, 1000, 10000 and 25000 seedlings per hectare (the *Abies Alba* source plot as referenced in (Hammond and Niklas 2009) was such a plot size). As a result of this extensive range of plantings, the effect of initial planting density on the forest dynamics is examined through the life of the forest with the possibility that forest heights will vary greatly for similar forest volumes. In effect the level of influence of number density, volume, basal area, height, space and light intensity (resource availability) on the forest dynamics was extensively investigated in order to distinguish what various forest heights reveal about forest volume.

4.4.2 The Influence of Number Density

Within forest conditions under high number density, individual trees will grow with tall and thin stems with less emphasis on mechanical stability due to the sheltering effects of neighbours. Canopy components would be solely located in the upper realms of the stem due to light competition. Under low number density conditions the lack of competition for light, as well as less protection, allows a tree to focus on reproductive capability and mechanical stability. The result being that a different distribution of height and DBH will exist.

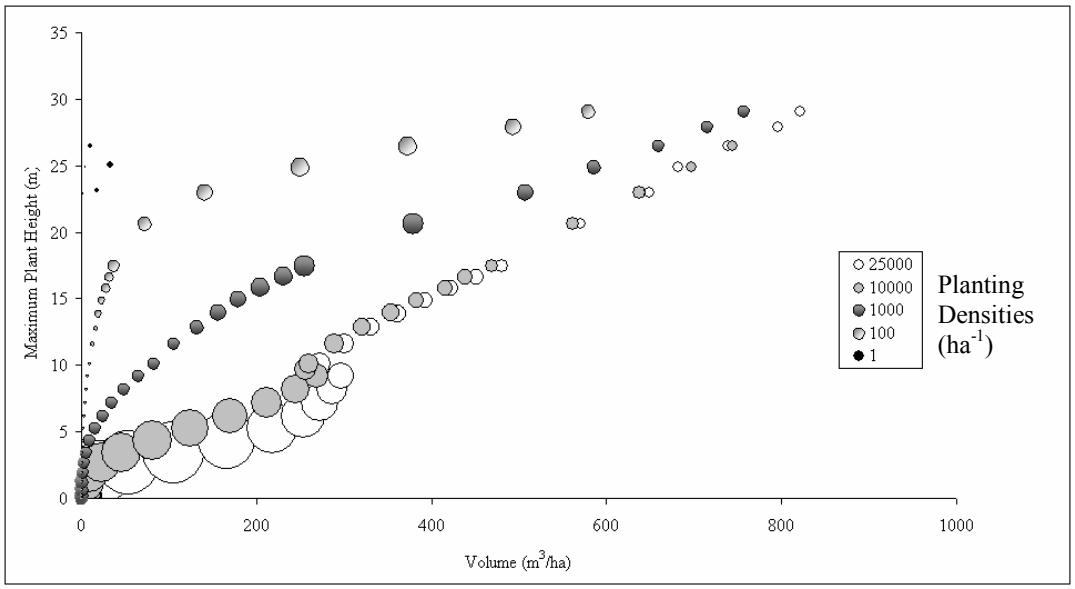

Figure 4.1. *Abies Alba* SERA modelled Maximum plant heights over a period of 100 years against stand volume per hectare. Larger circles represent larger number densities with changes resulting from competitive thinning of the initial planting densities.

The same trend is apparent between Maximum Tree Height and Stand Age for all planting densities simulated by SERA but when Maximum height values are plotted against stem volume (Figure 4.1) correlation is only evident between the high density planting cases of 10000 and 25000 stems ha^{-1}. These high planting density values are realistic for initial seeding with a particular study showing the presence of up to 763 seeds/m^2 (Granström 1982). The problems related to biomass estimation using height-based allometry are immediately apparent. For example, a SERA generated forest with a Maximum plant height of 25m could be contained within a forest volume of any from 32, 250, 586, 681 or 697 m^3/ha. Although the allometry suggests that the Maximum height of a plant will relate favourably to the volume it appears through SERA predictions that such a relationship is less stable for the community scenario. Interest is paid to the full volume density range of the forest so that insights can be provided into behaviour both above and below typical backscatter saturation levels, which at P-Band can be as high as 200 tha^{-1}.

In each species case, the conclusion remains the same that the number density clearly affects the relationship between height and volume with each case indicating that the Maximum heights capable within the forest are achieved at lower volumes when the initial planting density is less. This imbalance between forest dynamics would indicate that forest Maximum height to volume is a relationship which relies on the total basal area or planting density of the stand to define it. In each case studied here, as would be expected under the same resource limitations, the data converge at high volumes so that the Maximum height of the forest is uniform across all planting densities. This does not signify a strong relationship but rather tells us that forest configurations eventually converge to replicate one another in a space filling and constant resource environment. If this is a common case then it is possible that the knowledge of number density at this stage of growth may be used to infer forest volume.

With such variation in Maximum forest height for particular volumes, an assessment of the number density relationship to H100, Mean height, and Lorey's height is explored with immediate results showing a better relationship between Mean height and volume under number density variations (Figure 4.2), with the relationship of volume to Lorey's height (Figure 4.3) improving slightly on the relationship exhibited by Maximum height. H100 is not shown here as it largely follows the trends of Maximum height, particularly with large planting densities with these heights best suited to establishing forest age rather than volume.

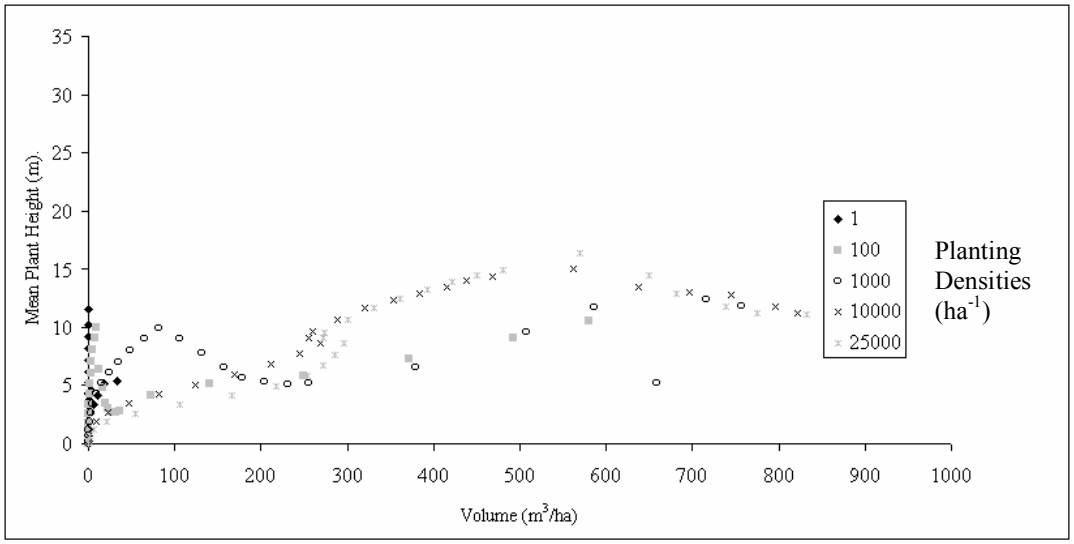

Figure 4.2. SERA modelled *Abies Alba* Mean plant heights against stand volume over a period of 100 years for various planting densities per hectare. For number density variations associated with each planting density the reader is referred to the trends shown in Figure 4.1.

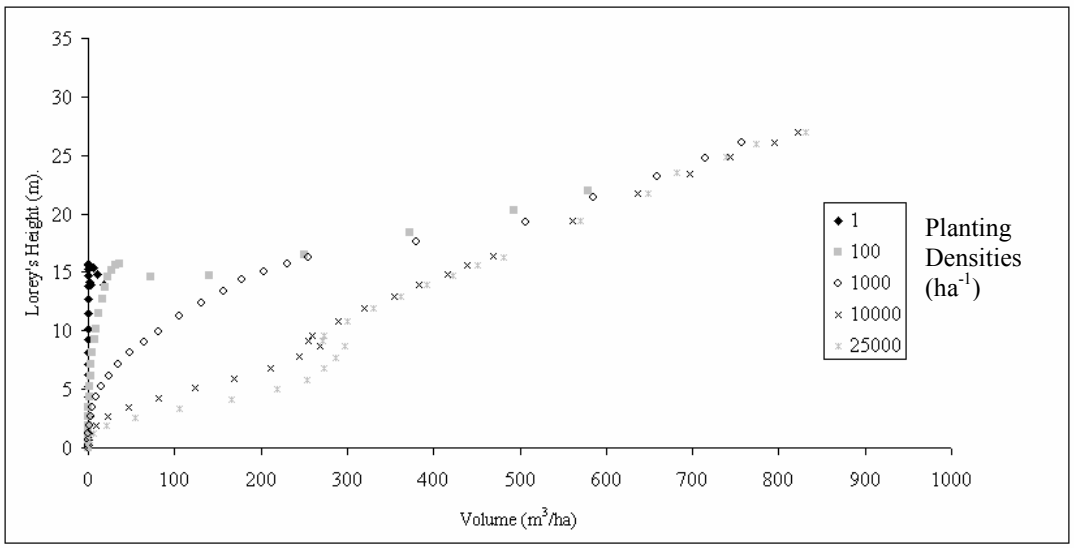

Figure 4.3. SERA modelled *Abies Alba* Lorey's heights against stand volume over a period of 100 years for various planting densities per hectare. For number density variations associated with each planting density the reader is referred to the trends shown in Figure 4.1.

4.4.3 The Influence of Species Variation

Figure 4.4 shows the variations that exist in forest Maximum tree height as a consequence of species variation for a particular planting density. The mixed species plots incorporate all featured species. For Mean plant height, familiar trends exist over the 100 year period with *Abies Alba* being a slight exception to the trend. Each data set exhibits behaviour to suggest the existence of a species optimum Mean height over the time period in question. When these height data are plotted against volume it appears that the Maximum height is a good indicator of forest volume at volumes above 300m^3/ha across all species when planting density is constant, with similar conclusions for H100 and Lorey's height (Figure 4.5). Mean height (Figure 4.6) as a comparison produces trends that indicate its potential as a useful parameter for indicating forest volume regardless of species.

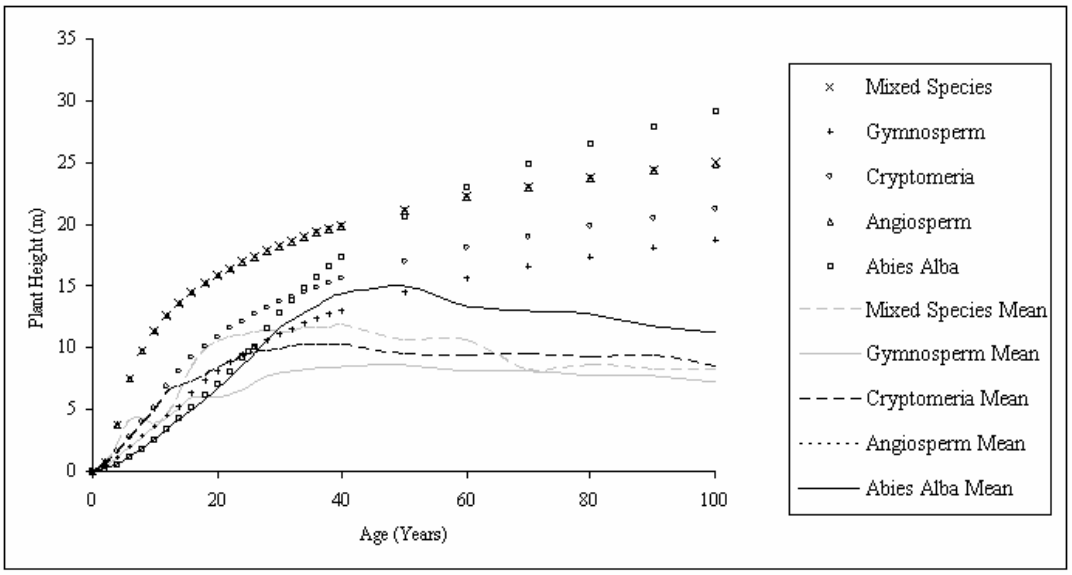

Figure 4.4. SERA modelled Maximum and Mean plant heights within forests of initial planting density of 10000 stems. Species definition is given in the legend along with identification of mean data.

The effect of species produces similar trends at various planting densities but in general the variation of species has a small effect on the relationship between Mean forest height and forest volume in comparison to planting density variation. Although primarily Mean height and then Lorey's height appear to be the most consistent height classifications for volume estimation on an interspecies level, small variations in Mean plant height from the expected trajectory could result in large variations in volume estimation due to the low rate of change of Mean height per unit volume. Quantifying the difference between the two least correlated species datasets could be used to provide a SERA predicted error estimation associated with each height.

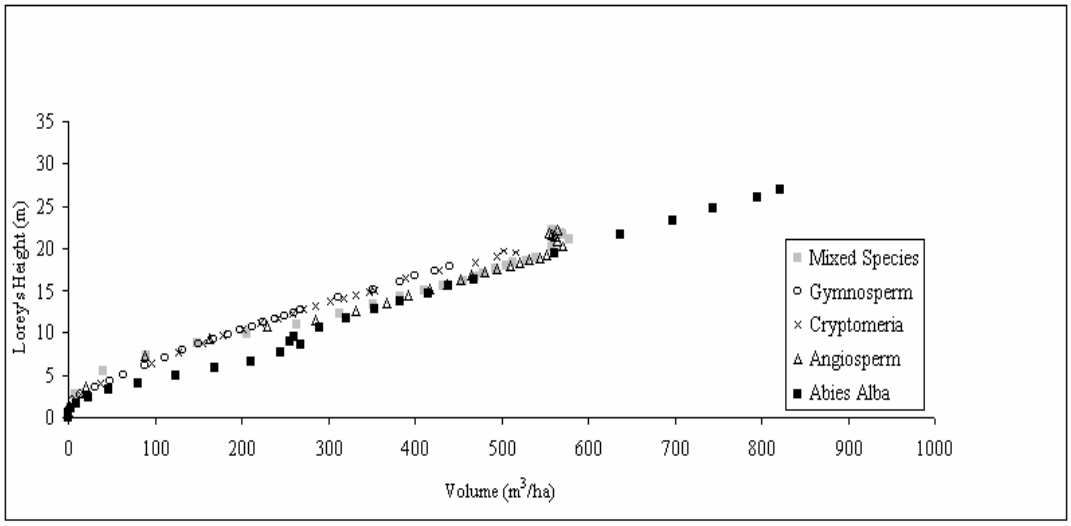

Figure 4.5. SERA modelled Lorey's height against forest volume plotted for different species at planting densities of 10000 ha^{-1}.

For any particular planting density the interspecies trends appear to resemble one another but do not hold as well under variation of both species and planting densities. A key question is then whether the possibility exists that knowing the current number density could be sufficient for determining volume across species using an interferometrically retrieved height and quantifying the potential errors in estimation using plots such as those of Figures 4.5 and 4.6. The data in Figure 4.1, showing the

effects of planting density, on the relationship suggest this could be possible in mature forests where number densities are predicted by SERA to converge.

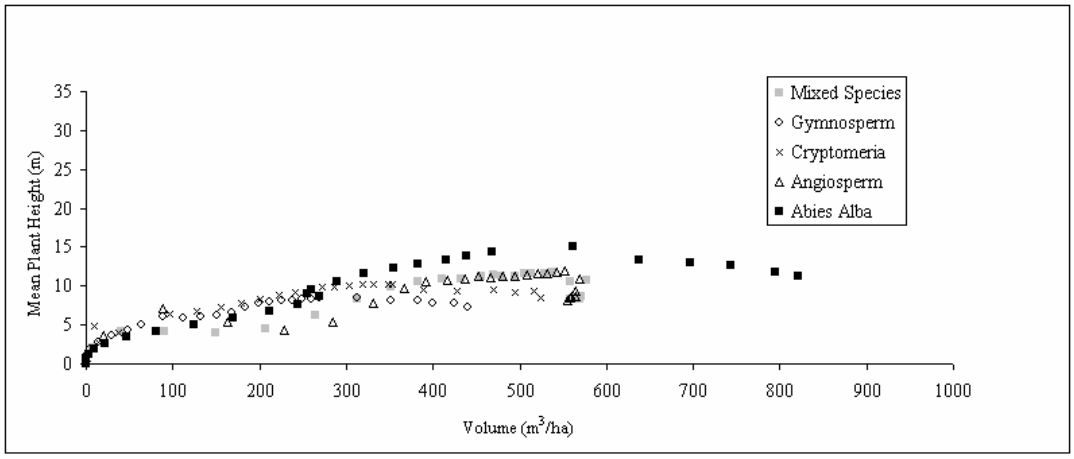

Figure 4.6. SERA modelled Mean forest plant heights against forest volume plotted for different species at planting densities of 10000 ha^{-1}.

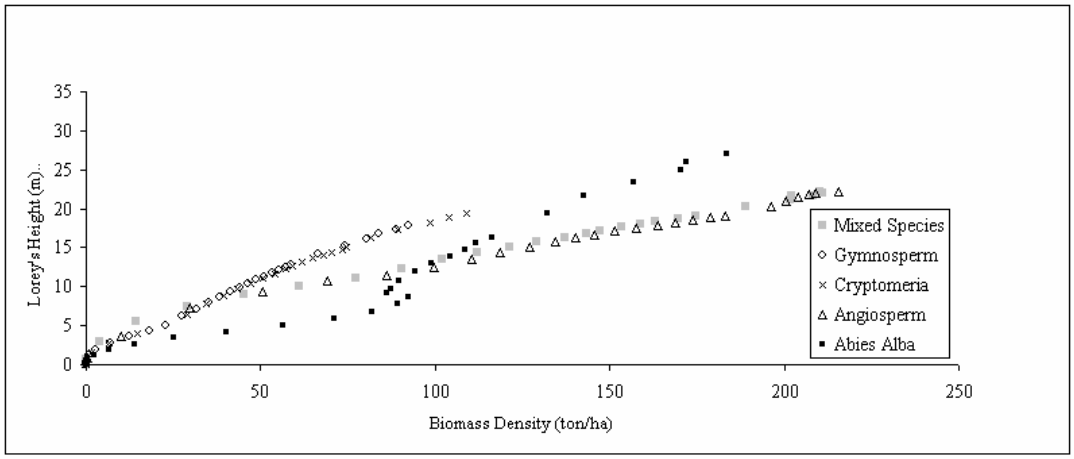

Figure 4.7. SERA modelled Lorey's height against stem biomass density plotted for different species at planting densities of 10000 ha^{-1}.

Consideration of the relationship of height with biomass density is also important when comparing across species. When examining stands in such a way, variations to the trends exhibited between volume and height may be apparent as a result of wood density variations from species to species, a consideration that is not required when exploring within a single species. SERA has the ability to predict mass based on field

calculated wood density values for each species and although small differences are exhibited the general trends remain the same with Mean height continuing to produce the greatest correlation with biomass density across each different species stand. Comparison of Lorey's height with respect to both volume and biomass density highlights how difficult it is to correlate across species (Figure 4.7) with Lorey's height only improving slightly on the offerings of H100 and Maximum height correlation levels.

Tables 1 and 2 contain the R^2 data relating each height classification when compared to equations representing the best fit through all data sets examined in Table 1 and for the best fits associated with each individual species set in Table 2. The "All Data" section in Table 1 provides information for all datasets used in this study which are combined to create a best fit for each height classification, the absence of this section in Table 2 is due to the species specific equations used. Figure 4.8 shows the spread of the height data with respect to the volumes predicted by SERA. Note the best fit equation for Mean plant height which represents the particular Mean Plant H "All Data" equation used in Table 1.

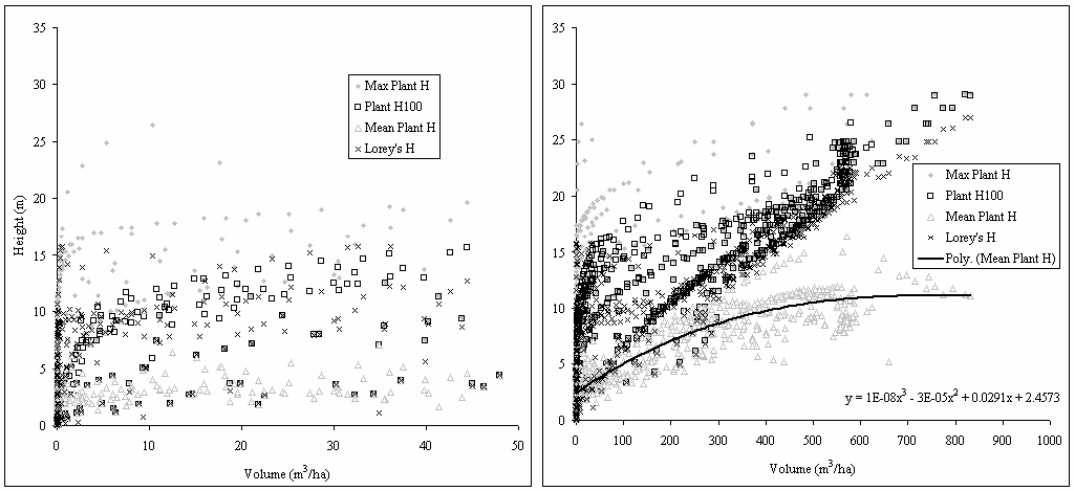

Figure 4.8. SERA modelled height data for all featured forest configurations under the same environmental conditions of light intensity and space (left) shows data up to $50m^3ha^{-1}$ while on (right) data is shown across the entire range up to $1000m^3ha^{-1}$. Legend provides height classification.

Table 4.1. R^2 values associated with the combination of all forest composition data sets with default resources. Predicted values used for comparison generated from "all data" equations associated with best fitting curves for each height classification using all data sets.

	Max Plant H	Max Stem H	H100 Plant	H100 Stem	Mean Plant H	Mean Stem H	Lorey's Height
All Data	0.51	0.51	0.73	0.73	0.75	0.76	0.71
Abies Alba	0.47	0.47	0.75	0.75	0.64	0.66	0.62
Cryptomeria	0.56	0.56	0.78	0.78	0.86	0.86	0.75
Generic Angiosperm	0.60	0.60	0.75	0.75	0.82	0.82	0.79
Generic Gymnosperm	0.55	0.55	0.72	0.72	0.78	0.78	0.73
Mixed Species	0.65	0.65	0.81	0.81	0.88	0.89	0.85

Table 4.2. R^2 values associated with each individual forest composition data set with default resources. Predicted values used for comparison were generated using best fitting curves from SERA generated data for each individual species data for each height classification.

	Max Plant H	Max Stem H	H100 Plant	H100 Stem	Mean Plant H	Mean Stem H	Lorey's Height
Abies Alba	0.45	0.45	0.70	0.70	0.64	0.66	0.50
Cryptomeria	0.51	0.51	0.71	0.71	0.90	0.64	0.73
Generic Angiosperm	0.49	0.49	0.70	0.70	0.82	0.82	0.82
Generic Gymnosperm	0.50	0.50	0.70	0.70	0.81	0.81	0.73
Mixed Species	0.55	0.55	0.79	0.79	0.88	0.89	0.82

4.4.4 The Influence of Environmental Conditions

When discussing the influence of environmental conditions on forest height dynamics, the factors that have the most significant effect on the growth of the forest are related to the life cycle. Forest growth requires light and carbon dioxide, water, space, and nutrient availability. With SERA, the dynamics of the forest in relation to light intensity can be manipulated as well as the ability to constrain the area in which the forest can grow. Of particular interest is how light intensity affects the nominated classes of H100 and Lorey.

4.4.4.1 Light Intensity

Forests experience different light intensities depending on their latitudinal location due to the angle of illumination and increased amount of atmosphere which the light must traverse at high latitudes. This section considers the consequences of light intensity reduction predicted by SERA on height to volume relationships. For the *Abies Alba* datasets the relationship variations resulting from light intensity fluctuations appear to apply across all planting densities. The general trend over a 100 year period is for forests exposed to lower light intensities to grow on average at a faster rate of height per unit volume as the forest as a whole accumulates less carbon over time for height gain as a result of reduced resources. Ultimately over the 100 year period the Maximum height and total volume accumulated are less for the low light intensity forest behaving in a manner of a slow developing forest. The variations are a result of increased thinning per unit volume within the forest to enable each surviving tree to capture the same level of light required for growth. The 100% light intensity stand will therefore allow more stems to grow to their maximum potential resulting in higher trees and higher volumes in part due to a higher and efficient rate of thinning per year. Similar behaviour is examined in the modelling conducted in (Murrell 2009) as a result of slow growth rates.

Due to the variations in forest structure caused by light variations, the relationship of Maximum forest height to forest volume does not hold across all light intensities and is affected proportionally to the amount of light intensity reduction. A greater rate of change of forest Maximum height with volume is displayed for lower intensities but the gradient increase is not necessarily linear. Similar findings are evident for the Mean height of the forest but with the surprising aspect being that forests subjected to lower intensity light can produce the maximum values of forest Mean height, predicted for *Abies Alba* at low planting densities. This trend suggests that there are fewer smaller trees at particular times due to the low light intensity therefore the mean value would be biased to the size of the more abundant older and larger trees. Although thinning rates are altered by the variation in light, the allometry of trees is not predicted by SERA to vary under these conditions.

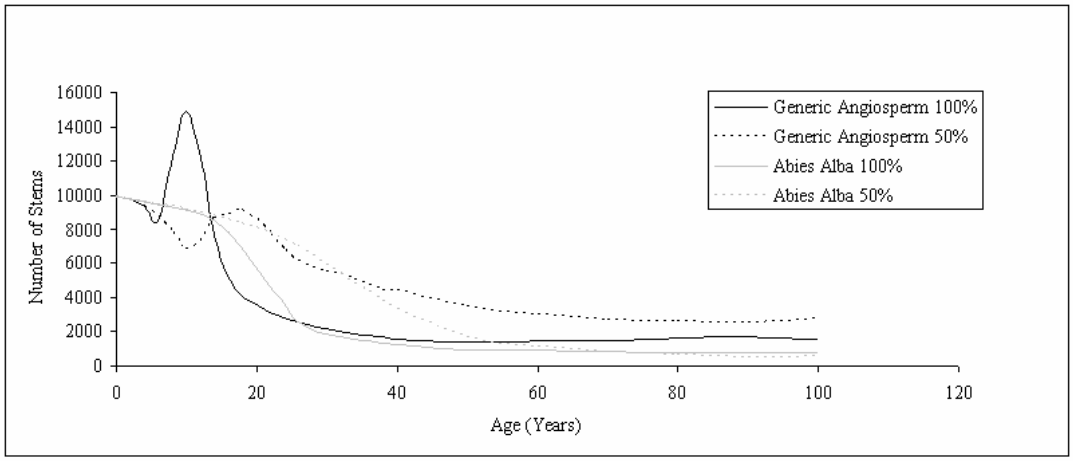

Figure 4.9. SERA modelled thinning with respect to age for *Abies Alba* and Generic Angiosperm. Planting densities of 10000ha^{-1}. Legend shows light intensity as a percentage and species variations.

For the generic angiosperm cases the rate of thinning is different to that seen for *Abies Alba* (Figure 4.9). The most significant difference being that, following early mortality, there is a greater surge in new growth seen for Angiosperms. The populations under light constraints produce reduced levels of this regrowth at later stages in accordance with light reduction. For angiosperms under light intensity

restrictions it is difficult to relate the Mean height of the forest to the volume contained within with the Mean height being almost constant as forest volume increases.

The Angiosperm communities also show evidence of an optimum volume varying according to the light intensity. With a limitation in resources this optimum value reduces as expected for a theory linking resources with the amount of live biomass a plot can support. The Maximum plant height for a particular volume still remains higher in the presence of greater light intensity and this appears an interspecies trend. The Mean height is also much more closely related to volume regardless of light intensity but when the data is plotted a problematic scenario is introduced where small Mean height changes can indicate very different volume values due to the shallow gradient. This in practice could signify a lack of a durable relationship between Maximum height, H100 or Mean height with volume under the constraints of light limitation, but the relationship with Lorey's height shown in comparison to H100 (Figure 4.10) does not suffer in the same way, with a more general level of increase in height registered for all increases in stand volume.

All forest variations modelled here show that the more light intensity a forest is subject to, the greater the rate of thinning per year. This is a direct result of the dynamics of the forest, which in the presence of sufficient resources will dictate an optimum tree growth to satisfy "fitness" needs. A forest that demands a balance between these "fitness" parameters will grow thicker and attain height with no compromise for stability linking total basal area of the stand to the forest volume and elevating the relevance of Lorey's height. When compared to basal area increase at high volumes Lorey's height exhibits less change in height for small changes in basal area than is shown for H100, in a similar fashion to the volume case of Figure 4.10. (Inversely as already stated the rate of thinning per unit volume is lower for the greater intensity of light suggesting a more efficient method of thinning while increasing volume).

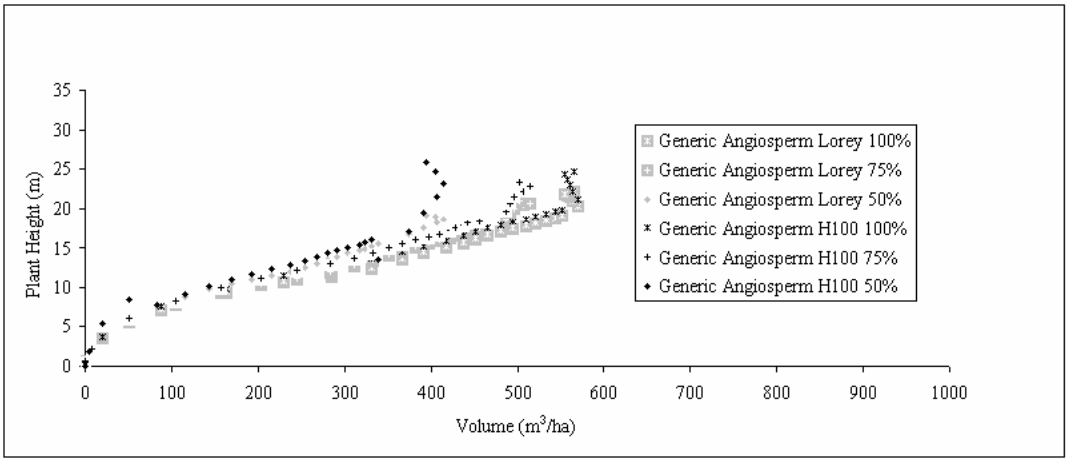

Figure 4.10. SERA modelled angiosperm populations of initial planting density of 10000 ha^{-1} exposed to varying percentages of light intensity. Show for Lorey's height and H100 against volume.

For each species, when light intensity is reduced, the number of stems making up a particular volume also reduces. This suggests that the trees under light restrictions are bigger for any particular forest volume, but as the rates of thinning over time show, the forest with less light thins slower as it undergoes competitive growth at a slower rate. This is seen by the reduced level of carbon accumulation in the SERA data. After 100 years SERA predicts that the stand with the least light will consist of more trees but with a lower Mean height as their growth has been stunted and thinning rates are less efficient as trees struggle to exert dominance. At any particular stand age the volume associated with the lower light intensity is lower as would be expected in a natural setting. The maximum volume over the 100 year period is therefore significantly lower for the stands exposed to reduced light intensity with all volumes showing a lower basal area for the lower light intensity, highlighting the effects of limiting resources. In Figure 4.11 it is shown how light variations are evident in the relationship of height to volume for each height classification. The relevance of these findings is discussed in Chapter 4.5.2.

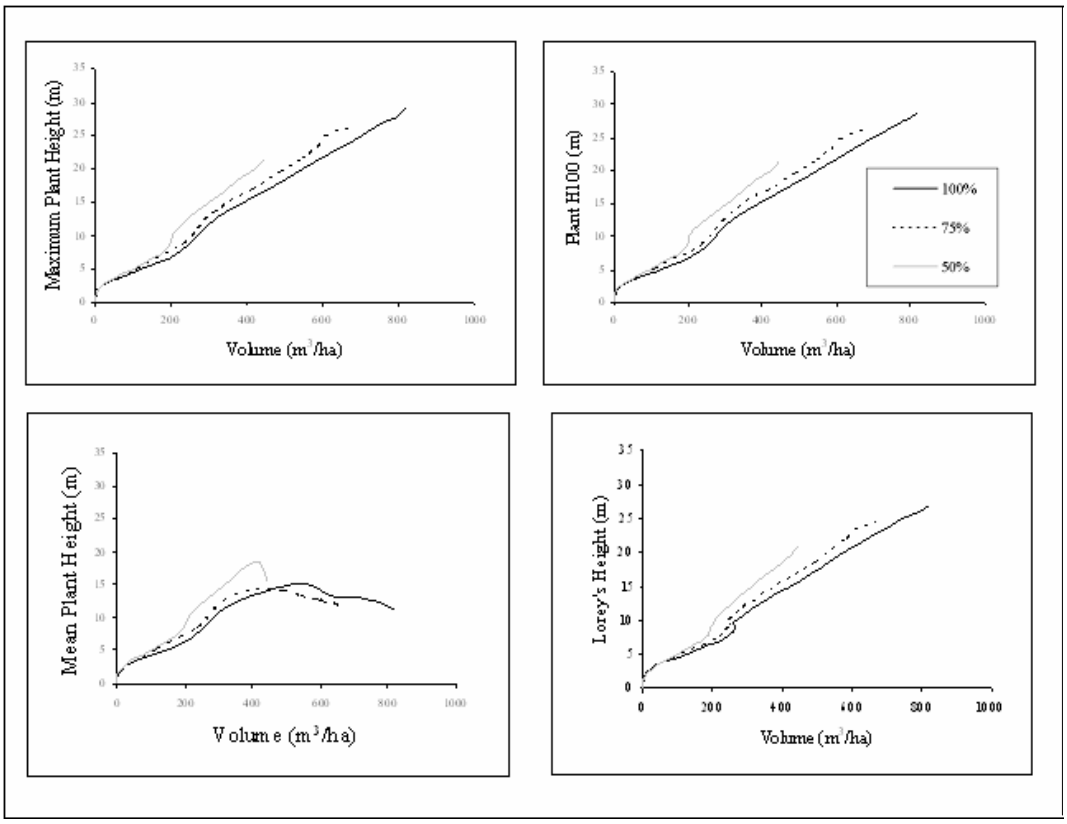

Figure 4.11. SERA modelled *Abies Alba* stands of planting density 10000ha^{-1} exposed to variations in light intensity (100%, 75%, 50%). Data shown clockwise from top left for Maximum, H100, Lorey's and Mean plant height.

4.5 Discussion

4.5.1 The Relationship Between Forest Height and Volume

All species and planting density data exposed to 100% light intensity over a 1ha area are plotted in Figure 4.8 in the form of Maximum, Mean, H100 and Lorey plant heights. The variations due to planting densities can be clearly seen for the data of H100 and Maximum plant height in which both show similar trends, albeit at different height levels. Lorey's height is also affected but shows a tighter relationship with volume. On the other hand the Mean forest height shows a consistent correlation with the volume of the forest as highlighted by the line of best fit; a cubic polynomial

producing an R^2 value of 0.75 between predicted and actual Mean height. This is slightly more accurate than the linear best fit which produces a lower R^2 of 0.67.

Regardless of species, planting density or basal area, the relationship between Mean height and volume remains more consistent than the other height classes investigated. Tables 1 and 2 show the R^2 correlation values of predicted volume against actual volume as provided by the relationship of all species data and individual species data respectively. Correlations are also improved on removal of stems < 2m high, but by doing so, the accuracy of the macroecological forest description is reduced.

The relationship between Maximum plant height and volume produces an R^2 value of only 0.51 for the combination of all datasets equation shown in Table 4.1 and thus appears clear that this parameter is not representative of forest volume. For both the Table 4.1 and 4.2 descriptions Angiosperm and Gymnosperm communities are represented well by their relationship of forest Mean height to forest volume, and poorly represented by Maximum height. On a singular species level the correlation of Lorey's height is high with the exception of the *Abies Alba* data set, which H100 provides a better correlation and suggests that Lorey's height is more applicable for use across species. For the generic relationship between height and volume using all species data the correlation of H100 with volume is slightly higher when referred to all datasets but when applied to three of the five species compositions it is Lorey's height that is better correlated. Of the 11 scenarios displayed in Tables 4.1 and 4.2 the outcome is for Lorey's height to produce the best correlation in 7 cases.

Each dataset used in this section highlights the problem of using Maximum plant height as an indicator of forest volume with all corresponding R^2 values consistently lower than the others. When the individual forest compositions are considered separately the Mean plant height of a forest is still typically the best indicator of forest volume, with *Abies Alba* being the exception through its preferred relationship with H100. It may be the case that *Abies Alba* forest volume is weighted towards the

small selection of larger trees. Maximum height, and to a lesser extent H100, do not appear entirely representative descriptors of the community with these height descriptions representing only the most dominant individuals which SERA predicts do not define the volume status of the whole community. Lorey's height (in a similar fashion to H100 and Maximum height) is biased towards the larger trees but given that it has better correlation than H100 or max height, yet poorer correlation compared to the mean, its relative success is probably due to the fact that it accounts for all trees.

4.5.2 Regarding Resource Constraints

The *Abies Alba* data are used as a direct comparison of the full 1 ha, 100% light intensity area with the varying environmental configurations as previously shown in Figure 4.11. By interpolating the data to allow a percentage analysis of the correlation of height values with volume at increments of $2m^3$, the variation between 100% and 50% light intensity produces larger variations when Mean height is considered; showing an average 34% data variation compared to 22% for Maximum height and 30% for H100 with Lorey's height showing a 25% variation. For 75% light the variations are 3%, 4%, 8%, and 4% respectively. When it comes to available area with constant planting number the results, as would be expected, vary considerably from the control situation. This is particularly true for the 0.25 ha case. Under these conditions of shrinking area it is the Mean height which undergoes the least mean percentage variation for both the 0.5 and the 0.25ha areas with 38% and 102% variations respectively. Results for Lorey's height of 67% and 163% are very similar to those produced for Maximum height and H100. These variations appear very high but result from 50% and 75% reductions in available area while maintaining the number of planted stems. When these areas are upscaled to give volume per hectare the results are much more closely linked but this highlights the potential problems that may exist if the ground area available for forest growth is not classified correctly.

Forest stand variations can be a result of age, species composition, population, forest management, and environmental conditions. Of these variables each has the ability to influence the collective forest allometry. Due to the dynamic ability of the forest to manage varying resource availability the thinning levels vary among planting densities in order to attain optimum conditions. A clear convergence in stem numbers for all planting densities is evident in the data at a volume of $300m^3$/ha for *Abies Alba*. Amongst planting densities, the amount of time it takes to achieve the optimal conditions varies. Such behaviour predicted by SERA indicates that the Mean heights of the *Abies Alba* forests will be the same regardless of planting density if these heights are achieved at volumes above $300m^3$/ha where the convergence suggests identical forests. In this way the forest combats the obstacles of resource and space allocation by resorting to the optimum structure to guarantee maximum efficiency through mortality and regrowth. In this scenario the number of stems and species would be adequate to infer forest volume. Alternatively this convergent behaviour may be related to an artefact from the measured data of (Cantiana 1974) used to create the SERA model, but the convergent behaviour still remains consistent with an optimum forest theory related to basal area sustainability with similar behaviour exhibited for Corsican pine in (Baker et al. 1994).

Although increasing planting density both reduces the space and light available to each individual tree it does not alter the optimum conditions for the plot – these are controlled by the maximum resource levels of the environment. These conditions will be unrelated to planting densities as thinning regulates the numbers to ensure an optimum structure satisfying the resources available. The effect of altering individual environmental conditions such as reducing space and varying light intensity will reduce the optimum conditions of the stand. For example a reduction in space will reduce the available nutrients and therefore reduce the total basal area the stand can sustain although the nutrient resources per ha. will not be affected by such changes. Reducing the light intensity will reduce the resources per ha. and consequently the ability of the trees to photosynthesise efficiently and to acquire carbon as effectively.

The analysis of the individual variations must therefore be viewed in a different light to the effects of overcrowding as not all trees are resource limited through overcrowding while all will be in the case of light reduction. Where these scenarios differ significantly is in the relationship of forest volume to height measurements. Within SERA a reduction in space while maintaining planting number, results in a greater rate of thinning as the forest is forced to behave in a similar manner as it would when faced with overcrowding. This is in keeping with the natural behaviour where the degree of clumping of stems should decrease through the size classes due to density dependence removing individuals that are close to one another in space, and in particular those individuals that are close to an adult (Getzin et al. 2008; Kenkel 1988; Moeur 1997; Murrell 2009; Sterner et al. 1986). This happens to such an extent within SERA that a similar number of stems within different sized areas will produce different forest volumes, particularly for Maximum height, but it is hoped when they are upscaled to the same volume density the values will match more closely but not exactly due to required changes in dynamics.

SERA predicts that if a plot can sustain a particular number of trees it will do so by using the maximum allowable basal area that resources allow and will thin according to this optimum value. The forest-level allometry is effectively altered without variations on an individual level. The effect this has on forest volume and height relationships is therefore to have a higher Mean height and Maximum height for any particular absolute volume of forest in a smaller area. When scaled to the same volume density units the relationship between height and volume will be almost identical at higher volume densities if the resources are identical but the exact size of the planting area must be known to allow this.

If the same personal space restrictions are placed on individual trees, regardless of stand area, then it would typically be expected that the growth would be the same, but this is not necessarily the case. Although faced with reduced space, there is always the potential to achieve more within a larger area. A tree's existence is bounded by

the limits of nature. This means that an area which can only be a 50% forested area (with 50% deemed uninhabitable, possibly due to contamination or early deforestation) cannot become a forested area with 75% capability which only experiences an uninhabitable area of 25% without outside intervention. Similarly a forest in an area with 50% less light intensity cannot increase the intensity of light captured within this area through thinning beyond the limits of the supply. The forest has to adapt to these unmovable resource limitations and as a result the height to volume relationships imposed by the variation of planting density differ from the relationships that exist when the resource supply is physically capped for example. Where a dense population is modelled the optimum conditions for space and light can be achieved regardless of the amount of space originally assigned to individual trees or the initial level of standing. Every planting density will be able to achieve the optimum structure given time, given the required thinning.

4.5.3 The Relevance of Lorey's Height

The studies carried out in this work show that in general Mean plant height holds the strongest relationship with tree volume regardless of variations in species, number density, light intensity, and stand area while maintaining planting numbers. As this work was carried out with the consequences for remote sensing as a primary concern, the ability of remote sensing to measure average forest height are here considered. The three principle remote sensing techniques for forestry measurements of optical (reflected), laser, and radar systems are often assumed to be capable of deducing the Maximum height of the forest, conditions allowing, but their ability to acquire Mean height and to verify using ground data is much less certain.

If the SAR scattering phase centre of a forest is to be better understood and better related to the physical aspects of a forest, the main source of the scattering must be defined. At high frequency bands such as X and C the dominant scattering mechanism in the forest is the volume scattering from the canopy (Sarabandi and Lin

2000)with the height of the effective phase scattering centre dependent on the wavelength and polarisation (multi-wavelength SAR interferometry has revealed the differences in vertical locations of effective phase scattering centres (Balzter et al. 2003a). As the frequency is reduced, and the wavelength increased, the dominant scattering is associated with gradually larger branches, for example VHF would be dominated by the stems located deeper in the canopy (Smith and Ulander 2000). Assuming a direct relationship between Maximum forest height and scattering phase centre is not always appropriate, even at X-Band, see (Hajnsek et al. 2009).

Further to this it is known that the larger the scattering object, the larger the scattering. In any of the cases involving scattering centres the scattering will be weighted towards branches of a particular size, which remain more susceptible to scattering at a particular wavelength. It would then seem apparent that the SAR scattering phase centre can be associated with an average height rather than the Maximum height of a forest. In the case of mid- to long- wavelength microwave frequencies this average height will be weighted by the size of the stems (Brolly and Woodhouse 2010). Such weighted forest measurements are similar to those favoured by Lorey's height and H100.

As the evidence points towards the scattering phase centre being related to an average height measurement it is suggested here that for use at long wave microwave frequencies (P and L Bands) the average height measurement will be of a similar nature to Lorey's height with measurements weighted by the basal area of each individual tree rather than a selection of the largest trees as with H100. H100 also happens to be the designated height classification proposed for the European Space Agency BIOMASS mission (Davidson 2008). Lorey’s height allows the average forest height to be closely linked with the larger trees, but not being overly biased by a small subset of the largest trees (as in H100). For mono-cultures we might expect the difference to be insignificant, but for natural, mixed-age forests, it is likely to be more so.

Although not a mean height, the relationship of Lorey's height with volume has been tested using SERA. The statistics resulting from this reveal the accuracy to which it can determine volume as being at a level bounded by those of Mean height and Maximum height measurements with similar correlations recorded to that shown for H100. Although not able to match the accuracy of Mean height, Lorey's height remains a more relevant measure in terms of radar and LiDAR scattering. For these reasons it is Lorey's Height that is suggested here for use in volume studies given that it is the most relevant forest height, of those investigated, to the location of the scattering phase centre.

Although LiDAR does not operate over similar bandwidths to Radar it does produce height results biased towards the tallest trees. With the high extinction rate of optical sensors through forest canopies this is expected but the reduced accuracy when surveying conifer plantations means that the height recorded by the sensor will tend to be less than the Maximum height of the forest. Lorey's height would once again be a reasonable evaluation of the inferred height from the LiDAR measurements with allometry suggesting that the taller trees will have larger basal areas and also because Lorey's height considers the entire visible community rather than simply selecting a sample of 100 trees.

4.5.4 An Alternative Relationship

The problem with height as an indicator of volume is of particular significance in the cases of resource limitation and space competition. A single stem existing within a single hectare plot will provide a Maximum height that is equal to the Mean height which is also equal to Lorey's height. In cases such as this the relationship of each height class with volume will be the same yet completely different from the relationships exhibited in communities of trees. With regards to interferometric SAR the height retrieved from the system will not correspond to Maximum height and

therefore will not correspond to the other classes investigated in this work. In areas that meet such criteria the need to incorporate environmental conditions into a height classification are required for height to inform on forest volume. If the plot capability is known in terms of the total basal area per hectare it is able to support then the presence of a reduced number of stems within this area will allow the relationship between height and the volume to be refined. If for example a plot can sustain $30m^2$/ha of a particular species then the presence of only $3m^2$/ha in a scene can be deemed to be 10% of the stand capability. Within any particular collection of stands undergoing similar forest dynamics the relationship between Maximum forest height and volume can be constrained into a relationship following the process of equation (4.3) here named "Mod Lorey Height". This process requires knowledge of the optimum basal area of the stand per ha (which may be determined from an appropriate model) as well as current basal area and Maximum tree height values which can be retrieved from current optical remote sensing methods (Wulder et al. 2000) for example relating the canopy size of the forest and tree respectively to the required values (Gill et al. 2000; Popescu et al. 2003; Wu and Strahler 1994). Area restrictions are considered by dividing the current absolute basal area by the fractional area occupied to provide the relative basal area per ha. Knowledge of species to determine the potential basal area of a stand is required in addition to the knowledge of any resource restrictions and potential for growth.

This process can account for all planting densities and species for both complete and partial area coverage.

$$\text{Mod Lorey Height} = \frac{(\text{Current Basal Area / Fraction of hectare available})}{(\text{Potential Basal Area per hectare})} \times \text{Maximum Height} \qquad (4.3)$$

Mod Lorey Height can then be plotted against volume calculated by dividing the absolute volume value by the fraction of the area available for growth which in forested areas will typically be 1, resulting in a data spread as shown in Figure 4.12 for *Abies Alba* and Angiosperm data. The correlation across species, planting

densities, and resource limitation shows the potential of such measurements if the maximum sustainable basal area of a species in a region can be estimated.

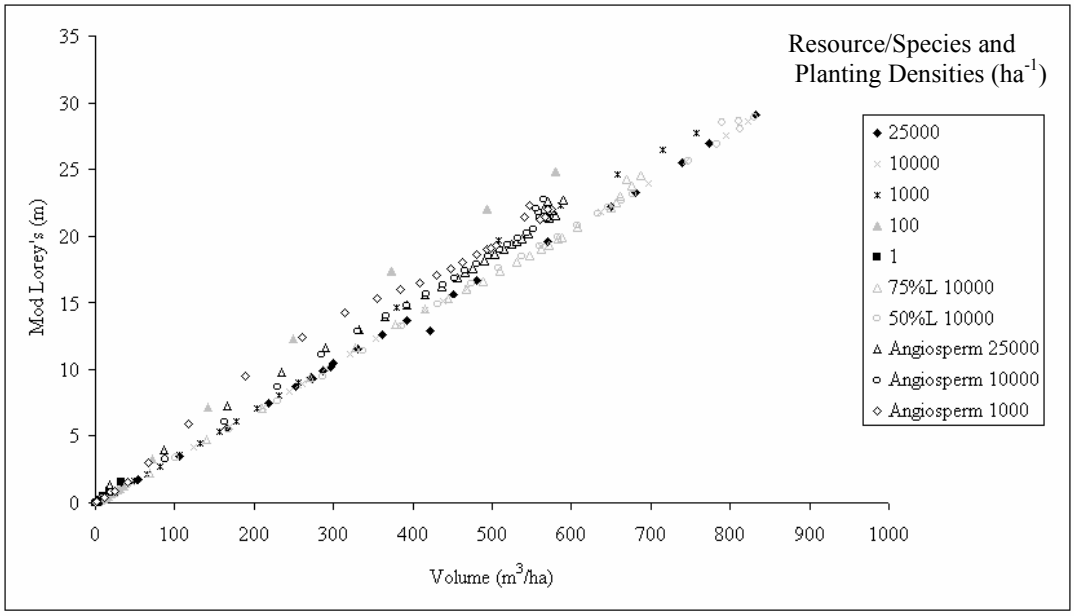

Figure 4.12. Mod Lorey height eq.(4.3) for various planting densities of *Abies Alba* and Angiosperms. Data also plotted for reduced light intensities (L). All data are *Abies Alba* except those signified.

If InSAR measurements of height were related to such a measurement as Mod Lorey, a height measurement that takes into account environment, and the nature of scattering through basal area dependence and Maximum height (indicating the weight and first instance of scattering), then a generic relationship with volume may be obtainable. This is an area that requires empirical analysis to determine validity.

4.6 Conclusions

Forest height and volume are intricately linked, but it is Mean height that is most related to forest volume; across species, planting density, and resource variation. The possible variations in the relationship between Maximum height and volume under the same conditions are extremely variable, even when considered within the confines

of a monospecies scenario. When light is restricted it has been shown that the trees can not grow to the same maximum heights within the time frame of the study, therefore SERA predicts that at the highest plant heights the relationship with volume will significantly break down. Through the same conditions, the relationship of Mean height remains significantly more consistent.

As a result of these findings it is important to identify when the SAR phase centre or the equivalent for LiDAR can be associated with the Mean height of the forest. LiDAR would be required to measure the Maximum height of each tree in order to ascertain a mean value, which is not economically or mechanically feasible, and methods involving SAR are similarly complex. While Maximum height and H100 are good predictors of volume across areas of variable resources and size, the inability of Maximum height to successfully predict volume across species boundaries, as well as amongst various planting densities, is a significant deficiency to its use in large area remote sensing. Therefore with regards to SAR remote sensing in particular, the weighting of the average height in favour of the basal area to produce Lorey's Height allows a greater connection with the nature of microwave scattering than offered by H100 or Maximum height. Microwave scattering is dominated by relatively larger structures according to particular ratios between the wavelength of the incident wave and the size of the object. Any scattering phase centre, if deemed to be related to average height, would be weighted towards the relatively larger structures. For LiDAR the physical connection is not as clear but appears to be valid due to its relation to larger trees.

The variation in the correlations between the examined height classifications and their relationships with volume have shown how the way we interpret forest height can vastly influence our forest volume estimations. As the heights often used in empirical studies tend to be related to Maximum height or samples of this measure it is clear that large errors exist through association with this parameter and may be greater when used at changing locations. The feasibility of remotely sensing Mean height

remains low and as the benefits of a relationship with H100 are less obvious and inherently less correlated with scattering physics this work recommends the use of Lorey's height as an alternative to the H100 measure. Lorey's height accounts for all trees, weighting the measurements towards the most dominant scatterers in a similar manner to radar interactions. If height measurements retrieved from LiDAR and SAR data correspond to Lorey's height then it is also possible for basal area to be inferred through the additional knowledge of the number of trees within the study area, exhibiting clear advantages over the sample based H100 measure.

It is important to keep in mind that this study relies heavily upon SERA, its use as a modelling tool is primarily based on its ability to predict empirically monitored behaviour. The ability to vary the allometry within the model using species definition allows forests of various allometric identities to be modelled independently and collectively within SERA. In effect this study has analysed the effects of individual allometry variations on the height-to-volume relationships of the forest through species definition. It has also, significantly, evaluated the consequences of collective forest allometry variations resulting from resource limitation and number density fluctuations to show that forest height and volume follow a complex relationship dependent on many environmental and physical factors with self thinning one such factor.

5 Vertical Backscatter Profile of Forests Predicted by a Macroecological Plant Model.

Matthew Brolly and Iain H. Woodhouse

Summary

The initial work of this chapter was conducted in 2009 and submitted to International Journal of Remote Sensing in 2011, it is currently in review. This chapter introduces the radiative transfer model RT2 described in Chapter 3.4 and is used here in conjunction with the tree growth model WBE of Chapter 3.1. As a collaboration between two independent models this work investigates the backscatter behaviour associated with tree structure, governed by the rules of resource supply upon which the WBE model is built. The WBE model in the form presented in this chapter allows user defined variations in scaling and number density. These variations allow the effects of vertical structure within a forest of identical stems to be analysed. Its simplistic form and provision of information regarding number density and size within a multi-layer environment makes it an excellent companion for RT2.

This chapter provides an investigation into how vertical forest structure influences the SAR backscatter return by analysing the contribution made by individual branching layers and focusses on the direct volume scattering. The aim is to obtain a description of backscatter behaviour through the vertical profile of the forest which can be related to the number density and size of branches. This aims to establish the macroecological factors influencing backscatter responses. The backscatter behaviour in itself is analysed with regards to the scattering theories of Optical and Rayleigh scattering with hypotheses for potential backscatter behaviour directly related to these scattering theories and their particular dependencies discussed. The implications of vertical forest structure on the interpretation of interferometric data are considered in this chapter through the discussion of dominant scattering layers. This provides a

direct link with Chapter 4 in which the implications of horizontal stand structure and vertical distribution of volume on interferometric data interpretation were discussed.

This chapter addresses the following questions:

1. How does number density and size distribution within a generalised forest structure affect the vertical location of dominant backscatter?
2. How does scattering regime change affect the distribution of backscatter?
3. Do the assumptions made by (Crispin Jr and Maffett 1965) (Chapter 2.3) apply in a forest scattering scenario?
4. How does scattering behaviour within the vertical profile of a forest inform on structure and what are implications for forest remote sensing?

To address these questions this chapter uses the theories of Crispin and Moffat described in Chapter 2.3, that scattering within the Mie resonance region can be described by an extension of the Optical scattering regime, and using WBE and RT2 investigates how structural effects and changing scattering regimes can directly affect the scattering centre of a forest. With regards to the relationships between forest height and volume described by SERA in Chapter 4 this study provides modelling evidence for the location of scattering centres below the top surface of the canopy as a consequence of number density and size distribution. It provides evidence for the importance of classifying height correctly for interferometry when used with allometry (see Chapter 1.4). Further investigation of the profiles produced in this study and interferometric consequences are conducted in Chapter 6 while the relationship between forest structure, scattering regime, and backscatter behaviour form a significant part of Chapters 7 and 8.

This work including the modelling procedures was conducted by myself and influenced by the work of (Woodhouse 2006b). Additional help was provided by Dr. Woodhouse with idea development and editing services within a supervisory role.

5.1 Abstract

This study describes a new application of a macroecological model to describe the vertical profile of radar backscatter through a forest canopy. Given layers of equally sized cylindrical scatterers, the model predicts that one layer within the forest canopy dominates the backscatter profile. This prediction is based on both first order theoretical approximations and results from a radiative transfer model parameterised by the macroecological model. This model is used to pre-empt specific backscatter trends with results predicting that Rayleigh and Optical backscatter follow negative and positive exponential trends respectively when plotted with respect to backscattering coefficient and branching level through the canopy. A maximum value is predicted by the model associated with the branching level located at the transitional zone between Rayleigh and Optical scattering. This finding follows directly from the size density distribution within a forest combined with dramatic reductions in cross-sectional trends exhibited through the transition. It is a result unrelated to resonant scattering or the effects of penetration depth. The feasibility of describing radar interactions using geometric optics is explored when limits are imposed on the physical optics scattering solution.

The findings offer a significantly new way of understanding the distribution of scattering from differently sized elements in a canopy, and challenges the widely held assumption that backscatter-biomass relationships saturate due to increased opacity of the canopy.

5.2 Introduction

In (Woodhouse 2006b) it was described how the macroecological plant model described by (West et al. 1997) could be used to parameterise a radar backscatter model, with the aim of predicting trends in backscatter and height as a function of vegetation biomass. This approach provided a new framework for making the

Random Volume over Ground (RVoG) model (Treuhaft and Siqueira 2000) incrementally more realistic.

The aim of this article is to consider how this macroecological approach to simplifying forest structure can describe the vertical profile of the backscatter response. The vertical profile is important in determining the relationship between scattering phase centre and forest height (Sarabandi and Lin 2000), in the modelling of polarimetric interferometry (Lavalle et al. 2009) and in radar tomography (Cloude et al. 2009; Cloude and Papathanassiou 2003; Cloude and Papathanassiou 2008b).

5.3 The Forest Structure Model

The macroecological model used is the "general model for structure and allometry of plant vascular systems" (WBE) developed by West, Brown and Enquist (West et al. 1999b), (West et al. 1997). The WBE model has roots in a macroecological approach to explain allometric scaling law origins (Niklas 1994), later modified to describe plants with branching architectures. Despite some important limitations this model has key advantages making it an appropriate first-order linkage between simple backscatter modelling and models of biological function.

The WBE model is also generically based on the constraints of biomechanics and resource distribution. The generic nature means that it can adequately describe "tree-like" branching that results as a consequence of underlying biophysical constraints of fluid flow and rigidity (unlike fractal scaling models), but as a consequence of its genericness it is not well suited to describing properties of specific species.

5.3.1 Plant Structure from the WBE Model

The advantages and disadvantages of using WBE for radar backscatter studies have been discussed in depth in (Woodhouse 2006b) and in Chapter 3 of this thesis. We

also take from this work the rationale for considering a range of empirical values of many key variables, rather than relying solely on generalised macroecological predictions favoured by (West et al. 1997). For completeness, however, the main power law relationships are summarised below.

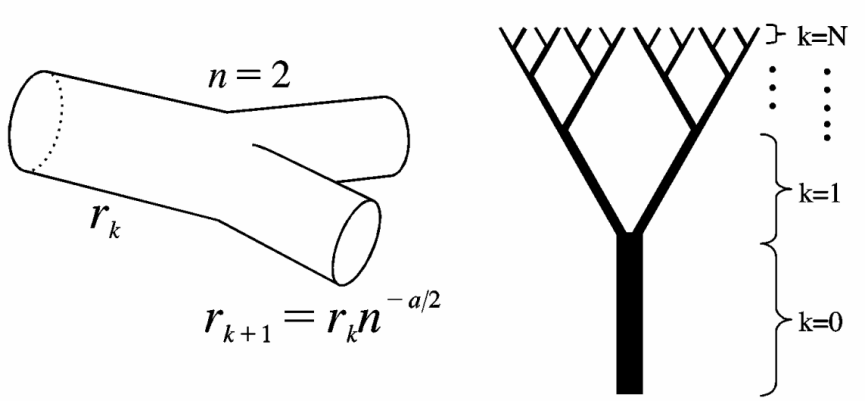

Figure 5.1. Main parameters in WBE model: scaling factor, *a*, branching ratio, *n*,. branching level *k,* and total number of branching levels for particular tree, *N*.

5.3.2 Generalised Allometric Predictions

The WBE model characterises geometric plant structure through a number of power laws derived from biological and biomechanical considerations of resource distribution within the plant (Enquist et al. 1999; Enquist et al. 1998a; Enquist et al. 1998b; West et al. 1997, 1999b).

The model uses five variables to describe the size and number of branch elements of a tree: (1) a scaling factor, *a*, determining how radii of branches change, or scale, within the plant; (2) the branching ratio, *n*, the number of daughter branches derived from one parent; (3) the length-to-radius constant of proportionality; (4) radius of leaf petiole, r_N; and (5) number of branching levels *N*. In actual trees, all five of these parameters lie within a small range of values, and are likely species-specific. In broadleaf species *N* is likely to be related to the tree age and is the only variable that

would normally change over time. The age of conifers should perhaps be more appropriately represented by increasing n with older branches producing a greater number of daughters, but further development of WBE would be required for full incorporation of such a trend.

The WBE branching network runs from the trunk (level 0) to the leaf petiole (level N) (see Figure. 5.1) with an arbitrary level in the plant branching network denoted by k. Note, however, that we might expect biomechanical properties of tilted branches in the canopy to differ from vertical stems. The value of n is typically 2 for broadleaf (decurrent) species, and larger (up to 5 or more) for conifers (excurrent). Within empirical studies, and specifically within literature on modelling radar backscatter, the value of a ranges from 2/3 to 4/3, with outwith values occurring very rarely, and are usually stem allometry associated (Woodhouse 2006b; Zianis and Mencuccini 2004). For excurrent trees, the value for a in the branching structure is often approximately 2/3, representing geometric similitude, but stems can be better represented by some value greater than 7/6, similar to the case of stress similarity related to a = 4/3. Note that a value of a=2/3 coincides with geometric similitude models of plant structure, consistent with many observations of conifers (Niklas 1994), but not dicots, which are more appropriately described by the elastic similarity model, $a \approx 1$. Values of a>1 for stems are also suggested by other empirical data (Zianis and Mencuccini 2004). When the scaling factor is a=1, this describes the special case of the area-preserving "pipe model" (Shinozaki et al. 1964), whereby the plant is described by tightly packed pipe bundles.

5.3.3 Branch Length

The WBE model utilizes biomechanical constraints that predict some optimal relationship between branch length, l and radius, r, such that:

$$l_k \propto r_k^{2/3a} \tag{5.1}$$

The stem level is represented by k=0, so that l_0 represents trunk height, and r_0 radius (assumed to equate to half diameter at breast height (DBH) in field studies).

5.4 Methodology

5.4.1 Modelling Strategy

Using branching descriptions given in previous section, it is possible to model a tree canopy as N levels of branching cylinders, going from k=0 to k=N, as shown in Figure. 5.1. The WBE model can then be used in one of two ways. Firstly, it is possible to make a first order estimate of backscatter trends with height using some approximations based on whether the cylinders lie in the Rayleigh or Optical scattering domain. The second is to use WBE to parameterise a full multi-layered radiative transfer model to predict backscatter response.

5.4.2 First Order Estimate of Trends

In this case we consider the backscatter trends as a function of branching level, k. If we further assume that the length at each branching level is indicative of layer depth we can also consider the trends as a function of height, z. Note, however, that while k need not correlate directly with z, it will tend to correlate with depth into crown, such that the smallest elements are located on outer parts of the crown. The crown shape itself is not described by WBE so is not considered, although it is recognised that this would be an important consideration in some circumstances particularly at high radar frequencies although the effect of shape is reduced when considering a monospecies, mono-age forest at the stand level.

Let us consider two extremes: (1) where the branch cylinders lie completely in the Rayleigh scattering domain; and (2) where they lie entirely in the domain of Optical scattering. The projected backscatter within these regions is visualised in Figure 3.4

Chapter 3.3 of this thesis with further examples found in (Walton and Young 1984) and chapter 11 of (Skolnik 1970). Although these theories were developed for spherical elements, the Rayleigh, Optical and Mie theories can be used with other fundamental shapes such as "spheres, plates, cylinders and the like" (Woodhouse 2006a). Previous work by Karam et al. (Karam and Fung 1988) suggested the Genaralised Rayleigh-Gans (GRG) approximation would be appropriate for the consideration of infinite cylinders, but it is also clear in this work that the trends remain the same between both the Rayleigh approximation and the GRG with the radiative transfer model used in this work regarding the scatterers as infinite cylinders. In the Rayleigh case we assume the backscatter from each cylinder increases with the square of the volume (Smith and Ulander 2000), while for Optical we assume it increases with physical cross-section (Kononov and Ka 2008). At the transition between these regimes lies Mie scattering – here we make an approximation that assumes resonant behaviour "averages out" across this region giving the cumulative effect of a distribution of branch sizes, an assumption supported by empirical results in (Crispin Jr and Maffett 1965; Lopes et al. 1991), and (Mougin et al. 1993).

WBE allows us to address the relative contribution to the backscatter from the different branching levels as both branch size and number density vary. In both Rayleigh and Optical scattering, the backscatter is greater for larger cylinders, as area and volume will both be larger, but for any given canopy the number density increases as the cylinders get smaller. Higher in the canopy, there are a greater number of smaller scatterers. The dominating factor must then be determined: is it the increase in size of scatterers or their decrease in number that dominates the backscatter? As this study is grounded firmly on the importance of backscattering trends the following equations are presented as a series of proportionalities (Cox et al. 2002; Holt 1959; Knott et al. 2004). The coefficients are as outlined by the WBE model parameters.

For Rayleigh scattering the total radar cross-section (RCS) of the k-th branch level, with N_k elements, is given by the square of the branch volume, V, multiplied by the number of branch elements:

$$\sigma_{Rayleigh} \propto N_k V_k^2. \tag{5.2}$$

Using the relationship between length and radius of equation (5.1), we can then write the proportional relationship using the already introduced variables and manipulate as follows:

$$\begin{aligned}
&\sigma_{Rayleigh} \propto N_k r_k^4 l_k^2 \\
&\propto N_k r_k^4 r_k^{4/3a} \\
&\propto \left(\frac{r_0}{r_k}\right)^{2/a} r_k^{(12a+4)/3a} \\
&\propto r_0^{2/a} r_k^{(12a-2)/3a}.
\end{aligned} \tag{5.3}$$

The relationship, $r_k = r_N n^{(N-k)a/2}$ can then be introduced, which is a rewritten expression from WBE, recognising r_N, r_0 and n, number of daughter branches from any parent, to be constant for any individual decurrent tree as preferred by WBE (Woodhouse 2006b), allowing the expression to become:

$$\sigma_{k,Rayleigh} \propto n^{-k(6a-1)/3}. \tag{5.4}$$

The trend for Rayleigh scattering is shown here as an inverse exponential of branching level, k, governed by n, the number of daughter branches, and a, the scaling parameter. The maximum backscatter originates from the largest branches with size dominating over number density when all branches scatter according to the Rayleigh definition of equation (5.4). This result is most amply illustrated by VHF radar measurements whereby the stems of the trees dominate the backscatter response, as seen in (Melon et al. 2001) and (Smith-Jonforsen et al. 2005). While this derived result could be taken for granted, it should be noted that theoretically, at least, a branching structure could exist with a=1/6 meaning that the backscatter contribution

would be equal for all branching levels. However, we have not yet encountered evidence for such a low value of a therefore simulations are not carried out for such low values.

In a similar manner, the scenario whereby the radii of all the branches are large enough for the cylinders to scatter completely in the Optical region is now considered. In this case the radar cross section for level k scales with the physical cross-section, A:

$$\begin{aligned}\sigma_{Optical} &\propto N_k A_k \\ &\propto N_k r_k l_k \\ &\propto r_0^{2/a} r_k^{(3a-4)/3a} \\ \sigma_{k,Optical} &\propto n^{k(4-3a)/6}.\end{aligned} \tag{5.5}$$

Here we assume a sufficiently thin canopy that occlusion is insignificant (as monitored through examination of extinction values within the backscatter modelling process) and geometric optics applies.

Again equation (5.5) shows an exponential trend, but positive as a result of number density exerting greater influence than increasing cylinder sizes. Whereas for complete Rayleigh scattering the maximum contribution is at k=0 (the stem), for complete Optical scattering the maximum contribution is at k=N with the majority of the scattered energy coming from the smallest branch elements at the top of the canopy. This corresponds to the common understanding that at short wavelengths, backscatter is dominated by smaller elements and is influenced more by number density. (Note that this is the case even when canopy is low density and attenuation is negligible).

However, this need not always be the case – the Optical exponent is significantly smaller so that the effect is not as dramatic, and reduces as a gets larger, such that it will be independent of k when a=4/3, and negative thereafter. Again we have not

found sufficient empirical evidence to suggest values of a larger than 4/3 for trees, although investigations by (Chave et al. 2001) and (Zianis and Mencuccini 2004) have published values which slightly exceed 4/3 based on previously published data. The expression ultimately shows that under normal circumstances, within forests with regards to Optical scattering, the number density has the dominant effect on backscatter.

In both cases the result is an exponential trend of total backscatter with branching level, but with opposite signs (for $1/6<a<4/3$) such that in the general case there will be a stage whereby the top of the canopy is still Rayleigh scattering but that the lower, larger branches have entered the Optical region. The combined effect is one branching level that dominates the scattering. When canopy opacity is low, this dominant level will correspond to the layer where the radii of the branches lie within the Mie scattering region. This result is in keeping with established understanding of backscatter from forests – that scattering is dominated by a particular branch radius in the Mie region defined as $0.1\lambda < 2\pi r < 10\lambda$ (Moosmuller and Arnott 2009; Woodhouse 2006a). Note, however, that here the result follows directly from the size density distribution combined with dramatic reduction in cross-section from Rayleigh to Optical, and is not related to "resonant" scattering or penetration depth. This presents a new way of understanding the distribution of scattering from differently sized canopy elements.

5.4.3 Geometric Optics Assumptions

In this section we provide further justification for the use of a simplified geometric optics approach to modelling the trend in backscatter from a cylinder. The physical optics formula for the radar cross section of a cylinder is shown below where k is the wavenumber, r the cylinder radius, l the cylinder length and θ represents the incident angle from broadside:

$$\sigma_{cyl}^{0} = krl^2 \cos^2\theta \left[\frac{\sin(kl\sin\theta)}{kl\sin\theta} \right]^2$$

(5.6)

By taking an average value over a symmetric window of incidence angles centred at $-\theta_w \leq 0 \leq \theta_w$ the average radar cross section of a cylinder becomes the integral:

$$\overline{\sigma_{cyl}^{0}} = \frac{1}{\theta_w} \int_0^{\theta_w} krl^2 \cos^2\theta \left[\frac{\sin(kl\sin\theta)}{kl\sin\theta} \right]^2 d\theta \tag{5.7}$$

As this window approaches zero the small angle approximations of $\cos\theta=1$ and $\sin\theta=0$ apply, and following a change of variable and subsequent integration we get the closed form formula for the average RCS of a cylinder around broadside, equation (5.8) (see also Hestilow 2000):

$$\overline{\sigma_{cyl}^{0}} = \frac{rl}{\theta_w} \left[Si(2kl\theta_w) - \frac{\sin^2(kl\theta_w)}{kl\theta_w} \right]$$

(5.8)

According to the rules of the sine integral function Si(x), as the argument (x) approaches zero, Si(x) will tend to x. Similarly by taking the limit of the angular window tending to zero we can rewrite equation (5.8) as below:

$$\overline{\sigma_{cyl}^{0}} = \lim_{\theta_w \to 0} \frac{rl}{\theta_w} \left[Si(2kl\theta_w) - \frac{\sin^2(kl\theta_w)}{kl\theta_w} \right] = \frac{rl}{\theta_w} \left[2kl\theta_w - kl\theta_w \right] = krl^2$$

(5.9)

Where the window tends to zero and is approximately representative of the broadside angle the average radar cross section is proportional to the frequency and the cylinder volume. But in the limit of large arguments where $2kl\theta_w$ is large the function Si(∞) tends to $\pi/2$. Under the limits of $kl\theta_w$ tending to infinity (equation (5.10)) we can write the equation for average RCS of a cylinder as in equation (5.11):

$$\lim_{kl\theta_w \to \infty} \frac{\sin^2(kl\theta_w)}{kl\theta_w} \to 0$$

(5.10)

$$\overline{\sigma^0_{cyl}} = \frac{\pi r l}{2\theta_w}$$

(5.11)

This frequency invariant equation is then a function of the physical cross section of the cylinder in accordance with geometric optics. A full progression of the working is found in (Hestilow 2000).

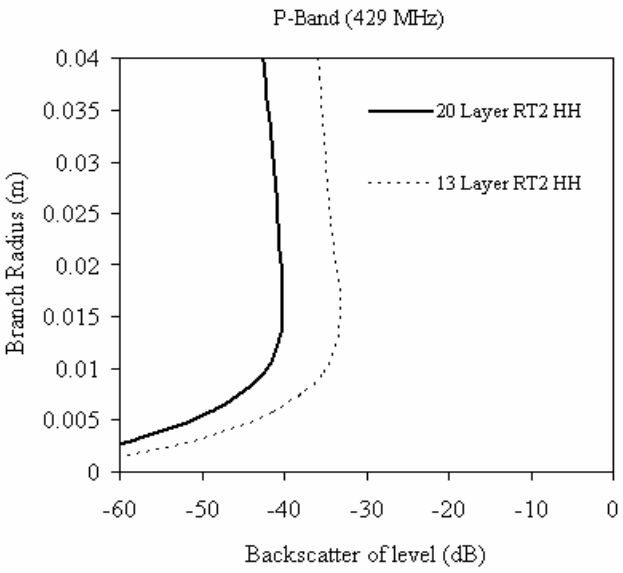

Figure 5.2. RT2 P-Band HH backscatter from 20 and 13 layer forests. Trends remain the same with respect to branch radii although when compared with branching layer the trend differs due to location of dominant radius on different branching levels.

5.4.4 Attenuation Considerations

As a forest matures, the dominant layer rises higher in the canopy with additional growth concentrated in the lowest branching levels, specifically in the stem. When forest thinning maintains a constant forest basal area, the upper part of the canopy

does not change with forest growth as increasing branch numbers for individual trees are exactly balanced by decreasing tree numbers. The result is that saturation on backscatter biomass plots could occur not because of increasing opacity, but because of the biophysical constraints of forest growth combined with Rayleigh-Optical transitions. The role attenuation plays in this work is not considered significant and is visualised in Figure 5.2 which consists of a high (20 Layers) and low attenuation (13 Layers) example, similar trends are exhibited, and the effect is shown through modelling to be independent of frequency. Similarly in Figure 5.3 where attenuation is varied by reducing the number of trees present. In each case penetration is monitored to ensure transmission through each layer. Visualising the role of attenuation is necessary due to the inbuilt attenuation considerations found in radiative transfer models when energy is transmitted to deeper lying layers. This is shown in Figure 5.4 where backscatter from a series of uniform layers is modelled. The effects of layer attenuation are shown here to enforce the understanding that the vertical backscatter trends exhibited in this work will not be driven solely by attenuation with other factors clearly playing a part.

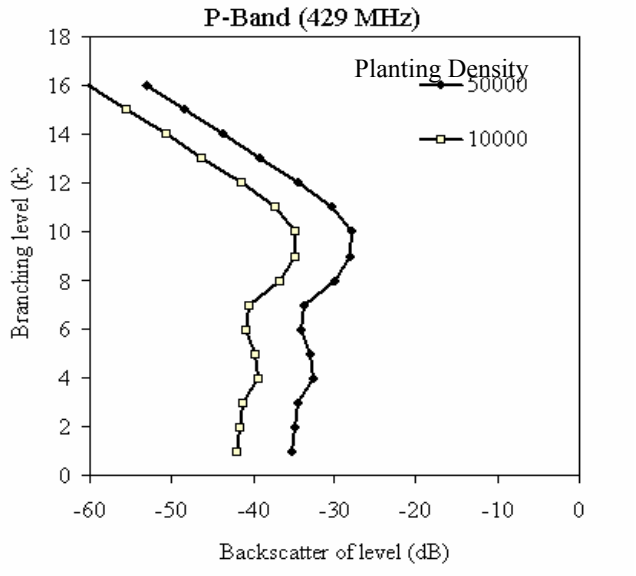

Figure 5.3. RT2 P-Band HV polarisation backscatter from each branching level of forest consisting of 18 branching levels with initial planting densities of 10000 and 50000ha^{-1}. Trends remain regardless of planting density.

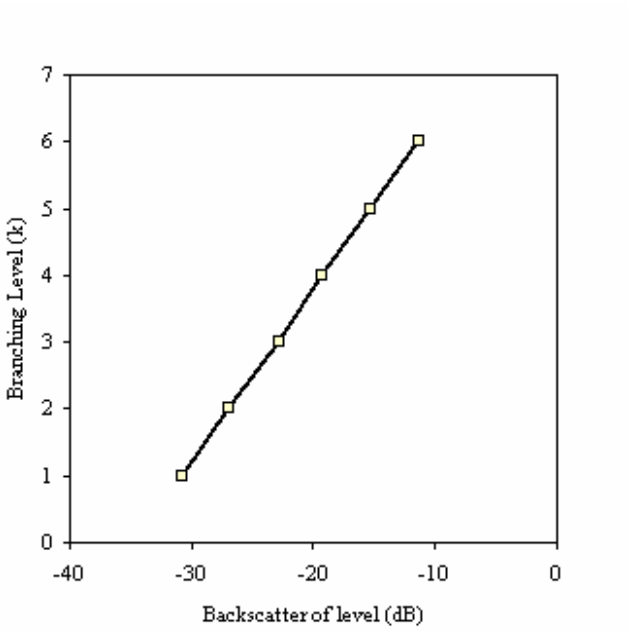

Figure 5.4. RT2 HV polarisation P-Band backscatter variation in presence of 6 identical branching layers in terms of numbers and size. Attenuation from each layer results in reduced backscatter from the lowest layers.

5.5 Results

5.5.1 Radiative Transfer Modelling

RT2, (Cookmartin et al. 2000) a multi-layer second order radiative transfer model (similar to the MIMICS model used in (Imhoff 1995b) and the UTACAN model used in (Woodhouse and Hoekman 2000)), was used to investigate trends in vertical backscatter profiles relative to different WBE associated values, with an emphasis on scaling exponent *a*, at P-band (0.7m).).

RT2 is a fully polarimetric, second-order solution to the radiative transfer equations that treats vegetation canopy as a plane-stratified multilayer region over a rough surface. In this model simple geometric forms are used, for example, plant stems are represented as finite-length cylinders, while leaves can be modelled as plane-circular or elliptical discs. The multilayer facet of this package allows different sized

cylinders to be positioned on different layers in accordance with WBE model structure. For the branches and stems in this instance scatterer shapes are cylinders based on the infinite cylinder scattering solution (Lin and Sarabandi 1995; Stiles and Sarabandi 1996) with uniform axial distribution. The branches also have spherical distribution of inclination angles.

Each layer of the RT2 model was comprised of equal-sized, randomly oriented cylinders parameterised by WBE for a given n (which determines branching rate) and a (determining subsequent size scaling of branches). This includes the stems (k=0), with the comparison between vertical and non-vertical stems and their effect on the backscatter also considered (and identified to produce higher volume backscatter when orientated non-vertically but with negligible effect on important trends). Each layer in RT2 corresponds to a branching layer in WBE. The petiole radius, the dielectric properties of each cylinder and the constant of proportionality, all remain fixed with a radar incidence of 25 degrees used throughout as used in modelling studies at VHF and P-Band by (Chauhan et al. 1991). Note that in this study, the contribution from the ground is ignored since interest lies only in the vertical profile through the canopy, not total backscatter.

The result of parameterising RT2 using WBE is that total backscatter can be broken down into contributions from different branching levels and therefore heights within the canopy. This is shown in Figure 5.5 in which it is shown how backscatter with respect to height matches with the theoretical contributions of Optical and Rayleigh scattering derived from the equations (5.4) and (5.5). In this scenario the theoretical Optical backscatter appears to be the main contributor at levels below k=4 corresponding to the lowest branching levels and largest branches. At heights above k=4 the contribution is Rayleigh dominated, hence the shape of the RT2 response as a function of branching level with the gradient of the Rayleigh section matching closely to the modelled solution based on equation (5.4).

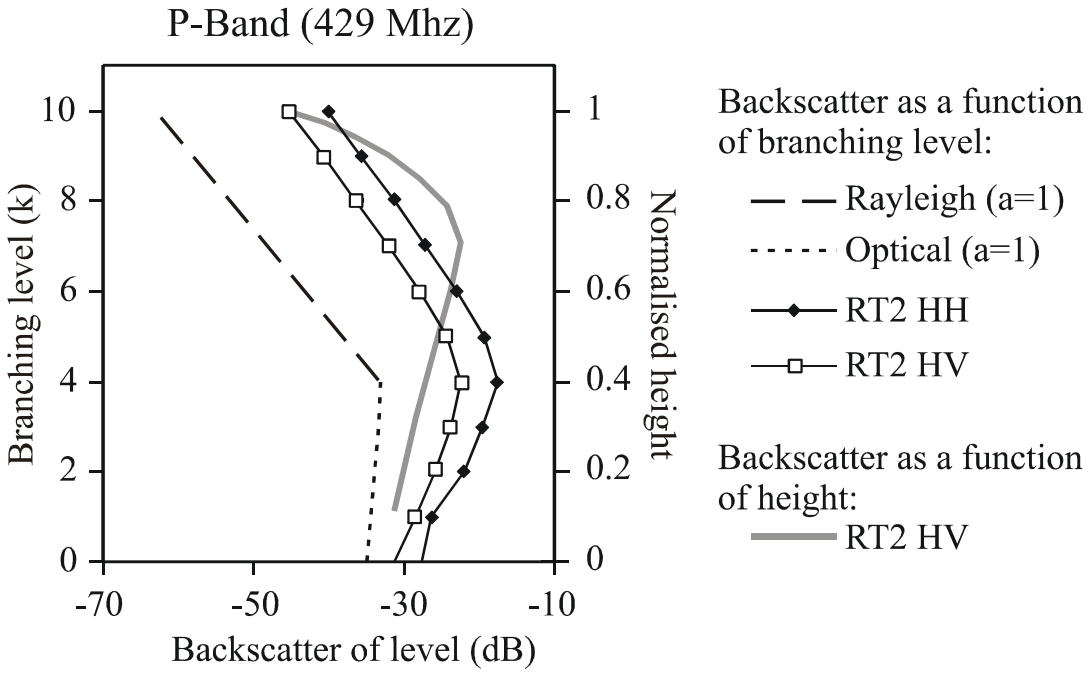

Figure 5.5. P-Band backscatter as function of branching level and height showing vertical profile for a relatively sparse forest case of 500 stems ha^{-1} following thinning from a planting density of 100000 stems ha^{-1}. Theoretical trends for Optical and Rayleigh from equations (5.4) and (5.5) included using arbitrary units. RT2 modelling results shown for HH and HV polarisations as function of branching level, *k*. HV results also shown as a function of normalised height in the canopy.

A similar relationship is seen for VHF band shown in Figure 5.6 (a) where, again, distinctive contributions to the backscatter are associated with Rayleigh and Optical scattering. In both Figures 5.5 and 5.6 (a) the peak backscatter contribution originates at the branching level, and height, corresponding to the interception of the theoretical Rayleigh and Optical scattering contributions. As we know there exists a region of Mie scattering between these scattering regimes we assume that this region averages out due to its periodic behaviour with respect to the size of object and wavelength, we then define this point as the transition from Rayleigh to Optical. This result supports the theoretical prediction that this transition is the most probable cause, and location, of a dominant scattering layer.

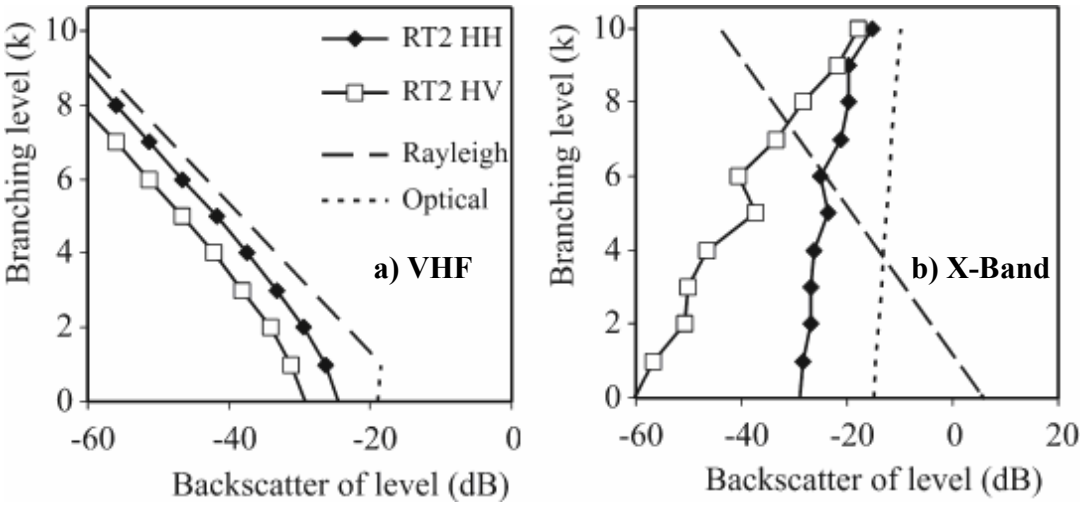

Figure 5.6. RT2 model results for (a) VHF-Band and (b) X-Band SAR data parameterised using WBE under identical scaling parameters (different to those of Figure 5.2). Theoretical Optical and Rayleigh trends from equations (5.4) and (5.5) included.

In Figure 5.6 (b) it is shown that there is no contribution to the backscatter from Rayleigh scattering due to the minimum size of the branching elements used in the modelled forest with respect to the wavelength of X-Band (0.03m). The minimum branch size, the petiole radius, is 0.0015m in comparison to the expected Rayleigh-Mie transition radius of 4.8×10^{-4}m. As a consequence of this, the Rayleigh relationship of equation (5.4) has no contribution to the backscatter, a fact which does not escape inspection of Figure 5.6 (b). The lack of transition from Rayleigh to Optical scattering does not indicate that backscatter saturation effects will not occur with respect to volume but simply that the initial Rayleigh scattering component will be absent. Modelling of much smaller scattering elements reveals the existence of the dominant branch size at X Band and likewise for larger branches at VHF (see Figure 5.7) which also includes P-Band data. The absence of a dominant scattering layer in a natural setting may be due to multi-age or multi-species stand composition.

For the 10GHz (X-Band) case, Figure 5.6 (b), the opposite relationship is seen to that of VHF with the HH modelled data matching the theoretical representation of Optical

scattering. In this case the dominant scattering level is clearly the highest branching level appearing to contain little contribution from Rayleigh scattering with the ratio of wavelength to branch radius at this frequency such that the smallest branches of the forest are completely within the Optical scattering regime.

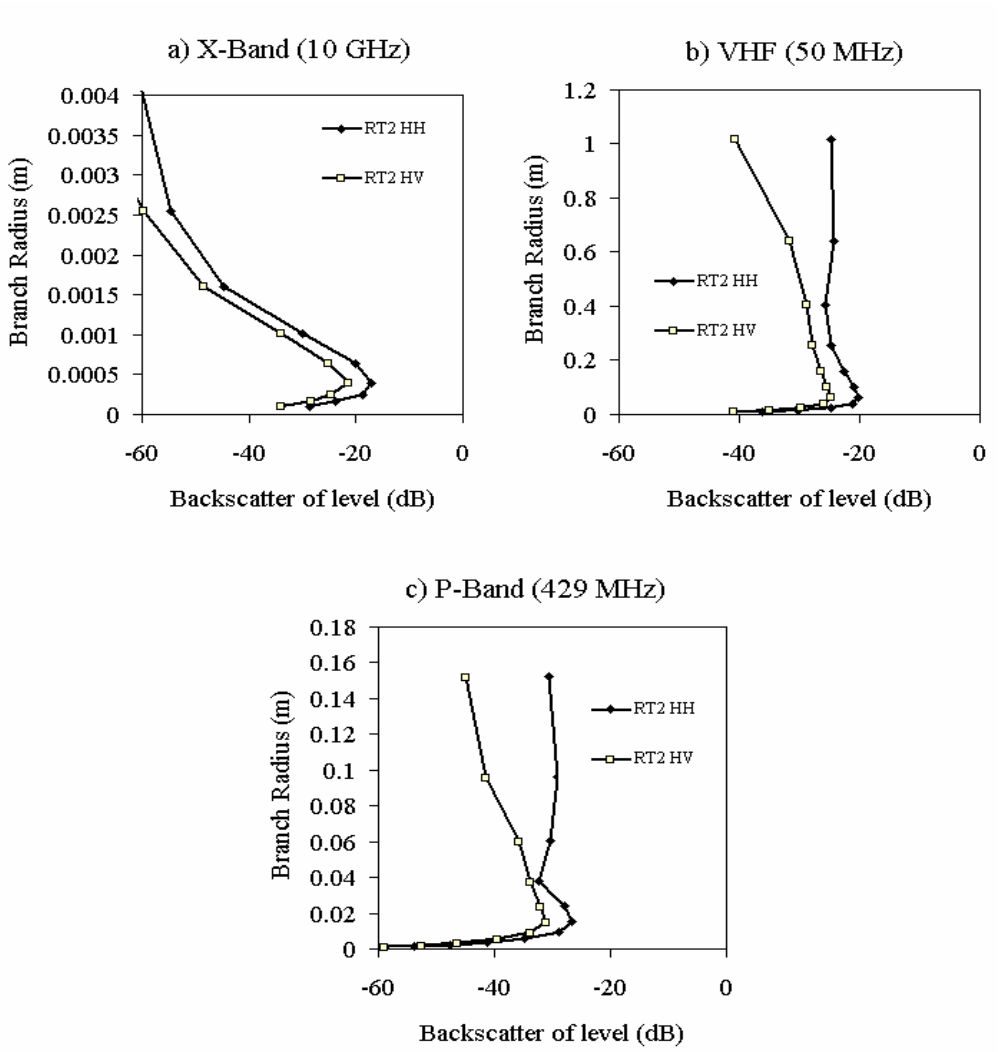

Figure 5.7. RT2 Multifrequency backscatter analysis of identical forests as a result of particular branch radii occupying branching levels and dominating backscatter. Branching radius of dominant branching layer reduces with reducing incident wavelength.

Figure 5.7 shows the dominant height, branching radius and branching level, illustrating that the dominant radius reduces in height location within the canopy

when the incident frequency is reduced. The relationship between backscatter and the ratio of wavelength to scatterer size is a relationship of mutual dependence. Within the WBE model this indicates that the dominant radius will become larger with an increasing wavelength. The resultant backscatter distribution among the branching levels for the VHF frequency of 50MHz shows that the dominant branching layer appears to be at the branching layer 0 but does not match the theoretical description of Rayleigh scattering.

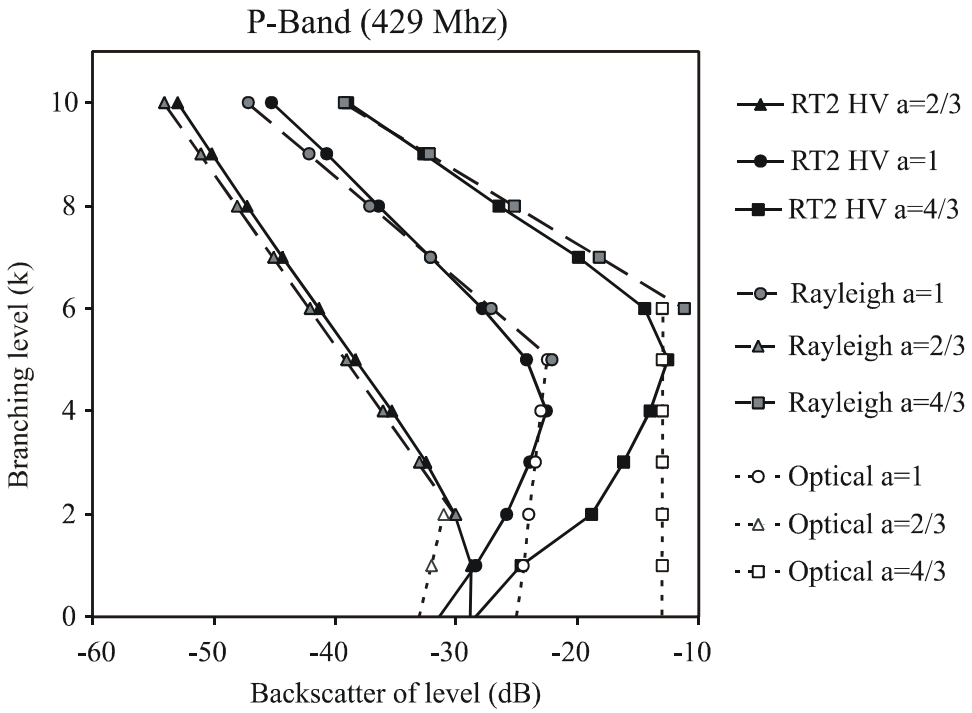

Figure 5.8. RT2 model results for P-Band SAR parameterised using WBE. Backscatter trends plotted against branching level for large planting density of 100000 ha^{-1} before undergoing large scale thinning with each additional layer increment. Backscatter values show trends not absolute values. Theoretical trends for Optical and Rayleigh contributions from equations (5.4) and (5.5) included.

The effect of the scaling parameter on the vertical backscatter distribution is investigated in Figure 5.8 and is such that the larger the scaling parameter the higher the location of the dominant branching level. Results are shown in the figure for scaling parameters a=2/3, a=1, and a=4/3 with stem DBH and height for a=1 being

0.096m and 11.8m, for a=2/3 being 0.03m and 1.35m and for a=4/3 0.3m and 34.87m respectively. Within the vertical profile this suggests that the branching radius of dominance remains the same irrespective of overall forest scaling parameter value, a result verified through multiple simulations and shown as a function of radius in Figure 5.7. One consequence of varying scaling parameter is that the number density per unit volume of the branches at a similar branching level will differ, although for each modelled backscatter response the number of branching elements in a particular branching level will remain the same due to constant n. The number density per unit volume will vary in such a way that it will be lower for the larger branch length increments incurred by lower scaling parameters. This is a consequence of the WBE relationship of equation (5.1). Several planting densities exposed to thinning rates which maintain stand basal area with each growth increment have been trialled through this study ranging from 50 to 500000 trees per hectare with the same conclusions evident. Typical basal areas are around $30 m^2 ha^{-1}$ (Chave et al. 2001).

The peak backscatter response in the 429MHz (P-band) case corresponds to the branching layer with a radius of approximately 0.010–0.015m lying within the expected transition from Rayleigh to Optical scattering with regards to the approximate limits of the Mie scattering regime stated as $0.1\lambda < 2\pi r < 10\lambda$ (Moosmuller and Arnott 2009; Woodhouse 2006a), with the transition to Mie scattering from Rayleigh scattering in the region where $2\pi r$ is approximately 0.1λ. 0.011m would therefore satisfy the radius value in the equation $kr/0.1 = 1$ for P-band. For 10GHz (X-band) the expected radius value is smaller than the petiole radius (0.0015) used in this study whereas for 50MHz (VHF-band) this value would be in the region of 0.09m. For any given modelled canopy, as a forest develops, the dominant layer becomes higher in the canopy since further additional growth takes place mostly in the lowest branching levels. Note that when a=1, and the basal area remains constant as volume increases (signifying a forest in balance with its resources, the upper part of the canopy does not change with growth so that the number density of the dominant layer remains constant with increasing biomass.

However, when the rate of thinning is such that basal area increases, or for scaling parameter less than 1, the canopy properties change, with the upper layers progressively becoming denser, increasing the proportion of Rayleigh scatterers.

5.6 Discussion

5.6.1 Predictions and Implications

This work offers one key prediction; that backscatter will be dominated by a single scattering layer, resulting from the transition from Rayleigh to Optical scattering. For the low opacity case, the trends are exponential relationships, but with opposite signs – for Rayleigh scattering the backscattered power decreases with depth into the canopy, whereas for Optical scattering it decreases with height. Once the largest branching elements encroach into the Optical regime, results indicate a single dominant scattering level. Both trends are governed by the scale parameter and are based on an assumption that backscatter for each layer scales as the number density multiplied by the square of the cylinder volume for Rayleigh or by the physical cross-sectional area for Optical scattering.

An important follow-up use of this model would be to explicitly consider the impact of number density variations on the height profile since a high thinning rate would reduce canopy opacity and therefore influence penetration depth through the canopy. One important implication of this work is that it may offer an explanation for the varieties of behaviour observed in standard radar backscatter-biomass plots. In some cases, there are transitions from positive to negative correlations following apparent "saturation" in the literature for X, C and L-band data in (Ranson et al. 1997), (Rauste et al. 1994) and less obviously (but still apparent) in (Baker et al. 1994), (Imhoff 1995b), and (Dobson et al. 1992). Elsewhere, (Ranson et al. 1997) observed an increasing positive correlation with P-band beyond the widely recorded saturation limit of 100-200 tha^{-1}. It is proposed that these patterns are a result of the backscatter

being dominated by the single scattering layer, which can change as canopy number densities vary, influencing both the total backscatter, but also the penetration depth due to increasing attenuation.

5.7 Conclusions

Sensitivity at longer wavelengths to deeper, larger elements in a forest canopy need not happen because of resonance (larger elements always scatter more), nor need it be related to opacity (penetration depth) of the canopy. The particular sensitivities as modelled by RT2 appear to relate to the balance of individual element cross sections and number densities at each branching level. The geometrical construction of a tree is such that the number density of branching elements is greater at higher levels and decreases with canopy depth, inverse to branch size. The level of this increase can be described by macroscopic scaling properties.

Simulations involving the RT2 radiative transfer model at several planting densities, and using multifrequency simulations correspond with the theory that a dominant scattering level is present due to transition in scattering from Rayleigh to Optical caused by the increase in size of branching elements with canopy depth and a switch in dependence from number density, with regards to Optical scattering, to size, with regards Rayleigh. This holds true for the majority of typical microwave frequencies used in forestry applications but different situations exist at the extremes such as for VHF (Fransson et al. 2000b). In the case of VHF, branching elements are believed to predominantly scatter in the Rayleigh regime due to the large wavelength to branch radii ratio. Inversely the relationship at high frequency bands such as C or X will always be dominated by Optical scattering by the smallest scatterers on the canopy top surface.

6 A study of forest vertical structure estimation using coherence tomography coupled to a macro-ecological scattering model

S.R. Cloude, M. Brolly, I.H. Woodhouse

Summary

This chapter was written in 2009 and published in the Proceedings of IGARSS 09. It combines the ideas of the two previous chapters by using vertical backscatter profiles generated in the manner of Chapter 5 and considers similar discussions regarding interferometry to that of Chapter 4. Each of these chapters relate the scientific work to the importance of forest structure when interpreting radar data.

This chapter asks the following questions:

1. How well do coherence tomography methods replicate forest heights using modelled vertical backscatter distributions?
2. Is the Random Volume over Ground model (RVoG) (Chapter 1.3.2) of attenuation appropriate for describing forest backscatter and adequate for use in height inversion?
3. How well do Gaussian and Legendre spectrum coherence tomography methods compare to RVoG?
4. How does alteration in the vertical forest structure change the effectiveness of these methods?
5. How do modelled compare to empirical findings from an empirically surveyed forest?
6. What effect does forest structure have on the interpretation of coherence tomography data?

This chapter aims to answer these questions by employing the WBE (Chapter 3.1) model for forest structure and the RT2 radiative transfer model (Chapter 3.4) to simulate backscatter behaviour. Forest structures typical of the WBE design (Chapter 3.1; (West et al. 1997)) are used with comparisons also created by the variation of branching distributions to produce fuller canopies. Using coherence tomography the ability of each method to replicate the backscatter distribution of these modelled forests is tested. An accurate forest height inferral is the desired outcome. Comparison of the methods deemed successful using modelled data is conducted with respect to empirical data from the Remningstorp test site with modelled data provided for multiple baselines and spectrum orders.

The main body of this work was written by Professor Cloude with all inclusions relating to the WBE model, forest structure and radiative transfer provided by myself. All forest modelling, including WBE modifications and backscatter modelling was conducted by myself with the application of the Legendre function and subsequent work carried out by Professor Cloude. Editing responsibilities were conducted by all authors.

6.1 Abstract

In this paper we combine a macroecology forest model with a numerical scattering code to estimate the vertical scattering profile of L-band penetration into forests. Using these simulations and the methods of coherence tomography we examine whether using the "Random volume over ground" model (RVoG), a mixture of Gaussians, or the 1st and 2nd orders of the Legendre spectrum are able to replicate the vertical volume backscatter profile of WBE simulated forests in the absence of ground scattering and using one or two interferometric baselines. Different forest structures are examined based on the distribution of branching through the height of the forest and are compared with experimental data collected from Remningstorp test

site Sweden. We also show that structure and the dominance of ground scattering have an important impact on interferometric coherence and hence on height retrievals based on single baseline polarimetric interferometry. We conclude with some suggestions for dual baseline extensions to allow for better height and structure estimation in future sensors.

6.2 Introduction

This paper is concerned with a study of the use of single-pass radar interferometry to estimate vertical structure variations in forested environments. It has been shown in previous studies that forest height can be estimated using polarimetric interferometry or POLInSAR (Cloude 2006; Cloude and Papathanassiou 2003), but here we show that there is potential also for estimating vertical structural parameters related to species variations and growth conditions. Key to our study is a fusion of two ideas; the first is use of a macroecology model for forest structure and its coupling to a radar backscatter simulation to obtain a vertical scattering profile. We then couple this to a 3-D radar imaging technique called coherence tomography (CT), which enables reconstruction of the vertical profile up to a resolution dependent on the number of baselines available. Particular interest is paid to the ability of methods involving the Legendre spectrum. We show calculations at L band and conclude as to the potential of this technology for application in future single-pass interferometer missions such as Tandem-L (Krieger et al. 2009).

6.3 Methodology

In this study we make extensive use of a macroecological vegetation model first developed by West Brown and Enquist (West et al. 1997) (the WBE model) and developed for radar applications by Woodhouse (Woodhouse 2006b). WBE characterises the geometric structure of a plant, and by extension to a collection of plants in mutual competition, through a number of power laws derived from

biological and biomechanical considerations. Figure 6.1 shows how the multi-scale aspects of the model can be used to build structure.

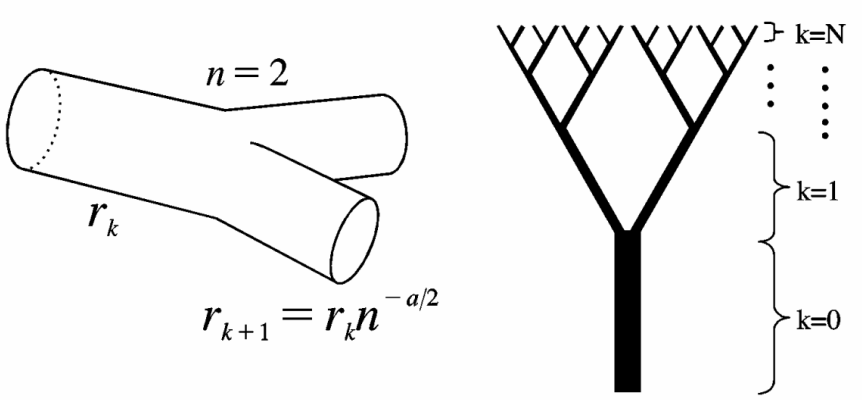

Figure 6.1. Main parameters in WBE model: scaling factor, *a*, branching ratio, *n*, branching level *k,* and total number of branching levels for particular tree, *N*.

In summary, it proposes a 6-parameter model to represent variations in both horizontal and vertical structure as described below:

a = scale factor (how radii of branches change within the plant). For example, *a* = 1 is area preserving pipe model. A more typical value is around 2/3, but variations occur between species. Generally speaking, low values of *a* are associated with 'bushy' canopies while large values with bulky stems.

N = number of branching levels (level 0 trunk, level N petiole).

n = branching ratio (number of daughter branches from parent), for example, *n* = 2 for broadleaf species and *n*= 6 for conifers.

r_k – radius of cylinder at scale k, so r_0 = radius of trunk and r_N radius of petiole.

l/*r* = length-to-radius ratio of cylinders. The WBE proposes an optimum power law relationship between branch length and radius.

These five are augmented by an additional parameter governing horizontal scale variations. These are of particular importance for any remote sensing technique that

measures spatial average parameters rather than individual tree properties. Such is the case for low-to-moderate resolution spaceborne SAR systems such as SIR-C, RADARSAT, ASAR, and LightSAR operating in the ScanSAR mode (Currie and Brown 1992). (ScanSAR achieves a wide swath coverage by periodically switching—on the fly—the antenna pointing in several range "subswaths" (Guarnieri and Rocca 1999)). In the case of ERS SAR data, a low resolution image is commonly used to refer to an image with spatial resolutions ranging from 100 to 200m). This parameter derives from the stem density (number of stems/ha) and often relates to the thinning practices in a forest.

d = thinning exponent. This ranges from 0 for constant number density (no thinning) to 3 for situations with a high rate of stem mortality not driven by competition alone.

These structure parameters have an impact on the estimation of biomass from height for example. According to WBE model height h is related to average biomass M by a power relation of the following form (Woodhouse 2006b):

$$M \propto h^{(6a+2-3da)/2} = h^x \tag{6.1}$$

We see that the relationship depends on structure, primarily via the two parameters a (relating to vertical structure) and d (relating to horizontal structure).

6.4 Coupled Ecology and EM Scattering Model

Using the branching description given in the previous section, it is possible to model a tree canopy as N levels of branching cylinders, going from k=0 to k=N, as shown in Figure 6.1. The WBE model can then be used to parameterise a full multi-layered radiative transfer model to predict the backscatter response. Here we employ RT2, a multi-layer second order radiative transfer model (Cookmartin et al. 2000) similar to the MIMICS model used in (Imhoff 1995b) and the UTACAN model used in

(Woodhouse and Hoekman 2000). RT2 was used to investigate the trends in backscatter associated with different values of *a* and *d*, at L-band wavelengths (λ = 0.2m) and for 25 degrees incidence. Each layer of the RT2 model was comprised of equal-sized cylinders parameterised by the WBE for a given *n* and *a*. Each layer in RT2 corresponds to a branching layer in WBE. The petiole radius, the dielectric properties of each cylinder and the constant of proportionality, all remain fixed. In this way we can obtain direct estimates of the average vertical scattering profile through a forest, taking into account single and multiple scattering as well as wave extinction effects. Our objective is now to see to what extent such profiles can be reconstructed by single or dual baseline radar interferometry.

6.5 Coherence Tomography

To estimate vertical structure, we propose a technique for 3-D radar imaging called coherence tomography (CT), which can be used to estimate a band-limited form of the vertical scattering profile (Cloude 2006). This technique, in distinction to other tomographic approaches, requires data for only 1 or 2 baselines and hence is well suited for application to future single-pass space sensors such as Tandem-L. Details of the coherence tomography approach can be found in (Cloude 2006, 2007). In general there are four approaches to CT in the literature, the original RVoG model (Cloude and Papathanassiou 2003; Treuhaft et al. 1996) which is a two –layer model composed by a vegetation layer (trunks, branches, leaves or needles) and a ground layer. The vegetation layer is modelled as a layer of given thickness h_v and random orientation with wave extinction σ. This model fits the best exponential profile to the data. The next approach is to use a mixture of Gaussians originally proposed in (Garestier et al. 2008; Treuhaft et al. 2002) and extended for finite bounds in (Garestier et al. 2008) and finally the Legendre spectrum to first or second order (Cloude 2007). Here we consider the performance of each of these for single and dual baseline estimation. Figure 6.2 shows a sample L-band forest profile obtained from the WBE model and used in RT2. The trees have a height of 21m and a general

structure of branches becoming smaller and more numerous with each additional branching layer moving away from the forest floor. The tree structure presented in Figure 6.1 can be used by the reader to establish a visual connection with the general structure of the forest. In modelling terms they are generated by the following parameters a= 4/3, d= 0, stem density = 2000 trees/ha and biomass around 150 t/ha. In the centre we see the predicted backscatter (in dB) while on the far right the corresponding normalised vertical profile. We see scattering is dominated by the upper canopy layer, but the scattering shows a peak below the top due to the variation of cylinder size with height embedded in the WBE approach. This is a typical non-RVoG type profile.

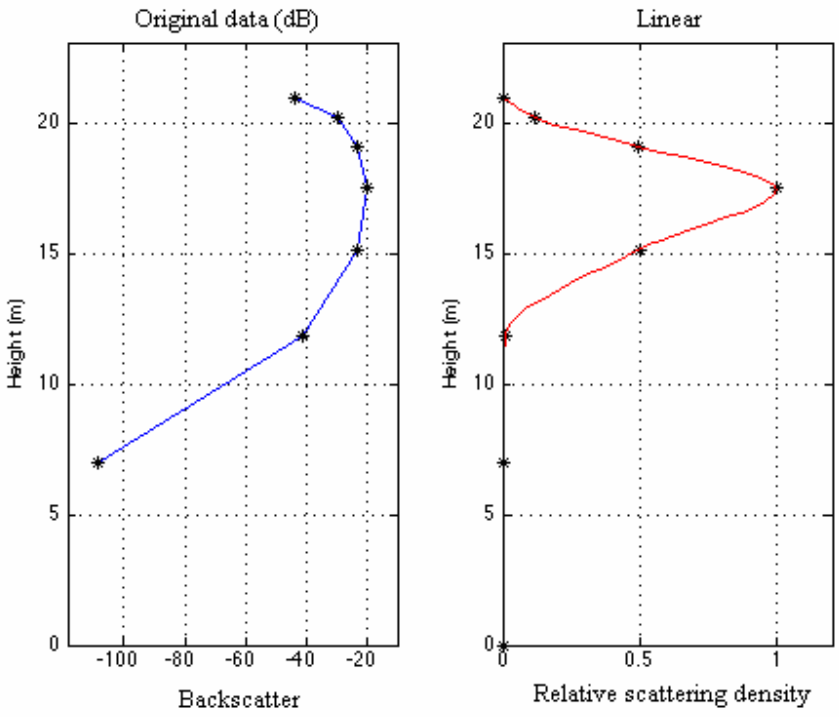

Figure 6.2. RT2 HV L-Band vertical scattering profile for a 21m pine forest model produced using RT2. Backscatter shown on (left) and relative scattering on (right) using linear values.

We can now use this profile to predict the observed interferometric coherence for a single pass L-band interferometer (Cloude 2006; Cloude and Papathanassiou 2003).

The results are shown in Figure 6.3. Here in black we show the coherence for the actual profile and in green, red and magenta the coherence contribution from the zeroth (SINC), second and fourth order Legendre expansions (Cloude 2007). We note that the coherence predicted is much higher than those observed in real L-band data (Cloude and Papathanassiou 2003; Eriksson et al. 2003). One reason for this can be the presence of surface scattering (which is here ignored). We can however use our volume-only coherence to bound the effect of arbitrary surface scattering (assuming a random volume) as shown in blue in Figure 6.3. Here we show the effect of mixing our volume prediction with surface scattering by calculating the minimum coherence observable by the interferometer (Cloude and Papathanassiou 2008a). These coherence bounds are much more in line with those seen in experimental data (Lee et al. 2008). We can now use this coherence to estimate the profile using single baseline coherence tomography. Figure 6.4 shows results for four different methods.

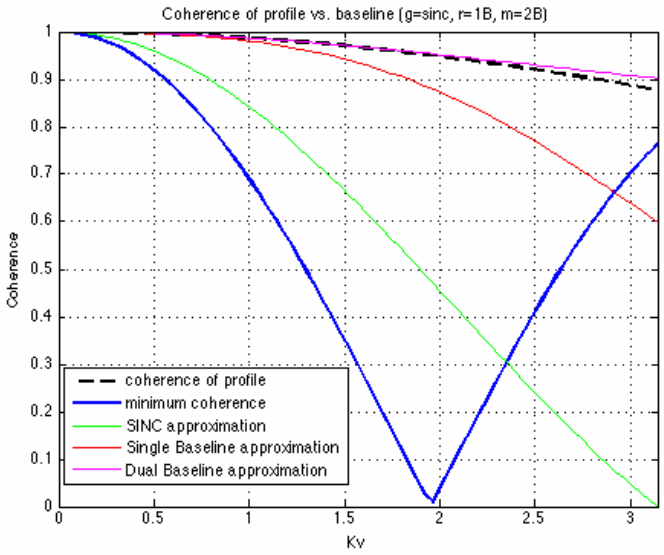

Figure 6.3. Predicted interferometric coherence for vertical profile of figure 6.2 and variable baseline/height product K_v (Vertical Wavenumber).

We see a slight underestimation of height and poor reconstruction of the actual shape from a single baseline (the Gaussian provides the best fit). With two baselines we can do much better as shown in Figure 6.5. Here on the right we show the Legendre

spectrum (up to 7th order) of the true profile and on the left show the various reconstructions for single (red), dual (magenta) and triple (blue) baselines. One baseline produces 3 orders of Legendre spectrum while further additional baselines add two orders each. We see that dual baselines already provide a good estimate. We can further simulate the case for smaller pine tree forest structures as shown in Figure 6.6. The structure sees a greater value of *n* in the older branches. Here we have a fuller canopy from ground to top. Its Legendre spectrum is shown on the far right and again we note significant spectral components beyond the single baseline case (shown in red) with very different spectral amplitudes observed for each order in comparison to those of Figure 6.5. Again, as with the scenario of Figure 6.5 the Gaussian basis function as is shown in Figure 6.4 produces a shape more fitting to volume-only scattering.

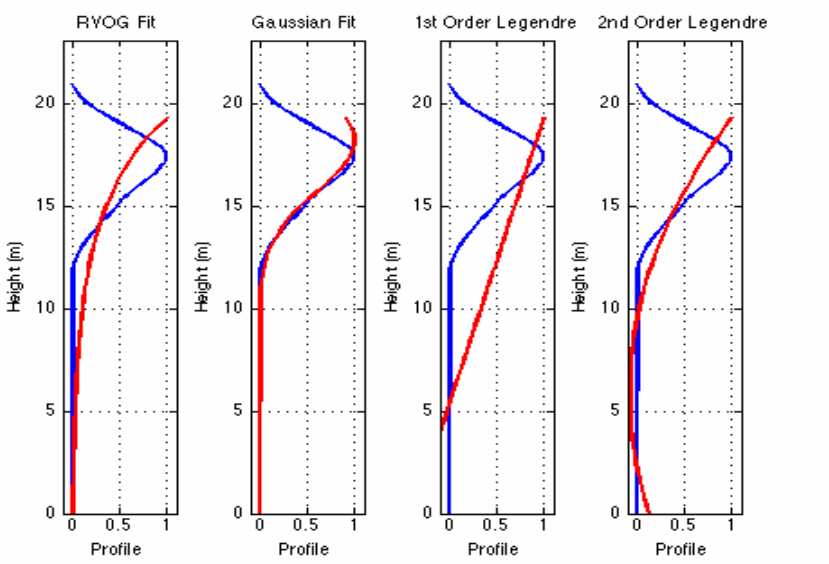

Figure 6.4. Estimated heights and profiles (red) using different coherence tomography techniques versus the true RT2 HV profile (blue). From (left) to (right) RVoG model of increasing attenuation with depth, Gaussian function, Legendre function 1st order, and Legendre function 2nd order.

6.6 Comparison With Experimental Data

We now move on to compare these simulations with profiles reconstructed from a real pine forest. We use L-band repeat-pass POLInSAR data from the DLR E-SAR system for the Remningstorp test site in Sweden. The prevailing tree species are Norway spruce, Scots pine and birch with a dominant soil type of till with a field layer, where present, of blueberry and narrow thinned grass. Tree heights are in the order of 20m with local maxima of up to 30m. The topography is fairly flat with terrain elevation above sea level ranging between 120 and 145m. Ground measurements have been taken at the test site for decades making it an ideal location for remote sensing experimentation and has been used in studies such as (Fransson et al. 2008; Lee et al. 2009; Lee et al. 2008; Tebaldini 2009; Ulander et al. 2000).

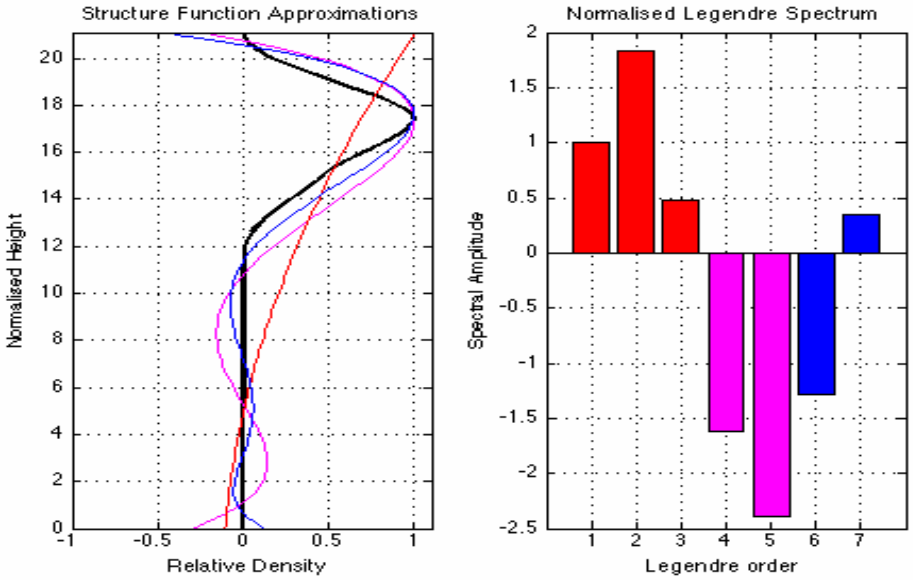

Figure 6.5. Legendre spectrum estimates of RT2 L-band profile (right) and corresponding reconstructions (left) for a 21m forest model featuring a concentration of branching elements towards the top of the canopy. Red represents single, magenta double, and blue triple baseline datasets and corresponding Legendre spectrums. Black represents actual profile.

For this forest test site, reference LiDAR height data is also available to provide a test of height estimation accuracy as used in (Lee et al. 2008). Figure 6.7 shows profiles from coherence tomography using the 'optimum' volume polarisation channels i.e. the ones with the minimum surface component across all possible polarisation states (Cloude and Papathanassiou 2003) for sample pixels in short (upper) and tall (lower) trees. In blue we show profiles reconstructed from the radar coherence but using the LiDAR height and in red the radar derived height and profile. Notice that for the shorter trees the profile *increases* with depth, indicating significant effect of the surface layer scattering. The taller trees are less affected but from the 2nd order Legendre response we see some evidence of a surface component even here. Again we see how the Gaussian and Legendre estimations are much more appropriate for height inversion than the commonly used RVoG model.

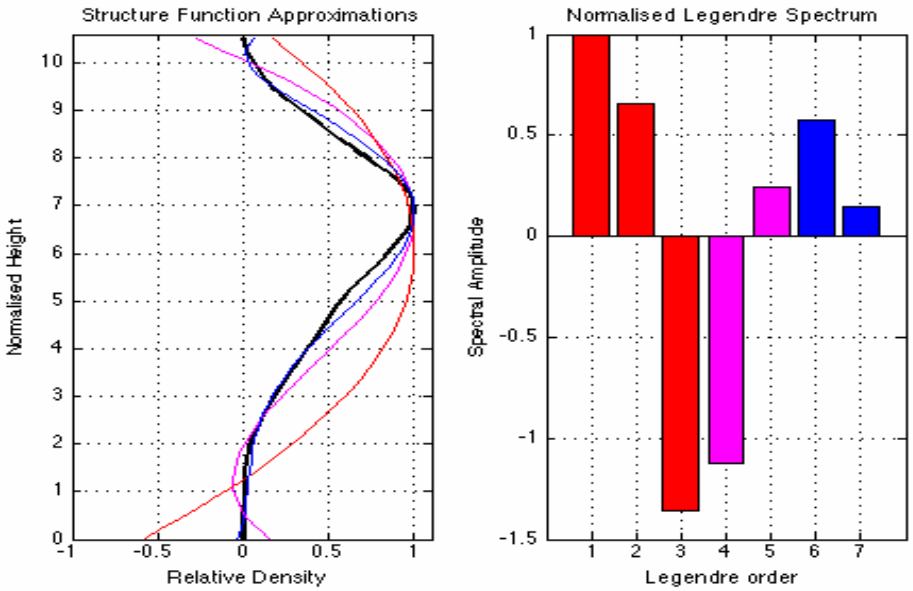

Figure 6.6. Legendre spectrum estimates of RT2 L-band profile (right) and corresponding reconstructions (left) for a shorter pine tree forest featuring a fuller canopy from ground to top. Red represents single, magenta double, and blue triple baseline datasets and corresponding Legendre spectrums. Black represents actual profile.

This varying surface component has an effect on forest height estimation at L-band as shown in the azimuth transect in Figure 6.8. Here we show vertical profiles with LiDAR height in black (here taken as the truth) and the radar estimate in white. Notice the clear correlation between radar height underestimation and dominant surface scattering in the vertical profile.

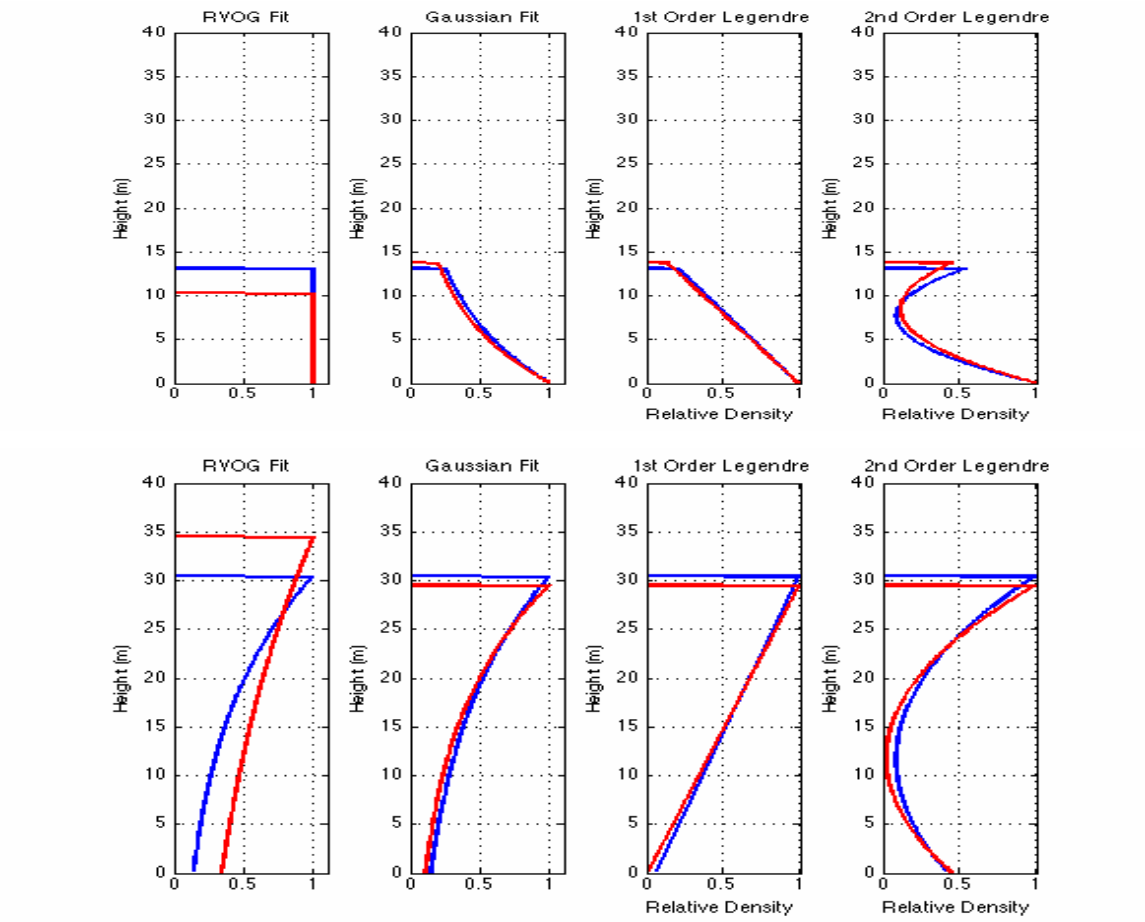

Figure 6.7. Sample L-Band profiles (red) from Remningstorp forest test site for small (upper) and tall (lower) trees with LiDAR derived true heights in blue. Shapes differ significantly from profiles of Figures 6.4, 6.5, and 6.6 as specific data from each branching level provided from RT2 modelling is not obtainable from empirical acquisition. In addition the data from Remningstorp features ground scattering not used in the RT2 simulations which serves to enhance lower canopy contribution.

6.7 Conclusions

In this paper we have shown, using a combination of a macroecology forest model and a numerical scattering code, how the volume scattering vertical profile is dominated by structure effects rather than simple extinction (as classically proposed in the RVoG model). This impacts on the estimation of height using single-pass interferometry, which can be underestimated without the required knowledge of structure. We have used experimental data to show that the effect of surface scattering cannot be ignored at L-band, even in tall forests, and hence that the observed coherence spectrum in real POLInSAR data cannot be assumed to contain a volume-only scattering channel. We therefore propose the following approach to the estimation of structure and isolation of volume scattering based on these results.

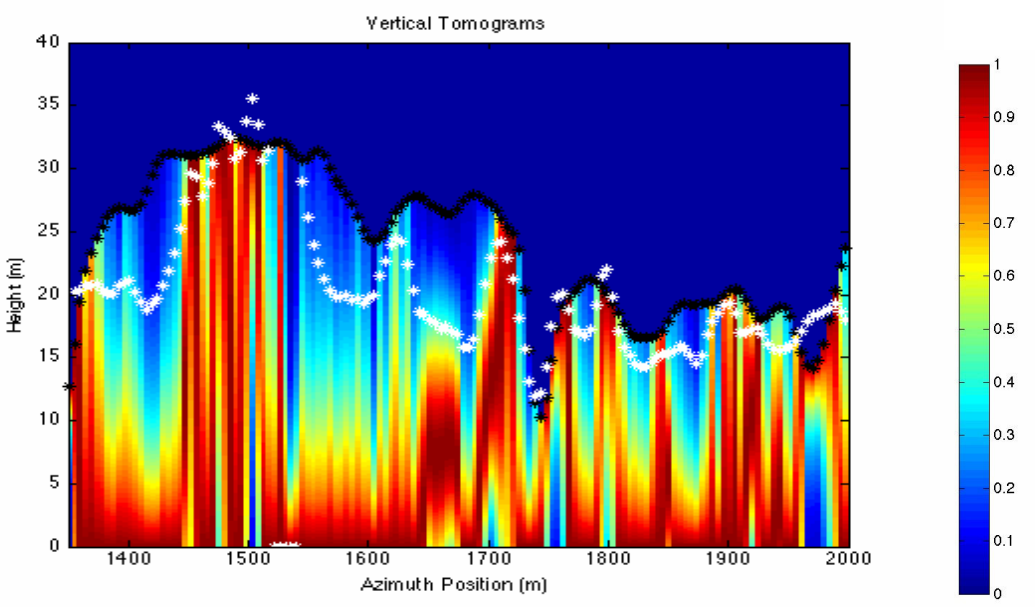

Figure 6.8. Variation of L-band profile for a transect through E-SAR data intensity of scattering shown in RGB colour key. Radar height estimation is shown in white, in situ height measurements represented by black. Correlation of radar height underestimation with dominant surface scattering is shown through the location of high intensity (red) scattering concentrated close to ground surface.

We suggest dual baseline POLInSAR could be used, even ‘incoherently’ i.e. without relative phase calibration, for independent Gaussian basis tomography along the coherence line with matching of Gaussian parameters between baselines to remove the residual surface component and efficiently reconstruct the volume only profile. Future studies will address this proposal in more detail.

7 A "Matchstick Model" of Microwave Backscatter from a Forest

Matthew Brolly and Iain. H. Woodhouse

Summary

The work of this chapter was conducted in 2009 and was submitted to Ecological Modelling in 2011. It is currently in review. The themes of this chapter are linked to the work of Chapter 5. In Chapter 5 the focus is the vertical backscatter distribution of the forest, here the horizontal structure in terms of stem number density, and size is considered. The importance of branching architecture is reduced in this work with the focus on the use of long microwave SAR. In both chapters the importance of the scattering regime is emphasised with analysis of the effects of variation in distribution, size and number density of forest constituents. Both chapters consider mono-age and mono-species forests as the main focus. The work of this chapter also relates to Chapter 4 through the depiction of a forest as a series of vertical cylinders. Here the effects of thinning and planting density are explicitly considered in a controlled scenario whereas in chapter 4 the variations in number density were species and environmentally defined indirectly through SERA.

Modelling observations (Woodhouse 2006b) and empirical data (Imhoff 1995b) have shown that forests can present varying volume saturation levels as a result of different number densities or structural factors. SAR backscatter saturation is typically considered an effect of energy attenuation within the canopy with saturation behaviour exhibited at particular volume densities associated with the incident EM waves. If saturation can occur at lower volume densities, particularly for forests with lower initial planting, then another factor must contribute. This chapter attempts to explain this behaviour through analysis of the relationship between scattering regimes and the forest scatterers and aims to answer the following questions:

1. Can forests be represented at long radar wavelengths as a collection of vertical cylinders?
2. In the absence of attenuating features of branching and foliage are saturation effects exhibited when backscatter is plotted against increasing volume?
3. Can this behaviour be described using Rayleigh and Optical scattering definitions?
4. How does such behaviour inform on the macroecological status of the forest?
5. Does a variation in thinning rate and therefore number density have a direct impact on the trends of backscatter observed with increasing forest volume?
6. Do these dependencies make a unique proportional relationship between backscatter and volume obtainable?

To answer these questions the Matchstick Model (Chapter 3.3) is used. By allowing the effects of backscatter from long wave microwaves to be studied in a controlled scenario the influence of macroecological changes on backscatter saturation behaviour can be investigated. The simple scenario of the Matchstick Model allows scattering to be described as a contribution of Rayleigh and Optical (Non-Rayleigh) scattering allowing a comparison with radiative transfer data from identical forests produced from RT2 (Chapter 3.4). This paper also lays the theoretical groundwork for the use of SERA derived forests (Chapter 3.2 and (Hammond and Niklas 2009)) in a radiative transfer scenario (Chapter 8). SERA is shown in the subsequent chapter to provide a more heterogeneous forest environment than can be produced by the Matchstick or WBE models (which are necessarily simplistic to enable development of the theories), providing a testing ground for the theories developed in this chapter to be explored independently of forest architectures defined by user inputs.

The main body of this chapter including the modelling procedures were conducted by myself. Additional help was provided by Dr. Woodhouse with editing and idea development within a supervisory role.

7.1 Abstract

Given that the majority of biomass is contained in the stems of trees within forests (as much as 90%), a new radar modelling approach is proposed here wherein the stems are the major biomass contributor in the context of Synthetic Aperture Radar backscatter sensitivity to forest biomass. The new model regards stems as "matchsticks" consisting of constant radius, constant density, and constant dielectric properties. Furthermore, by considering only the larger constituents of the forest a clearer understanding of the correlation of biomass with backscatter from P and VHF Band SAR can be obtained.

Using backscatter data produced from the RT2 radiative transfer model this paper considers the effects of SAR scattering when interacting with forest stands consisting of identical vertical stems, or matchsticks. SAR frequencies of 50MHz (VHF) and 429MHz (P-Band) are used to generate a comparative radar interaction data. These not only allow a comparison of the scattering of SAR signals of different wavelengths but also of how interactions with stems can reveal novel clues as to the source of the backscatter saturation phenomenon of forests. Removing the volume scattering aspect of a forest would be expected to eliminate the saturation behaviour which occurs at increasing levels of biomass density, an effect believed to be due to extinction effects, but is shown here to not be the case. Results reveal that saturation can occur even for the single stem case where increasing the size of this stem through the radii associated with Rayleigh, Mie and Optical scattering will result in backscatter saturation behaviour as the biomass density is increased. Consistent with this finding, a forest of solely vertical stems will exhibit saturation behaviour at lower biomass density values when lower planting densities of similar stems are used. In this study the backscatter model considers the ground contribution to be negligible but does include the double bounce as a result of interactions between the stems and ground.

Also considered are Mie backscatter oscillations which are shown to average out when using both non-vertical stems and random radius values about a mean, both independently and collectively. These "Mie" effects can also be removed by altering the incident SAR angle. These findings allow a reduction of the backscattering scenario of forests to a two- region problem involving solely Rayleigh and Optical scattering. This serves to further provide an explanation as to the origin of saturation, whereby the balance between the optical scattering increase and the matchstick number density decrease cancel each other out.

The important conclusion is that backscatter does not measure biomass, but measures structural trends that are correlated with biomass in different ways, driven by stand level competition, resource use, etc. As a result different forest growth regimes should expect different backscatter-biomass trends.

7.2 Introduction

Modelling vegetation as a random volume over a ground (RVoG) provides a simple, deductive tool for understanding microwave backscatter from a forest (Treuhaft et al. 1996). It forms the basis of height determination from polarimetric interferometry (Papathanassiou and Cloude 2001) and, with its history in the Water Cloud Model (Attema and Ulaby 1978), continues to support the widely held assumption that saturation of backscatter with increasing biomass is always driven by increased canopy opacity. However, these models fail to capture one key physical aspect of a forest, namely that the stems often contain the majority of the standing biomass (up to 90% according to a study of 332 angiosperm and 343 conifer dominated communities (Cannell 1982)), and similarly for tropical species (Bastien-Henri et al. 2010). This is important for two reasons: (1) at long wavelengths (P-band and longer) stems make a significant contribution to the total backscatter (Smith and Ulander 2000), (Smith-Jonforsen et al. 2007), and (2) that total backscatter within an area is determined by

the number of stems as well as their individual shapes and sizes (Smith-Jonforsen et al. 2007), (Imhoff 1995b). While backscatter increases with increasing stem size, an increase in biomass can typically be associated with a corresponding rapid decrease in the number density of stems.

In order to understand the balance of these conflicting trends, this paper introduces a new deductive model of forest backscatter based on a collection of identical cylindrical stems, with no canopy. By combining the simplified representations of the backscatter trends from individual stems based on (Smith and Ulander 2000), (Fransson et al. 2000b), and (Fransson et al. 2004) with the generalised stem dynamics observed in macroecological studies (West et al. 1999a), this model is able to explain the range of observed backscatter-biomass trends published in the last 30 years. Understanding the trends in radar backscatter measurements of forests is undeniably important from scientific, economic and policy related standpoints, since one of the most important applications of remote sensing is the monitoring of forests and their contribution to the terrestrial carbon cycle and related policy issues such as REDD (Gibbs et al. 2007).

In this paper we introduce a "Matchstick" model approach to simplify the forest structure. It builds on earlier models developed for VHF measurements (Smith and Ulander 2000) by incorporating generalised stem parameters from studies in macroecology (following on from (Woodhouse 2006b)). Our key question is as follows: is radar backscatter a good indicator of stem volume (biomass) per unit area when only the tree stems are considered? The concept that "structure" may influence backscatter is not new (see (Imhoff 1995b), for example) but here we expand this concept to introduce a formalised model at the stand level based on generalised biological principles. The validity of the model and its limitations are demonstrated by comparing model predictions to both radiative transfer model results and previous empirical studies at VHF, and P-Band (50MHz, 429MHz).

7.3 Methods and Theory: The Matchstick Model

Simple, single layer models of microwave scattering from a forest have treated the target surface as either a dielectric slab with constant properties suspended above the ground (Bush and Ulaby 1976) or a layer of sparsely distributed identical dielectric scatterers. These scatterers can be spheres, as in the Water Cloud Model (Attema and Ulaby 1978), or random cylinders (Peake 1959) which may be randomly oriented, (now referred to as the Random Volume Over Ground (RVOG) model, (Papathanassiou and Cloude 2001), (Mette et al. 2004a)) or with a systematic orientation (Treuhaft et al. 1996), (Smith et al. 2002). These models share one important common feature in that none of them considers the change in number density of tree stems associated with biomass changes.

Remaining within the realms of simple, single-layered models, we describe here a model based on a single layer of stems, which we call the "Matchstick Model". It is an oriented layer of cylinders and as such the model is most suited to P-band wavelengths or longer. The stems are identical and always (near) vertical, and do not account for tapering. The forest biomass is assumed to be directly proportional to the total volume of the cylinders in a similar fashion to the relationships explored in (Fang et al. 1998) in which a simple linear relationship between stand biomass and volume is shown to exist for all the main forest types in China. In that work a direct relationship established between stem volume and biomass was shown to slightly underestimate biomass. Similar relationships are used in (Valentine et al. 1984) and documented in (Philip 1994), while (Le Toan et al. 1992) states the link between stem volume and biomass within the context of a radar survey. Changes in area biomass are therefore a result of changes in cylinder size and number density. Since the stem volume-biomass relationship is expected to be both species and site specific, our primary application of the model is to explore trends in backscatter associated with biomass changes (rather than simulate absolute values). A visual representation of

the model is demonstrated in Figure 7.1, with the parameter *d* describing the nature of thinning defined in Chapter 7.3.2.

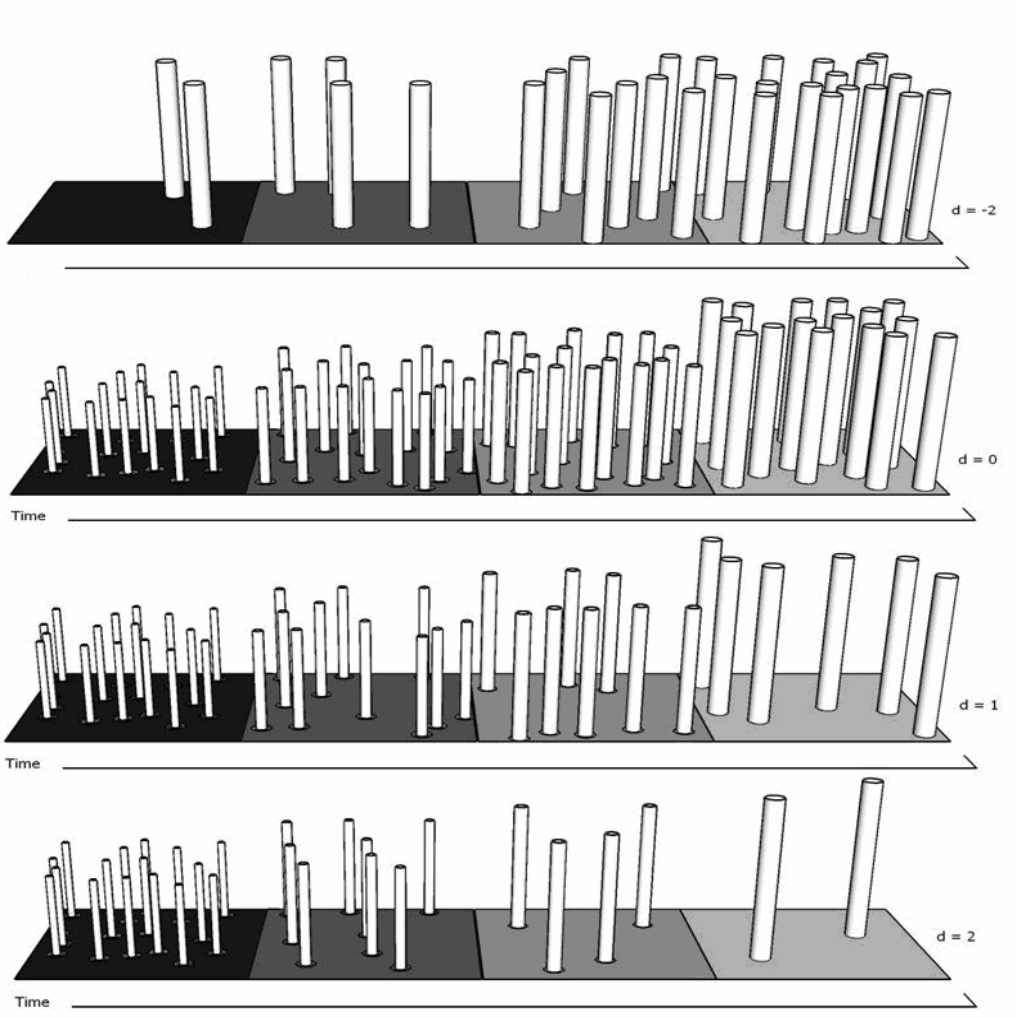

Figure 7.1. Representation of collection of cylinders in four forest settings. Area is schematic representation. From top to bottom *d*=-2, *d*=0, *d*=1 and *d*=2 representing various thinning regimes. Where *d* is positive the progression from left to right can represent a single stand changing over time or simply the state of four neighbouring plots at any one time. When *d* is negative the progression can not be considered with respect to time (and therefore stems growth) but can represent neighbouring stands, shown here with no stem size variation.

Chapters 7.3.1 and 7.3.2 describe how we can characterise the changes in stem size and number density using general macroecology principles. The two sections after

these (7.3.3, 7.3.4) describe the twofold modelling approach. Firstly, we consider trends in backscatter from varying sized cylinders using a simple model. Following this we corroborate these trends using a full radiative transfer model, RT2, described in Chapter 3.4. In each case the modelled scenario is that of a developing forest with increasing biomass. In reference to Figure 7.1, although it can be assumed that when thinning, *d*, is zero or greater the data points in this study represent a single hectare forest changing over time they can just as easily refer to neighbouring hectare plots at differing stages of growth within a large forest or plantation. This would always be the case for negative *d* values. This is particularly relevant in an expanding forest where a plot of new growth would mimic the characteristics of early stage forest. Modelling a single stand across a number of years does not take account of variations that may exist in terms of ground conditions and other environmental factors that may directly affect the growth of the forest but in spite of this, this method allows a direct analysis of the effect of size and number distribution on the trends of backscatter return. This method of forest modelling is therefore directly relevant to studies presented in the literature, as the acquisition of a wide range of biomass values to enable scientific analysis involves the survey of forest stands of varying stages of growth, and is particularly true within monospecies stands in which the allometry of individual trees is assumed to vary very little, and resource levels to remain fairly consistent, within neighbouring stands.

7.3.1 Individual Stem Characteristics

In this study the variables that determine individual stem sizes are (1) a scaling factor, *a*, which determines proportional change of cylinder shape to cylinder size, (West et al. 1997), (Woodhouse 2006b):

$$l \propto r^{2/(3a)} \tag{7.1}$$

(where, l is stem length and r, radius), and (2) the length-to-radius constant of proportionality, m, so that:

$$l = mr^{2/(3a)} \tag{7.2}$$

This allometric formulation utilises biomechanical constraints that predict some optimal relationship between l and r. Decurrent trees (most broadleafed species) are appropriately described by the elastic similarity model, a = 1, whereas a =2/3 is the value that represents geometric similitude, $l \propto r$, which (Niklas 1994) reports is consistent with many observations of excurrent species (most conifers). Empirical data suggest that stems have often been better represented by some value greater than $a = 7/6$, similar to the case of stress similarity, a condition related to $a = 4/3$. In the interests of space, we do not present all model results for differing values of a, given that backscatter trends remain consistent for $2/3 < a < 4/3$, even if absolute values vary. Instead, we stick to a default choice of a=1, representing the idealised "pipe" model in the WBE branching model.

The constant of proportionality, m, is more diverse than observed values of a. Reported values range from approximately 5 to 163 in the dataset of (Cannell 1982) which includes 675 forest communities. The default value in this study is chosen to be 20 due to its frequency of occurrence in this dataset. We will show that while absolute values vary, the general trends remain similar for large m variations.

7.3.2 Stem Number Densities (Populations)

In radar measurements it is not usually possible to measure individual trees. The Matchstick Model therefore incorporates variability in both stem size, and stem number density within a population. In the current work we only consider populations of identical stems so that variability of biomass per unit area is governed only by variability in size and number. This is a reasonable representation of managed monocultures and for many single species forest areas where one size dominates. For

example see (Zenner and Peck 2009) for red pine managed stand statistics showing range of size distributions within mature stands..

In any forest biome, the number of trees of a given size is limited by the available resources, and the balance between new growth and tree mortality (including herbivory and fire). These may vary both spatially and temporally. The relationship between the size (radius, r) and number of trees, N, can be characterised by a "thinning factor", d, such that

$$N \propto r^{-d} \tag{7.3}$$

(See also (Woodhouse 2006b)). Although called a "thinning factor" it need not apply only to the change in a population over time (or a spatial surrogate, as in different aged managed stand) – we use it here as a general description of the size-number relationship. Figure 7.1 visually describes the impact of d and demonstrates the relationship between size, number density and volume. When d=0, N is constant and total volume increases linearly with the volume of each stem. This is typical of young, actively growing forest (such as regeneration) where trees have yet to utilize all available resources, and tree mortality is near zero. Here, biomass per unit area will be positively correlated with N.

When d=2, there is a dramatic decrease in N. The total volume still increases since the collective basal area remains constant (since each stem's basal area increases with r^2) while stem height increases. This is typical of many forests, especially in the tropics, or in managed forests where thinning has been applied in order to maintain basal area. It is exactly this dramatic change in structure associated with increasing areal volume that the Matchstick Model tries to characterise (and is not incorporated into other simple single layer models). In this case the biomass per unit area is inversely proportional to N.

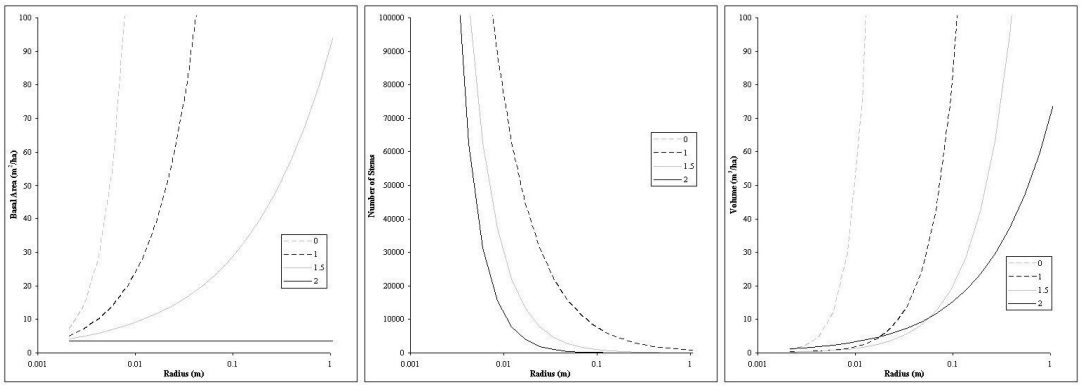

Figure 7.2. Relationship of basal area (left), number of stems (centre), and volume (right) with respect to branch radius for varying thinning parameters representing identical single stem size forests starting from initial planting of 500000 stems per ha. Legend represents values of thinning parameter, *d*. Variations in *d* highlight how particular volumes and basal areas can be represented by different stem numbers and radii as a consequence of thinning.

For $d = -2$ (relating number increases and neglecting corresponding radius increases) the cylinders are identical; increasing volume per unit area corresponds to increasing *N*. This is typical of a resource-limiting case, such as savannas, whereby tree numbers are limited due to competition for scarce resources such as water, but where trees do grow they often need only grow to a sufficient height to outperform grasses and avoid fire and herbivory (Sankaran et al. 2008). In these cases biomass per unit area will again be positively correlated with *N*.

Thinning is directly related to the resources available per tree within an area which in turn has an effect on the backscatter response. The amount of thinning that takes place within a forest directly affects forest number density and therefore backscatter (Champion et al. 1998). Changes in number density then have a significant effect on the space available for growth (Ginn et al. 1991; Waring 1983) and with the growth of a tree determining the stem size and tree height it will have a direct influence on backscatter (Castel et al. 2002; Imhoff et al. 2001).

In the modelling results that follow, we look at different forests that begin with a finite number of small trees (the "planting density", *p*) which then grow and reduce in number, as given by *N*. We are then able to describe the impact of both *d* and *p* on the backscatter trends associated with increasing volume (and by implication, biomass). The range of basal areas and volume used within this study cover realistic values of up to $100m^2$/ha and $1000m^3$/ha respectively (Shula 1989), (Cannell 1982), (Kinnunen et al. 2007). How volume, basal area and *N* change with *d* is illustrated in Figure 7.2.

7.3.3 Scattering Considerations

The simple model offered here considers the limiting case of cylinders with circumferences smaller than 0.1λ of a wavelength on the one hand, and much larger than 10λ on the other. For the sake of simplicity, we refer to these limits as corresponding to "Rayleigh" and "Optical" scattering, respectively. In the Rayleigh case we assume the backscatter from each cylinder increases with the square of the cylinder volume, and for the latter, it increases with the physical cross-section (Kononov and Ka 2008). At the transition between these two regimes lies resonant scattering, here we make an approximation that assumes the resonant behaviour "averages out" across this region due to the cumulative effect of a distribution of stem sizes. This assumption is supported by empirical results in (Lopes et al. 1991), and (Mougin et al. 1993) and considered more completely in Chapter 7.4.3.

Following the formulation by (Smith and Ulander 2000) based on VHF backscatter from individual stems at a polarisation P (H or V), we can write the radar cross section of a single tree stem as

$$\sigma_{PP} = \frac{4\pi}{L^2}\left| r_P(\theta)\frac{k^2(\varepsilon_r - 1)}{\pi(\varepsilon_r + 1)}\right|^2 V^2 \tag{7.4}$$

where V is stem volume, $r_p(\theta)$ is the Fresnel reflection coefficient of the surface, ε_r is the relative dielectric permittivity of the trunk, and L is the attenuation. Given the

simplicity of the Matchstick Model it is reasonable to consider all of these parameters, except *V*, to remain constant. The one point of discussion is whether it is an appropriate assumption for the attenuation, *L*. (Smith and Ulander 2000) give a convincing case as to why this would be so at VHF wavelengths, but it is less clear whether this would be appropriate for, say, P-band. A compelling case for the importance of attenuation would normally be made based on evidence of saturation in the backscatter-biomass curves. However, it is just such an interpretation based on the Water Cloud model that we wish to challenge with the Matchstick Model. Indeed, the results presented in this paper demonstrate that the impact of thinning on the backscatter can be sufficient to cause saturation even when attenuation due to a thickening canopy and increasing number of scatterers is ignored. Attenuation in this case does not refer to any scattering variations that may occur on the individual level due to scattering regime change as these variations are considered an important part of the theories presented here. Saturation in itself is therefore not evidence of increasing attenuation by the forest layer.

In summary, we argue that we can characterise the trend in backscatter from each stem in the Matchstick Model as follows. For Rayleigh scattering:

$$\sigma_{Rayleigh} \propto V^2 \tag{7.5}$$

Using the relationship between length and radius of (7.1), the proportional relationship can then be written with respect to *r* and *a* as follows. The radar cross section per unit area is proportional to the cylinder volume:

$$\begin{aligned} \sigma^0_{Rayleigh} &\propto N\, r^4 l^2 \\ &\propto N r^{(12a+4)/3a} \end{aligned} \tag{7.6}$$

For Optical scattering, the normalised radar cross section scales with the physical cross-section:

$$\begin{aligned}\sigma^0_{optical} &\propto N\ A \\ &\propto Nrl \\ &Nr^{(3a+2)/3a}\end{aligned} \tag{7.7}$$

This is in accordance with the laws of geometric optics which under certain limitations is an acceptable simplification of the scattering formula for the physical optics of a cylinder. The physical optics formula for the radar cross section of a cylinder is shown below where k is the wavenumber, r the cylinder radius, l the cylinder length and θ represents the incident angle from broadside:

$$\sigma^0_{cyl} = krl^2 \cos^2\theta \left[\frac{\sin(kl\sin\theta)}{kl\sin\theta}\right]^2 \tag{7.8}$$

By taking an average value over a symmetric window of incidence angles centred at $-\theta_w \leq 0 \leq \theta_w$ the average radar cross section of a cylinder becomes the integral:

$$\overline{\sigma^0_{cyl}} = \frac{1}{\theta_w}\int_0^{\theta_w} krl^2 \cos^2\theta \left[\frac{\sin(kl\sin\theta)}{kl\sin\theta}\right]^2 d\theta \tag{7.9}$$

As this window approaches zero the small angle approximations of $\cos\theta$ =1 and sin θ = 0 apply, and following a change of variable and subsequent integration we get the closed form formula for the average radar cross section of a cylinder around broadside, equation (7.10) (see also Hestilow 2000):

$$\overline{\sigma^0_{cyl}} = \frac{rl}{\theta_w}\left[Si(2kl\theta_w) - \frac{\sin^2(kl\theta_w)}{kl\theta_w}\right] \tag{7.10}$$

According to the rules of the sine integral function Si(x), as the argument (x) approaches zero, Si(x) will tend to x. Similarly by taking the limit of the angular window tending to zero we can rewrite equation (7.10) as below:

$$\overline{\sigma^0_{cyl}} = \lim_{\theta_w \to 0}\frac{rl}{\theta_w}\left[Si(2kl\theta_w) - \frac{\sin^2(kl\theta_w)}{kl\theta_w}\right] = \frac{rl}{\theta_w}\left[2kl\theta_w - kl\theta_w\right] = krl^2 \tag{7.11}$$

Where the window tends to zero and is approximately representative of the broadside angle the average radar cross section is proportional to the frequency and the cylinder volume. But in the limit of large arguments where $2kl\,\theta_w$ is large, the function Si(∞)→ π / 2. Under the limits of $kl\theta_w$ tending to infinity (equation (7.12) we can write the equation for average radar cross section of a cylinder as in equation (7.13):

$$\lim_{kl\theta_w \to \infty} \frac{\sin^2(kl\theta_w)}{kl\theta_w} \to 0 \tag{7.12}$$

$$\overline{\sigma^0_{cyl}} = \frac{\pi r l}{2\theta_w} \tag{7.13}$$

This frequency invariant equation is then a function of the physical cross section of the cylinder in accordance with geometric optics. A full progression of the working is found in (Hestilow 2000).

If the geometric optics is valid it can be stated that within P-Band at 429MHz the radius value of a scatterer coinciding with the transition from Rayleigh to Mie is about 0.01m and the radius value of a scatterer which coincides with the transition from Mie to Optical is approximately 1.1m, so scatterers greater than 0.01m are deemed Optical scatterers for the purpose of this study.

An application of this simple approach is shown through Matchstick Model data in Figure 7.3, whereby the backscatter is shown as logarithmic plots for 4 different planting densities in the absence of thinning (*d=0*). Two distinct phases are visible. The Rayleigh scattering is represented by low biomass density data points, the region exhibiting a broad distribution among planting densities. The population density has a significant effect on the backscatter level in the Rayleigh. As the scattering transitions into Optical it is apparent that the relationship is less sensitive to the planting density. Note the similarities between the Matchstick Model representations of geometrical (Figure 7.3 (left)) and physical optics (Figure 7.3 (right)).

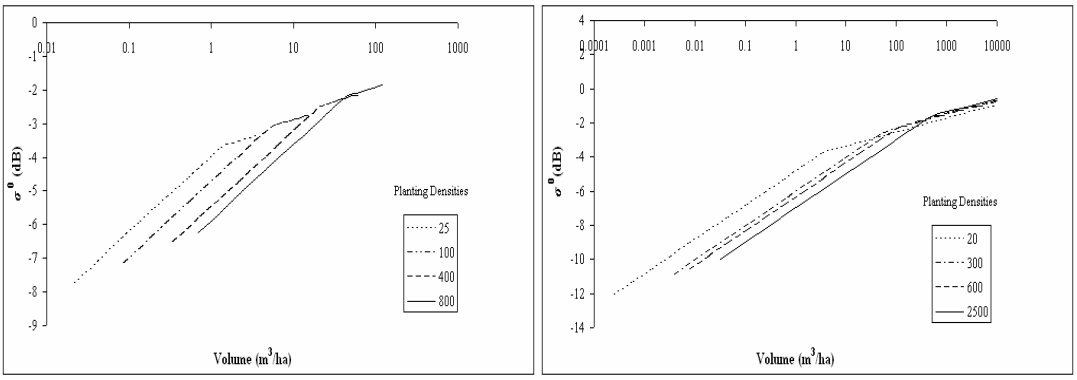

Figure 7.3. Simple Matchstick Model predictions produced from varying planting densities per ha. Data based on the combination of two equations representing the correlation of Rayleigh backscatter with the square of the volume Eq.(7.5), and the correlation of Optical backscatter with basal area Eq.(7.7). Planting densities vary in each figure and are chosen to achieve similar volume values. Figure (left) represents geometric optics and (right) physical optics. Note the similarity in trends.

7.3.4 Radiative Transfer Modelling Using RT2

RT2 is a multi-layer second order radiative transfer model similar to the MIMICS model used in (Imhoff 1995b) and the UTACAN model used in (Woodhouse and Hoekman 2000). It is described in (Cookmartin et al. 2000) where it was used for modelling crop backscatter and in (Balzter et al. 2003b) for forests. In the current study, RT2 was used to investigate the backscatter from the Matchstick forest for a range of scenarios. RT2 is a fully polarimetric, second-order solution to the radiative transfer equations that treats vegetation canopy as a plane-stratified multilayer region over a rough surface. Its use in this instance is limited to a single plane with only vertical stems existing over a rough surface. The scattering properties of all plant components are derived from their depictions as simple geometric forms but here we only consider plant stems, represented as finite-length cylinders. The reader is referred to Chapter 3.4 of this thesis.

7.4 Results

7.4.1 Model data

In this modelling process initial planting densities from 1 to $1x10^7$ trees per hectare were used. This selection was made to encompass realistic planting densities as well as extreme cases which are less likely (for forest conditions) which can be reduced significantly in numbers through each growth increment according to the thinning regime. As well as the variation of planting density, the scaling is altered via the constant of proportionality *m* and scaling exponent *a*. Data has been modelled for both VHF and P-Bands. Typical variations, due to changes in *m*, manifest as minute changes in trends, but show increased backscatter associated with longer stem lengths for similar radii.

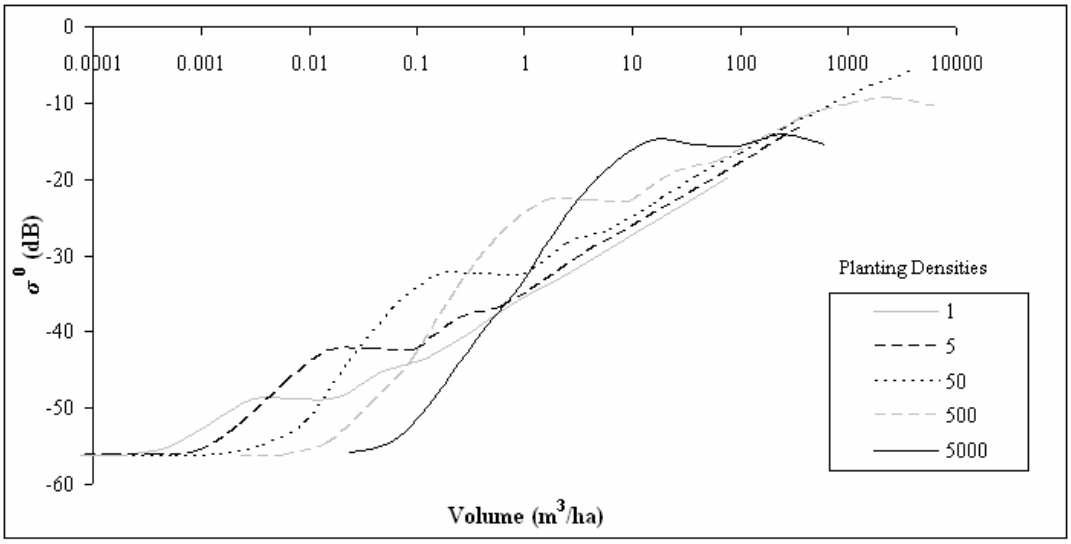

Figure 7.4. RT2 modelled VV P-Band data for multiple planting densities per ha. in the absence of thinning. Number densities maintained at planting density level for duration of growth signifying zero mortality.

In a similar fashion to the Matchstick Model predictions of Chapter 7.3.3, RT2 backscatter data is plotted against the log of the volume (with zero thinning, as in

Figure 7.3). The common feature regardless of planting density is the clustering of data points at higher volumes around a common trend in backscatter values, Figure 7.4. The low volumes featured in this figure are a consequence of the need to avoid extremely high basal areas resulting from higher initial planting densities in the absence of thinning. Therefore avoiding potential interference of stems with one another and deviation from the assumption of low attenuation.

7.4.1.1 Saturation Effects

When a single stem is modelled in RT2 it already shows saturation like effects (even for very low stem volume) due to the transition to Optical scattering as the single stem grows with each increment. In itself, this is an important observation that should be borne in mind when plotting backscatter-biomass trends. 50MHz VHF data shows similar saturation trends. The theoretical transition points between Rayleigh and Mie, and Mie and Optical scattering are determined by the ratio of wavelength to radius.

Data were modelled for sparse as well as dense (Figure 7.5) stem scenarios with the backscatter values of each of these planting densities represented with respect to the radius. The trend is independent of planting density and scaling properties.

The use of longer wavelengths in SAR forest remote sensing has consistently been observed to move the point of backscatter saturation to higher biomass values (Table 7.1). This effect is normally attributed to decreasing opacity of the forest canopy as wavelength increases. For example, (Smith and Ulander 1998) describe the theory of attenuation limitation as, “fundamentally linked with the high attenuation through the top of the foliage and the backscatter sensitivity to small-scale structures”. When considering low numbers of single stems this attenuation is significantly reduced, and the large-scale structures (of the order of the wavelength) dominate the backscatter, with modelling showing saturation still occurring. Such statements allow a direct

comparison with the Matchstick Model predictions which feature zero attenuation effects. Any saturation effects produced through modelling of solely stems, in concurrence with the Matchstick Model, is devoid of attenuation. It would then appear no longer appropriate to state attenuation as the sole cause of saturation, but rather a more complex issue related to stem radius, number density trends and wavelength. With regards to saturation, Table 7.1 expresses reported levels from empirical data in the literature.

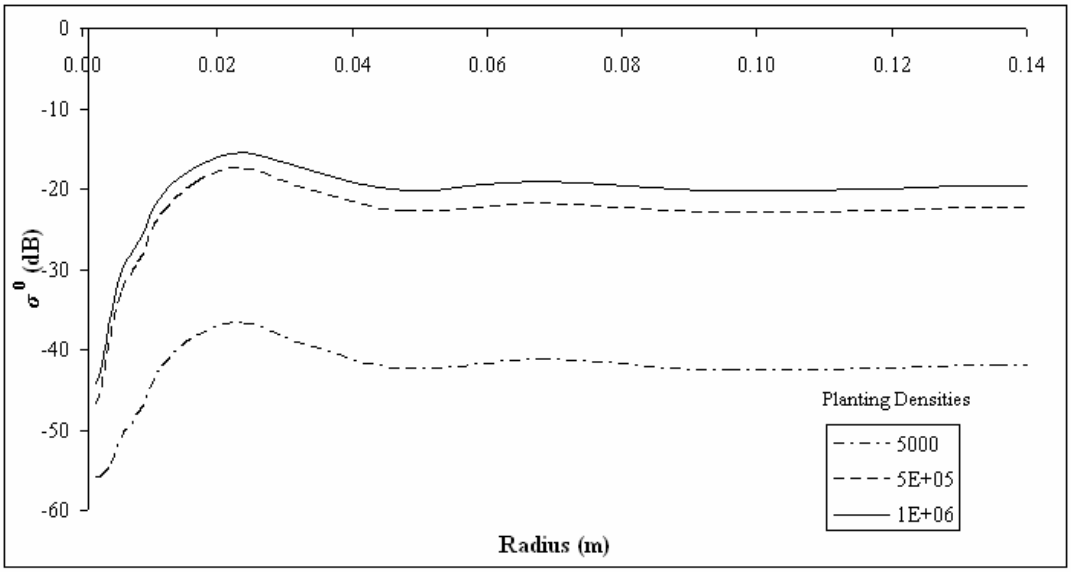

Figure 7.5. RT2 modelled data for P-band VV backscatter with *d*=2 thinning. Legend shows planting densities prior to thinning which reduce the numbers significantly at each growth increment. For the 1 million planting density there are 244 stems when the radius equals 0.1m.

7.4.1.2 The influence of Stem Radii on SAR Data.

In any particular instance in the absence of thinning, the number density remains constant with lengths and basal areas becoming larger as a result of radii increase. Only the introduction of stem thinning will alter this. Individual backscatter from a stem is seen to vary for any particular volume for different constants of proportionality. This is primarily due to different length and radii combinations that

make up these particular volumes. In order to concentrate on consistent stem-specific values, backscatter can be shown in terms of the radii of the stems (Figure 7.5).

The transition point between the theorised Mie scattering regime and the Optical and Rayleigh scattering regimes appear to be an accurate representation as to when the saturation process occurs, signifying a clear dependence on radius. Trends appear to be independent of the constant of proportionality and saturation is only dependent on the scattering change from Rayleigh to Mie through the dependence on stem radius. Significantly increasing the constant of proportionality only increases the level of backscatter and does not alter the trend with an equal significance.

7.4.2 Saturation

7.4.2.1 Initial Findings

Modelling has shown that saturation can theoretically be caused by a change in scattering regime and is affected by factors such as radius, and length. Saturation is generally associated with the rapid decrease in the rate of change of backscatter with increasing stem volume, and therefore biomass density. This, in effect, is not saturation by definition as saturation signifies a cessation in correlation between backscatter and volume. The following modelling procedures serve to provide an explanation as to the existence of this effect using the concept of the thinning factor d introduced in (Woodhouse 2006b). The majority of modelling so far has assumed a thinning factor of 0. This assumes that no thinning takes place within the forest, signifying perpetual growth. This scenario, as it sounds, is unnatural due to the limited resources of a forest, the main factor behind natural thinning processes. In addition, managed thinning is a prevalent procedure in managed plantations as a means of achieving maximum useable wood from a particular species. For biomass retrieval schemes the effects of thinning are an important aspect that must be taken into account (Castel et al. 2002).

Table 7.1. SAR observed "saturation" limits. (Patenaude 2003)

SAR biomass saturation values	Acquisition	Frequency	Biomass Density (B) or Volume (V) Saturation	Sources
Northern Conifers, France	Airborne Backscatter amplitude	P-band L-band	B: 200 t/ha B: 100 t/ha	Dobson et al. (1992)
Northern Michigan	Orbital Polarimetric and modelling.	C-Band (SIR), X-Band (SIR)	B: 250 t/ha	Dobson et al. (1995)
Boreal Conifer, Sweden	Satellite Backscatter amplitude	C-Band(ERS-1), L-Band(JERS-1)	V: 64 m^3/ha V: 143 m^3/ha	Fransson and Isrealsson (1999)
Norway spruce, Sweden	Airborne Backscatter amplitude	VHF	No Volume Saturation	Fransson et al. (2000)
Coniferous Europe and North America.	Airborne Backscatter amplitude	P-Band, L-Band, C-band	B: 100 t/ha B: 40 t/ha B: 20 t/ha	Imhoff (1995)
Tropical	Satellite Interferometric coherence	L-Band (JERS)	B: 60 t/ha	Luckman et al. (1998)
Boreal, Canada	Satellite Multifrequency and polarisation	C-band (SIR) X-band (SIR)	B: 200 t/ha ratio between L-band HH and C-Band HV.	Ranson et al. (1995)
Northern Maine	Airborne, Multifrequency and polarisation	L-band , P-band, C-band	B: 150 t/ha (using HV polarisation)	Ranson et al. (1994)
Tropical transition region Cameroon	Satellite Backscatter, polarisation (HH/HV)	L-band (JERS-1, ALOS PALSAR)	100-150 Mg ha^{-1} biomass (JERS-1, HH), 150-200 Mg ha^{-1} (ALOS PALSAR, HV)	(Mitchard et al. 2011)
Tropical savanna, woodland and forest/savanna Cameroon, Uganda, Mozambique	Satellite Backscatter, polarisation (HH/HV)	L-band (ALOS PALSAR)	No real prediction accuracy above 200 Mg ha^{-1}	(Mitchard et al. 2009)

The main effect of introducing a thinning factor to forest modelling is the direct change in basal area resulting from a loss of stems while growth in the remaining stems continues. This factor is believed to be the main driving factor of backscatter saturation with respect to volume, with the basal area of a stem directly dependent on radius. As the height of the stems increase with each increment, the forest volume is still expected to increase, with the notion that fewer larger stems will contain a

greater volume than several smaller stems (Figure 7.1). In the case of *d* being equal to 2 the total basal area of a plot of stems will remain constant. If the total basal area of a fixed zone remains constant as the stems increase their individual basal areas, then the number of stems must reduce. As the stems begin to scatter in the Optical regime the backscatter becomes dependent on the number of stems and the basal area of each individual stem. Thinning is related to the radial increases in the stem through the equation:

$$N = r_k^{-d}.r_0^{d}.pdens \tag{7.14}$$

Where subscript $_k$ represents an incremental increase in radius from the initial value associated with the subscript $_0$. Between the values *d=0* to *d=2* the rate of change of backscatter with volume is expected to reduce. When this rate of change in backscatter is zero at *d=2*, the basal area is assumed to be constant as volume increases in accordance with the nature of Optical scattering (equation 7.7).

According to the simple Matchstick Model, when *d=2*, the backscatter signal will saturate in the Optical region. When *d* is not equal to this value the basal area will continue to increase or decrease with a continual increase in backscatter (Figure 7.6). The basal areas featured are higher than typical basal areas but were chosen to allow the use of more data points and enable closer comparison between different thinning levels.

For *d=2* thinning, the number of stems will reduce with each size increment but collective volume will increase as remaining stems become taller and thicker. As a result, backscatter will continue to increase within the Rayleigh regime and show a distinct correlation between the backscatter and the volume. Through the Optical regime backscatter will remain constant. As Optical backscatter is directly related to the area of individual stems multiplied by the number present, or in essence total basal area, then zero basal area increase indicates zero backscatter increase manifesting in a zero gradient.

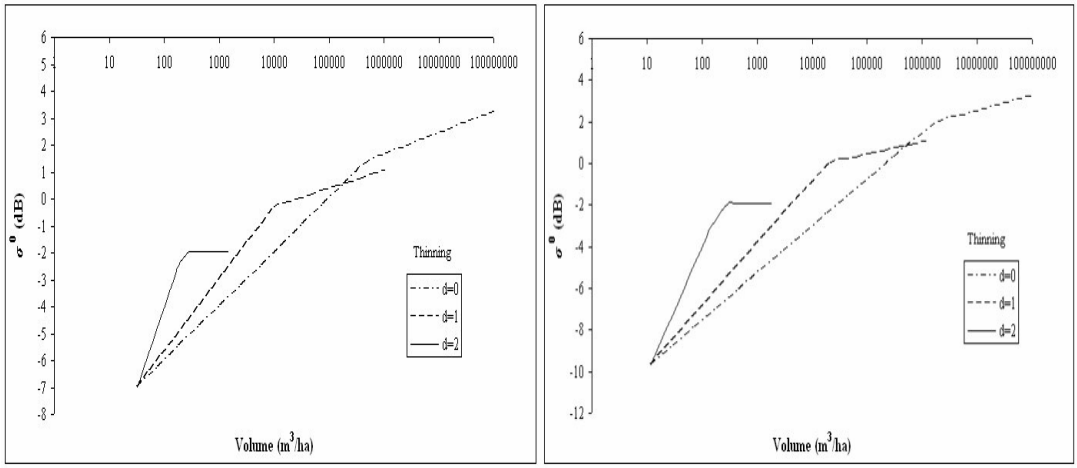

Figure 7.6. Matchstick Model representation using physical optics (left) and geometric optics (right) of backscatter associated with thinning. *d=2* shows backscatter for constant total basal area at 35m^2/ha as forest volume increases, *d=0* shows increasing basal area from initial 35m^2/ha, and *d=1* shows increasing basal area from 35m^2/ha. Initial planting density 2.5x10^6 per ha. Note that *d=2* exhibits classic saturation while *d=0* thinning reaches excessive volume values not intended to be representative of natural forests but to highlight trends.

Modelling to visualise these scenarios, using RT2, was performed on data featuring variations in the thinning exponent, *d*. The constant of proportionality *m* and the initial planting density were also varied. These variations provide a broad analysis of possible stem structures produced by nature and allow comparison with the simplistic Matchstick Model (Figure 7.6). The modelling explored volumes up to and beyond noted values. These values of volume are far higher than featured saturation values in empirical studies (Table 7.1). Through modelling, when a thinning factor of *d*=2 is applied, saturation occurs. Alternatively when *d*=1.5 a change in the gradient of the backscatter-volume trend line is seen but not necessarily saturation. If this modelling is correct then the existence of saturation, even at VHF band, is not entirely dependent on the volume present but also on the forest thinning and in turn the change in total basal area and stem numbers. According to physical laws, equation (7.7), in the absence of significant attenuation and with increasing basal area backscatter will increase. The gradient of increase within the Mie and Optical regimes will be greater for a *d*=1 than a *d*=2 forest. The transition between Rayleigh and

Optical scattering therefore becomes less significant when plotting backscatter against biomass density at low thinning values up to reasonable volume limits.

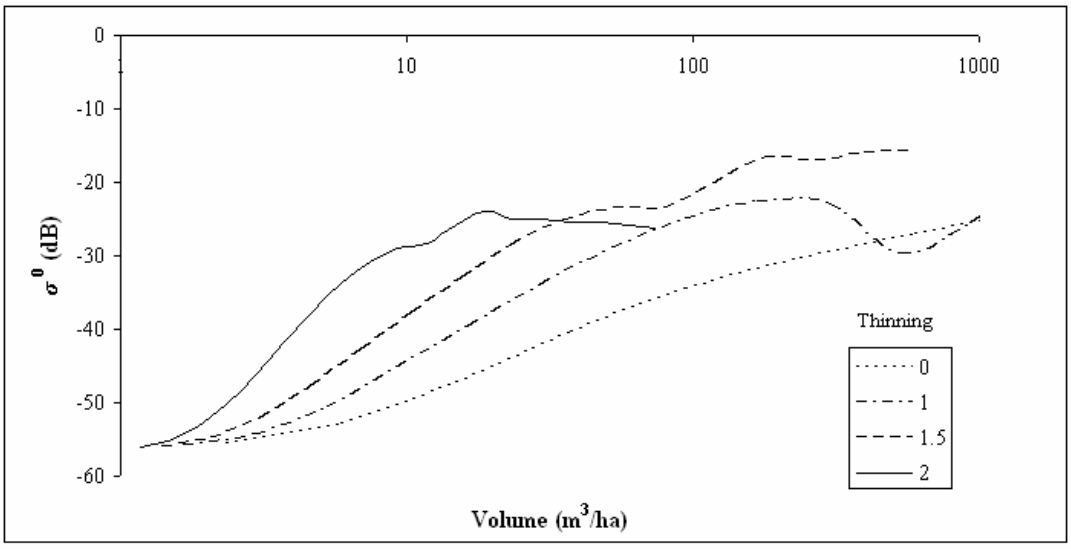

Figure 7.7. RT2 modelling backscatter results for VHF-Band VV incident waves of 50MHz frequency on a forest of initial planting density of $5x10^5$ stems per ha. under different thinning regimes. Chosen polarisation emphasises trends.

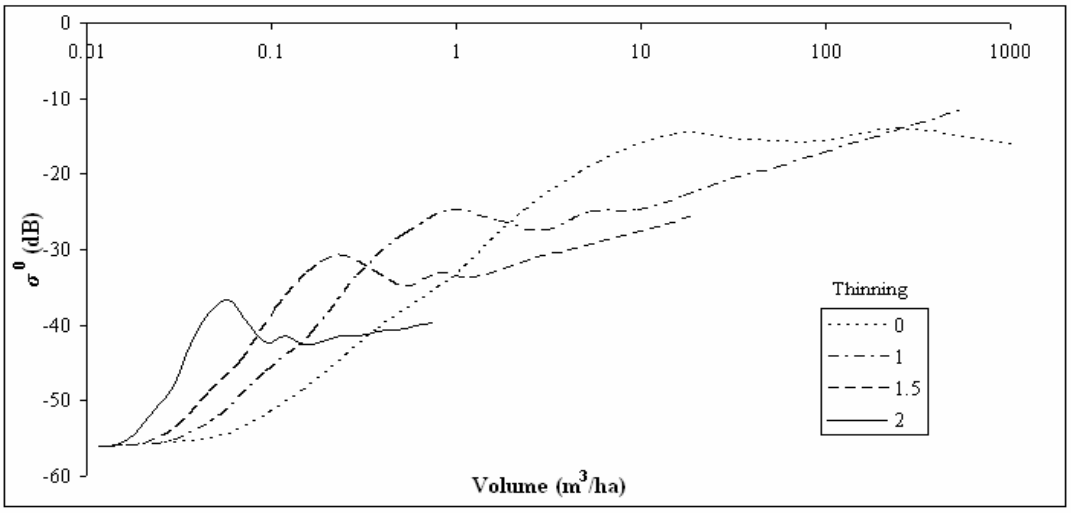

Figure 7.8. RT2 modelling results for P-Band VV incident on initial planting density of $5x10^3$ stems per ha. when thinning regime is varied between d=0 and d=2. Chosen polarisation emphasises trends.

When full trees are considered in a natural forest, the canopy will at some point reach a level where it will remain constant as stems continue to grow. According to

empirical studies at 429MHz (Table 7.1), at a biomass density in the region of 100 to 200t/ha, it is expected that saturation will take place. This theory then suggests that the cross-sectional area of a collection of similar sized branches may have a constant total cross-sectional area which scatters optically. As the smaller branches will scatter optically at a smaller wavelength, saturation for these frequencies will therefore occur at lower biomass values offering an additional explanation why saturation at higher frequencies occurs at lower biomass densities. Figures 7.7 and 7.8 show how the saturation volume varies with thinning and may not correspond with planting density for both VHF and P-Bands respectively.

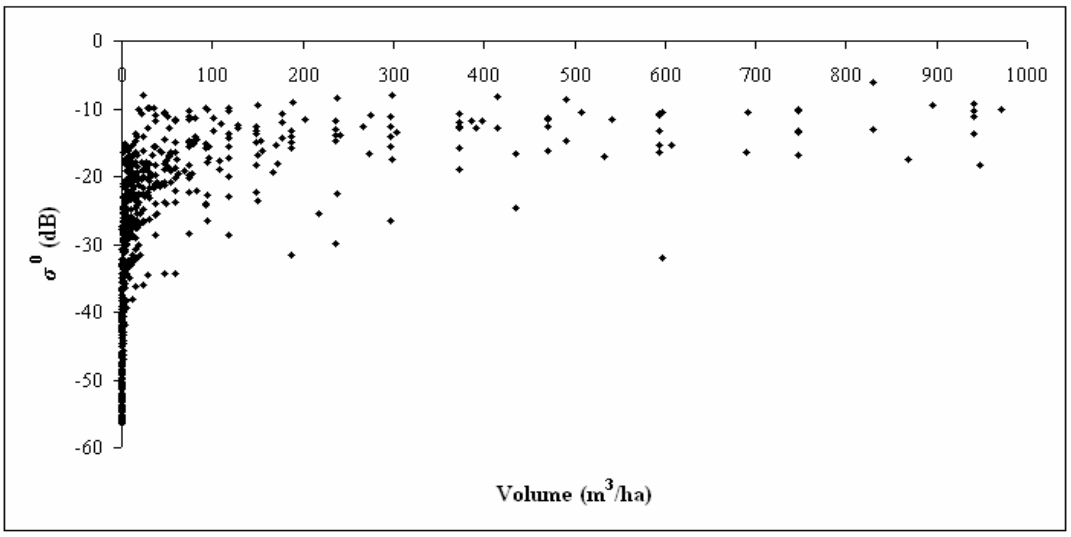

Figure 7.9. RT2 VV polarised P-Band backscatter values for various planting densities, thinning exponents, scaling parameters, and constants of proportionality. Similar trends exist for VHF data. The non-uniqueness of backscatter to volume relationship is apparent. Low volume data is included although such low volume values may only be present in modelled data.

The consequences of the dependency of forest backscatter on number density, thinning parameter, scaling exponent, and constant of proportionality as explored in the previous sections are evident in Figure 7.9. The relationship between forest volume and forest backscatter appears largely non unique with several forest volumes producing similar backscatter values when these parameters are varied. The consequences for prospective backscatter intensity surveys to estimate forest volume

or biomass are apparent based on these modelling results. Similar trends are shown in empirical studies with the tendency to fit curves based on prior knowledge of the shape of the saturation curve. Examples of this can be found in (Mitchard et al. 2009; Neeff et al. 2005; Wagner et al. 2003).

In addition to these observations, it is noticeable that the 429MHz datasets show evidence of oscillation at volumes associated with saturation with an average over this range required to show gradient variations associated with thinning. These oscillations could relate to the Mie oscillatory trends existing between Rayleigh and Mie scattering and should not be disregarded without consideration.

7.4.3 Mie Oscillations

In order to investigate the possibility of Mie oscillations in the region of saturation the modelling procedures were altered. Originally every backscatter value was associated with a volume determined from a collection of identical stems whose number at any particular point was controlled by initial planting density and thinning factor. It is thought by changing this depiction to something slightly more realistic, any oscillations will be non existent. To increase the realism, a series of randomly generated stems were used. The stems were chosen to possess radii values within one standard deviation of the mean. In essence this variation transforms a mono-sized forest into a multi-sized forest, in keeping with natural forest growth. In addition the backscatter was simulated for collections of stems orientated at random angles over a spherical distribution while still possessing the same dimensions as the vertically aligned collections.

Under the new conditions of modelling, the thinning factor was maintained at a value of d=2 and an initial planting density of $10x10^6$ was used, a significantly high value due to the large thinning effect of d=2 with each size increment. These parameters would allow an approximately constant basal area over the test site and allow a

reasonable value of volume at all stages of the forest growth through each radius increment representative of natural settings with initial increments resulting in high mortality.

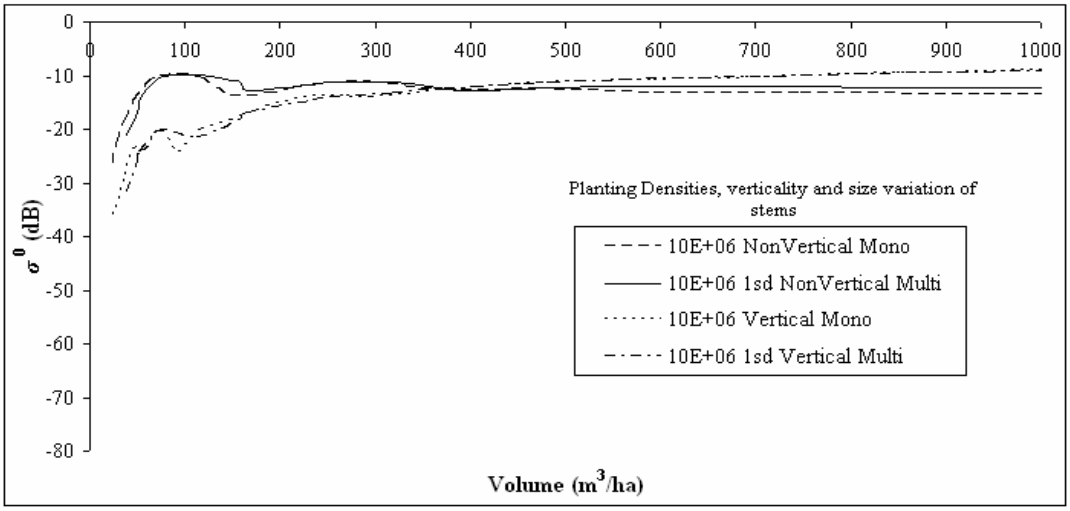

Figure 7.10. RT2 VV P-Band data of 429MHz for initial forest planting density of $10x10^6$ stems per ha. with thinning d=2, featuring vertical and non-vertically aligned stems of multi and mono radii forests. Saturation seen in presence of approximately 1220 stems at $373m^3$/ha for vertical stems. Note number density reduces significantly with every size increment as volume increases. Polarisation chosen to emphasise trends.

Modelling the forest in this new way allows comparison of forests consisting of: 1) mono sized vertical stems 2) multi size vertical stems, 3) mono size non-vertically aligned stems and 4) multi size non-vertically aligned stems (Figure 7.10). By modelling these alternate forest structures while maintaining the Matchstick Model ethic it can also be determined whether the mono and vertical nature of the stems at each volume increment have any bearing on the presence of Mie oscillations and in effect the backscatter. In the presence of a single object, Mie oscillations would be expected, and it is assumed that the same behaviour, to some extent, is exhibited with a collection of identical stems. As such these oscillations are not generally seen or noted in empirical data possibly due to the large stem numbers present and their variable sizes.

At 35 degrees incidence the data appears largely unaffected by Mie oscillations. At both 429MHz (Figure 7.10) and for VHF the same trends are apparent with higher backscatter in general for non vertical stems at VV but lower for HH as a result of stronger double bounce contribution. When non vertical stems are modelled there is little difference in backscatter whether the stems are homogeneously or heterogeneously sized. This is apparent when modelling vertical stems, despite the identical trends existing between the two datasets. When these scenarios are modelled at lower incidence angles oscillations are evident in the mono sized stems alone, this oscillatory behaviour at lower incidences is removed by varying the size distribution of the stems but also by introducing non-vertical stems of random angles over a spherical distribution. At 35 degrees incidence these oscillations are not evident.

Introducing non-vertical stems appears to remove the oscillations at volumes consistent with Mie scattering at low incidence angles without an effect on the Rayleigh region. In a natural forest setting, in a climax forest, stems will appear to be very similar in size but not identical. These stems which appear very similar in size are more accurately described using a distribution about a mean value. Empirical SAR backscatter values can be extremely variable in terms of correlation with volume. It is for this reason that these data are shown, highlighting the effect on backscatter that verticality and size distribution have on the resultant backscatter. Within the Matchstick Model set up, the stem sizes could be less constrained and yet still provide sensible correlation with the backscatter to coincide with more natural settings. The negative trends in the data following saturation could be construed as a result of the presence of non vertical stems over such great an angular range. Saturation does not appear to be affected by the parameters varied here but backscatter intensity is significantly influenced by the size distribution and orientation of stems.

7.5 Discusssion

SAR backscatter has been shown to correlate empirically with the standing biomass density of forests (Karam et al. 1993), yet robust generic relationships have remained elusive. The correlation is often thought to be dependent on the incident SAR wavelength and the volume of the forest. RVoG or Water Cloud Model explains these trends as the increasing volume of vegetation resulting in increasing backscatter, and saturation caused by the increasing forest opacity. The significance of the Matchstick Model presented here is that it challenges those models and provides an alternative explanation by considering macroecological trends in forest stem size and number that determine the consolidation of the biomass material, which has been previously shown to impact on backscatter, (Imhoff 1995b); (Woodhouse 2006b); (Dobson et al. 1995). Saturation need not be caused by increased opacity, but rather, by the physical structure of the forest as it moves from low biomass to high biomass, including the changes in stem number densities.

When structure (i.e., size and number density) is highly correlated with biomass, the backscatter-biomass trend also has a strong correlation. However, such structural trends are highly varied in nature – in some areas biomass is positively correlated with size and number density, while in others it is positively correlated with size but negatively correlated with stem density. When backscatter is modelled across a variety of realistic radii, basal areas and number densities (the large planting densities used in this study produce realistic number densities following only a few growth increments), the result has no clear trend (Figure 7.9). If backscatter is not a robust measure of biomass even for a simple single layer Matchstick Model, then we must urge great caution when trying to apply generic trends across different forest biomes. The important conclusion is that backscatter does not measure biomass, but measures structural trends that are correlated with biomass in different ways, driven by stand level competition, resource use, etc. As a result different forest growth regimes

should expect different backscatter-biomass trends. In this respect, VHF does not avoid interrogation. With regards to 50MHz data the transition from Mie to Optical scattering is believed to occur at radii of approximately 9.54m. Trees of this size do not occur in nature (General Sherman has a diameter of 11m) and as a result complete saturation would not necessarily be expected in empirical data when using this wavelength. However, the modelled results presented here also establish that robust trends are not possible with VHF when averaging backscatter over many stems. CARABAS (Smith 2000) demonstrates such consistently good results because they resolve individual trees and thinning rates are irrelevant.

7.6 Conclusions

We have introduced the "Matchstick Model" as a new deductive approach to modelling backscatter from a forest. As the majority of a forest's biomass is concentrated in the stems it would seem reasonable to remove all but the stems from the modelled forest and consider this a realistic representation of natural biomass distribution when considering long wavelength SAR. The model predicts that SAR forest backscatter saturation can be caused by tree stem scattering going from one scattering regime to another, combined with a stem thinning rate. These transitions produce two distinct phases in backscatter with regards to a forest increasing in volume. The model explains why a robust and consistent backscatter-biomass trend has been so elusive – because forests accumulate biomass in different ways, and these differences have profound influence on the backscatter, even in very simple cases.

The model reinforces the risk of not considering forest structure when using backscatter as an indicator of biomass, and is a word of warning for possible future satellite instruments such as BIOMASS (Le Toan et al. 2010) or descendants of DESDynI (Donnellan et al. 2008). This work builds a foundation in which to explore how to account for variability in planting densities and thinning rates, and this will form the focus of future studies.

8 SAR backscatter trends as a consequence of the emergent properties of tree populations

Matthew Brolly and Iain. H. Woodhouse

Summary

This Chapter extends the applicability of concepts introduced in Chapters 4, 5 and 7. It does this by incorporating the SERA forest model (Chapter 4) into a radiative transfer SAR backscatter scenario, by analysing the backscatter dependence on scatterer size and therefore scattering regime (Chapters 5 and 7) , and by focussing on the behaviour of long SAR wavelengths (P-Band, VHF) upon interaction with forests consisting solely of stems (Chapter 7). The use of SERA allows the theories presented in Chapter 7 to be analysed using an independent model providing forest geometry details based on species specific allometric identities. The hypotheses of this chapter concern the nature of the saturation effect and its relationship with forest total basal area. It is believed from the results of Chapter 7 that the SAR backscatter saturation effect as forest volume increases is driven by the Optical scattering behaviour of forests. Although the transition from Mie to Optical scattering requires the presence of large radii scatterers, Chapters 5 and 7 showed how an Optical description of Mie scattering behaviour is adequate. This is particularly true for multi stem size forests (see Chapter 7.4.3). A greater level of heterogeneity in stem sizes is produced by SERA and is therefore expected to amplify the averaging effect. Due to the dependence on forest basal area of Optical scattering it is predicted that the nature of the saturation curve can inform on the variation of basal area across the forest stand (see Chapter 2.3).

This chapter asks the following questions:

1. Using the independent forest growth model SERA to parameterise RT2, are the theories of the Matchstick Model of Chapter 7 regarding basal area dependence verified by the modelled backscatter?
2. Does thinning as a consequence of space and light competition in SERA forests actively influence the backscatter relationship with forest volume?
3. How does backscatter from SERA forests relate to stem size distribution in terms of their classification as Rayleigh or Optical scatterers?
4. If Optical scatterers dominate the forest does backscatter follow a physical cross section dependency, and if Rayleigh dominated is it volume squared?
5. How does theoretical backscatter using SERA forest data, and based on Rayleigh and Optical theories, compare to RT2 modelled backscatter?

This Chapter aims to address the questions and hypotheses by modelling the backscatter returns of various SERA forests using RT2. Mono-species and multi-species forests are generated and examined in terms of their backscatter relationships to macroecology. The detailed geometry of SERA stems allows the analysis of backscatter contributions from different size scatterers therefore scattering regimes and to determine influential macroecological factors. This study helps to establish links between theoretical backscatter descriptions (Chapter 2.3) and the macroecology of heterogeneous forests. Ultimately the comparison between modelled backscatter and theoretical descriptions will determine whether describing forest backscatter as a combination of Rayleigh and Optical scattering is appropriate. Ideally such work will lead to the accurate inferral of macroecological changes; particularly in number density and basal area (see Chapter 3.3.2 and Chapter 7).

The work featured in this paper was entirely produced by myself including idea formulation and work undertaken. Influence was provided by S. Hammond and Prof. Niklas of Cornell University regarding SERA, acknowledged as a significant contribution to this work. Additional help and editing was provided by Dr. Woodhouse within a supervisory role.

8.1 Abstract

This study describes the use of a plant and forest structure model (SERA) which actively combines the fields of allometry, macroecology and empirical studies, in conjunction with radiative transfer theory for forest microwave interactions. SERA (Spatially Explicit Reiterative Algorithm), has the ability to parameterise generic and specific gymnosperm and angiosperm characteristics based on empirical studies and the consequences of light and space competition. It provides a widely varied tree size distribution while maintaining allometric consistency to produce a natural-like forest representation at an easily defined stage of growth. A radiative transfer model, RT2, parameterised by SERA is used to analyse the backscatter variations resulting from changes to the forest stand as a result of light and space competition showing that the slope of the saturation curve provides information as to the thinning rate and therefore basal area changes. It is determined that forest SAR backscatter can be described using two equations related to volume and basal area. The nature of these equations is such that they describe the saturating behaviour of forests seen at high volumes and in the absence of canopy attenuation. Modelled data predicts that backscatter is directly related to forest basal area from an early age when forest volume is increasing. When this is not the case it is assumed to be a result of attenuation of the dominant stem-ground interaction due to the presence of an excessive number of forest stems. SERA uses canopies for light interception but to remove their attenuating influence, and reinforce the concepts of this work, only stems provide backscatter values. This work reveals that backscatter saturation need not be a direct result of attenuation but more a comment on forest dynamics and the influence of forest basal area.

8.2 Introduction

Models such as the "Water Cloud Model" (WCM) (Attema and Ulaby 1978) and "Random Volume over Ground" (RVoG) (Papathanassiou and Cloude 2001) have become two of the most widely used simplifications of microwave scattering from forests, and are widely seen as an adequate representation in terms of total backscatter. Effective exploitation of airborne and spaceborne SAR requires a theoretical understanding about the relationship between backscatter and forest volume/biomass. It is a widely held view, resulting from the nature of the WCM, that the saturation of backscatter is a result of the increasing attenuating properties of forest canopies – saturation occurs when the forest layer effectively becomes opaque to the microwaves. However, there is modelling evidence showing saturation for lower planting densities (Woodhouse 2006b), as well as empirical evidence when comparing Savanna and coniferous forest saturation levels from JERS-1 datasets of (Santos et al. 2002) and (Fransson and Israelsson 1999). Supporting theories exist concerning the effect of total basal area on Optical backscatter (Brolly and Woodhouse 2010) that suggest that the WCM may not be as generally applicable as is widely thought. In particular, saturation may be caused by other factors, such as the ratio of dominant stem radius to wavelength (Smith-Jonforsen et al. 2007; Smith and Ulander 2000).

In (Woodhouse 2006b) it was initially shown how macroecology could be used to aid the process of forest modelling using remote sensing. The model used was the "General model for structure and allometry of plant vascular systems" (WBE) (West et al. 1997), which has its roots in an explanation for the origin of allometric scaling laws. Despite some important limitations this model displays key advantages that make it an appropriate first-order linkage between simple backscatter modelling and models of biological function. WBE is based on the constraints of biomechanics and resource distribution for a single plant. SERA (Spatially Explicit Reiterative

Algorithm) on the other hand, is an area model that has similar macroecological principles imbedded, but uses them to model plant (tree) communities. It achieves this by accounting for light and space competition as SERA was designed "to evaluate how different species compete in a world space whose physical attributes, are clearly defined" (Hammond and Niklas 2009).

In this work the SERA description of forest population structure is used as input to a radiative transfer model, RT2, to simulate radar (microwave) backscatter values expected from airborne or spaceborne radar imagers (Cookmartin et al. 2000).

8.3 Methods

8.3.1 SERA

SERA (introduced in Chapter 3.2) is a forest growth model which accurately reproduces the community dynamics of a collection of trees competing for light and space resources. According to (Enquist et al. 1998a) a variety of plant ensembles are observed to "self-thin" in accord with the same or very similar scaling exponents to one another. As a result of this, SERA was designed to incorporate this self management technique to allow evaluation of how different species compete when the physical attributes, such as the direction and intensity of incident sunlight are clearly defined. SERA provides a first estimate of the outcome of forest dynamics in a homogeneous environment from the onset of plantation until a user-defined point. Variability of water and nutrient resources are not considered. The computer simulations are discussed exclusively in the context of competition for light and space as a starting point for assessing competing theories purporting to explain the real world behaviour of plants, particularly forests.

Within SERA each plant is intentionally simplified to consist of a single photosynthetic surface elevated by a single stem. Similar concepts have been explored in (Niklas 2000) and (Chave 1999) but in this work the canopy is only used

to determine ensemble growth. Whereas some models represent the canopy as a flat disc, SERA treats each canopy as a hemispheric layer of uniform thickness. The angle of solar incidence is time averaged to 0 degrees such that the projected canopy area is the total photosynthetic area available for each plant. For the purpose of the backscatter modelling, we consider only longer wavelengths and therefore do not include the canopy.

One of the advantages of SERA is that it requires relatively few input variables, consisting of 20 species specific parameters and representative values. Of these variables only six scaling exponents are required to generate a species. Unlike WBE, the relationships in SERA that govern allocation of stem mass to stem diameter and height allow a transition from stem geometric self-similarity to geometric non-similarity. Such considerations were given in (Woodhouse 2006b). SERA allows scaling exponents to change within the lifetime of a stem with the scaling change found empirically to occur around the onset of maturity. SERA also minimises input parameters by assuming species similarities (Gifford and Foster 1989; Taiz and Zeiger 2002).

SERA consistently predicts that plant lifetimes scale as the ¼ power of body mass, a scaling relationship that has been reported for diverse plant species (Marbà et al. 2007). A number of naturally occurring scaling relationships also emerge as the direct result of competition for light and space, even in a simple homogeneous scenario. Many of the scaling relationships predicted by SERA also emerge from WBE suggesting that SERA and other mathematical/theoretical explanations for observed real-world scaling relationships have conceptual common ground. When plants violate physical laws, such as the Euler-Greenhill mechanical relationship governing the buckling height of a stem (Niklas and Spatz 2004), the result is death. Mortality also results from light deprivation or stochastic/age-dependent processes. In this way SERA's "self-thinning" closely replicates empirical trends.

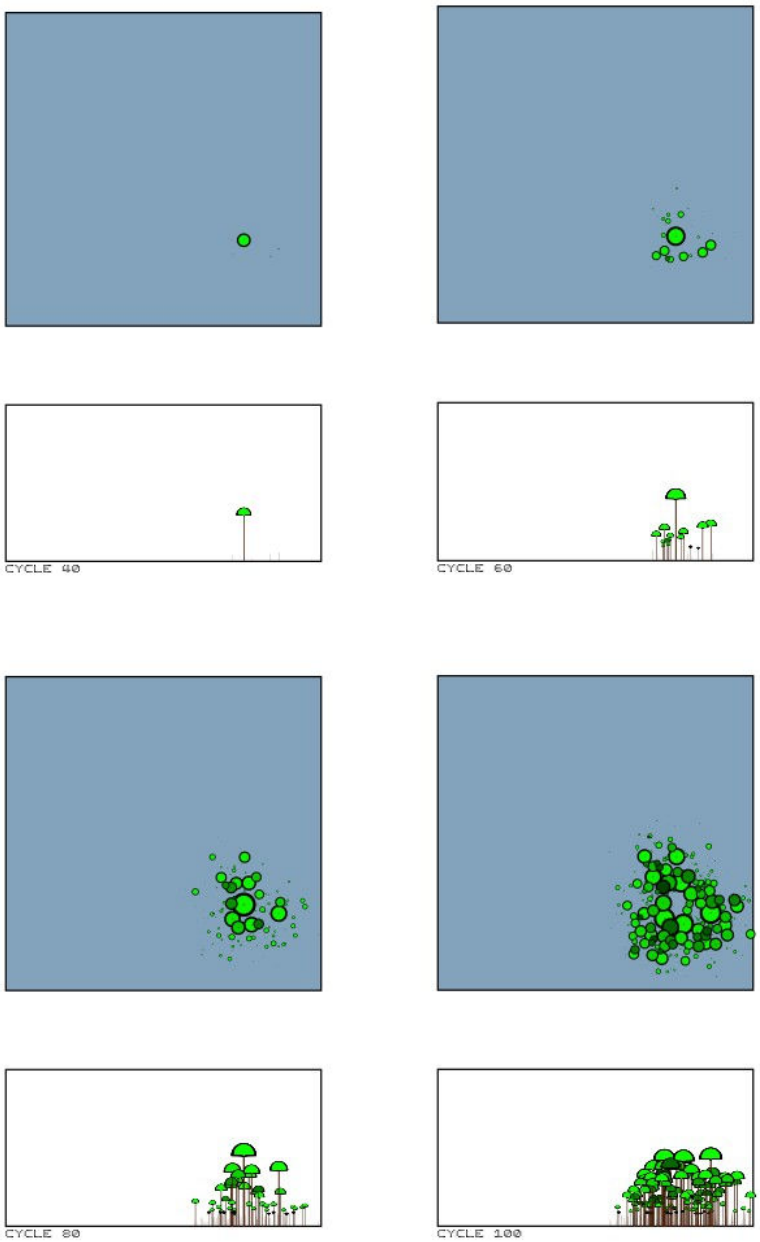

Figure 8.1. Horizontal and bottom-up representation of *Abies Alba* forest emanating from single stem. Glimpses (clockwise from top left) at 40, 60, 80, and 100 years over 1ha. Brown represents stems, darkness of green represents level of canopy shading, for example bright green represents unshaded canopy. Blue represents sky, indicating zero canopy cover between ground and sky.

SERA's robustness was assessed biologically through comparison with the ensemble behaviour of thoroughly investigated and collated empirical data. The world wide compendium for forestry data compiled by (Cannell 1982) was used as a reference to survey the primary literature published before 1982 to identify long term studies of monospecific forests. Of these the most useful data set for any species was for a single *Abies Alba* population documented every 5 years for 95 years starting 10 years after initial planting (referenced and used in (Hammond and Niklas 2009)). Cannell (Cannell 1982) was then used to statistically characterise 332 angiosperm and 343 conifer dominated communities to emulate the dynamics of "generalised" populations.

The high extent to which SERA was successful at emulating the behaviour of real forest populations is documented in (Hammond and Niklas 2009). The true capability of SERA is its ability to predict the fate of a species under varying degrees of spatial and temporal heterogeneity. Figure 8.1 emphasises the visual capabilities of SERA when presenting a randomly seeded forest.

8.3.2 Rayleigh and Optical Scattering Theory

In (Brolly and Woodhouse 2010) it was shown that it is possible to make a first order estimate of trends of backscatter using some approximations based on whether the stem cylinders lie in the Rayleigh or Optical scattering domain. In a similar fashion the trends in backscatter as a function of stem radius are considered here. The three possibilities that exist are: (1) the stem specifications lie completely in the Rayleigh scattering domain, (2) they lie entirely in the domain of Optical scattering, and (3) the stems consist of both size classes spanning both domains. In the Rayleigh case we assume the backscatter from each cylinder increases with the square of the volume, and for Optical, it increases with the physical cross-section (Moosmuller and Arnott 2009). At the transition between these two regimes Mie scattering is dominant but an approximation is made that assumes resonant behaviour of Mie "averages out" across

this region giving the cumulative effect of a distribution of stem sizes (see Chapter 7.4.3). This assumption is supported by multi frequency empirical results, for example (Lopes et al. 1991) and (Mougin et al. 1993).

Using the data provided by SERA the forest can be segregated according to whether the stems are expected to scatter in the Optical or Rayleigh regimes with the corresponding backscatter generated accordingly.

For Rayleigh scattering, the total radar cross-section (RCS) of the collection of N stems, is given by a proportionality to the square of the stem volume multiplied by the number of stems within the stand (Smith and Ulander 2000):

$$\sigma_{Rayleigh} \propto N V^2 \tag{8.1}$$

Due to the nature of this scattering the maximum backscatter will originate from the largest branches with size dominating over number density when all stems are Rayleigh scatterers.

In a similar manner, the scenario whereby the radii of all the stems are large enough for the cylinders to lie completely in the Optical region is considered (equation (8.2)). In this case the RCS of the stand scales with the physical cross-section or total basal area according to the relationship between geometric and physical optics as published in (Hestilow 2000) and evident under particular scaling properties of the scatterer with the physical and geometric optics solutions corresponding when scaling follows particular conditions (Hestilow 2000), see also Chapter 2.3.

$$\sigma_{Optical} \propto N A \tag{8.2}$$

The ratio of radius to incident wavelength governs the nature of scattering. For this work the limits are determined by equations (8.3) and (8.4) which describe the Rayleigh-Mie boundary and the Mie-Optical boundary respectively. These limits are the same as those outlined in (Woodhouse 2006a) and (Moosmuller and Arnott 2009).

Equation (8.3) represents the significant boundary in this work determining Rayleigh and non-Rayleigh scatterers.

$$\frac{(2\times\pi\times r)}{(0.1\times\lambda)}=1 \tag{8.3}$$

$$\frac{(2\times\pi\times r)}{(10\times\lambda)}=1 \tag{8.4}$$

If the backscatter is solely generated by Optical scattering then as the number of stems reduces the backscatter will decrease, but as the size of the remaining stems increase and the individual basal areas increase, the backscatter will do so also. Therefore there may exist a scenario whereby the reduction in numbers and the increase in the basal areas of the largest stems would result in equilibrium and therefore backscatter saturation.

8.4 Modelling Strategy

By coupling the SERA model to radiative transfer theory and incorporating the ideas of the "Matchstick Model" (Brolly and Woodhouse 2010) only one layer of scatterers describing the stem properties is required. The limits of this layer are defined by the height of the tallest stem present at any time, and the ground surface, a typical consideration for longer microwave wavelengths. The radiative transfer model used here is RT2 (Saich 1993), a multi-layer second order radiative transfer model similar to the MIMICS model used in (Imhoff 1995b) and the UTACAN model used in (Woodhouse and Hoekman 2000). It is described in (Cookmartin et al. 2000) where it was used for modelling crop backscatter. In the current study, RT2 was used to investigate the backscatter from the SERA forest for a range of scenarios. RT2 is a fully polarimetric, second-order solution to the radiative transfer equations that treats the vegetation canopy as a plane-stratified multilayer region over a rough surface. Its

use in this instance is limited to a single plane with only vertical stems described by SERA existing over a rough surface. Here we consider only plant stems which are represented as finite-length cylinders and we consider like polarised HH backscatter due to its sensitivity to vertical structures.

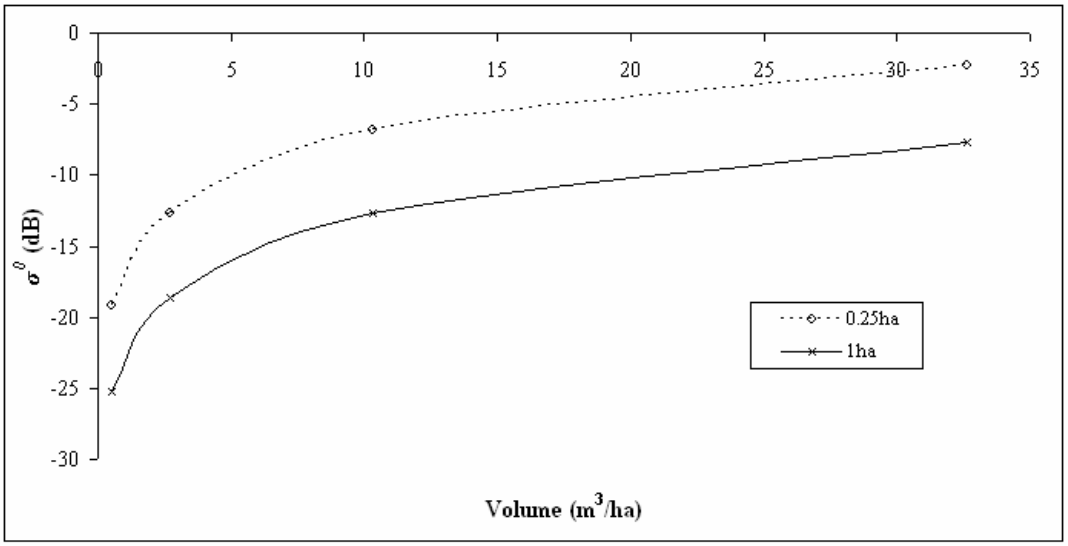

Figure 8.2. RT2 modelled HH backscatter representation of the forest depicted in Figure 8.1 emanating from a single stem from 40 years onwards. Backscatter in dB normalised to both 1ha and 0.25ha.

Due to the limitations of RT2, in terms of the number of allowed scatterer sizes, each dataset representing the test stand was divided into 64 size classes (information for each single stem is recorded and used during the analysis and creation of equal size classes). These 64 size classes were then distributed within this layer. In effect the scatterers could be theoretically positioned anywhere within this layer but will always remain vertical. With this in mind the test stand parameterisation for RT2 represents the total volume and number density of individual size classes but the precise coordinates and their individual effects are not transferred from SERA to RT2. For this reason this backscatter investigation can only comment on trends of normalised backscatter over a large enough area that contains the 64 class sizes and not on the contribution of each individual tree. Figure 8.2 shows a typical backscatter-volume

plot produced using RT2 representing the forest scenario of Figure 8.1 devoid of canopy. Data are shown normalised for the full displayed hectare area and also for the quarter hectare area that the simulated forest occupies. Similar trends are exhibited by both.

When generating forest data, SERA allows the user to determine the "world" size, starting population, and maximum number of cycles (years). In each simulation, world space was maintained as a hectare while the other values were varied in order to identify trends over a 100 year period. In this work 3 case studies are presented representing Angiosperms, Gymnosperms and a combination of both. These 3 "forests" are subjected to the same conditions and allowed to grow unmanaged for a 100 year duration. Following the simulated growth, separate backscatter values can be generated for the total volume, the Rayleigh volume, and the Optical (Non-Rayleigh) volume using the limits defined by equation (8.3). With these distinctions made and their backscatter values generated, a comparison of the individual contributions to the total backscatter can then be made. As well as this, theoretical values are calculated, based on equations (8.1) and (8.2), to show whether the total backscatter can be represented as a saturating effect caused by transitions from one scattering regime to another in conjunction with forest dynamics. By inferring a relationship between the Rayleigh volume and backscatter in the form of equation (8.1) and between the Optical basal area and backscatter as in equation (8.2), theoretical backscatter values for these components can be established and combined to provide a theoretical total backscatter based on just two types of scattering. Multifrequency analysis can also be carried out to aid investigation and to infer an inverse relationship between wavelength and forest saturation age. This process will provide further evidence as to the radius-wavelength ratio association to backscatter.

For each species composition, the effects of volume, basal area, number density, and height were investigated in order to highlight significant links between HH backscatter and forest constitution. All of the following work is carried out using

SERA to generate the forests and RT2 or theoretical equations to generate backscatter levels. Analysis is primarily concerned with the working theories of Optical and Rayleigh backscatter.

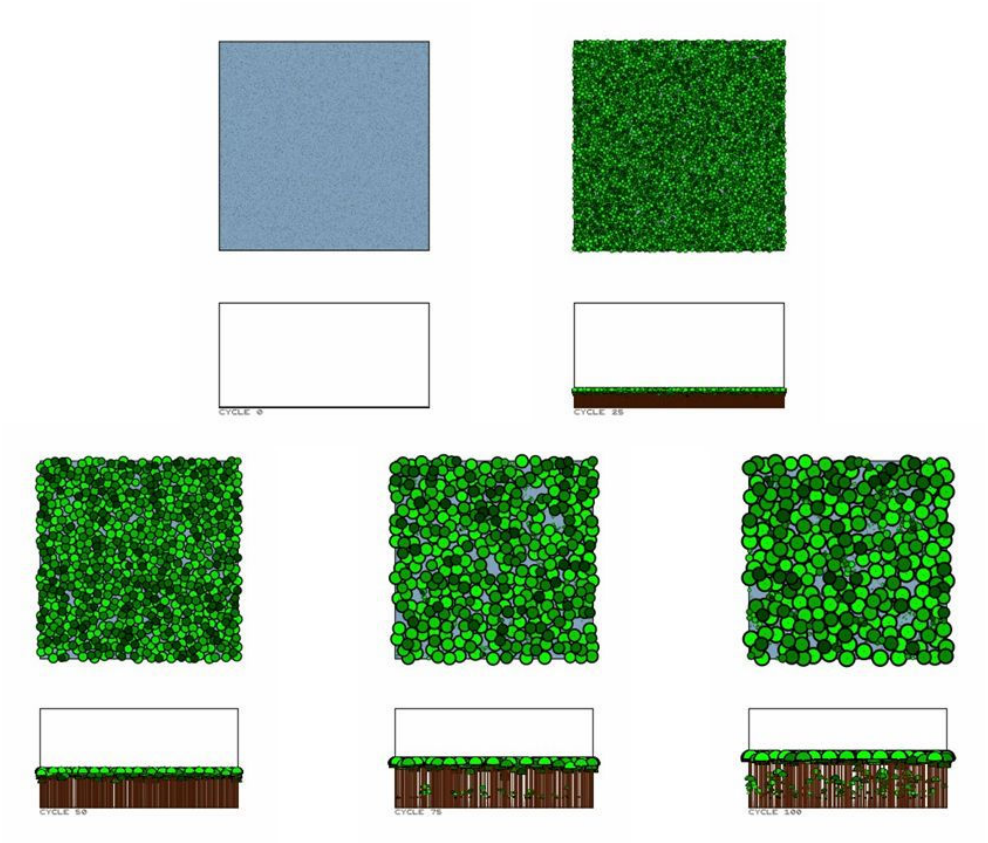

Figure 8.3. Horizontal and bottom-up representation of *Abies Alba* forest before canopy removal. Glimpses clockwise from top left at 0, 25, 50, 75 and 100 years over 1ha. Brown represents stems, darkness of green represents level of canopy shading, for example bright green represents unshaded canopy. Blue represents sky, indicating zero canopy cover.

Three scenarios were examined; these scenarios were the forest configurations of a) *Abies Alba* (Gymnosperm), b) Generic Angiosperm (Angiosperm), and c) Mixed Species (Gymnosperm and Angiosperm). Figure 8.3 shows a typical visualisation of SERA derived data at 0, 25, 50, 75 and 100 years. This particular forest is for the *Abies Alba* forest. Each forest can be viewed in a similar fashion using horizontal and

bottom up views. These figures highlight the potential of this modelling procedure to both aid backscatter interpretation as well as to identify how the evolution of a forest can directly affect this in a visual as well as numerical way.

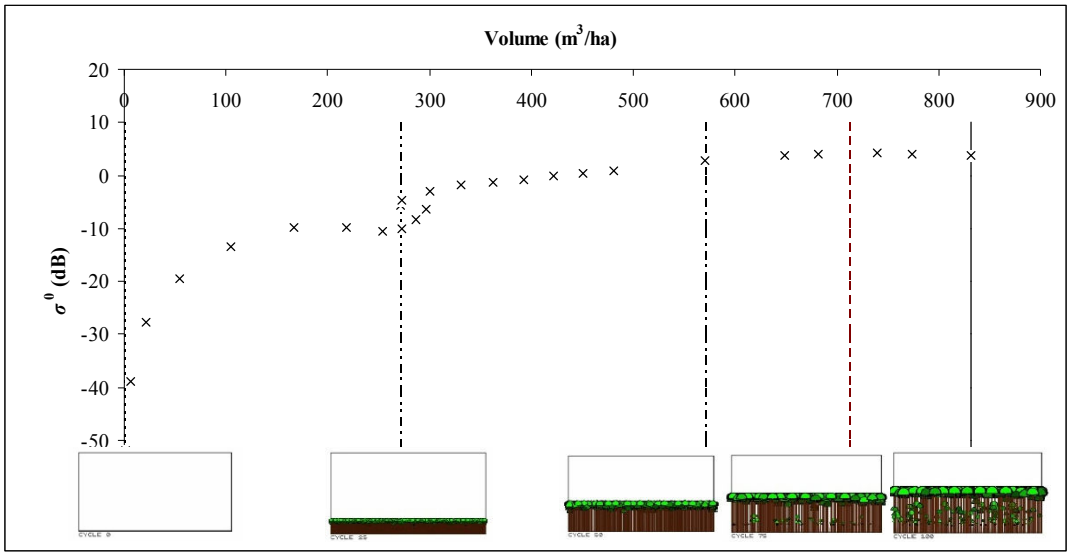

Figure 8.4. RT2 modelled P-Band HH Backscatter and volume values shown with respect to the visual appearance of the SERA *Abies Alba* forest at 0, 25, 50, 75 and 100 years old, left to right respectively. Note that backscatter and volume values are representative of stems.

Each forest in this study is based on an initial planting density of 25000 seeds, to mimic the empirically monitored forest of *Abies Alba* used as a comparison for the SERA model. The numerical description of the forest progression is given in Table 8.1. for scenario a) with the backscatter against volume per ha. plotted in Figure 8.4.

The backscatter for *Abies Alba* follows the typical saturation pattern commonly reported in forest SAR studies (Baker et al. 1994; Imhoff 1995a). As the forest volume increases, the returned backscatter does so also. When the volume reaches a certain limit the increase in backscatter per unit volume reduces significantly until under certain circumstances the increase saturates, signalling a zero increase in backscatter per unit volume. This is seen at approximately 650m^3/ha, a significantly large volume density but the steady decline in backscatter change with volume begins

at a much lower volume. In a similar fashion (Baker et al. 1994) noted that the "gentler rise" occurred at ages beyond 20 years for the empirically monitored *Corsican Pine*, similarly here for the modelled *Abies Alba*. The most common explanation for this saturation behaviour is given as attenuation resulting from increasing density of canopy components. This would appear to be an acceptable explanation when taking into account the visualisations shown in Figure 8.4 but for these scenarios all backscatter is generated for a single layer with a zero canopy component. Alternate explanations must therefore be considered bearing in mind the backscatter contributions of Rayleigh and Optical scatterers in this scenario when plotted against volume, with modelled Rayleigh scattering at high volumes appearing to contribute very little to total backscatter. As the volume values and visualisations suggest, there will inevitably be an increase in attenuation as a forest's size increases. At very short wavelengths the attenuating effects will be caused by the smaller canopy branches but at longer wavelengths the attenuating effects of the canopy will have less influence. With the removal of canopy considerations the backscatter values are therefore not influenced or compromised by canopy attenuation. The inconsistency evident in the backscatter curve of Figure 8.4 can be explained through numerical evaluation of Table 8.1 which indicates that the backscatter levels are susceptible to interference from the vast numbers occupying the limited space producing unsustainably large basal areas (comparison with Table 8.2 affirms this).

With the theories proposed by the "Matchstick Model" (Brolly and Woodhouse 2010) and acquired modelling evidence, including that of SERA, it is believed that the saturation behaviour exhibited in each scenario is not in fact associated with attenuation. In (Brolly and Woodhouse 2010) it was predicted that saturation effects are due to the presence of optically scattering branches or stems. In that work the forest was controlled by the presence of mono-sized stems so that the transition from Rayleigh to Optical scattering could be easily monitored. In this work using SERA the more realistic scenario of multi-sized, multi-generational stems occupying any particular stand are considered.

Table 8.1. *Abies Alba* forest data.

Age (years)	Stems	Vol. (m3/ha)	Basal (m2/ha)	H100 (m)	Opt.Vol (m3/ha)	Ray.Vol (m3/ha)
0	24809	0.00	0.00	0.02	0.00	0.000
2	24409	0.06	0.26	0.23	0.00	0.059
4	24010	1.08	1.68	0.65	0.00	1.084
6	23562	6.41	5.27	1.22	0.00	6.406
8	22950	21.79	11.57	1.89	21.72	0.077
10	22318	53.76	20.57	2.65	53.76	0.000
12	21403	105.29	31.29	3.46	105.29	0.000
14	18829	166.42	40.19	4.33	166.42	0.000
16	14720	218.18	43.92	5.24	218.18	0.000
18	10753	253.18	43.32	6.19	253.18	0.000
20	7598	272.58	40.26	7.17	272.58	0.000
22	5477	286.08	37.04	8.18	286.08	0.000
24	4048	296.66	34.11	9.22	296.66	0.000
25	3128	271.53	29.81	9.67	271.53	0.000
26	2685	272.81	28.35	10.14	272.81	0.000
28	2227	300.30	27.82	11.57	300.30	0.000
30	1926	330.27	27.71	12.78	330.27	0.000
32	1716	361.67	27.95	13.87	361.67	0.000
34	1558	392.70	28.27	14.86	392.70	0.001
36	1429	422.11	28.61	15.76	422.11	0.003
38	1317	450.68	28.98	16.60	450.68	0.003
40	1245	480.89	29.56	17.38	480.89	0.005
50	896	570.17	29.33	20.57	570.16	0.012
60	872	649.25	29.84	22.92	649.23	0.022
70	838	681.19	28.95	24.84	681.17	0.023
80	854	739.32	29.71	26.46	739.30	0.021
90	839	774.21	29.83	27.80	774.18	0.027
100	818	831.55	30.85	28.98	831.53	0.022

The contribution to the total backscatter of the different sized stems is expected to show that complete saturation is very rarely achieved in nature due to the continual regrowth taking place beneath the dominating upper canopy, especially upon senescence with a more common occurrence for a gradual change in backscatter per unit volume to be observed. This suggests that a climax forest continues to have a continuing volume contribution from Rayleigh scatterers in both the canopy and from the floor.

Although the general saturation curve is manifest in each dataset, the effect of a rapidly increasing basal area and the subsequent drop off to a more sustainable level appears to have a profound effect on backscatter. In a similar way to that seen in (Baker et al. 1994), it would appear that single species gymnosperm forests have a tendency to overstretch themselves in terms of basal area accumulation per area. This area of change coincides with the fluctuation in backscatter around 270m^3/ha. in Figure 8.4 highlighting how "self-thinning" and basal area have a direct influence on backscatter levels.

Table 8.2. Angiosperm forest data.

Age (years)	Stems	Vol. (m^3/ha)	Basal (m^2/ha)	H100 (m)	Opt.Vol. (m^3/ha)	Ray.Vol. (m^3/ha)
0	24825	0.00	0.00	0.04	0.00	0.000
2	24400	0.97	1.21	0.80	0.00	0.971
4	23039	44.12	12.68	3.77	43.95	0.445
6	15733	153.33	21.68	7.51	153.33	0.000
8	12167	227.12	24.49	9.76	227.12	0.003
10	9776	277.03	25.63	11.36	276.87	0.167
12	7471	316.11	26.39	12.60	315.91	0.201
14	5871	348.82	26.89	13.62	348.70	0.116
16	4776	377.12	27.29	14.47	377.01	0.117
18	4043	397.31	27.31	15.20	397.24	0.073
20	3519	418.74	27.55	15.85	418.66	0.084
22	3087	437.81	27.78	16.43	437.73	0.080
24	2814	457.96	28.16	16.95	457.91	0.053
25	2664	464.69	28.16	17.19	464.63	0.063
26	2527	471.38	28.17	17.43	471.31	0.063
28	2364	488.82	28.50	17.86	488.76	0.068
30	2141	496.76	28.28	18.26	496.69	0.074
32	2038	507.91	28.36	18.64	507.85	0.067
34	1954	515.26	28.26	18.99	515.20	0.057
36	1869	521.50	28.14	19.32	521.44	0.060
38	1763	531.02	28.20	19.63	530.96	0.060
40	1683	537.98	28.17	19.92	537.92	0.063
50	1415	539.36	27.61	21.17	559.31	0.052
60	1407	568.25	26.98	22.19	568.20	0.048
70	1232	586.58	27.08	23.03	586.55	0.035
80	1262	587.96	26.50	26.51	587.90	0.056
90	1415	577.94	25.63	24.35	577.88	0.052
100	1556	556.05	24.68	24.74	555.99	0.060

The backscatter data for scenarios b) and c), defined previously, are shown in Figure 8.5 for RT2 simulated Total backscatter, Optical backscatter and Rayleigh backscatter with both cases exhibiting very similar behaviour. The mixed species forest composition emphasises the competitive dominance of angiosperms over gymnosperms as time elapses, with the forests of the generic angiosperm and mixed composition almost identical in number and structure as the forest matures. As a result the backscatter data is very similar. Table 8.2 shows the specific data for the generic gymnosperm forest.

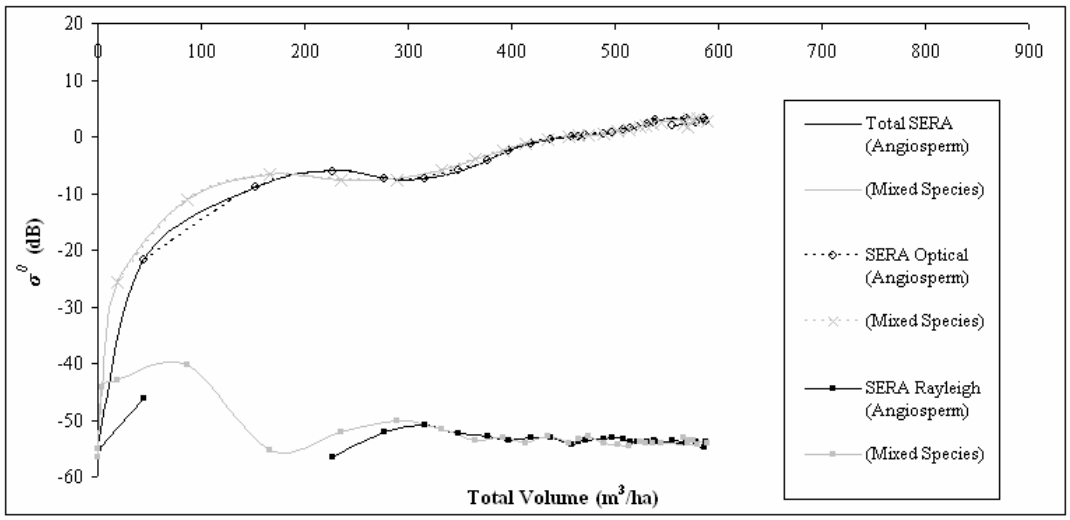

Figure 8.5. RT2 P-Band HH backscatter associated with SERA generated stem forests over a 100 year period. RT2 backscatter generated for total forest, Optical forest and Rayleigh forest according to limits of equation (8.3) for scenarios b) and c).

In both cases the total backscatter appears to progress in a more uniform way than for the *Abies Alba* scenario. Thinning is at a much greater level and basal area and volume increase at a steady rate with no obvious overexpansion. The mixed species forest example consists of 6 variations of species. These six comprise *Abies Alba*, generic angiosperm with additional shade constant, generic angiosperm, generic gymnosperm, generic gymnosperm featuring the *Abies Alba* specific photosynthesis constant, and generic gymnosperm with the *Cryptomeria* photosynthesis constant.

When planted in equal numbers the dominant species after 100 years becomes the generic angiosperm with a gradual reduction in the overall percentage of gymnosperm contribution from an early age.

8.5 Results

8.5.1 Forest Data Comparison of Mono and Multi Species Plots

In order to apply the theoretical values of backscatter based on equations (8.1) and (8.2), the backscatter must be separated into both Rayleigh and Optical scatterers according to equation (8.3), with Optical denoted as anything non Rayleigh. With the stems separated into their respective scattering size classes the backscatter created by the Rayleigh scatterers can be plotted against the squared volume which they occupy. Similarly the Optical backscatter can be plotted against the basal area. By doing this the constants associated with equations (8.1) and (8.2) can be obtained and used to predict the theoretical backscatter values for the entire volume based on the combined results of the simple equations. The results of this process indicate whether the backscatter and saturation within a forest can be considered a simple combination of two scattering types.

The data provided by this process has already been touched upon and shown to produce negligible Rayleigh contribution at high volumes but a noteworthy one at low volumes (Figure 8.5). If these relationships in scattering are in fact reliable, theoretical values for Rayleigh scattering and Optical (Non-Rayleigh) scattering can be generated. By combining the Rayleigh and non-Rayleigh backscatter datasets the robustness of the relationship is tested through its correlation with the total backscatter produced using the combination of SERA and RT2. High correlation would suggest that equations governing backscatter as a ratio of stem size to wavelength are correct. This would provide an explanation within this modelling

scenario for the saturation effect as forest volume increases beyond certain limits, which in the manner of the Matchstick Model and SERA is brought about by a reducing number of stems increasing their individual volumes and basal areas. The influence of "self thinning" on backscatter is highlighted through these relationships. Importantly reductions in stem number are also shown to reduce the effect of signal interference so that any saturation will be a result of the physical laws of scattering and not attenuation.

The thinning component of (Woodhouse 2006b) considered that at a particular volume the forest can adopt a thinning exponent which would indicate a constant forest basal area. Such a thinning routine would be implemented in a climax forest when resources must be rationed. At different stages of the forest's growth, this thinning value tends to vary. These variations are often noted as an increasing rate of thinning with age as volume increases beyond forest maturity. If the vast majority of scatterers are Optical scatterers, a feature more common in a mature forest, irrelevant of SAR frequency, and the basal area remains approximately constant, then saturation of backscatter will be as predicted by equation (8.2). Such a theory suggests that the reason the values of volume at saturation points can vary for the same incident wavelength is that the nature of the forest structure, as its components compete for light and space, determines saturation. If resources are limited the saturation would be expected to occur at a lower volume as fewer trees would be able to grow into the range of Optical scattering. Oppositely if they are in abundance then saturation would be expected at a higher volume. In a similar fashion, saturation could be described by age variations and through the types of age stand structures that exist (TASS) (Shvidenko et al. 1996).

With regards to the importance of volume and basal area in determining saturation, SERA predicts that forests, and the trees within them, consistently appear to reach an optimum condition. This relationship between the optimum basal area and volume of particular species can be seen in Figure 8.6. As the dominant species in the mixed

forest is the Angiosperm it is no surprise that the cases of Angiosperm and Mixed species data converge at higher levels of basal area and volume. The *Abies Alba* data on the other hand shows the behaviour seen in mono-species gymnosperm plantations of over extension in terms of basal area and then rapid die back. Correlation is still shown with the other species but only at volumes below $100m^3$/ha and above $300m^3$/ha. From the data produced by SERA, a particular stand area has the ability to sustain a much larger volume of *Abies Alba* than the Angiosperm species, with the Angiosperms appearing to reach their optimum volume at approximately $600m^3$/ha while *Abies Alba* does not reach its optimum within the 100 year study limit. As for basal area, for each case the optimum basal area is in the region between $25m^2$/ha and $30m^2$/ha with a reduction in basal area only occurring if the optimum volume has been reached or over extension occurs. At this point the constraint in volume dominates over basal area. With height continuing to increase, the forest must therefore scale back in numbers in order to not exceed this optimum volume value.

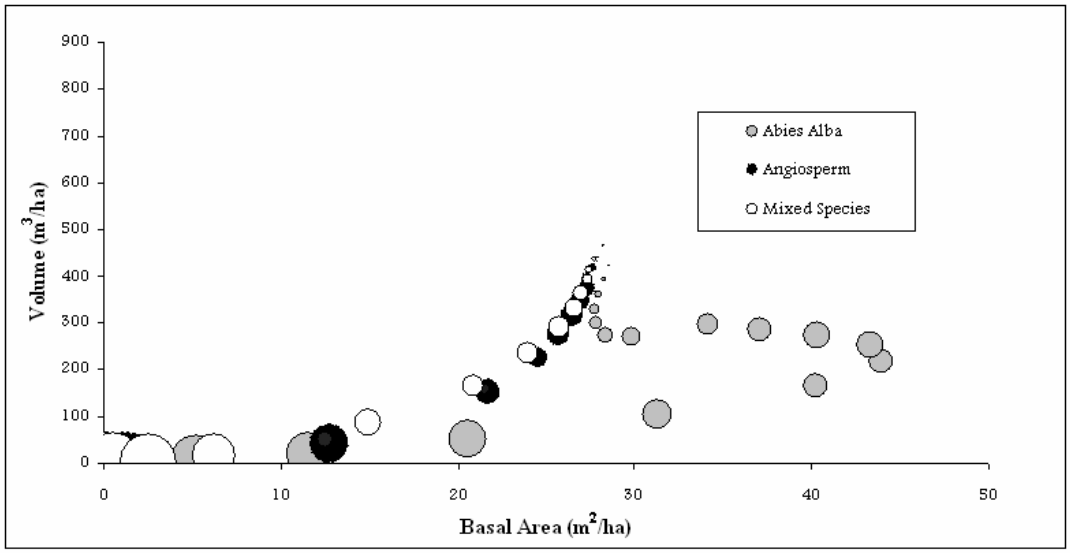

Figure 8.6. Volume per hectare of stems plotted against Basal Area per hectare for 3 SERA cases. Circles represent number of stems, the larger the area the larger the number of stems. Initial planting density 25000 per ha.

8.5.2 Backscatter Consequences of Scattering Regime Transitions

Backscatter increases as the volume increases irrespective of the fluctuations in basal area seen for the *Abies Alba* case of Figure 8.4. With respect to volume the backscatter appears slightly higher for the other two cases shown in Figure 8.5, although only at levels above 300m^3/ha. As for the thinning, the rate for *Abies Alba* is much more variable in comparison to the other two cases as is apparent through the circle representation of number density shown in Figure 8.6.

With regards to the findings concerning basal area and volume constraints, the SERA-RT2 backscatter, and the SERA-Theoretical backscatter, both corresponding to the total volume per ha, are plotted in Figures 8.7-8.10 for the 3 examined cases. The backscatter appears to follow the expected trajectories of a growing forest which at mature levels thins close to a level that maintains basal area (Woodhouse 2006b) and as a result approximately constant backscatter is recorded as volume increases. In each case the theoretical trajectory matches well with the P-Band RT2 generated backscatter above volumes of 300m^3/ha. At these volumes the majority of stems are scattering optically and with the basal area values consistently within the region of 25m^2/ha to 30m^2/ha the backscatter assumes a very small fluctuating rate of change. This backscatter increase corresponds to the level of basal area increase up to volumes of approximately 600m^3/ha in the cases involving angiosperms and to the end of the data range for the *Abies Alba* case. If the 600m^3/ha level is assumed to be the optimum (or maximum) volume sustainable by generic gymnosperms then up to this volume level the relationships laid out in equations (8.1) and (8.2) hold. Beyond this level SERA predicts that the behaviour of the forest is altered as it attempts to balance volume and basal area constraints rather than the previous process of increasing volume while maintaining basal area. The basal area increases are represented by the increases in circle area representing data points in the figures in question. It is apparent that basal area varies very little above 300m^3/ha but increases

gradually prior to this, with *Abies Alba* the exception, showing a rapidly increasing and subsequently decreasing value.

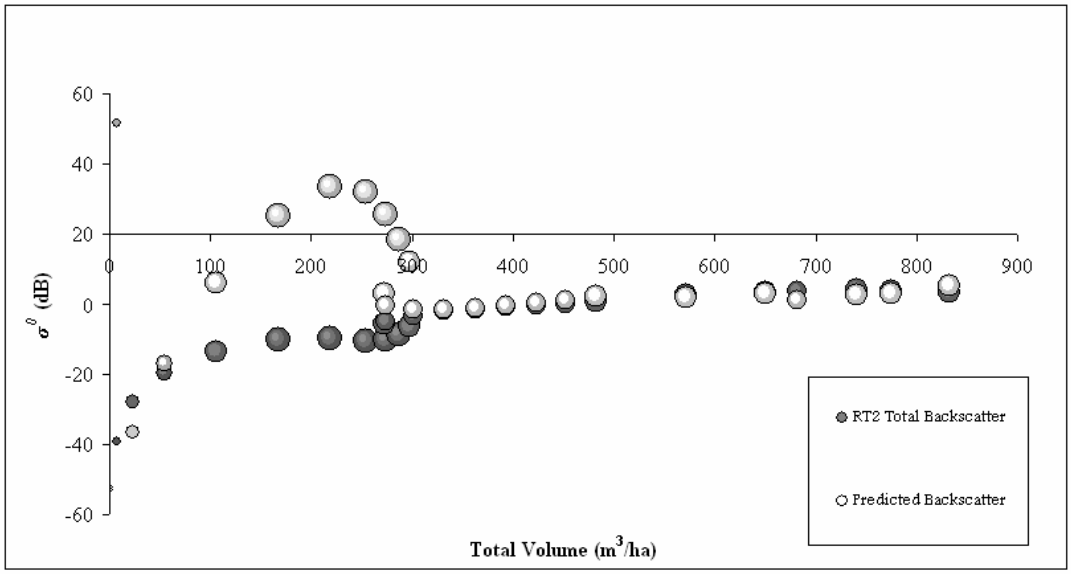

Figure 8.7. P-Band HH *Abies Alba* backscatter with respect to volume per hectare. RT2 generated backscatter of SERA forest shown alongside theoretical calculation of backscatter with respect to volume. Circle area signifies relative basal area quantity per hectare.

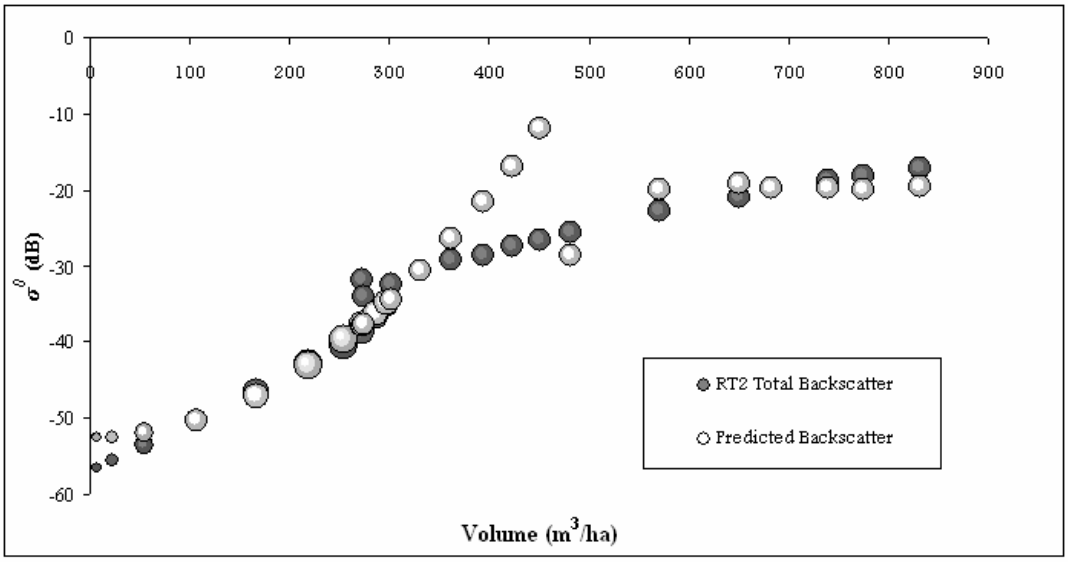

Figure 8.8. VHF HH *Abies Alba* backscatter with respect to volume. RT2 generated backscatter of SERA forest shown alongside theoretical calculation of backscatter with respect to volume. Circle area signifies relative basal area quantity per hectare.

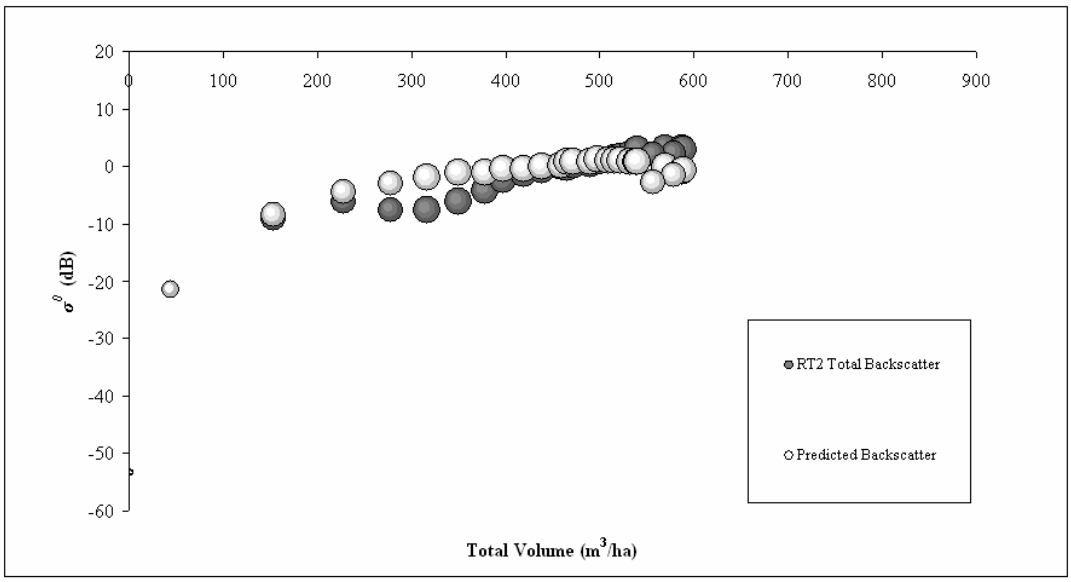

Figure 8.9. P-Band HH Generic Angiosperm backscatter with respect to volume. RT2 generated backscatter of SERA forest shown alongside theoretical calculation of backscatter with respect to volume. Circle area signifies relative basal area quantity per hectare.

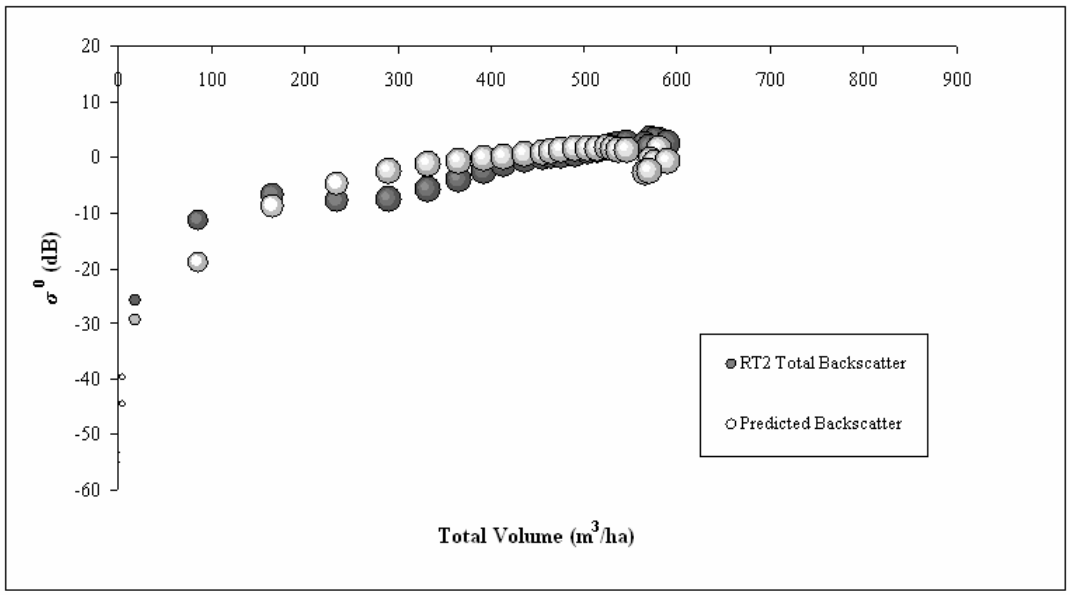

Figure 8.10. P-Band HH Mixed species backscatter with respect to volume. RT2 generated backscatter of SERA forest shown alongside theoretical calculation of backscatter with respect to volume. Circle area signifies relative basal area quantity per hectare.

Significantly in the case of *Abies Alba* the theoretical interpretation of backscatter does not fit the RT2 data at volumes between 50 and 300m^3/ha, Figure 8.7. In this region of volume, the basal area reaches unsustainable levels. As a result it would be expected that the backscatter will be much higher in this region due to its dependence on Optical backscatter. This is manifest in Figure 8.7 through the theoretical representation. It is clear that the RT2 data does not follow the theory in this region, with the backscatter being overestimated. Applying the theory to the work of (Baker et al. 1994) on *Corsican Pines* would result in a similar outcome, with no great increase in backscatter seen for the large increase in basal area exhibited by the forest. Reasons for this anomaly could be assigned to the overcrowding of the forest causing interference on the backscatter returns; the nature of the forest at this moment in time is such that, according to the classification used here, there are no Rayleigh scatterers within the forest. As volume increases from 50m^3/ha to 300m^3/ha there is no further Rayleigh contribution under the constraints of equation (8.3). The same dataset, with VHF backscatter, does not suffer from the same level of overestimation in the theory. The volumes at which the basal areas are elevated lie within the Rayleigh region at VHF and therefore the backscatter is correlated with the volume squared coupled with the longer, less attenuating wavelength of VHF, Figure 8.8.

For *Abies Alba*, at both P-Band and VHF, there is decorrelation at the transition from Rayleigh to Optical scattering between the theory and the backscatter, the anomalous results showing a data spike in the theoretical backscatter. For VHF this spike is located in the region of 350-500m^3/ha, the spike in P-Band is centred at approximately 6.4m^3/ha as can be seen in Figure 8.7. Both points mark the last data entry before the largest stems are theoretically considered to become large enough to scatter Optically. Significantly, if the Rayleigh to Optical boundary was reduced to a smaller stem radii these spikes would not occur as the data points would come under the Optical relationship of basal area. It is perfectly feasible then to say that the boundaries of equations (8.3) and (8.4) are not exact and liable to vary on a small scale, anomalous results would be minimised by considering such variations closely.

Alternately, under thinning conditions associated with Angiosperms, the impacts at these transition zones are greatly reduced. This may be due to the wide variability of stem radii in Angiosperm communities allowing a more even spread of values while for *Abies Alba* there is less variation and larger radii steps due to the yearly collective mass accumulation rates.

For the cases involving Angiosperms there is a distinct correlation between the theoretical and the RT2 generated backscatter values. The anomalies identified for *Abies Alba* are not replicated and the theories correlate extremely well with the RT2 produced data. Basal area and volume undergo a similar increase for both non *Abies Alba* cases following a generally accepted progression of forest growth. No over extension and die back is seen for either the mixed or Angiosperm datasets. The similarities and differences in the backscatter of the three data sets can be related to Figure 8.11 showing how the stem numbers thin with age. The differences between *Abies Alba* and the other cases are obvious, particularly over the first 30 years of growth when the recorded basal areas reach unsustainable levels.

Figure 8.11. Stem number thinning with passing years for all cases. Circle size represents relative basal area changes, larger circles represent larger basal area.

The success of interpreting forest scattering using the ideas laid out in the Matchstick Model (Brolly and Woodhouse 2010) in conjunction with SERA and RT2 is highlighted through the correlations seen between the datasets. The R^2 values for P-Band and VHF are shown in Table 8.3. The effect that the overextended basal area has on the *Abies Alba* data is only seen at P-Band as the VHF data is more dependent on the volume squared within this region of over extension. The spike in the theoretical backscatter is also much more significant at P-Band. This scenario is seen through the great differences in R^2 describing the theoretical backscatter using equations (8.1) and (8.2) with the limits of (8.3) and its likeness to the RT2 generated backscatter.

Table 8.3. Correlation between theoretical values based on relationship with basal area and RT2 backscatter.

Species	R^2	
	P-Band	VHF
Abies Alba	0.45	0.92
Angiosperm	0.96	0.90
Mixed	0.97	0.92

In order to determine the low correlation between RT2 and theory, the thinning rate of the *Abies Alba* stand was increased to that of the Angiosperm and Mixed species allowing the two tone scattering regime theory to match up extremely well with the RT2 generated backscatter. Complications related to basal area over expansion are avoided. This correlation shows that the mismatch between the theory and RT2 in the original *Abies Alba* case is not due directly to the specific species but an occurrence related to the basal area and number density; features of macroecological importance governing forest dynamics. In essence at a particular frequency the backscatter will be limited by a particular level of basal area. By applying the same forest dynamics to the *Abies Alba* case as experienced by the other two cases the same number of stems can be present at each age of each forest. The *Abies Alba* RT2 backscatter of such a

forest matches the theory to produce an R^2 value of 0.95. This crude matching only takes into account the largest stems within the stand when reducing the number density through the removal of any new growth, but it highlights how the large basal area, caused by the presence of many small scatterers, interferes with the backscatter return. As such it is deemed that the smallest scatterers act to interfere with the important larger stem interactions, specifically the double bounce mechanism.

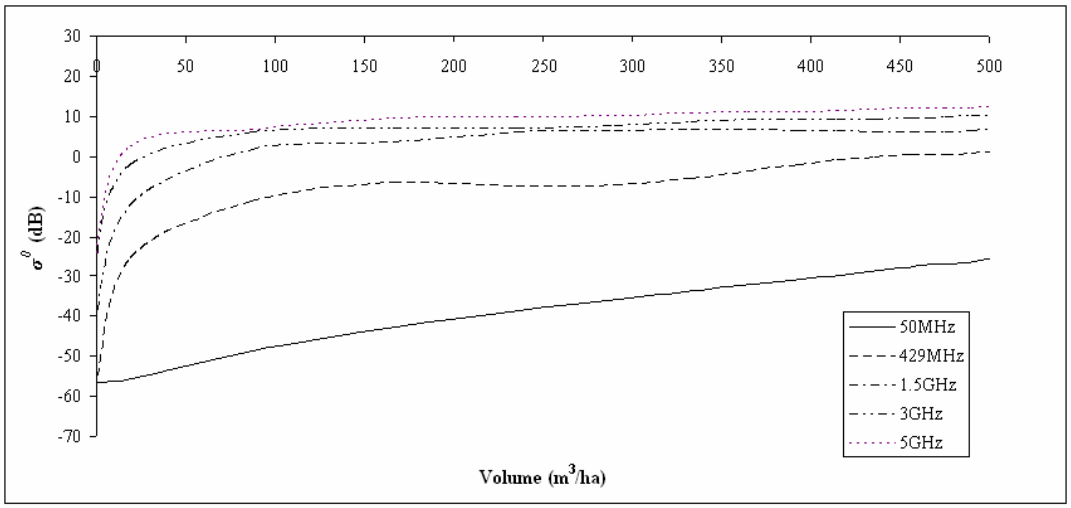

Figure 8.12. RT2 modelled multifrequency HH backscatter for mixed forest of scenario c) (section 8.5) against volume per hectare. Only vertical stems present over single layer. 25000 initial stems per ha. for each case.

Multifrequency backscatter analysis of the mixed species forest of scenario c) from Chapter 8.5 is visualised in Figure 8.12. The expected trend in backscatter behaviour is exhibited with saturation occurring at higher volumes for lower incident frequencies with the highest frequencies producing the highest intensity of backscatter. Of particular interest is the fact that this typical behaviour is exhibited in the absence of canopy attenuation with saturation exhibited within the volume range of 0 to 500 m^3/ha for frequencies from 5GHz down to 429MHz. Low saturation volumes apparent here can be explained by the basal area consistency following transition to Optical scattering which occurs at lower volumes for higher frequencies due to the sensitivity to smaller scatterers. The 50MHz data on the other hand does

not show saturation behaviour within the displayed volume range, with the transition of dominant scatterers to Optical scattering not occurring until much higher volumes than the other frequencies shown.

8.6 Discussion

A forest growth model (SERA) was used to investigate the theoretical possibility of forest SAR backscatter and saturation being caused by the inherent physics of electromagnetic scattering in relation to forest dynamics rather than due to commonly held assumptions of signal attenuation. As is often published, the reasons for saturation at large forest biomass levels have consistently been attributed in this way. The assumption is such that as the size of a forest increases, the ability of an EM signal to penetrate through the forest canopy towards the ground is reduced. This belief is backed up by the fact that short wavelength radar saturates at much lower biomasses in a widely accepted and undebated understanding of EM waves. This is empirically an aspect of all electromagnetic studies such as GPR surveys in which the penetration depths of particular wavelengths are well known and analysed (Smith and Jol 1995).

The existence of attenuation in relation to EM waves is not here debated but rather its importance to the particular scenario of SAR forest backscatter saturation. How the contribution of attenuation is assessed in this context is carried out through the removal of canopy scatterers, as such making the forest transparent. Such a method, as proffered in (Brolly and Woodhouse 2010) through the Matchstick Model, uses solely the wavelengths most sensitive to the larger forest components, the stems, which can contain up to 90% of a forest's biomass (Cannell 1982). As a result of this, the attenuating effects of the canopy are removed physically and theoretically from the scenario following the cessation of the forest growth model run, allowing an investigation between wavelength, scatterer size (stem), and number density. It has been reported in (Fransson et al. 2000b) that backscattered radar signal saturates at a

constant level for SAR systems using microwave frequencies at forest biomass above 40-100t/ha with the reasons for this "constant" attenuation level said to be due to the high attenuation in the canopy, but such statements are believed here to be untrue. P-Band SAR frequencies are included in this generalisation and have been shown to saturate over a large range of volumes (Patenaude 2003).

In this study the frequency 429MHz is the principal frequency of investigation with a wavelength of 0.7m. Many studies have quoted this frequency to saturate at between 100 to 200 t/ha ($167m^3$/ha – $333m^3$/ha), but as the theories presented here would suggest these saturation figures are not dependent on the biomass of the forest, but on the size of its constituent components and the methods, man made or natural, of controlling size dynamics. In a typical forest 333 m^3/ha represents a biomass at which the forest has had several years of growth and has become mature. When a forest has achieved this status the most consistent forest parameter is the total basal area of the stand. Using SERA (Hammond and Niklas 2009) and simulating, from conception, 3 separate forests consisting of *Abies Alba*, generic gymnosperm and the forest consisting of mixed species, each forest has shown that for this level of volume the change in basal area per year of growth is less than 1% every year. With the nature of Optical scattering being proportional to the basal area increase of the stand (Moosmuller and Arnott 2009; Woodhouse 2006a) the backscatter would be expected to saturate if the rate of increase of basal area with volume stagnates. According to equation (8.2) if there is no increase in basal area then there will be no increase in backscatter. This statement is indeed true if the forest is entirely devoid of Rayleigh scatterers, but with the existence of regrowth in each of the simulated forests there remains a small contribution from Rayleigh scattering proportional to the volume squared (Smith and Ulander 2000) and equation (8.1). Due to the nature of this backscatter, small increases in volume will result in a much greater increase in backscatter than that caused by similar basal area increases. By modelling forests devoid of canopy, it is perfectly viable that complete saturation could be observed but due to the dynamism of a forest this is unlikely in a natural setting. Figure 8.12 helps

to explain the relationship between forest backscatter, volume, and frequency. In a single layer defined by the height of the largest stem, the trends are considered to be driven by stem size rather than extinction with stable saturation more apparent for higher frequencies for which more of the forest will scatter optically.

SERA has predicted that a forest will grow to reach an optimum basal area as well as an optimum volume. In biological terms the forest can only be sustained within the confines of the allocated area and in accordance with the nutrients available, when these are expended only senescence followed subsequently by regrowth or additional growth to the survivors will take place. At such times the volume and basal area will be temporarily reduced until the gap can be filled. At this point it would appear that different backscatter values to those expected are possible in response to the change in number density and total size and structure changes of the forest. These backscatter changes are proposed to be directly related to the variation in the mix of Rayleigh to Optical scatterers resulting from mature death and regrowth. By coupling SERA with RT2 it has been shown that the Optical and Rayleigh scattering contribution influence the saturation effects encountered in forest SAR surveys and are directly affected by adverse growing dynamics within a forest. By separating the forest into Rayleigh and Optical scatterers and calculating theoretical backscatter values based on simple equations defining two scattering types, the fit to the RT2 modelled backscatter values represents corroborating evidence pertaining to the nature of saturation. For the 3 simulated forests, R^2 values at P-Band of 0.45 for *Abies Alba*, 0.96 for generic angiosperm, and 0.97 for the mixed species represent a successful correlation between the theory and the radiative transfer data with the low result for *Abies Alba* being discussed earlier and explained as a feature of forest overcrowding and uncertainties in boundaries assigned to the Rayleigh size limits. For VHF the correlation is trustworthy with *Abies Alba* producing R^2 of 0.92, with the generic angiosperm and mixed species giving values of 0.90 and 0.92 respectively; high values of correlation but generally lower than at P-Band due to the increase in proportion of Rayleigh scatterers.

8.7 Conclusions

In natural climax forests, with canopy features, the contribution of predominantly Rayleigh scatterers across the microwave range can be more significant than the negligible status they have been given by the modelling work here. Although it will be expected that their contribution will be to attenuate the signal, canopy scatterers will also be expected to increase the volume squared proportional backscatter quotient. In a mature forest there may be enough continual new Rayleigh volume growth in the under-storey to allow the backscatter of the forest to increase beyond the apparent saturation points, regardless of basal areas although additional volume growth in the canopy may not be encountered. This is believed to be one of the main reasons that complete saturation is rarely measured. If a forest features an active canopy as well as regrowth on the forest floor then there will be a consistent Rayleigh presence. This is even true at very high SAR frequencies at which the sensitivity to scatterers in the higher echelons of the forest is high. At low frequencies such as VHF the contribution of Rayleigh scattering will be prominent up to high volumes due to the ratio of wavelength to radius, although the sensitivity to smaller scatterers will be low resulting in lower intensity values than would be seen for a similar forest surveyed using a shorter wavelength.

Across two incident frequencies regarding three forest stands, five out of six studies showed that SERA forests predicted that backscatter is largely influenced by forest basal area. All 3 cases using VHF showed high correlation between RT2 generated backscatter and the values predicted by theory using constants derived from the RT2 data. For P-Band two out of three cases provided the same result. Each of these scenarios points to a relationship between the forest and backscatter that is driven by early forest growth through increasing basal area of optically scattering forest constituents. When basal area remains consistent only small changes in backscatter are noted with backscatter levels assumed to be a result of backscatter contribution

from senescence of larger trees and forest regrowth. The anomalous scenario is that of P-Band for *Abies Alba* with the backscatter only loosely associated with the basal area increase, and being largely overestimated by the theory. This lower correlation is due to forest overexpansion and interferance with the important double bounce scattering, a dominant mechanism at P-Band and longer wavelengths (Saatchi and McDonald 2002). Attenuation is not believed to influence the saturation in the absence of this behavioiur.

Although there remains work to be done in this area this study provides evidence to counteract the belief that forest SAR saturation is a result simply of canopy attenuation. Although the existence of attenuation is not debated, its role in saturating the backscatter return is questioned by the existence of trends upon removal of attenuating influences. What is left is an analysis of two scattering types combining in a forest situation to provide total backscatter. Saturation is therefore not expected to fit any particular model or correlation with biomass but rather with size of forest components in conjunction with existing dynamics. Many tree species have similar allometric scaling exponents and in combination with forest dynamics the majority of stems will reach a certain biomass at a certain age. This age may represent a size of stem which will scatter optically and as a result of the majority of stems, and total stem volume, consisting of Optical scatterers, saturation behaviour will be seen.

9 Thesis Discussion

This thesis has been provided in the form of five individual studies with each disseminating an independent scientific finding but are linked through the key factors of the forest, macroecology and remote sensing. Each study has incorporated a macroecological model to simulate both forest growth and structure and in four of the five studies radiative transfer backscatter modelling has been used to obtain links between forest form and structure and the SAR backscatter response. The research studies included in this thesis have followed a progression from an analysis of forest structure in terms of the relationships between forest volume and height (Chapter 4) to conclude with a study of the same structures from a backscatter perspective relating to forest volume (Chapter 8). In the intermediate chapters the impact of both vertical and horizontal structural variations have been examined. In Chapters 5 and 6 forests of mono-size and mono-aged trees were used to provide vertical backscatter profiles of a forest at a particular moment in time while in Chapter 7 these same mono-sized forests were used to provide the horizontal backscatter profile for a series of stands representing different ages. These stands could be considered the same stand at various times or neighbouring stands of different ages. The significance of the findings of these chapters in relation to the questions and hypotheses provided in Chapter 1 are here discussed with the first question the main focus of this study. Each of the experimental chapters (4-8) are concerned with the effects of variation in either the vertical or horizontal forest structure. Horizontal variations are defined by the effects of self thinning with visual examples of this provided in Figure (3.4) with a more explicit analysis of thinning variation given in Chapter 7. Vertical structure variations are also defined by thinning on a stand scale but a more significant impact on the vertical distribution of biomass is made by scaling variations between branching levels and general allometry considerations (Chapter 1.4).

Chapter 4 focusses on the structure of a heterogeneous forest which can vary over time in both its horizontal and vertical distribution of biomass. As the forests in this

chapter do not possess branching architecture the effect of scaling on the vertical distribution is negligible with the structure largely a result of mortality and regrowth. Structural variation is typically associated with stand age and thinning rates are driven by competition. An example of the vertical distribution of stem and canopy biomass predicted by SERA is shown in the appendix Chapter 12.4 where this distribution is described in terms of biomass per metre. Chapter 4 considers the consequences of these structural variations on the relationship between forest height and forest volume and subsequently for the use of interferometry. These variations are significant for the inferral of forest height to indirectly estimate forest volume through allometry. This method has been used in studies such as (Mette et al. 2003), (Wegmuller and Werner 2002) and (Hajnsek et al. 2009). The work of Chapter 4 indicated that forest mean height is the the most accurate indicator of forest volume (see Figures (4.1, 4.2, and 4.4) for comparison) but its success is diminsihed by the difficulties associated with attaining such height measurements from field measurements. Also, and more significantly for remote sensing studies no definable relationship between mean forest height and the scattering physics of SAR is easily obtainable. As a consequence a trade off between an accurate height measurement for establishing forest volume and an applicable height measurement related to SAR scattering is required. In this study Lorey's height is suggested as a compromise as it offers a more reliable and applicable height classification than the other alternatives of maximum height and H100, see Tables (4.1 and 4.2). The fact that forest volume and height are shown to possess no unique relationship as a result of both horizontal and structural variations as a forest grows regardless of the height classifications chosen serves as a warning to studies that employ allometric conversions (see Figure 4.8). The work of Chapter 4 is an example of how vertical and horizontal heterogeneity across forest stands have a significant impact on the use of remote sensing for forestry.

The interferometric implications of structural variation implied by Chapter 4 are explored in Chapters 5 and 6 with the effects of variation in the vertical plane examined. In these chapters the consequences of number density and size distribution

within the vertical profile of the forest are the focus. Chapter 5 analyses the consequences of structural variations resulting from scaling exponent changes between parent and daughter branches (Figure 5.8) while Chapter 6 incorporates increased values of possible daughter branches, *n*, from each parent to provide a fuller canopy (see Chapter 6.5) with coherence tomography used both with the original WBE and with the scaling variant of the model. What both of these chapters highlight is that the vertical profile of backscatter can be used to determine scattering phase centres both in intensity and interferometric studies and is affected significantly by structural variations, particularly within canopies. This is not just a result of SAR frequencies (Figure 5.6) but also as a result of the distribution of biomass through number density and size variations. Typically the RVoG model of attenuation (Treuhaft and Siqueira 2000) has been deemed adequate to describe the SAR saturation effect over forests and also the vertical distribution of backscatter. In Chapters 5 and 6 the use of this model is brought into question due to its inability within the scope of these scenarios to represent the shape of backscatter.

The importance of number density and size variation is emphasised in Chapter 5 when describing the shape of the vertical SAR backscatter profile of a forest. Due to branch size variation within a canopy and the relationship of each individual branch to the wavelength of the incident SAR frequency it is possible that scattering regime transitions occur (see Chapter 2.3). These scattering transitions are shown to influence the shape of the vertical backscatter profile and determine the maximum backscatter locations within the canopy as a consequence of the dependencies of these scattering regimes. The scattering trends resulting from these transitions are further explored in Chapters 7 and 8 using the Matchstick Model and the more heterogeneous SERA model (see Chapters 3.2 and 3.3) to examine the effects of horizontal structural variation resulting from thinning. In Chapter 7 the structural variations are largely confined to the horizontal plane due to the mono-sized stems that occupy the studied forests but in Chapter 8 horizontal and vertical structural heterogeneity are both considered. The work of Chapter 8 reinforces the findings of this thesis concerning

the effects of scattering regime transitions on backscatter trends by indicating that saturation does not have to be an effect of attenuation but can be caused by the changing structure and increasing size of a forest and the resultant change in backscattering behaviour.

Of key importance to this study are the particular influences on forest structure played by macroecological parameters. It has been emphasised that tree structure impacts on backscatter trends, see (Castel et al. 2002; Dobson et al. 1992), here forest structure variations are assigned to effects of stand scale macroecological variations. The impact on backscatter trends of those considered in this study are discussed here:

- **Thinning**

Thinning is seen in this study to be the largest influence on backscatter trends both with respect to forest volume and forest height. Forest dynamics are largely seen to be driven by this behaviour. In Chapters 4 and 8 thinning is determined by species specific relationships provided by SERA which determine the stochastic probabilities of mortality and also of how thinning can be driven by competitive behaviour. These thinning measures ensure that gaps appear in the forest landscape allowing regrowth to occur. An example of this can be seen in Figure 8.3 which shows gaps appearing for a SERA modelled forest. The implications of this being that the forest becomes a multi-age environment where trees of different sizes share the same stand. This is evident in Chapter 4 where heterogeneity in vertical size reduces the effectiveness of height to volume relationships. In Chapter 7 thinning operates in a different manner with mortality induced by a user defined thinning rate. The subsequent mortality provides space for existing trees to expand. No regrowth is considered by the model therefore the forests are represented by mono-age and mono-size stems as depicted by *d=1* or *d=2* thinning in Figure 3.4. In the absence of thinning the same number of stems may represent a forest stand for a large period of time without mortality as represented by the *d=0* thinning of Figure 3.4. Such thinning behaviour is similar to that exhibited by managed plantation forests with stands largely represented by a

common age and height value to ensure maximum yields. In Chapters 5 and 6 thinning is not an active part of the investigation but the thinning behaviour chosen ensures that canopy extinction does not influence the backscatter distribution. Although each vertical profile is a snapshot of an individual stand at a particular time the forests of Chapters 5 and 6 are modelled to allow transmission through the canopy. In the absence of thinning, forests of multi branching layers may become dense and produce a large drop off in backscatter when the density of the forest is such that occlusion is influential.

Thinning is also seen to be the driving force behind forest backscatter saturation. In the absence of thinning, saturation will be dominated by attenuation, but in the presence of thinning saturation is a function of forest basal area and scattering transition. When using the WBE model, the SERA model and the Matchstick Model (Chapters 3.1, 3.2, 3.3) the total basal area of a forest is seen to either level off at a particular value (Figure 8.4) or can be manipulated to do so through user defined inputs of $d=2$ (Figure 7.10). In each case the backscatter contribution is seen to follow this constant total basal area value if the forest is of a mature size and in an area that suggests a resource limited value. This can be visualised in Figures (7.6-7.8) from Chapter 7, and through analysis of Figures (8.4) and (8.5) and the data of Table (8.2) also see appendix Chapter 12.3. What these results suggest is that in the absence of significant attenuation the SAR backscatter saturation behaviour is driven by the total basal area of the forest. As this appears the case when forests are of a particular maturity, the relationship then applies to large stems, with the ratio between scatterer and incident wavelength significant. For radar frequencies the higher the value the smaller the radius required to cause a transition from Rayleigh to Optical scattering suggesting lower forest volume levels of saturation due to the dependence of Optical scattering on the physical cross section of a scatterer. Figure (8.12) exhibits the frequency variation in saturation behaviour for a heterogeneous forest in age and size and is not considered an effect of attenuation. This is especially true throughout this

study as long SAR frequencies of L, P and VHF Band are used as well as canopy free forests in Chapters 7 and 8.

As the evidence suggests thinning to be the driving force behind SAR backscatter saturation over forests it consequently has direct influence on other specific macroecological parameters. Examination of these parameters provides further information on why thinning has such an influence on backscatter trends.

- **Number Density**

Chapter 5 provides the most significant evidence of how number density variations impact on backscatter behaviour. Thinning in a forest not only reduces the number of stems as visualised in Figure 3.4, but also reduces substantially the number of branches within a canopy layer of a forest. When thinning reduces the number of branches within a layer in the generalised setting of a WBE forest the proportion of smaller branches will be most significantly reduced due to their abundance in the vertical structure. One stems loss leads to many branch losses. The significance of this is the scattering behaviour exhibited by branches on either side of the scattering transition described in Chapter 2.3. The association of dominant influence of number density in Optical scatterering and size in Rayleigh scatterering means that a thinning imposed reduction in numbers could lead to alteration of the vertical backscatter profile of a forest similar to the examples shown in Figure (5.8).

For the horizontal structure the effect on number density is also significant with Chapters 4, 7 and 8 highlighting how forest stands must thin the number density of stems due to both space restrictions and to allow individuals to grow to greater sizes. The typical occurrence is for number densities to reduce and individual sizes to increase as volume increases. The reduction in the number density of larger stems is then a precursor to SAR backscatter saturation as a reduction in number density allows basal area to remain constant across a forest stand increasing in volume. This again indicates the importance of scattering being dominated by the Optical regime so

that when number density has been reduced sufficiently in the presence of a dominant distribution of Optical sized scatterers saturation occurs. Apparent in Figure (8.5).

- **Basal Area**

The total basal area has been shown through the modelling in this thesis to be the driving force behind the saturation effect. This is due to the relationship of Optical scattering with the physical cross section of scatterers. The effect on basal area caused by thinning is a direct consequence of number density reduction. Thinning of stem numbers does not necessarily reduce the rate of volume increase of a forest over time due to the continuing accumulation by the remaining stems in both height and basal area (Figure 7.2) but thinning can severely inhibit the increase in total forest basal area as is the case for *d=2* thinning shown in Chapter 7. When visualised using Figure 3.4 and the work of Chapters 7 and 8, thinning can be seen to significantly alter the relationship between forest volume and forest basal area with multiple forest volumes being possible for the same forest basal areas. This is a result of the variable relationship between height and volume (see Chapter 4). What this also implies is that the relationship between SAR backscatter and forest volume can not be unique as future mission proposals using SAR backscatter such as BIOMASS (Le Toan et al. 2010; Scipal et al. 2010) assume. This non-uniqueness is seen explicitly in Figure (7.9) from RT2 modelling of Matchstick Model forests and through the backscatter dependence on basal area seen in Chapter 8 for forests beyond a particular maturity. It is also seen through the backscatter behaviour related to thinning levels of close to *d=2* which provide constant forest basal area for the life of the forest as depicted in Figures (7.6-7.8).

- **Size Distribution (Scaling)**

Scaling is the least affected parameter by forest thinning. As an inherent part of a species make up, in this study where user defined variables are used the scaling remains the same through the life of the forest. Examples of this are in the studies incorporating the WBE model. Chapters 5, 6 and 7 all rely on this model to provide

scaling information through all branching layers but in Chapter 7 this is minimised to stem size increments. As a result of only considering stems the backscatter trends resulting from scaling variation are minimal with the relationship between backscatter and basal area maintained albeit at different backscatter intensity levels. Where thinning does influence scaling is when the SERA model is used. The SERA model (Chapter 3.2) possesses different allometric identities (see appendix Chapter 12.2 for examples) dependent on whether maturity has been reached. As a result of the mortality and regrowth allowed by SERA, trees possessing different allometric identities can exist within the same forest stand. Additionally within multispecies stands the dominant behaviour of one species over another will alter the balance of one allometric identity over another.

Where scaling is of most interest is in the work of Chapters 5 and 6 where the distribution of branching and size within the vertical profile are affected by variations. The conclusions of Chapter 5 are not dependent on the scaling as shown from the similar trends displayed in Figure (5.8) where the dominant backscattering layer is a result of the nature of Optical and Rayleigh scattering. What the results shown in this figure do indicate is that changes in scaling can alter the vertical location of dominant layers within the profile. As a result the scaling variations are predicted to have implications for interferometric studies such as examined in Chapter 6 where two different forest structures in terms of branching are seen to have different vertical backscatter profiles subsequently different interferometric interpretations, see Figures (6.5) and (6.6). The result of such modifications in fullness of canopy is for the structure approximation using coherence tomography to produce less accentuated spikes, occurring relatively lower in the vertical profile. A fuller canopy from ground to top with varying branch sizes within each layer lowers the vertical location of interferometric dominance within the canopy. In a similar way a multi-age, multi-species forest representing many scaling identities would present a varied distribution of branch sizes within the vertical profile. The dominance of a particular layer would still be deemed a result of the number density of a branch size.

- **Volume**

Volume is not shown in any experimental chapters to be responsible for saturation behaviour. The relationship between backscatter and volume is largely confined to the early stages of forest growth representing the low volumes on a backscatter saturation curve. Proportionality between Rayleigh scattering and the squared volume of a scatterer (Chapter 2.3) ensures that backscatter saturation can only occur with constant volume. It is therefore not possible for volume to be responsible for saturation in the forests studied here unless an attenuation related explanation is indeed the case. Volume to height relationships examined in Chapter 4 also highlight how volume is not dependent on the structure of the forest. Its most significant contribution is apparent in Chapters 5 and 6 where the shape of the backscatter profiles are dependent on the number density dependence of Optical scatterers and the volume of the Rayleigh scatterers as in Figure (5.5).

Although these macroecological factors are deemed to be influential in forming the backscatter trends of empirical data, their influence is dependent on the nature of the active scattering regimes. This thesis has explored the macroecological effects on the backscatter and has crucially linked these effects to the physics of scattering. For horizontal forest structure the most simple structures to model are the stems which contribute significantly to total forest volume and specifically to P-Band backscatter through double bounce interactions (Saatchi and McDonald 1997). By simplifying the modelling scenario to consider solely stems the particular effects of macroecological variations and influence of scattering regime change could be examined in a controlled environment allowing the Matchstick Model concept existing as a result of the findings of Chapter 5 concerning scattering regimes to be used in Chapter 7 and further examined in Chapter 8. The comparison of the radiative transfer data and the results of simple calculations involving two equations representative of scattering have exposed clear similarities in observed saturation effects for increasing forest volume.

10 Thesis Conclusions

This thesis offers a unique synthesis across biophysical models and radiative transfer theory to provide an analysis of the effects of some macroecological parameters on the backscatter return from forests. In so doing it examines both vertical and horizontal backscatter distributions and the macro ecological trends associated with them.

Each piece of work featured in this thesis has addressed a question related to the radar backscatter behaviour of forests. Of particular focus has been how the different forest dynamics used in this work influence the interpretation, and therefore the estimation, of forest volume/biomass. The importance of findings such as those presented in this thesis relate primarily to furthering the understanding of the radar scattering relationship with vegetation. The consequences of this new understanding is to impact on future remote sensing missions either by advising on the potential of a particular survey method or to offer insight on the interpretation of data retrieved from operational missions. This is especially befitting of research intended to operate at P-Band wavelengths or longer.

An example of such a prospective mission is the European Space Agency's proposed BIOMASS mission (Le Toan et al. 2010; Scipal et al. 2010), which will incorporate both intensity and interferometric P-Band data to provide forest global biomass observations as part of its scientific mission. Of particular significance to such missions is the potential structural influence of the forest on interferometric data and its interpretation which will be used to obtain height measurements for allometric conversion to biomass estimates (see Chapters 4, 5, and 6) and indeed the structural variations that appear to influence the relationship between SAR backscatter and forest volume (see Chapters 7 and 8). What this thesis adds to the understanding of these scenarios is that the dynamics of forest structure have an key role in defining the observed SAR backscatter responses and trends.

This thesis makes several contributions to further the understanding of SAR backscatter behaviour of forests through the modelling undertaken. These are:

- Through modelling using a forestry growth model forest it is demonstrated that volume does not possess a unique relationship with forest height. Of the height classifications investigated mean height is shown to have a greater association with volume than is exhibited by maximum, H100, and Lorey's height but its applicability to remote sensing is diminished by the inability of methods such as SAR and LiDAR to measure all trees within a forest. Lorey's height is suggested as a more appropriate height class for association with volume through remote sensing as it maintains qualities of the mean height measurement as well as the remote sensing methods through the consideration of all trees but by weighting the height measurement towards the larger.
- P-Band volume scattering from within the vertical profile of a forest is defined by the number density and size of the scatterers at each layer rather than being determined by biomass and attenuation. Based on the assumption that SAR backscatter within a forest can be described as either Rayleigh or Optical scattering, RT2 modelling data reinforces the theory that Rayleigh backscatter is dominated by the size of the scatterers and Optical backscatter is dominated by the number density. A dominant scattering layer is shown to exist where branches in the region of scattering transition produce maximum backscattering intensity.
- L-Band vertical backscattering profiles which, in empirical data features a peak in intensity below the surface of the canopy, similar to those of Chapters 5 and 6, can not be sufficiently represented by the RVoG model which describes backscatter through an exponential signal decay. This is due to the volume scattering vertical profile being dominated by structure effects rather than simple extinction. More appropriate descriptions are found using Gaussian or Legendre solutions which can better describe these effects but require additional interferometric baselines to accurately infer volume from height measurements.

- P-Band and VHF backscatter saturation behaviour can be reproduced using a forest description of solely identical cylinders to represent stems. Saturation behaviour is shown through modelling to be produced as a consequence of Optical backscatter being dependent upon the total physical cross section of the stems rather than as a consequence of increasing extinction as volume increases. This is possible through the intervention of thinning which allows forest volume to increase while number density is reduced leading to a direct association between saturation and forest thinning. Thinning determines total basal area variations as a forest increases in volume.
- Even for longer wavelengths, mature forests are dominated by Optically scattering constituents which determine that SAR backscatter increase is driven by basal area increases as forest volume grows.
- The relationship between forest volume and forest backscatter is shown to be non-unique in the presence of identical vertical stems representing forests as well as in the presence of a heterogeneous stem height and size distributed environment as a consequence of the association with forest basal area.
- Vertical and horizontal forest structure, manifested through number density and size variations, can significantly influence the backscatter trends of backscatter with volume, and with height. The extent of this influence is evident where different thinning practices or species-specific scaling are employed.

As with any study this thesis has limitations. The most significant limitation of the study being that it is purely model-based with reliance on published literature to verify the findings. In the interests of completeness future empirical work would be required to validate the relevance of this thesis' findings with particular interest paid to forest basal area values, which are not as commonly referred to in the literature as forest biomass. In addition the existence of a test forest with exact inventories and regular SAR data would be an exceptional source for theoretical studies such as this. Additional limitations relate to the nature of the modelling. Particularly important in this sense is that only one radiative transfer model was used to calculate backscatter

values. The use of additional models would potentially corroborate the findings published here and would add further significance to the presented conclusions.

Potential future work on this subject would concentrate on the use of interferometry. With intensity measurements shown to be particularly structure dependent the relationship of interferometry, and polarimetric interferometry, to forest height must be better understood. Chapters 4, 5 and 6 provided a series of examples of how interferometric data is not entirely understood and it is thought that modelling using interferometric models in collaboration with similar forest models to those used in this thesis would allow a greater insight into the nature of scattering phase centres. In such work there lies the potential of using multi-frequency and multi-polarisation data to infer a high level of structural detail in the vertical profile. Such successes would then lead to a potential increase in the accuracy of biomass estimates across forest stands.

This thesis has tackled the subject of forest remote sensing using a deductive approach aiming to provide, through the modelling procedures carried out, general explanations that encompass a large range of radar backscattering behaviour exhibited by forest ecosystems. This is in contrast to the more common inductive approach of reasoning from the particulars of empirical studies of specific forests to explain the universal scenario. This thesis has aimed to achieve these explanations by relying on a minimal number of generalised macroecological predictions.

"The grand aim of all science is to cover the greatest number of empirical facts by logical deduction from the smallest number of hypotheses or axioms."

Albert Einstein (1879-1955)

11 References

Andersen, H.E., McGaughey, R.J., Carson, W.W., Reutebuch, S.E., Mercer, B., & Allan, J. (2003). A comparison of forest canopy models derived from LIDAR and INSAR data in a Pacific Northwest conifer forest. *International Archives of Photogrammetry and Remote Sensing, 34*, 211-217

Anderson, C. (2000). User and programmer guide for RT2. In, *Space Syst. Group Tech. Rep. YD/000293/D1995*. London, U.K: BAE Systems

Askne, J., Santoro, M., Smith, G., & Fransson, J.E.S. (2003). Multitemporal repeat-pass SAR interferometry of boreal forests. *Geoscience and Remote Sensing, IEEE Transactions on, 41*, 1540-1550

Askne, J.I.H., Dammert, P.B.G., Ulander, L.M.H., & Smith, G. (1997). C-band repeat-pass interferometric SAR observations of the forest. *Geoscience and Remote Sensing, IEEE Transactions on, 35*, 25-35

Attema, E.P.W., & Ulaby, F.T. (1978). Vegetation modeled as a water cloud. *Radio Science, 13*, 357-364

Baker, J.R., & Luckman, A.J. (1999). Microwave observations of boreal forests in the NOPEX area of Sweden and a comparison with observations of a temperate plantation in the United Kingdom. *Agricultural and Forest Meteorology, 98*, 389-416

Baker, J.R., Mitchell, P.L., Cordey, R.A., Groom, G.B., Settle, J.J., & Stileman, M.R. (1994). Relationships between physical characteristics and polarimetric radar backscatter for Corsican pine stands in Thetford Forest, UK. *International Journal of Remote Sensing, 15*, 2827-2849

Ballester-Berman, J.D., et al (2005). Retrieval of biophysical parameters of agricultural crops using polarimetric SAR interferometry. *Geoscience and Remote Sensing, IEEE Transactions on, 43*, 683-694

Balzter, H. (2001). Forest mapping and monitoring with interferometric synthetic aperture radar (InSAR). *Progress in physical geography, 25*, 159

Balzter, H., Cox, R., Rowland, C., & Saich, P. (2003a). Forest Canopy Height Mapping from Dual-Wavelength SAR Interferometry. In, *PolInSAR 2003* (p. 51). Frascati, Italy

Balzter, H., Luckman, A., Skinner, L., Rowland, C., & Dawson, T. (2007). Observations of forest stand top height and mean height from interferometric SAR and LiDAR over a conifer plantation at Thetford Forest, UK. *International Journal of Remote Sensing, 28*, 1173-1197

Balzter, H., Skinner, L., Luckman, A., & Brooke, R. (2003b). Estimation of tree growth in a conifer plantation over 19 years from multi-satellite L-band SAR. *Remote Sensing of Environment, 84*, 184-191

Bansal, R., King, R.W.P., & Wu, T.T. (1982). The Measurement of the Electric Field Inside a Finite Dielectric Cylinder Illuminated by a Plane Wave. *Microwave Theory and Techniques, IEEE Transactions on, 30*, 1282-1286

Bastien-Henri, S., Park, A., Ashton, M., & Messier, C. (2010). Biomass distribution among tropical tree species grown under differing regional climates. *Forest Ecology and Management*

Battaglia, A., Tanelli, S., Kobayashi, S., Zrnic, D., Hogan, R.J., & Simmer, C. (2010). Multiple-scattering in radar systems: A review. *Journal of Quantitative Spectroscopy and Radiative Transfer, 111*, 917-947

Beaudoin, A., Toan, T.L., Goze, S., Nezry, E., Lopes, A., Mougin, E., Hsu, C., Han, H., Kong, J., & Shin, R. (1994). Retrieval of forest biomass from SAR data. *International Journal of Remote Sensing, 15*, 2777-2796

Bergen, K.M., & Dobson, M.C. (1999). Integration of remotely sensed radar imagery in modeling and mapping of forest biomass and net primary production. *Ecological Modelling, 122*, 257-274

Bindlish, R., & Barros, A.P. (2001). Parameterization of vegetation backscatter in radar-based, soil moisture estimation. *Remote Sensing of Environment, 76*, 129-137

Bouman, B. (1991). Crop parameter estimation from ground-based X-band (3-cm wave) radar backscattering data. *Remote Sensing of Environment, 37*, 193-205

Brolly, M., & Woodhouse, I. (2010). A Matchstick Model of microwave backscatter from a forest: A change of regime. In, *Geoscience and Remote Sensing Symposium (IGARSS), 2010 IEEE International* (pp. 3295-3298). Honolulu, Hawaii: IEEE

Brown, S., Burnham, M., Delaney, M., Powell, M., Vaca, R., & Moreno, A. (2000a). Issues and challenges for forest-based carbon-offset projects: a case study of the Noel Kempff Climate Action Project in Bolivia. *Mitigation and Adaptation Strategies for Global Change, 5*, 99-121

Brown, S., Cookmartin, G., Morrison, K., McDonald, A., Quegan, S., Anderson, C., Cordey, R., & Dampney, P. (2000b). Wheat scattering mechanisms observed in near-field radar imagery compared with results from a radiative transfer model. In (pp. 2933-2935 vol. 2937): IEEE

Burton, R.F. (2010). Human allometry: Adult bodies are more nearly geometrically similar than regression analysis has suggested. *Medical hypotheses, 74*, 15-17

Bush, T., & Ulaby, F. (1976). Radar return from a continuous vegetation canopy. *IEEE Transactions on Antennas and Propagation, 24*, 269-276

Cannell, M.G.R. (1982). *World forest biomass and primary production data*: Academic Press New York

Cantiana, M. (1974). Experimental research into dendrometry and auxometry. Part II. Initial enquires concerning the biomass of the white fir. [in Italian] In, *Bulletin 5*. Florence, Italy: Instituto di Assestamento Forestale, University of Firenze

Castel, T., Guerra, F., Caraglio, Y., & Houllier, F. (2002). Retrieval biomass of a large Venezuelan pine plantation using JERS-1 SAR data. Analysis of forest structure impact on radar signature. *Remote Sensing of Environment, 79*, 30-41

Champion, I., Guyon, D., Riom, J., Toan, T.L., & Beaudoin, A. (1998). Effect of forest thinning on the radar backscattering coefficient at L-band. *International Journal of Remote Sensing, 19*, 2233-2238

Chauhan, N.S., Lang, R.H., & Ranson, K.J. (1991). Radar modeling of a boreal forest. *Geoscience and Remote Sensing, IEEE Transactions on, 29*, 627-638

Chave, J. (1999). Study of structural, successional and spatial patterns in tropical rain forests using TROLL, a spatially explicit forest model. *Ecological Modelling, 124*, 233-254

Chave, J., Condit, R., Aguilar, S., Hernandez, A., Lao, S., & Perez, R. (2004). Error propagation and scaling for tropical forest biomass estimates. *Philosophical Transactions of the Royal Society of London. Series B: Biological Sciences, 359*, 409

Chave, J., Muller-Landau, H.C., Baker, T.R., Easdale, T.A., Steege, H., & Webb, C.O. (2006). Regional and phylogenetic variation of wood density across 2456 neotropical tree species. *Ecological Applications, 16*, 2356-2367

Chave, J., Riera, B., & Dubois, M.A. (2001). Estimation of biomass in a neotropical forest of French Guiana: spatial and temporal variability. *Journal of Tropical Ecology, 17*, 79-96

Chen, W., Blain, D., Li, J., Keohler, K., Fraser, R., Zhang, Y., Leblanc, S., Olthof, I., Wang, J., & McGovern, M. (2009). Biomass measurements and relationships with Landsat-7/ETM+ and JERS-1/SAR data over Canada's western sub-arctic and low arctic. *International Journal of Remote Sensing, 30*, 2355-2376

Christensen, M., & Emborg, J. (1996). Biodiversity in natural versus managed forest in Denmark. *Forest Ecology and Management, 85*, 47-51

Cloude, S.R. (2006). Polarization coherence tomography. *Radio Science, 41*, RS4017

Cloude, S.R. (2007). Dual-baseline coherence tomography. *Geoscience and Remote Sensing Letters, IEEE, 4*, 127-131

Cloude, S.R., Brolly, M., & Woodhouse, I.H. (2009). A study of forest vertical structure estimation using coherence tomography coupled to a macro-ecological scattering model. In, *Geoscience and Remote Sensing Symposium,2009 IEEE International,IGARSS 2009* Cape Town: IEEE

Cloude, S.R., & Corr, D. (2003). Tree-height retrieval using single baseline polarimetric interferometry. In (pp. 14-16): Proceedings of ESA Workshop, POLInSAR

Cloude, S.R., & Papathanassiou, K.P. (1998). Polarimetric SAR interferometry. *Geoscience and Remote Sensing, IEEE Transactions on, 36*, 1551-1565

Cloude, S.R., & Papathanassiou, K.P. (2003). Three-stage inversion process for polarimetric SAR interferometry. *Radar, Sonar and Navigation, IEE Proceedings-, 150*, 125-134

Cloude, S.R., & Papathanassiou, K.P. (2008a). Forest Vertical Structure Estimation using Coherence Tomography. In, *Geoscience and Remote Sensing Symposium, 2008* (pp. V-275-V-278). Boston: IEEE

Cloude, S.R., & Papathanassiou, K.P. (2008b). Forest Vertical Structure Estimation using Coherence Tomography. In (pp. V-275-V-278): IEEE

Cloude, S.R., Papathanassiou, K.P., Woodhouse, I., Hope, J., Suarez Minguez, J.C., Osborne, P., & Wright, G. (2001). The Glen Affric project:: forest mapping using polarimetric radarinterferometry. *Geoscience and Remote Sensing Symposium, 2001. IGARSS'01. IEEE 2001 International, 4*

Cloude, S.R., Pottier, E., Ep, S.E.I., & Cnrs, N. (1996). A review of target decomposition theorems in radar polarimetry. *Geoscience and Remote Sensing, IEEE Transactions on, 34*, 498-518

Cookmartin, G., Saich, P., Quegan, S., Cordey, R., Burgess-Allen, P., & Sowter, A. (2000). Modeling microwave interactions with crops and comparison with ERS-2 SAR observations. *IEEE Transactions on Geoscience and Remote Sensing, 38*, 658-670

Cookmartin, G., Saich, P., Quegan, S., Cordey, R., Burgess-Allen, P., Sowter, A., & ONL, G.U. (1998). Using backscatter models to define the limits of crop information recovery from SAR data. In, *Proc. 2nd Int. Workshop: Retrieval of Bio- and Geophysical Parameters from SAR Data for Land Applications* (pp. 107-114.). Noordwijk, The Netherlands

Coomes, D.A., Duncan, R.P., Allen, R.B., & Truscott, J. (2003). Disturbances prevent stem size density distributions in natural forests from following scaling relationships. *Ecology Letters, 6*, 980-989

Cox, A., DeWeerd, A.J., & Linden, J. (2002). An experiment to measure Mie and Rayleigh total scattering cross sections. *American Journal of Physics, 70*, 620

Cramer, W., Bondeau, A., Schaphoff, S., Lucht, W., Smith, B., & Sitch, S. (2004). Tropical forests and the global carbon cycle: impacts of atmospheric carbon dioxide, climate change and rate of deforestation. *Philosophical Transactions of the Royal Society of London. Series B: Biological Sciences, 359*, 331

Crispin Jr, J.W., & Maffett, A.L. (1965). Radar cross-section estimation for simple shapes. *Proceedings of the IEEE, 53*, 833-848

Currie, A., & Brown, M.A. (1992). Wide-swath SAR. In (pp. 122-135): IET

Davidson, M. (2008). Candidate Earth Explorer Mission : Biomass (Report for Assessment). In P. Clissold (Ed.): European Space Agency

Davis, J.L., & Annan, A.P. (1989). Ground Penetrating Radar for High Resolution Mapping of Soil and Rock Stratigraphy. *Geophysical prospecting, 37*, 531-551

Debye, P. (1909). *Ann physik, 30*

Disney, M., Kalogirou, V., Lewis, P., Prieto-Blanco, A., Hancock, S., & Pfeifer, M. (2010). Simulating the impact of discrete-return lidar system and survey characteristics over young conifer and broadleaf forests. *Remote Sensing of Environment, 114*, 1546-1560

Dobson, M.C., & Ulaby, F.T. (1986). Active microwave soil moisture research. *Geoscience and Remote Sensing, IEEE Transactions on*, 23-36

Dobson, M.C., Ulaby, F.T., LeToan, T., Beaudoin, A., Kasischke, E.S., & Christensen, N. (1992). Dependence of radar backscatter on coniferous forest biomass. *Geoscience and Remote Sensing, IEEE Transactions on, 30*, 412-415

Dobson, M.C., Ulaby, F.T., Pierce, L.E., Sharik, T.L., Bergen, K.M., Kellndorfer, J., Kendra, J.R., Li, E., Lin, Y.C., & Nashashibi, A. (1995). Estimation of forest biophysical characteristics in Northern Michigan with SIR-C/X-SAR. *IEEE Transactions on Geoscience and Remote Sensing, 33*, 877-895

Dong, J., et al (2003). Remote sensing estimates of boreal and temperate forest woody biomass: carbon pools, sources, and sinks. *Remote Sensing of Environment, 84*, 393-410

Donnellan, A., Rosen, P., Graf, J., Loverro, A., Freeman, A., Treuhaft, R., Oberto, R., Simard, M., Rignot, E., & Kwok, R. (2008). Deformation, ecosystem structure, and dynamics of ice (DESDynI). In, *Aerospace Conference, 2008 IEEE* (pp. 1-13): IEEE

Dubayah, R.O., & Drake, J.B. (2000). Lidar remote sensing for forestry. *Journal of Forestry, 98*, 44-46

Dubois, P.C., Van Zyl, J., & Engman, T. (1995). Measuring soil moisture with imaging radars. *Geoscience and Remote Sensing, IEEE Transactions on, 33*, 915-926

Enquist, B., West, G., Charnov, E., & Brown, J. (1999). Allometric scaling of production and life-history variation in vascular plants. *Nature, 401*, 907-911
Enquist, B.J., Brown, J.H., & West, G.B. (1998a). Allometric scaling of plant energetics and population density. *NATURE, 395*, 163-165
Enquist, B.J., Brown, J.H., & West, G.B. (1998b). Allometric scaling of plant energetics andpopulationdensity. *Nature, 395*, 163
Enquist, B.J., & Niklas, K.J. (2001). Invariant scaling relations across tree-dominated communities. *NATURE, 410*, 655-660
Eom, H., & Fung, A. (1986). Scattering from a random layer embedded with dielectric needles. *Remote Sensing of Environment, 19*, 139-149
Eom, H.J. (1986). Regression models for vegetation radar-backscattering and radiometric emission. *Remote Sensing of Environment, 19*, 151-157
Eriksson, L.E.B., Santoro, M., Wiesmann, A., & Schmullius, C.C. (2003). Multitemporal JERS repeat-pass coherence for growing-stock volume estimation of Siberian forest. *Geoscience and Remote Sensing, IEEE Transactions on, 41*, 1561-1570
Faller, N.P., & Meier, E.H. (2002). First results with the airborne single-pass DO-SAR interferometer. *Geoscience and Remote Sensing, IEEE Transactions on, 33*, 1230-1237
Fang, J., Wang, G.G., Liu, G., & Xu, S. (1998). Forest biomass of China: an estimate based on the biomass-volume relationship. *Ecological Applications, 8*, 1084-1091
Ferrazzoli, P., & Guerriero, L. (1995). Radar sensitivity to tree geometry and woody volume: A model analysis. *Geoscience and Remote Sensing, IEEE Transactions on, 33*, 360-371
Floury, N., Le Toan, T., & Souyris, J. (1996). Relating forest parameters to interferometric data. In (pp. 975-977 vol. 972): IEEE
Floury, N., Le Toan, T., Souyris, J.C., & Bruniquel, J. (1997). A study of SAR interferometry over forests: theory and experiment. *Geoscience and Remote Sensing, 1997. IGARSS'97.'Remote Sensing-A Scientific Vision for Sustainable Development'., 1997 IEEE International, 4*
Fransson, J., Smith, G., Askne, J., & Olsson, H. (2001). Stem volume estimation in boreal forests using ERS-1/2 coherence and SPOT XS optical data. *International Journal of Remote Sensing, 22*, 2777-2791
Fransson, J.E.S., Gustavsson, A., Ulander, L.M.H., & Walter, F. (2000a). Towards an operational use of VHF SAR data for forest mapping and forest management. In (pp. 399-401 vol. 391): IEEE
Fransson, J.E.S., & Israelsson, H. (1999). Estimation of stem volume in boreal forests using ERS-1 C-and JERS-1 L-band SAR data. *International Journal of Remote Sensing, 20*, 123-137
Fransson, J.E.S., Magnusson, M., Olsson, H., Eriksson, L.E.B., Folkesson, K., Sandberg, G., Santoro, M., & Ulander, L.M.H. (2008). Detection of clear-cuts using ALOS PALSAR satellite images. In (pp. 1-4): VDE
Fransson, J.E.S., Smith, G., Walter, F., Gustavsson, A., & Ulander, L.M.H. (2004). Estimation of forest stem volume in sloping terrain using CARABAS-II VHF SAR data. *Canadian journal of remote sensing, 30*, 651-660

Fransson, J.E.S., Walter, F., & Ulander, L.M.H. (2000b). Estimation of forest parameters using CARABAS-II VHF SAR data. *IEEE Transactions on Geoscience and Remote Sensing, 38*, 720-727
Freeman, A., Durden, S., & Zimmerman, R. (1992). Mapping sub-tropical vegetation using multi-frequency, multi-polarization SAR data. In (pp. 1686-1689): IEEE
Freeman, A., & Durden, S.L. (1998). A three-component scattering model for polarimetric SAR data. *Geoscience and Remote Sensing, IEEE Transactions on, 36*, 963-973
Fung, A. (1966). On depolarization of electromagnetic waves backscattered from a rough surface. *Planetary and Space Science, 14*, 563-568
Fung, A.K. (1994). *Microwave scattering and emission models and their applications*. Norwood: Artech House, INC.
Garestier, F., Dubois-Fernandez, P.C., & Champion, I. (2008). Forest height inversion using high-resolution P-band Pol-InSAR data. *Geoscience and Remote Sensing, IEEE Transactions on, 46*, 3544-3559
Gehring, C., Park, S., & Denich, M. (2004). Liana allometric biomass equations for Amazonian primary and secondary forest. *Forest Ecology and Management, 195*, 69-83
Getzin, S., Wiegand, T., Wiegand, K., & He, F. (2008). Heterogeneity influences spatial patterns and demographics in forest stands. *Journal of Ecology, 96*, 807-820
Gibbs, H.K., Brown, S., Niles, J.O., & Foley, J.A. (2007). Monitoring and estimating tropical forest carbon stocks: making REDD a reality. *Environmental Research Letters, 2*, 045023
Gifford, E.M., & Foster, A.S. (1989). *Morphology and evolution of vascular plants*: WH Freeman and Co
Gill, S.J., Biging, G.S., & Murphy, E.C. (2000). Modeling conifer tree crown radius and estimating canopy cover. *Forest Ecology and Management, 126*, 405-416
Ginn, S.E., Seiler, J.R., Cazell, B.H., & Kreh, R.E. (1991). Physiological and growth responses of eight-year-old loblolly pine stands to thinning. *Forest Science, 37*, 1030-1040
Graham, A., & Harris, R. (2003). Extracting biophysical parameters from remotely sensed radar data: a review of the water cloud model. *Progress in physical geography, 27*, 217
Granström, A. (1982). Seed banks in five boreal forest stands originating between 1810 and 1963. *Canadian Journal of Botany, 60*, 1815-1821
Guarnieri, A.M., & Rocca, F. (1999). Combination of low-and high-resolution SAR images for differential interferometry. *Geoscience and Remote Sensing, IEEE Transactions on, 37*, 2035-2049
Guo, Z., Sun, G., Ranson, K.J., Ni, W., & Qin, W. (2008). The potential of combined Lidar and SAR data in retrieving forest parameters using model analysis. In (pp. V-542-V-545): Geoscience and Remote Sensing Symposium, 2008. IGARSS 2008. IEEE International
Hagberg, J.O., Ulander, L.M.H., & Askne, J. (1995). Repeat-pass SAR interferometry over forested terrain. *Geoscience and Remote Sensing, IEEE Transactions on, 33*, 331-340

Hajnsek, I., Kugler, F., Lee, S.K., & Papathanassiou, K.P. (2009). Tropical-Forest-Parameter Estimation by Means of Pol-InSAR: The INDREX-II Campaign. *Geoscience and Remote Sensing, IEEE Transactions on, 47*, 481-493
Hallberg, B., Smith-Jonforsen, G., & Ulander, L. (2005). Measurements on individual trees using multiple VHF SAR images. *Geoscience and Remote Sensing, IEEE Transactions on, 43*, 2261-2269
Hallikainen, M.T., Ulaby, F.T., Dobson, M.C., El-Rayes, M.A., & Wu, L.K. (1985). Microwave dielectric behavior of wet soil-part 1: empirical models and experimental observations. *Geoscience and Remote Sensing, IEEE Transactions on*, 25-34
Hammond, S.T., & Niklas, K.J. (2009). Emergent properties of plants competing in silico for space and light: Seeing the tree from the forest. *American Journal of Botany, 96*, 1430
Hellrigl, B. (1974). Experimental research into dendrometry and auxometry. Part I. Tabulation of the productivity of tree biomass. [in Italian]. In, *Bulletin 5*. Florence, Italy.: Instituto di Assestamento Forestale, University of Firenze
Hestilow, T.J. (2000). Simple formulas for the calculation of the average physical optics RCS of a cylinder and a flat plate over a symmetric window around broadside. *IEEE Antennas & Propagation Magazine, 42*, 48-52
Hill, D. (1988). Electromagnetic scattering by buried objects of low contrast. *Geoscience and Remote Sensing, IEEE Transactions on, 26*, 195-203
Hoekman, D.H., & Quiriones, M. (2000). Land cover type and biomass classification using AirSAR data for evaluation of monitoring scenarios in the Colombian Amazon. *Geoscience and Remote Sensing, IEEE Transactions on, 38*, 685-696
Holt, F. (1959). Geometrical optics approximation of near-field back scattering. *Antennas and Propagation, IRE Transactions on, 7*, 434-435
Hussin, Y., Reich, R., & Hoffer, R. (1991). Estimating splash pine biomass using radar backscatter. *Geoscience and Remote Sensing, IEEE Transactions on, 29*, 427-431
Hyyppä, J., Hyyppä, H., Inkinen, M., Engdahl, M., Linko, S., & Zhu, Y.H. (2000). Accuracy comparison of various remote sensing data sources in the retrieval of forest stand attributes. *Forest Ecology and Management, 128*, 109-120
Imhoff, M.L. (1995a). Radar backscatter and biomass saturation: ramifications for global biomass inventory. *Geoscience and Remote Sensing, IEEE Transactions on, 33*, 511-518
Imhoff, M.L. (1995b). A theoretical analysis of the effect of forest structure on synthetic aperture radar backscatter and the remote sensing of biomass. *Geoscience and Remote Sensing, IEEE Transactions on, 33*, 341-352
Imhoff, M.L., Johnson, P., Carson, S., Lawrence, W., Condit, R., Stutzer, D., & Wright, J. (2001). VHF radar mapping of forest biomass in Panama. *Geoscience and Remote Sensing Symposium, 2001. IGARSS'01. IEEE 2001 International, 1*
Isaacs, R.G., Jin, Y.Q., Worsham, R.D., Deblonde, G., & Falcone Jr, V.J. (2002). The RADTRAN microwave surface emission models. *Geoscience and Remote Sensing, IEEE Transactions on, 27*, 433-440
Isola, M., & Cloude, S.R. (2001). Forest height mapping using space-borne polarimetric SARinterferometry. *Geoscience and Remote Sensing Symposium, 2001. IGARSS'01. IEEE 2001 International, 3*

Karam, M.A., A. Amar et al. (1995). A microwave polarimetric scattering model for forest canopies based on vector radiative transfer theory. *Remote Sensing of Environment, 53*, 16-30
Karam, M.A., Amar, F., Fung, A.K., Le Vine, D.M., Mougin, E., Lopes, A., & Beaudoin, A. (1995). A Microwave Polarimetric Scattering Model for Forest Canopies Based on Vector Radiative Transfer Theory. *Remote Sensing of Environment, 53*, 16-30
Karam, M.A., & Fung, A.K. (1988). Electromagnetic scattering from a layer of finite length, randomly oriented, dielectric, circular cylinders over a rough interface with application to vegetation. *International Journal of Remote Sensing, 9*, 1109-1134
Karam, M.A., Fung, A.K., Lang, R.H., & Chauhan, N.S. (1992). A microwave scattering model for layered vegetation. *Geoscience and Remote Sensing, IEEE Transactions on, 30*, 767-784
Karam, M.A., LeVine, D.M., Amar, F., Fung, A.K., Mougin, E., & Lopes, A. (1993). Understanding the relation between the forest biomass and the radarbackscattered signals. In (pp. 573-575)
Kasischke, E.S., Christensen Jr, N.L., & Bourgeau-Chavez, L.L. (1995). Correlating radar backscatter with components of biomass in loblolly pine forests. *Geoscience and Remote Sensing, IEEE Transactions on, 33*, 643-659
Keller, M., Palace, M., & Hurtt, G. (2001). Biomass estimation in the Tapajos National Forest, Brazil:: Examination of sampling and allometric uncertainties. *Forest Ecology and Management, 154*, 371-382
Kenkel, N. (1988). Pattern of self-thinning in jack pine: testing the random mortality hypothesis. *Ecology*, 1017-1024
Ketterings, Q.M., Coe, R., van Noordwijk, M., Ambagau, Y., & Palm, C.A. (2001). Reducing uncertainty in the use of allometric biomass equations for predicting above-ground tree biomass in mixed secondary forests. *Forest Ecology and Management, 146*, 199-209
Kinnunen, J., Maltamo, M., & Paivinen, R. (2007). Standing volume estimates of forests in Russia: how accurate is the published data? *Forestry, 80*, 53
Kleinman, R.E. (1965). The Rayleigh region. *Proceedings of the IEEE, 53*, 848-856
Knight, P.A. (1997). Software design specification and test results. In, *BSATC document*
Knott, E.F., Shaeffer, J.F., & Tuley, M.T. (2004). *Radar cross section*: SciTech Publishing
Kobayashi, Y., Sarabandi, K., Pierce, L., & Dobson, M.C. (2002). An evaluation of the JPL TOPSAR for extracting tree heights. *Geoscience and Remote Sensing, IEEE Transactions on, 38*, 2446-2454
Kononov, A.A., & Ka, M.H. (2008). Model-Associated Forest Parameter Retrieval Using VHF SAR Data at the Individual Tree Level. *Geoscience and Remote Sensing, IEEE Transactions on, 46*, 69-84
Kozlowski, J., & Konarzewski, M. (2004). Is West, Brown and Enquist's model of allometric scaling mathematically correct and biologically relevant? *Functional Ecology, 18*, 283-289
Krieger, G., Hajnsek, I., Papathanassiou, K., Eineder, M., Younis, M., De Zan, F., Prats, P., Huber, S., Werner, M., & Fiedler, H. (2009). The tandem-L mission proposal:

Monitoring earth's dynamics with high resolution SAR interferometry. In (pp. 1-6): IEEE
Kugler, F., Koudogbo, F.N., Gutjahr, K., & Papathanassiou, K.P. (2006). Frequency effects in Pol-InSAR forest height estimation. *EUSAR 2006*
Kurz, W.A., & Apps, M.J. (1999). A 70-year retrospective analysis of carbon fluxes in the Canadian forest sector. *Ecological Applications, 9*, 526-547
Laboratory., F.P. (1999). Wood handbook: wood as an engineering material. In, *Gen. Tech. Rep. FPL-GTR-113*. Madison, WI. : U.S. Department of Agriculture, Forest Service
Lanari, R., Fornaro, G., Riccio, D., Migliaccio, M., Papathanassiou, K.P., Moreira, J.R., Schwabisch, M., Dutra, L., Puglisi, G., & Franceschetti, G. (1996). Generation of digital elevation models by using SIR-C/X-SAR multifrequency two-pass interferometry: The Etna case study. *Geoscience and Remote Sensing, IEEE Transactions on, 34*, 1097-1114
Lang, R.H., Chauhan, N.S., Ranson, K.J., & Kilic, O. (1994). Modeling P-band SAR returns from a red pine stand. *Remote Sensing of Environment, 47*, 132-141
Lang, R.H., H.A., Saleh (1985). Microwave inversion of leaf area and inclination angle distributions from backscattered data. *IEEE Transactions on Geoscience and Remote Sensing, GE-23*, 685-694
Lang, R.H., J.S., Sidhu (1983). Electromagnetic backscattering from a layer of vegetation: a discrete approach. *IEEE Transactions on Geoscience and Remote Sensing, 21*, 62-71
Lang, R.H., & Saleh, H.A. (1985). Microwave inversion of leaf area and inclination angle distributions from backscattered data. *Geoscience and Remote Sensing, IEEE Transactions on*, 685-694
Lavalle, M., Williams, M., Hensley, S., Pottier, E., & Solimini, D. (2009). Dependence of P-band interferometric height on forest parameters from simulation and observation. In, *Geoscience and Remote Sensing Symposium,2009 IEEE International,IGARSS 2009* (pp. IV-5-IV-8): IEEE
Le Toan, T., Beaudoin, A., Riom, J., & Guyon, D. (1992). Relating forest biomass to SAR data. *Geoscience and Remote Sensing, IEEE Transactions on, 30*, 403-411
Le Toan, T., et al (2001). On the relationship between forest structure and biomass. In, *3rd symposium on the retrieval of biogeophysical parameters from SAR data for land application.* Sheffield
Le Toan, T., Quegan, S., Davidson, M., Balzter, H., Paillou, P., Papathanassiou, K., Plummer, S., Saatchi, S., Shugart, H., & Ulander, L. (2010). The BIOMASS Mission: Mapping global forest biomass to better understand the terrestrial carbon cycle. *Remote Sens Environ, accepted*
Lee, S.K., Kugler, F., Papathanassiou, K., & Hajnsek, I. (2009). Polarimetric sar interferometry for forest application at p-band: potentials and challenges. In (pp. IV-13-IV-16): IEEE
Lee, S.K., Kugler, F., Papathanassiou, K.P., & Hajnsek, I. (2008). Quantifying temporal decorrelation over boreal forest at L-and P-band. In (pp. 1-4): VDE

Lefsky, M.A., Cohen, W.B., Harding, D.J., Parker, G.G., Acker, S.A., & Gower, S.T. (2002). Lidar remote sensing of above ground biomass in three biomes. *Global Ecology and Biogeography, 11*, 393-399
Lefsky, M.A., Harding, D.J., Keller, M., Cohen, W.B., Carabajal, C.C., Espirito-Santo, F.D.B., Hunter, M.O., & de Oliveira Jr, R. (2005a). Estimates of forest canopy height and aboveground biomass using ICESat. *Geophysical Research Letters, 32*, L22S02
Lefsky, M.A., Hudak, A.T., Cohen, W.B., & Acker, S. (2005b). Patterns of covariance between forest stand and canopy structure in the Pacific Northwest. *Remote Sensing of Environment, 95*, 517-531
Liang, Z., & Jin, Y.Q. (2003). Iterative approach of high-order scattering solution for vector radiative transfer of inhomogeneous random media. *Journal of Quantitative Spectroscopy and Radiative Transfer, 77*, 1-12
Lillesand, T.M., & Kiefer, R.W. (1987). Remote sensing and image interpretation
Lin, C.C., Hélière, F., Bensi, P., Thompson, A., Aguirre, M., Buck, C., Ludwig, M., Süss, M., Gallou, N., & Aloisio, M. (2008). ESA's SAR technology and future mission concept developments beyond sentinel-1. *EUSAR 2008*
Lin, Y.C., & Sarabandi, K. (1995). Electromagnetic scattering model for a tree trunk above a tilted ground plane. *Geoscience and Remote Sensing, IEEE Transactions on, 33*, 1063-1070
Lin, Y.C., & Sarabandi, K. (1999a). A Monte Carlo coherent scattering model for forest canopies usingfractal-generated trees. *Geoscience and Remote Sensing, IEEE Transactions on, 37*, 440-451
Lin, Y.C., & Sarabandi, K. (1999b). Retrieval of forest parameters using a fractal-based coherentscattering model and a genetic algorithm. *Geoscience and Remote Sensing, IEEE Transactions on, 37*, 1415-1424
Lopes, A., Mougin, E., Beaudoin, A., & Karam, M.A. (1991). Relating The Microwave Signatures Of Trees To Their Structure Results Of An Experimental/Theoretical Approach. *Geoscience and Remote Sensing Symposium, 1991. IGARSS'91.'Remote Sensing: Global Monitoring for Earth Management'., International, 1*
Luckman, A., Baker, J., Honzak, M., & Lucas, R. (1998). Tropical forest biomass density estimation using JERS-1 SAR: Seasonal variation, confidence limits, and application to image mosaics. *Remote Sensing of Environment, 63*, 126-139
Luo, X., Askne, J., Smith, G., Santoro, M., & Fransson, J.E.S. An analysis of InSAR coherence of boreal forests based on electromagnetic scattering modeling. In (pp. 16–20): Citeseer
Luo, X., Askne, J., Smith, G., Santoro, M., & Fransson, J.E.S. (2000). An analysis of InSAR coherence of boreal forests based on electromagnetic scattering modeling. In, *Proceedings ERS-Envisat Symposium*. Göteborg, Sweden
Madsen, S.N., Zebker, H.A., & Martin, J. (2002). Topographic mapping using radar interferometry: Processing techniques. *Geoscience and Remote Sensing, IEEE Transactions on, 31*, 246-256
Magnani, F., Mencuccini, M., Borghetti, M., Berbigier, P., Berninger, F., Delzon, S., Grelle, A., Hari, P., Jarvis, P.G., & Kolari, P. (2007). The human footprint in the carbon cycle of temperate and boreal forests. *NATURE, 447*, 849-851
Mandelbrot, B. (1977). *Fractals, Form, Chance and Dimension*. San Francisco

Freeman
Marbà, N., Duarte, C.M., & Agustí, S. (2007). Allometric scaling of plant life history. *Proceedings of the National Academy of Sciences, 104*, 15777
Marin, S. (1982). Computing scattering amplitudes for arbitrary cylinders under incident plane waves. *Antennas and Propagation, IEEE Transactions on, 30*, 1045-1049
Martin, J.G., Kloeppel, B.D., Schaefer, T.L., Kimbler, D.L., & McNulty, S.G. (1998). Aboveground biomass and nitrogen allocation of ten deciduous southern Appalachian tree species. *Canadian Journal of Forest Research, 28*, 1648-1659
Martinez, J.M., Floury, N., Le Toan, T., Beaudoin, A., Hallikainen, M.T., & Mäkynen, M. (2000). Measurements and Modeling of Vertical Backscatter Distribution in Forest Canopy. *IEEE Transactions on Geoscience and Remote Sensing, 38*
McDonald, K.C., Dobson, M.C., & Ulaby, F.T. (1990). Using Mimics To Model L-band Multiangle and Multitemporal Backscatter From A Walnut Orchard. *Geoscience and Remote Sensing, IEEE Transactions on, 28*, 477-491
McDonald, K.C., Dobson, M.C., & Ulaby, F.T. (1991). Modeling multi-frequency diurnal backscatter from a walnut orchard. *IEEE Transactions on Geoscience and Remote Sensing, 29*, 852-863
Melon, P., Martinez, J.M., Le Toan, T., Ulander, L.M.H., & Beaudoin, A. (2001). On the retrieving of forest stem volume from VHF SAR data: observation and modeling. *Geoscience and Remote Sensing, IEEE Transactions on, 39*, 2364-2372
Mette, T., Hajnsek, I., Papathanassiou, K., & Center, D. (2003). Height-biomass allometry in temperate forests performance accuracy of height-biomass allometry. *Geoscience and Remote Sensing Symposium, 2003. IGARSS'03. Proceedings. 2003 IEEE International, 3*
Mette, T., Papathanassiou, K., & Hajnsek, I. (2004a). Biomass estimation from polarimetric SAR interferometry over heterogeneous forest terrain. *Geoscience and Remote Sensing Symposium, 2004. IGARSS'04. Proceedings. 2004 IEEE International, 1*
Mette, T., Papathanassiou, K., Hajnsek, I., Pretzsch, H., & Biber, P. (2004b). Applying a common allometric equation to convert forest height from Pol-InSAR data to forest biomass. *Geoscience and Remote Sensing Symposium, 2004. IGARSS'04. Proceedings. 2004 IEEE International, 1*
Mette, T., Papathanassiou, K.P., Hajnsek, I., & Zimmermann, R. (2002). Forest biomass estimation using polarimetric SAR interferometry. *Geoscience and Remote Sensing Symposium, 2002. IGARSS'02. 2002 IEEE International, 2*
Mie, G. (1908). Contributions to the optics of diffusing media. *Ann physik, 25*
Mitchard, E., Saatchi, S., Lewis, S., Feldpausch, T., Woodhouse, I., Sonké, B., Rowland, C., & Meir, P. (2011). Measuring biomass changes due to woody encroachment and deforestation/degradation in a forest-savanna boundary region of central Africa using multi-temporal L-band radar backscatter. *Remote Sensing of Environment*
Mitchard, E.T.A., Saatchi, S.S., Woodhouse, I.H., Nangendo, G., Ribeiro, N.S., Williams, M., Ryan, C.M., Lewis, S.L., Feldpausch, T.R., & Meir, P. (2009). Using satellite radar backscatter to predict above-ground woody biomass: A consistent

relationship across four different African landscapes. *Geophysical Research Letters, 36*, L23401
Moeur, M. (1997). Spatial models of competition and gap dynamics in old-growth Tsuga heterophylla/Thuja plicata forests. *Forest Ecology and Management, 94*, 175-186
Moghaddam, M., & Saatchi, S. (1995). Analysis of scattering mechanisms in SAR imagery over boreal forest: Results from BOREAS'93. *Geoscience and Remote Sensing, IEEE Transactions on, 33*, 1290-1296
Moosmuller, H., & Arnott, P. (2009). Particle optics in the Rayleigh regime. *Journal of the Air & Waste Management Association, 59*, 2
Mougin, E., Lopes, A., Karam, M.A., & Fung, A.K. (1993). Effect of tree structure on X-band microwave signature ofconifers. *Geoscience and Remote Sensing, IEEE Transactions on, 31*, 655-667
Mougin, E., Proisy, C., Marty, G., Fromard, F., Puig, H., Betoulle, J., & Rudant, J. (1999). Multifrequency and multipolarization radar backscattering from mangrove forests. *Geoscience and Remote Sensing, IEEE Transactions on, 37*, 94-102
Murrell, D.J. (2009). On the emergent spatial structure of size structured populations: when does self thinning lead to a reduction in clustering? *Journal of Ecology, 97*, 256-266
Needham, T.D., Smith, J.L (1987). Stem count accuracy and species determination in Loblolly Pine plantations using 35mm aerial photography. *Phot. Eng. Rem. Sens., 53*, 1675-1678
Neeff, T., Dutra, L.V., dos Santos, J.R., Freitas, C.C., & Araujo, L.S. (2005). Tropical forest measurement by interferometric height modeling and P-band radar backscatter. *Forest Science, 51*, 585-594
Nelson, B.W., Mesquita, R., Pereira, J.L.G., Garcia Aquino de Souza, S., Teixeira Batista, G., & Bovino Couto, L. (1999). Allometric regressions for improved estimate of secondary forest biomass in the central Amazon. *Forest Ecology and Management, 117*, 149-167
Nelson, R., Krabill, W., & MacLean, G. (1984). Determining forest canopy characteristics using airborne laser data. *Remote Sensing of Environment, 15*, 201-212
Nghiem, S., Le Toan, T., Kong, J., Han, H., & Borgeaud, M. (1993). Layer model with random spheroidal scatterers for remote sensing of vegetation canopy. *Journal of electromagnetic waves and applications, 7*, 49-75
Niklas, K.J. (1994). *Plant Allometry: The Scaling of Form and Process*: University Of Chicago Press
Niklas, K.J. (2000). Modeling fossil plant form-function relationships: a critique. *Paleobiology, 26*, 289-304
Niklas, K.J., & Enquist, B.J. (2001). Invariant scaling relationships for interspecific plant biomass production rates and body size. *Proceedings of the National Academy of Sciences*, 41590298
Niklas, K.J., Midgley, J.J., & Enquist, B.J. (2003). A general model for mass-growth-density relations across tree-dominated communities. *Evolutionary Ecology Research, 5*, 459-468

Niklas, K.J., & Spatz, H.C. (2004). Growth and hydraulic (not mechanical) constraints govern the scaling of tree height and mass. *Proceedings of the National Academy of Sciences of the United States of America, 101*, 15661
Oh, Y., Sarabandi, K., & Ulaby, F.T. (1992). An empirical model and an inversion technique for radar scattering from bare soil surfaces. *Geoscience and Remote Sensing, IEEE Transactions on, 30*, 370-381
Papathanassiou, K., Reigber, A., & Coltelli, M. (1997). On the interferometric coherence: A multifrequency and multitemporal analysis. In (p. 319)
Papathanassiou, K.P., & Cloude, S.R. (2001). Single-baseline polarimetric SAR interferometry. *IEEE Transactions on Geoscience and Remote Sensing, 39*, 2352-2363
Papathanassiou, K.P., & Cloude, S.R. (2002). Single-baseline polarimetric SAR interferometry. *Geoscience and Remote Sensing, IEEE Transactions on, 39*, 2352-2363
Patenaude, G. (2003). Remote sensing and LULUCF carbon inventories in the UK. In, *DEFRA, 2003. UK Emissions by Sources and Removals by Sinks due to Land Use, Land Use Change and Forestry Activities*. (pp. pp. 9:1-9:59). London: Department for the Environment, Food and Rural Affairs (DEFRA)
Patenaude, G., Milne, R., & Dawson, T.P. (2005). Synthesis of remote sensing approaches for forest carbon estimation: reporting to the Kyoto Protocol. *Environmental Science & Policy, 8*, 161-178
Peake, W. (1959). Theory of radar return from terrain. In, *IRE National Convention Record* (pp. pp. 27-41)
Peters, R.H., & Wassenberg, K. (1983). The effect of body size on animal abundance. *Oecologia, 60*, 89-96
Philip, M.S. (1994). *Measuring trees and forests*: Wallingford (RU)
Pinel, N., Bourlier, C., & Saillard, J. (2010). Degree of Roughness of Rough Layers: Extensions of the Rayleigh Roughness Criterion and Some Applications. *Progress In Electromagnetics Research, 19*, 41-63
Popescu, S.C., Wynne, R.H., & Nelson, R.F. (2003). Measuring individual tree crown diameter with lidar and assessing its influence on estimating forest volume and biomass. *Canadian journal of remote sensing, 29*, 564-577
Quegan, S., Le Toan, T., Yu, J.J., Ribbes, F., & Floury, N. (2000). Multitemporal ERS SAR analysis applied to forest mapping. *Geoscience and Remote Sensing, IEEE Transactions on, 38*, 741-753
Quiñones, M.J., & Hoekman, D.H. (2004). Exploration of factors limiting biomass estimation by polarimetric radar in tropical forests. *Geoscience and Remote Sensing, IEEE Transactions on, 42*, 86-104
Raney, R.K. (1971). Synthetic aperture imaging radar and moving targets. *Aerospace and Electronic Systems, IEEE Transactions on*, 499-505
Ranson, K.J., & Sun, G. (1994a). Mapping biomass of a northern forest using multifrequency SAR data. *Geoscience and Remote Sensing, IEEE Transactions on, 32*, 388-396
Ranson, K.J., & Sun, G. (1994b). Northern forest classification using temporal multifrequency and multipolarimetric SAR images. *Remote Sensing of Environment, 47*, 142-153

Ranson, K.J., Sun, G., Weishampel, J.F., & Knox, R.G. (1997). Forest biomass from combined ecosystem and radar backscatter modeling. *Remote Sensing of Environment, 59*, 118-133
Rauste, Y., Hame, T., Pulliainen, J., Heiska, K., & Hallikainen, M. (1994). Radar-based forest biomass estimation. *International Journal of Remote Sensing, 15*, 2797-2808
Richards, J.A. (1990). Radar backscatter modelling of forests: a review of current trends. *International Journal of Remote Sensing, 11*, 1299-1312
Richards, J.A., Sun, G.Q., & Simonett, D.S. (1987). L-Band Radar Backscatter Modeling of Forest Stands. *Geoscience and Remote Sensing, IEEE Transactions on*, 487-498
Richmond, J. (1965). Scattering by a dielectric cylinder of arbitrary cross section shape. *Antennas and Propagation, IEEE Transactions on, 13*, 334-341
Rignot, E., Way, J., Williams, C., & Viereck, L. (1994). Radar estimates of aboveground biomass in boreal forests of interior Alaska. *Geoscience and Remote Sensing, IEEE Transactions on, 32*, 1117-1124
Rybicki, G.B., & Lightman, A.P. (1979). Radiative processes in astrophysics. *San Francisco*
Saatchi, S.S., & McDonald, K.C. (1997). Coherent effects in microwave backscattering models for forest canopies. *Geoscience and Remote Sensing, IEEE Transactions on, 35*, 1032-1044
Saatchi, S.S., & McDonald, K.C. (2002). Coherent effects in microwave backscattering models for forest canopies. *Geoscience and Remote Sensing, IEEE Transactions on, 35*, 1032-1044
Saatchi, S.S., & Moghaddam, M. (2000). Estimation of crown and stem water content and biomass of boreal forest using polarimetric SAR imagery. *Geoscience and Remote Sensing, IEEE Transactions on, 38*, 697-709
Saich, P. (1993). Theoretical Models for Forest Radar Backscatter. In: GEC-Marconi Research Centre
Saich, P. (1995). Software test specification. In, *BSATC document*
Saich, P. (2002). Review of Microwave Scattering from Vegetation
Saich, P., Cordey, R., Quegan, S., Williams, M., Baker, J., Luckman, A., Wielogorska, A., & Wooding, M. (1995). SAR retrieval algorithms for land applications. *Final report (3 vols), ESA contract, 10644*, 93
Saich, P., Rees, W., & Borgeaud, M. (2001). Detecting pollution damage to forests in the Kola Peninsula using the ERS SAR. *Remote Sensing of Environment, 75*, 22-28
Salas, W.A., Ranson, J.K., Rock, B.N., & Smith, K.T. (1994). Temporal and spatial variations in dielectric constant and water status of dominant forest species from New England. *Remote Sensing of Environment, 47*, 109-119
Sandberg, G., Ulander, L.M.H., Fransson, J.E.S., Holmgren, J., & Le Toan, T. (2009). Comparison of L-and P-band biomass retrievals based on backscatter from the BioSAR campaign. In (pp. IV-169-IV-172): IEEE
Sankaran, M., Ratnam, J., & Hanan, N. (2008). Woody cover in African savannas: the role of resources, fire and herbivory. *Global Ecology and Biogeography, 17*, 236-245

Santos, J., Lacruz, M.S.P., Araujo, L., & Keil, M. (2002). Savanna and tropical rainforest biomass estimation and spatialization using JERS-1 data. *International Journal of Remote Sensing, 23*, 1217-1229
Santos, J.R., Freitas, C.C., Araujo, L.S., Dutra, L.V., Mura, J.C., Gama, F.F., Soler, L.S., & Sant'Anna, S.J.S. (2003). Airborne P-band SAR applied to the aboveground biomass studies in the Brazilian tropical rainforest. *Remote Sensing of Environment, 87*, 482-493
Sarabandi, K., & Lin, Y.C. (2000). Simulation of interferometric SAR response for characterizing the scattering phase center statistics of forest canopies. *Geoscience and Remote Sensing, IEEE Transactions on, 38*, 115-125
Sarabandi, K., & Senior, T.B.A. (1990). Low-frequency scattering from cylindrical structures at oblique incidence. *Geoscience and Remote Sensing, IEEE Transactions on, 28*, 879-885
Scipal, K., Arcioni, M., Chave, J., Dall, J., Fois, F., LeToan, T., Lin, C., Papathanassiou, K., Quegan, S., & Rocca, F. (2010). The BIOMASS mission—An ESA Earth Explorer candidate to measure the BIOMASS of the earth's forests. In, *Geoscience and Remote Sensing Symposium (IGARSS), 2010 IEEE International* (pp. 52-55): IEEE
Sedjo, R.A., & Marland, G. (2003). Inter-trading permanent emissions credits and rented temporary carbon emissions offsets: some issues and alternatives. *Climate Policy, 3*, 435-444
Seker, S., & Schneider, A. (1988). Electromagnetic scattering from a dielectric cylinder of finite length. *Antennas and Propagation, IEEE Transactions on, 36*, 303-307
Sellers, P.J., et al (1992). Canopy reflectance, photosynthesis, and transpiration. A reanalysis using improved leaf models and a new canopy integration scheme. *Remote Sensing of Environment, 42*, 187-216
Shao, Y., Hu, Q., Guo, H., Lu, Y., Dong, Q., & Han, C. (2003). Effect of dielectric properties of moist salinized soils on backscattering coefficients extracted from RADARSAT image. *Geoscience and Remote Sensing, IEEE Transactions on, 41*, 1879-1888
Shinozaki, K., Yoda, K., Hozumi, K., & Kira, T. (1964). A quantitative analysis of plant form—the pipe model theory. I. Basic analyses. *Japanese Journal of Ecology, 14*, 97-105
Shula, R.G. (1989). The upper limits of radiata pine stem-volume production in NZ. *New Zealand Forestry*
Shvidenko, A., Venevsky, S., & Nilsson, S. (1996). Increment and mortality for major forest species of northern Eurasia with variable growing stock. *International Institute for Applied Systems Analysis, Laxenburg, Austria, WP-96–98, 68*
Skolnik, M.I. (1970). *Radar handbook, second edition*: McGraw-Hill New York
Smil, V. (2000). Laying down the law. *NATURE, 403*, 597-597
Smith-Jonforsen, G., Folkesson, K., Hallberg, B., & Ulander, L.M.H. (2007). Effects of Forest Biomass and Stand Consolidation on P-Band Backscatter. *Geoscience and remote sensing letters IEEE, 4*, 669

Smith-Jonforsen, G., Ulander, L.M.H., & Luo, X. (2005). Low VHF-band backscatter from coniferous forests on sloping terrain. *Geoscience and Remote Sensing, IEEE Transactions on, 43*, 2246-2260
Smith, D.G., & Jol, H.M. (1995). Ground penetrating radar: antenna frequencies and maximum probable depths of penetration in Quaternary sediments. *Journal of Applied Geophysics, 33*, 93-100
Smith, G. (2000). Radar Remote Sensing of Forests Using CARABAS and ERS. In, *Department of Radio and Space Science, School of Electrical and Computer Engineering*. Gothenburg: Chalmers University of Technology
Smith, G., & Ulander, L.M.H. (1998). Forest biomass retrieval using VHF SAR. *EUROPEAN SPACE AGENCY-PUBLICATIONS-ESA SP, 441*, 301-308
Smith, G., & Ulander, L.M.H. (2000). A model relating VHF-band backscatter to stem volume of coniferous boreal forest. *IEEE Transactions on Geoscience and Remote Sensing, 38*, 728-740
Smith, G., Ulander, L.M.H., Fransson, J.E.S., Walter, F., & Gustavsson, A. (2002). Forest stem volume retrieval with VHF-band SAR. In
Stebler, O., Meier, E., & Nüesch, D. (2002). Multi-baseline polarimetric SAR interferometry--first experimental spaceborne and airborne results. *ISPRS Journal of Photogrammetry and Remote Sensing, 56*, 149-166
Sterner, R.W., Ribic, C.A., & Schatz, G.E. (1986). Testing for life historical changes in spatial patterns of four tropical tree species. *The Journal of Ecology*, 621-633
Stiles, J.M., & Sarabandi, K. (1996). A scattering model for thin dielectric cylinders of arbitrary cross section and electrical length. *Antennas and Propagation, IEEE Transactions on, 44*, 260-266
Suganuma, H., Abe, Y., Taniguchi, M., Tanouchi, H., Utsugi, H., Kojima, T., & Yamada, K. (2006). Stand biomass estimation method by canopy coverage for application to remote sensing in an arid area of Western Australia. *Forest Ecology and Management, 222*, 75-87
Sun, G., K.J., Ranson (1995). A three-dimensional radar backscatter model of forest canopies. *Geoscience and Remote Sensing, IEEE Transactions on, 33*, 372-382
Sun, G., Ranson, K.J., Guo, Z., Zhang, Z., Montesano, P., & Kimes, D. (2011). Forest biomass mapping from lidar and radar synergies. *Remote Sensing of Environment*
Swarup, S., & Tewari, R. (1979). Depolarization of radio waves in jungle environment. *Antennas and Propagation, IEEE Transactions on, 27*, 113-116
Taiz, L., & Zeiger, E. (2002). Plant physiology 3rd. ed
Tang, K., & Buckius, R.O. (1998). The geometric optics approximation for reflection from two-dimensional random rough surfaces. *International journal of heat and mass transfer, 41*, 2037-2047
Tang, K., Dimenna, R.A., & Buckius, R.O. (1996). Regions of validity of the geometric optics approximation for angular scattering from very rough surfaces. *International journal of heat and mass transfer, 40*, 49-59
Tavakoli, A., Sarabandi, K., & Ulaby, F.T. (2002). Horizontal propagation through periodic vegetation canopies. *Antennas and Propagation, IEEE Transactions on, 39*, 1014-1023
Tebaldini, S. (2009). P-band sar tomography of the remningstorp forest site. In

Tewari, R., Swarup, S., & Roy, M.N. (1990). Radio wave propagation through rain forests of India. *Antennas and Propagation, IEEE Transactions on, 38*, 433-449
Treuhaft, R., & Siqueira, R. (2000). The Vertical Structure of Vegetated Land Surfaces from Interferometric and Polarimetric Radar. *Radio Science, 35*, 141-177
Treuhaft, R.N., Asner, G.P., & Law, B.E. (2003). Structure-based forest biomass from fusion of radar and hyperspectral observations. *Geophysical Research Letters, 30*, 1472
Treuhaft, R.N., Asner, G.P., Law, B.E., & Van Tuyl, S. (2002). Forest leaf area density profiles from the quantitative fusion of radar and hyperspectral data. *Journal of Geophysical Research, 107*, 4568
Treuhaft, R.N., & Cloude, S.R. (1999). The structure of oriented vegetation from polarimetric interferometry. *Geoscience and Remote Sensing, IEEE Transactions on, 37*, 2620-2624
Treuhaft, R.N., & Cloude, S.R. (2002). The structure of oriented vegetation from polarimetric interferometry. *Geoscience and Remote Sensing, IEEE Transactions on, 37*, 2620-2624
Treuhaft, R.N., Law, B.E., & Asner, G.P. (2004). Forest attributes from radar interferometric structure and its fusion with optical remote sensing. *BioScience, 54*, 561-571
Treuhaft, R.N., Madsen, S.N., Moghaddam, M., & van Zyl, J.J. (1996). Vegetation characteristics and underlying topography from interferometric radar. *Radio Science, 31*
Tsang, L., J. Kong (1981). Scattering of electromagnetic waves from random media with strong permittivity fluctuations. *Radio Science, 16*, 303-320
Tsang, L., & Kong, J. (1977). Theory for thermal microwave emission from a bounded medium containing spherical scatterers. *Journal of Applied Physics, 48*, 3593-3599
Tsang, L., Kong, J.A., & Shin, R.T. (1985). Theory of microwave remote sensing
Ulaby, F.T., & El-Rayes, M.A. (1987). Microwave dielectric spectrum of vegetation-Part II: Dual-dispersion model. *Geoscience and Remote Sensing, IEEE Transactions on*, 550-557
Ulaby, F.T., Moore, R.K., Fung, A.K. (1982). *Microwave Remote Sensing: Active and Passive Vol. II*. Reading, MA Addison-Wesley
Ulaby, F.T., Sarabandi, K., McDonald, K., Whitt, M., & Dobson, M.C. (1990). Michigan microwave canopy scattering model. *International Journal of Remote Sensing, 11*, 1223-1253
Ulaby, F.T., Siquiera, P. (1995). Polarimetric SAR Soil Moisture Inversion Algorithms. In, *Technical Memorandum 95-12*: University of Michigan
Ulander, L.M.H., Askne, J., Fransson, J., Gustavsson, A., Le Toan, T., Manninen, T., Martinez, J.M., Melon, P., Smith, G., & Walter, F. (2000). Retrieval of stem volume in coniferous forest from low VHF-band SAR. In (pp. 441-443 vol. 441): IEEE
Valentine, H.T., Tritton, L.M., & Furnival, G.M. (1984). Subsampling trees for biomass, volume, or mineral content. *Forest Science, 30*, 673-681
Wagner, W., Luckman, A., Vietmeier, J., Tansey, K., Balzter, H., Schmullius, C., Davidson, M., Gaveau, D., Gluck, M., & Le Toan, T. (2003). Large-scale mapping of boreal forest in SIBERIA using ERS tandem coherence and JERS backscatter data. *Remote Sensing of Environment, 85*, 125-144

Wait, J.R. (1955). Scattering of a plane wave from a circular dielectric cylinder at oblique incidence. *Can. J. Phys, 33*, 189–195
Wallington, E., & Woodhouse, I. (2006). Forest height retrieval from commercial X-band SAR products. *Geoscience and Remote Sensing, IEEE Transactions on, 44*, 863-870
Walton, E., & Young, J. (1984). The Ohio State University compact radar cross-section measurement range. *Antennas and Propagation, IEEE Transactions on, 32*, 1218-1223
Wang, H., & Ouchi, K. (2005). The relation between the order parameter of K-distribution in high-resolution polarimetric SAR data and forest biomass. In (pp. 4339-4342): Geoscience and Remote Sensing Symposium, 2005. IGARSS'05. Proceedings. 2005 IEEE International
Waring, R.H. (1983). *Estimating forest growth and efficiency in relation to canopy leaf area*: Academic Press
Waring, R.H., Way, J.B., Hunt Jr, E.R., Morrissey, L., Ranson, K.J., Weishampel, J.F., Oren, R., & Franklin, S.E. (1995). Imaging radar for ecosystem studies. *BioScience, 45*, 715-723
Way, J.B., Paris, J., Dobson, M.C., McDonals, K., Ulaby, F.T., Weber, J., Ustin, L., Vanderbilt, V.C., & Kasischke, E.S. (1991). Diurnal change in trees as observed by optical and microwave sensors: the EOS synergism study. *IEEE Transactions on Geoscience and Remote Sensing, 29*, 807-821
Weber, J.A., & Ustin, S.L. (1991). Diurnal water relations of walnut trees: implications for remote sensing. *Geoscience and Remote Sensing, IEEE Transactions on, 29*, 864-874
Wegmuller, U., & Werner, C. (2002). Retrieval of vegetation parameters with SAR interferometry. *Geoscience and Remote Sensing, IEEE Transactions on, 35*, 18-24
West, G.B., Brown, J.H., & Enquist, B.J. (1997). A General Model for the Origin of Allometric Scaling Laws in Biology. *Science, 276*, 122
West, G.B., Brown, J.H., & Enquist, B.J. (1999a). The Fourth Dimension of Life: Fractal Geometry and Allometric Scaling of Organisms. *Science, 284*, 1677
West, G.B., Brown, J.H., & Enquist, B.J. (1999b). A general model for the structure and allometry of plant vascular systems. *Nature(London), 400*, 664-667
White, J.D., Running, S.W., Nemani, R., Keane, R.E., & Ryan, K.C. (1997). Measurement and remote sensing of LAI in Rocky Mountain montane ecosystems. *Canadian Journal of Forest Research, 27*, 1714-1727
Wigneron, J.P., Ferrazzoli, P., Olioso, A., Bertuzzi, P., & Chanzy, A. (1999). A simple approach to monitor crop biomass from C-band radar data. *Remote Sensing of Environment, 69*, 179-188
Woodhouse, I., Wallington, E., & Turner, D. (2006). Edge effects on tree height retrieval using X-band interferometry. *Geoscience and Remote Sensing Letters, IEEE, 3*, 344-348
Woodhouse, I.H. (2006a). *Introduction to microwave remote sensing*: CRC
Woodhouse, I.H. (2006b). Predicting Backscatter-Biomass and Height-Biomass Trends Using a Macroecology Model. *Geoscience and Remote Sensing, IEEE Transactions on, 44*, 871-877

Woodhouse, I.H., & Hoekman, D.H. (2000). Radar modelling of coniferous forest using a tree growth model. *International Journal of Remote Sensing, 21*, 1725-1737
Wu, Y., & Strahler, A.H. (1994). Remote estimation of crown size, stand density, and biomass on the Oregon transect. *Ecological Applications*, 299-312
Wulder, M., Niemann, K.O., & Goodenough, D.G. (2000). Local maximum filtering for the extraction of tree locations and basal area from high spatial resolution imagery. *Remote Sensing of Environment, 73*, 103-114
Yoda, K. (1963). Self-thinning in over-crowded pure stands under cultivated and natural conditions.(In-traspecific competition among higher plants. XI.). *J Biol Osaka City Univ, 14*, 107-129
Young, H.E., Ribe, J.H., & Wainwright, K. (1980). Weight tables for tree and shrub species in Maine. *Maine. Life Sciences and Agriculture Experiment Station. Miscellaneous report (USA)*
Yueh, S.H., et al (1992). Branching model for vegetation. *Geoscience and Remote Sensing, IEEE Transactions on, 30*, 390-402
Zenner, E.K., & Peck, J.L.E. (2009). Characterizing structural conditions in mature managed red pine: spatial dependency of metrics and adequacy of plot size. *Forest Ecology and Management, 257*, 311-320
Zianis, D. (2003). The size-biomass allometry of forest trees : a global meta-analysis, novel methods for estimating forest biomass and a case study of Fagus moesiaca Cz. In
Zianis, D., & Mencuccini, M. (2004). On simplifying allometric analyses of forest biomass. *Forest Ecology and Management, 187*, 311-332

12 Appendices

12.1 Appendix 1

12.1.1 Preliminary Validations for Allometric Choices

After identifying the potential of using allometric relations for forest backscatter purposes a preliminary parameter study was conducted for use with allometric equations collected and published in (Zianis and Mencuccini 2004). The allometric equation under investigation is of the form $M = a.\ D^{\ b}$, with the a and b scaling exponents given in Zianis and Mencuccini and the diameter, '*D*', taken from 50 year old samples of each of the 8 tree species featured in the 1946 British Forestry yield tables to give biomass '*M*'. In this study 279 combinations of the '*a*' and '*b*' parameters were used, collated from empirical methods for various tree species including excurrent and decurrent types. Using these parameter combinations a series of possible biomass values were calculated for individual tree species. The distribution of which is seen below.

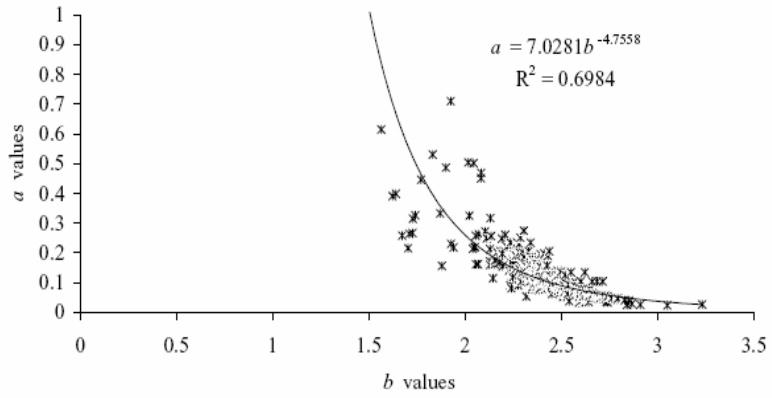

Figure A1.1.Relation of reported *a* and *b* scaling values. Taken from (Zianis 2003).

In figures A1.2 and A1.3 there is a large distribution of biomass values separated into bin ranges using the equations available. It is true that the parameters for the allometric equations were derived for particular tree species but also that there is a trend towards a certain range of values representing a Gaussian distribution.

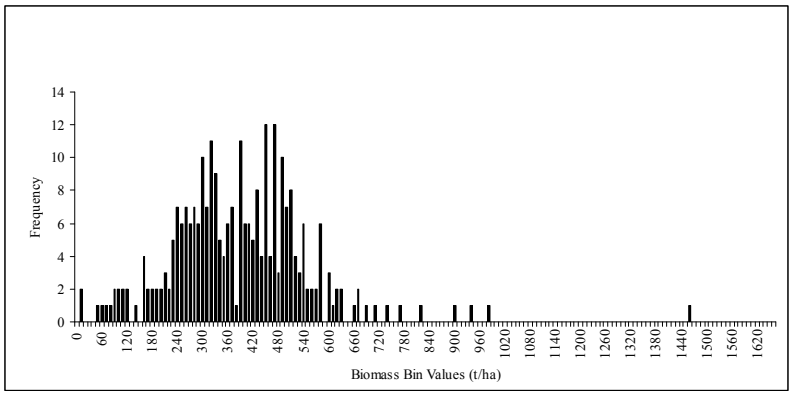

Figure A1.2. Histogram showing frequency of biomass values for European Larch within a particular range using exponents taken from Zianis and Mencuccini (2004) and diameter values from 1946 British forestry yield tables. Bin values represent biomass in ton/ha.

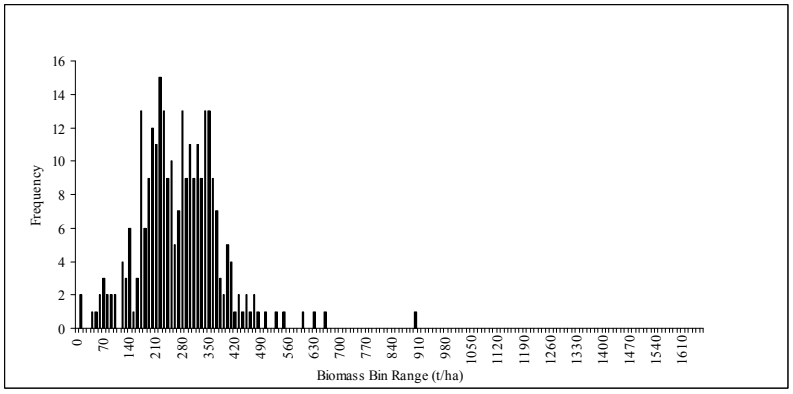

Figure A1.3. Histogram showing frequency of biomass values for Scots Pine within a particular range using exponents taken from Zianis and Mencuccini (2004) and diameter values from 1946 British forestry yield tables. Bin values represent biomass in ton/ha.

The b value predicted by the WBE model has the value of 2.67 which does not correspond exactly with the mean value of 2.3679 from the collation of allometric study values from the literature. This does not disprove the theoretical value but there is a distinct trend towards values for *b* of between 2.36 and 2.6. If the theory of a generic allometric equation were to exist or for a range of values to be acceptable then such a relationship as shown above would be expected. The incorporation of a range of values is recommended, rather than the use of solely the WBE prediction. The WBE model predicts a relationship between mass and radius of:

$$M \alpha r_0^{2(3a+1)/3a} \quad \text{(A.1)}$$

with the *a* value in this case determined by the geometry of the branching. These '*a*' values have been seen in nature to range from approximately 2/3 to 4/3. For example excurrent trees would be represented by exponent 'b' with a value of approximately 3 as a result of an *a* value of 2/3, while for decurrent it would be 2.67 when using the decurrent based WBE model with an *a* of 1. By dividing the equations into coniferous and broadleaf species the following statistical studies could be made and plotted.

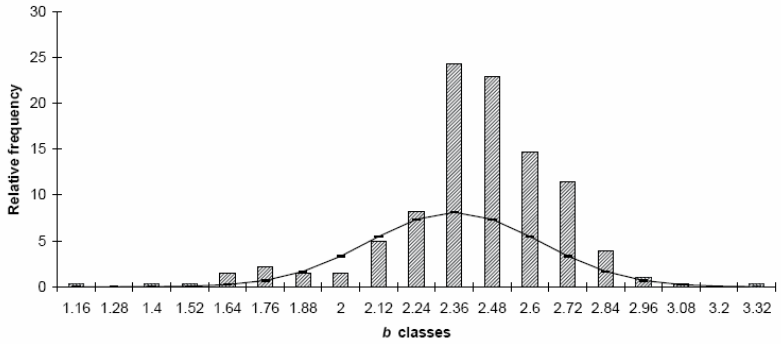

Figure A1.4. Relative frequency distribution of '*b*' values superimposed on normal curve taken from (Zianis 2003).

The distribution of values when segregated indicates a relatively small difference between '*b*' values of coniferous and broadleaf species. The mean value for coniferous can be seen to be lower than that of the broadleaf. The predictions of the WBE model are specifically tailored for broad leaf decurrent trees which may be the reason for the mean '*b*' value being closer to the WBE value of 2.67. It is also interesting to note the presence of parameters derived for "all species" such as that of (Martin et al. 1998) where a value of 2.663 for '*b*' coincides with certain values of both coniferous and broadleaf trees as well as with the WBE value.

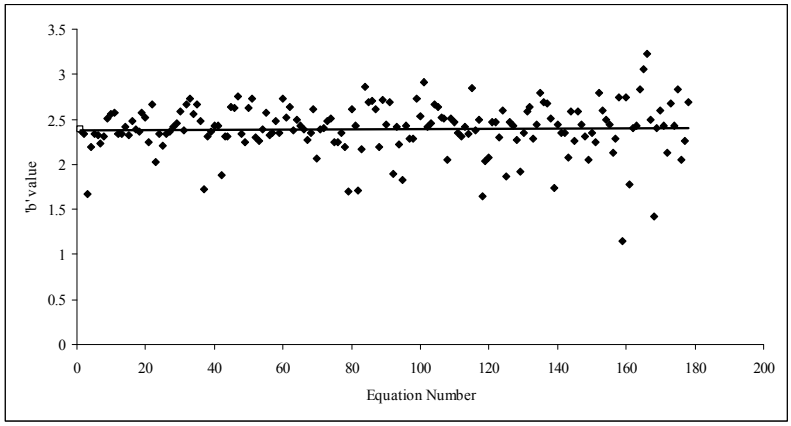

Figure A1.5. Distribution of '*b*' values from broadleaf allometric equations collated by (Zianis 2003). Mean value denoted by open data point.

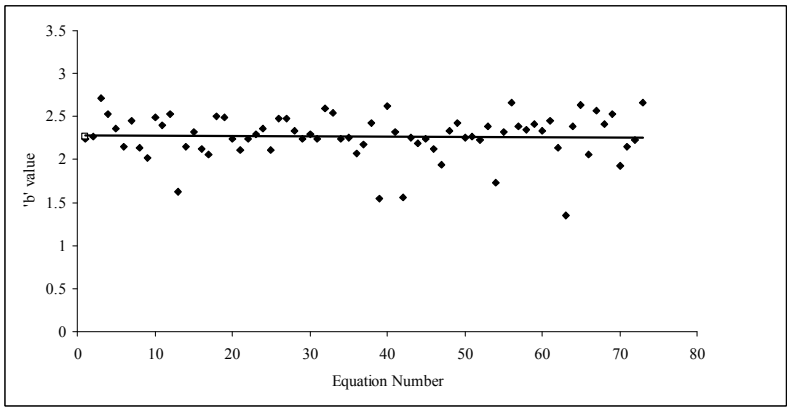

Figure A1.6. Distribution of '*b*' values taken from coniferous allometric equations collated by Zianis and Mencuccini (2004). Mean value denoted by open data point.

A useful conclusion to arise from this study is that it seems apparent that there exists a difference in scaling exponent for decurrent and excurrent trees. Although the results have not entirely agreed with the WBE predictions, the values still lie within a range within reasonable proximity to WBE predictions. As the WBE model refers to trends in nature this preliminary work serves to show that these trends do exist and that the range of values used in (Woodhouse 2006b) are appropriate for further use rather than assuming that all species scale the same.

12.2 Appendix 2

12.2.1 SERA Parameter File Examples

Table A2.1

Basic	Species:	Generic Angiosperm	*Abies Alba*	Generic Gymnosperm
	densityStem:	995.76	718.90	764.30
	densityLeaf:	500	923.43	923.43
	densitySeed:	497.88	359.45	479.00
	canopyTransmittance:	0.02	0.02	0.02
	fractionMinimumSurvival:	0.20	0.20	0.20
	heightLeafMax:	0.00030	0.00030	0.00030
	heightStemMax:	31.46	42.70	30.11
	youngsModulusStem:	9.65	7.40	7.33
	makeSeeds:	TRUE	TRUE	TRUE
	fractionSelfishness:	0.5	0.5	1.0
Reproduction	reproductionConstant:	0.0070	0.0997	0.5000
	reproductionExponent:	1.710	1.100	0.085
	numYearsGrowthMemory:	2.000	2.000	1.098
	massSeedMax:	0.008	0.600	0.085
	locSeedFormation:	[1.0,0,0.0]	[1.0,0,0.0]	[1.0,0,0.0]
	seedDispersalMethod:	[4,45,5]	[4,45,5]	[4,45,5]
	photoConstant:	1.51	1.53	0.58
	photoExponent:	-0.45	-0.46	-0.46
	canopyTransmittanceImpacts	FALSE	FALSE	FALSE
Photosynthesis	fractionCarbonToSeeds:	1	1	1
	fractMassSeedMaxToGerm:	0.8	0.8	0.8
	fractionSeedMassToPlant:	0.003400	0.000045	0.000317647
	fractionCarbonToStem:	0.99	0.99	0.99
Allometry	speciesConstant1:	0.86	0.94	0.72
	speciesExponent1:	1.02	1.00	1.04
	speciesConstant2:	0.1200	0.0397	0.2902
	speciesExponent2:	0.880	1.199	0.972
	speciesConstant3:	0.085	0.248	0.385
	speciesExponent3:	0.77	0.73	0.71
	speciesConstant20:	0.026	0.029	0.030
	speciesExponent20:	0.38	0.39	0.40
	speciesConstant7:	160.81	100.06	80.26
	speciesExponent7:	1.10	1.08	0.93
	speciesConstant8:	7.71	15.51	8.49

12.3 Appendix 3

12.3.1 Comparative Data for Cases (b) and (c) from Chapter 10

- Case (a): Described thoroughly in Chapter 10
- Case (b): Generic Angiosperm (Angiosperm)

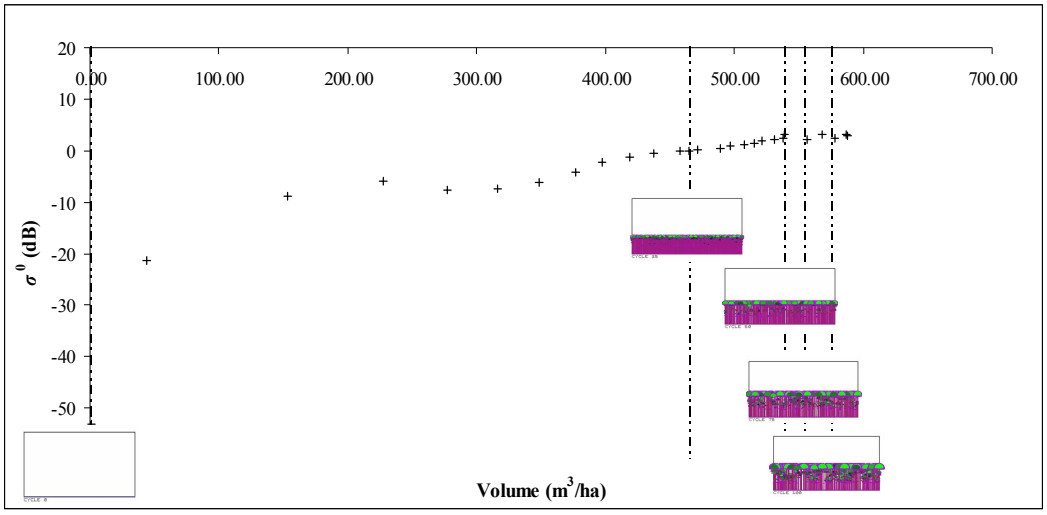

Figure A3.1. RT2 modelled P-Band HH Backscatter and volume values shown with respect to the visual appearance of the Angiosperm forest at 0, 25, 50 , 75 and 100 years old, left to right respectively. Note that backscatter and volume values are only representative of stems. Y axis position of images for display purposes only.

The generic angiosperm allometry was determined for SERA using the Cannell dataset. The allometry differs from *Abies Alba* through many parameters both physically and functionally. The forest progression data is given in Table 8.2. The visualisation of this progression is also included with the backscatter contribution associated with each stage of the forest growth, Figure A3.1. The backscatter, as a result of separating the scatterers into classes of Optical and Rayleigh, is also displayed alongside the total forest backscatter highlighting the large Optical contribution at 429MHz, Figure A3.2. The total backscatter is shown to progress in a

more uniform way than for *Abies Alba*. Thinning is at a much greater rate and basal area and volume increase at a steady rate. There is no obvious overexpansion.

- Case (c): Mixed Species (Gymnosperm and Angiosperm)

Table A3.1. Mixed Species forest data.

Age (years)	Stems	Vol. (m^3/ha)	Basal (m^2/ha)	H100 (m)	Opt.Vol. (m^3/ha)	Ray.Vol. (m^3/ha)
0	24788	0.00	0.00	0.06	0.00	0.000
2	24141	0.38	0.56	0.80	0.00	0.381
4	21465	18.70	6.26	6.26	19.40	2.014
6	16477	86.27	14.92	7.51	83.76	2.393
8	13004	165.61	20.86	9.76	165.60	0.015
10	10322	235.08	23.98	11.36	234.77	0.155
12	7642	289.63	25.67	12.60	289.42	0.213
14	5700	332.29	26.53	13.62	332.17	0.122
16	4567	364.48	26.87	14.47	364.42	0.063
18	3915	392.53	27.26	15.20	392.45	0.079
20	3389	413.94	27.36	15.85	413.88	0.060
22	2951	435.58	27.67	16.43	435.50	0.084
24	2713	455.71	27.99	16.95	455.65	0.061
25	2598	464.70	28.12	17.19	464.63	0.069
26	2506	474.66	28.31	17.43	474.76	0.086
28	2230	489.18	28.45	17.86	489.12	0.057
30	2027	502.80	28.53	18.26	502.75	0.047
32	1917	513.47	28.55	18.64	513.43	0.038
34	1842	524.64	28.60	18.99	524.59	0.053
36	1756	529.77	28.41	19.32	529.71	0.055
38	1668	536.50	28.31	19.63	536.50	0.052
40	1643	544.97	28.36	19.92	544.92	0.052
50	1335	580.10	28.50	21.17	580.06	0.040
60	1383	571.54	26.92	22.19	571.48	0.062
70	1563	575.05	26.61	23.03	574.99	0.060
80	1506	589.41	26.74	23.75	589.36	0.056
90	1619	565.68	25.35	24.35	565.60	0.073
100	1645	570.19	25.48	24.85	570.14	0.052

The mixed species forest example consists of 6 variations of species comprising *Abies Alba*, generic angiosperm with additional shade constant, generic angiosperm, generic gymnosperm with *Abies Alba* photo constant, and generic gymnosperm with *Cryptomeria* photo constant. When planted in equal numbers the dominant species

after 100 years becomes the generic angiosperm with a gradual reduction in the overall percentage of gymnosperm contribution to the community from an early age.

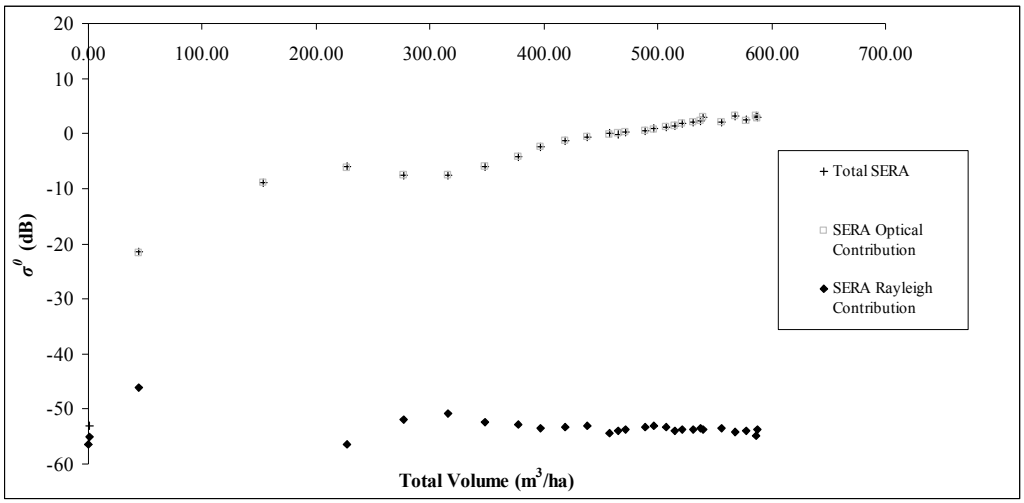

Figure A3.2. RT2 modelled P-Band HH backscatter associated with a SERA generated Angiosperm forest over a 100 year period in terms of Total, Rayleigh and Optical backscatter..

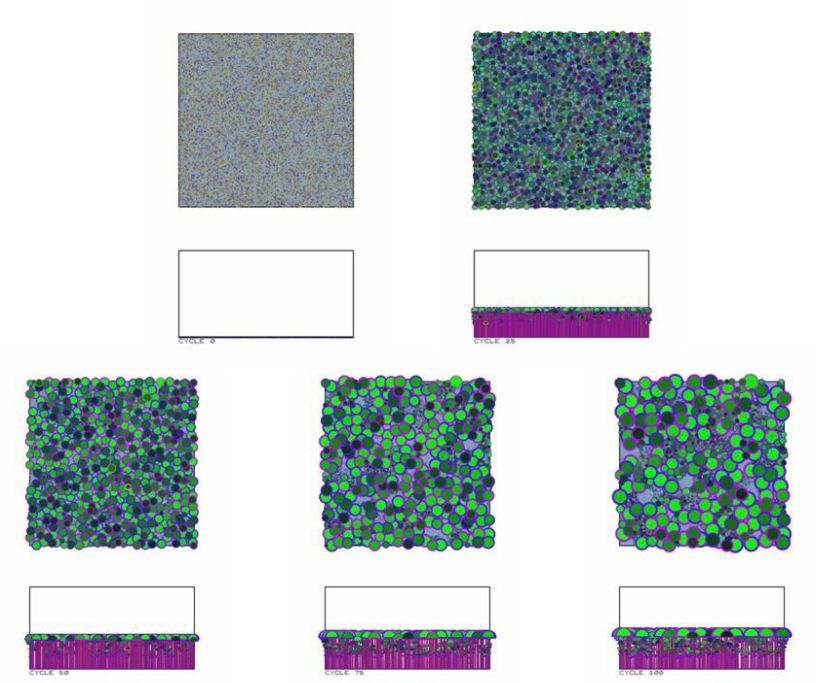

Figure A3.3. Horizontal and bottom-up representation of Mixed Species forest before canopy removal. Glimpses at 0, 25, 50, 75 and 100 years over 1ha. Purple represents stems, darkness of green represents the level of shading on the canopy. Blue represents sky, indicating zero canopy cover.

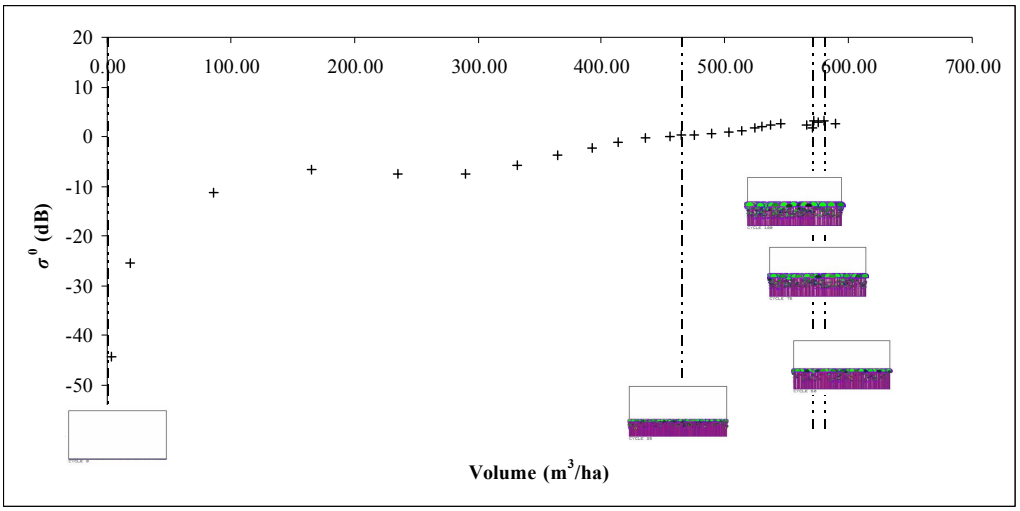

Figure A3.4. RT2 modelled P-Band HH Backscatter and volume values shown with respect to the visual appearance of the Mixed Species forest at 0, 25, 50 , 75 and 100 years old, left to right respectively. Note that backscatter and volume values are representative of stems. Y axis position of images due to space limitations.

Data is provided in the form of Table A3.1 and Figure A3.3 showing the forest's growth progression as well as backscatter values against volume in the form of total backscatter, Figures A3.4 and A3.5. A visual interpretation is also provided with respect to years of growth as well as volume in Figure A3.4. with the contributions of Rayleigh and Optical backscatter shown in Figure A3.5.

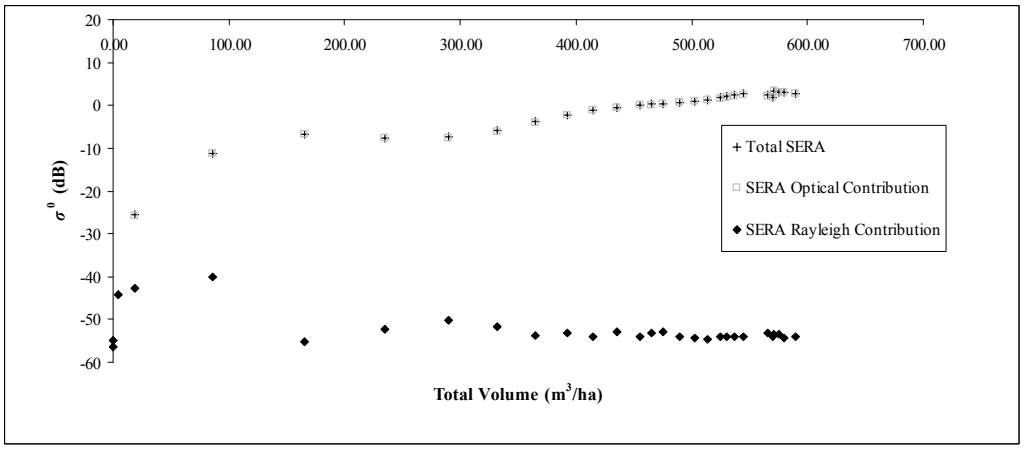

Figure A3.5. RT2 P-Band HH backscatter associated with a SERA generated stem forest of mixed species over a 100 year period. Backscatter shown for Total, Optical and Rayleigh backscatter.

12.4 Appendix 4

12.4.1 SERA Derived Vertical Biomass Distributions

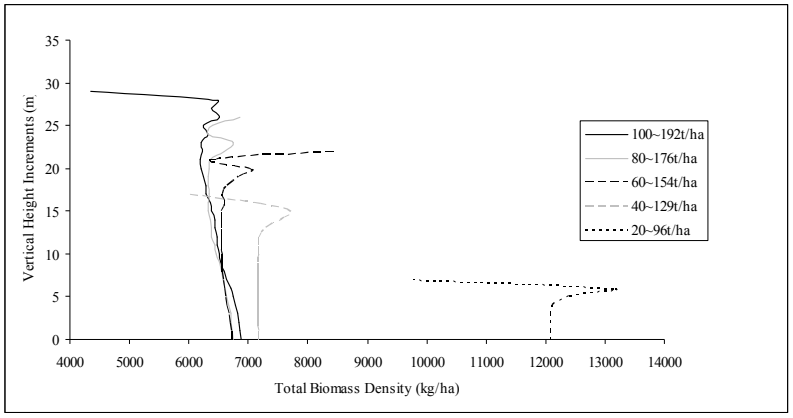

Figure A4.1: *Abies Alba* planting density 10000. Vertical biomass distribution within the forest over 1m increments for forest total biomass density after 20, 40, 60, 80 and 100 years. Total cumulative biomass density is shown in legend.

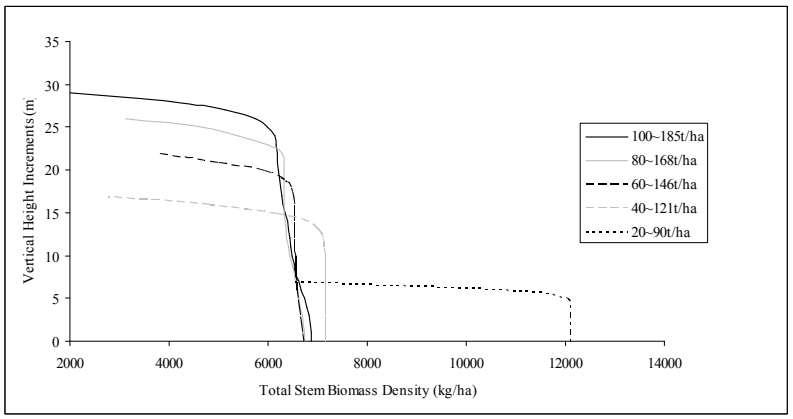

Figure A4.2: *Abies Alba* initial planting density 10000. Vertical biomass distribution within the forest over 1m increments for forest total stem biomass density after 20, 40, 60, 80 and 100 years. Total cumulative stem biomass density is shown in legend.

Examples from *Abies Alba*, Generic Gymnosperm, Generic Angiosperm, Mixed Species, *Cryptomeria*; years 20, 40, 60, 80, 100; starting population of 10000 are used. SERA has been used in this thesis for the primary purpose of predicting forest backscatter behaviour of different species growing in competitive environments. In addition it has been used to

model the relationships between forest "average" height and volume. An additional role that SERA can perform is in describing the distribution of forest biomass. Here its ability to model vertical biomass distribution is emphasised. For *Abies Alba*, *Cryptomeria*, Generic Gymnosperm, Generic Angiosperm, and a Mixed Species example, forests are generated for 20, 40, 60, 80 and 100 year periods. Each forest is assigned a starting population of 10000 and is limited to 100 years of growth. The areal constraints are limited to a single hectare with no outer growth allowed. The vertical distribution of the biomass in each of these forests is displayed using single metre increments to display how much biomass is present within each metre of the vertical profile. In the case of stems the largest biomass accumulation over a single metre increment will be associated with the metre spanning from the ground upwards. All stems must have a presence in this vertical region and as the study ventures higher into the canopy the stem contribution to biomass will drop off as fewer trees will scale the maximum forest height. In addition the canopy contribution is also included. Biomass values in kg are assigned by SERA and converted into biomass density of tonnes per hectare.

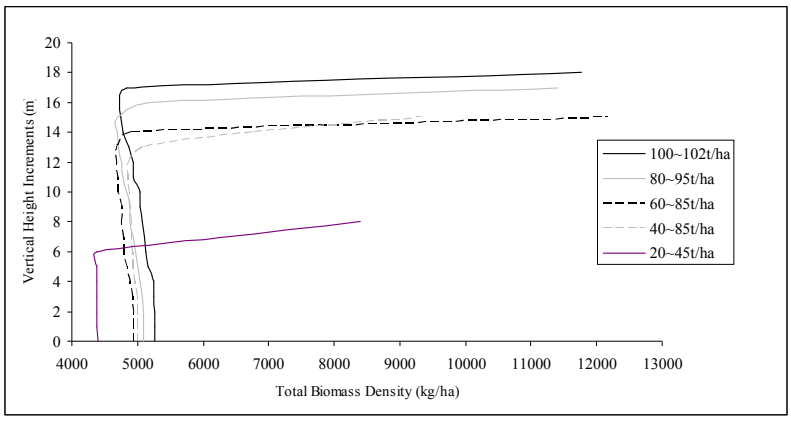

Figure A4.3: Generic Gymnosperm initial planting density 10000. Vertical distribution of biomass within forest over 1m increments, for total biomass density after 20, 40, 60, 80 and 100 years. Total cumulative biomass density is shown in legend.

In Figures A4.1 and A4.2 the vertical distribution of *Abies Alba* is shown in terms of total biomass and total stem biomass density. Where the total biomass density is considered the data consists of both stem and canopy. For the total stem biomass density distribution

the trend at each age is for the first metre in the vertical profile to initially contain the most biomass, with this level dropping gradually as profile height increases. The gradual biomass decrease suffers from a rapid drop off at the limits of the tallest stems as the profile reduces to zero beyond the forest limits. This behaviour is exhibited for all modelled examples when stem biomass density is solely considered. *Abies Alba* data differs from other examples in one crucial way, this is that the general trend is for the younger stands to possess more biomass in the first few metres than the older stands. This is a likely result of variations in the exhibited thinning behaviour with the thinning rate of *Abies Alba* such that a large reduction in stem numbers is apparent between the ages of 20 and 40 years in comparison to the thinning rates of other species.

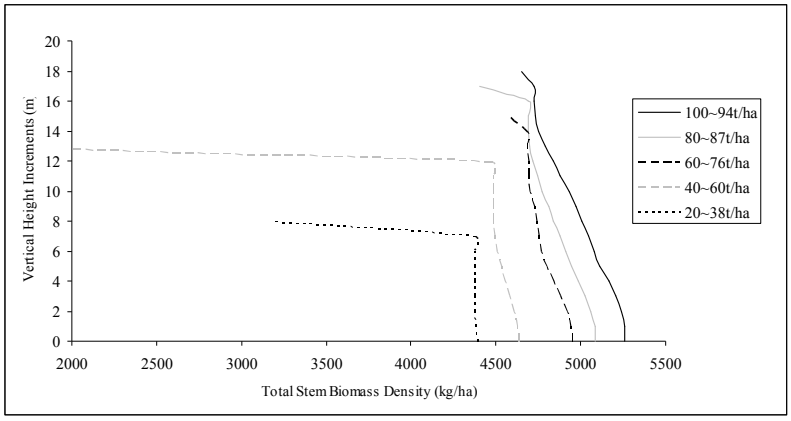

Figure A4.4: Generic Gymnosperm initial planting density 10000. Vertical biomass distribution within forest over 1m increments for total stem biomass density after 20, 40, 60, 80 and 100 years. Total cumulative stem biomass density shown in legend.

For total biomass density the inclusion of forest canopy reduces the familiarity of the biomass distribution between species but also due to the stochastic nature of forest growth. When plotting the vertical distribution of total biomass for each modelled example after 100 years of growth similarities are apparent for Generic Angiosperm and mixed species examples due to the gradual dominance of angiosperms over gymnosperms. The gymnosperm cases of generic gymnosperm and *Cryptomeria* both exhibit biomass drop offs per metre as the location of the canopy is increased upwards, but once the canopy is reached there is a very large increase in biomass, particularly for

the generic gymnosperm which indicates a majority of trees present in the forest are similar to the maximum height. The *Abies Alba* forest has a much less significant contribution to the total biomass density per vertical metre from the canopy biomass. The minimal increases due to the canopy at higher levels within the canopy can describe the *Abies Alba* vertical structure as either being a forest consisting of a variety of different heights which disperses the canopy contribution throughout the vertical structure or as a forest which assigns less biomass to the canopy components. Analysis of raw data shows that the tallest tree in the *Abies Alba* forest assigns a greater percentage of mass to the canopy than a generic angiosperm. As such the description of the vertical structure must be a result of a more widely distributed canopy.

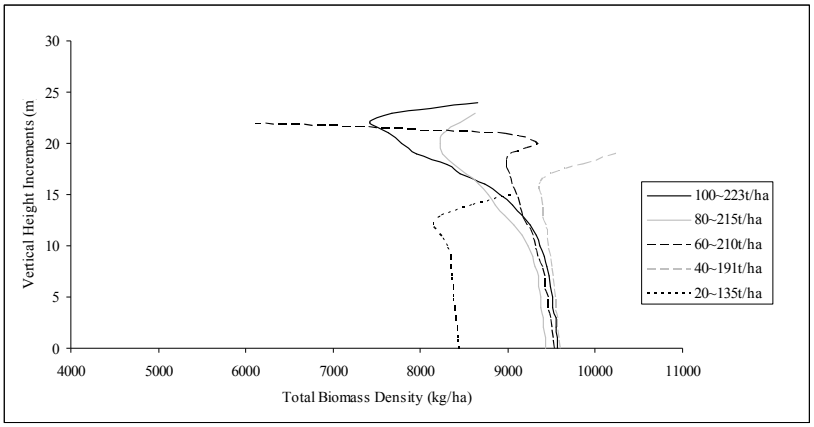

Figure A4.5: Generic Angiosperm, initial planting density 10000. Vertical biomass distribution within the forest over 1m increments for total biomass density after 20, 40, 60, 80 and 100 years. Total cumulative biomass density shown in legend.

This appendix highlights the further capabilities of Macroecological models for studies concerning remote sensing. Such studies with which these abilities can be associated are those that study vertical heterogeneity within a forest using radar backscatter and interferometry as in (Treuhaft and Cloude 1999) and (Treuhaft et al. 1996) and this thesis.

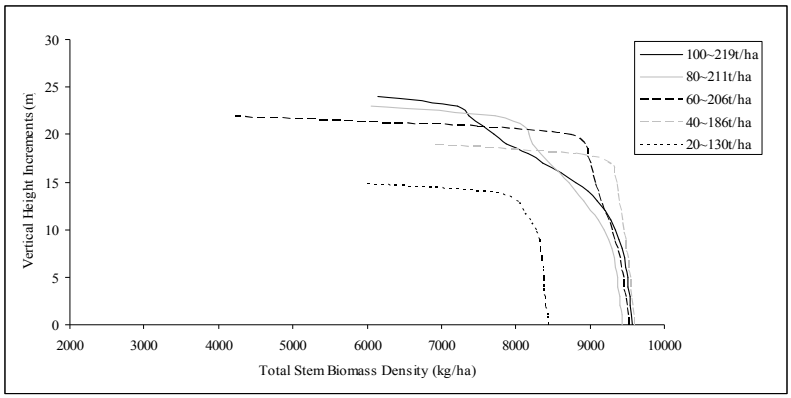

Figure A4.6 Generic Angiosperm, initial planting density 10000. Vertical biomass distribution within the forest over 1m increments for total stem biomass density after 20, 40, 60, 80 and 100 years. Total cumulative stem biomass density shown in legend.

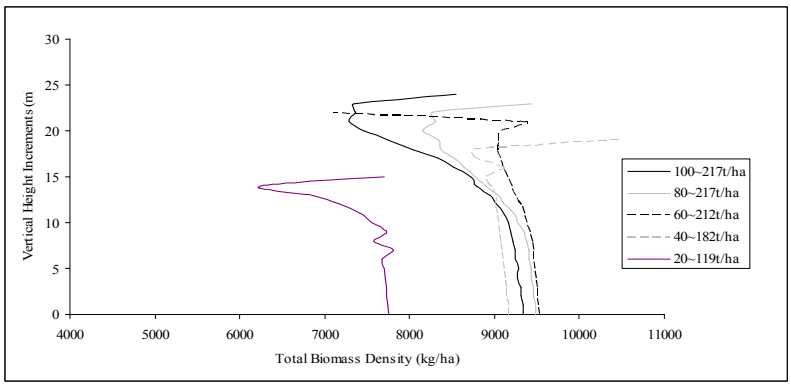

Figure A4.7: All Species initial planting density 10000. Vertical biomass within the forest over 1m increments for total biomass density after 20, 40, 60, 80 and 100 years. Total cumulative biomass density shown in legend.

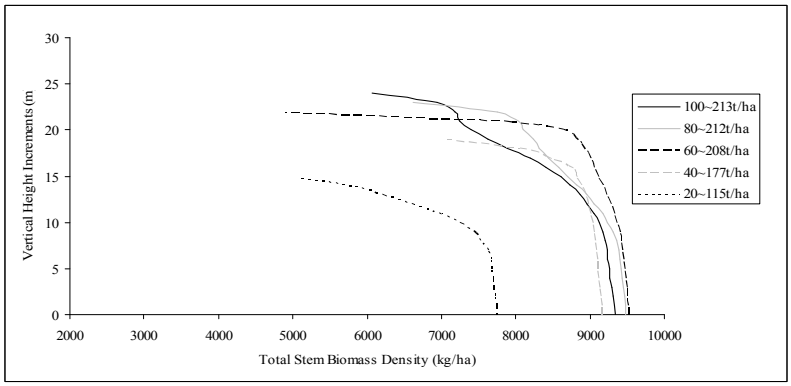

Figure A4.8: All Species initial planting density 10000. Vertical biomass distribution within the forest over 1m increments for total stem biomass density after 20, 40, 60, 80 and 100 years. Total cumulative stem biomass density shown in legend.